Impacts of liquefaction and lateral spreading on bridge pile foundations from the February 22nd 2011 Christchurch earthquake

A thesis submitted in partial fulfilment of the requirements for the

Degree of Masters of Engineering in Civil Engineering

at the University of Canterbury

By: **Anna Winkley**

Supervised by: **Professor Misko Cubrinovski**

Co-supervisors: **Dr. Alessandro Palermo, Dr. Brendon Bradley**

Department of Civil and Natural Resources Engineering

University of Canterbury

Christchurch, New Zealand

June 2013

Abstract

The M_w 6.2 February 22nd 2011 Christchurch earthquake (and others in the 2010-2011 Canterbury sequence) provided a unique opportunity to study the devastating effects of earthquakes first-hand and learn from them for future engineering applications. All major events in the Canterbury earthquake sequence caused widespread liquefaction throughout Christchurch's eastern suburbs, particularly extensive and severe during the February 22nd event. Along large stretches of the Avon River banks (and to a lesser extent along the Heathcote) significant lateral spreading occurred, affecting bridges and the infrastructure they support.

The first stage of this research involved conducting detailed field reconnaissance to document liquefaction and lateral spreading-induced damage to several case study bridges along the Avon River. The case study bridges cover a range of ages and construction types but all are reinforced concrete structures which have relatively short, stiff decks. These factors combined led to a characteristic deformation mechanism involving deck-pinning and abutment back-rotation with consequent damage to the abutment piles and slumping of the approaches.

The second stage of the research involved using pseudo-static analysis, a simplified seismic modelling tool, to analyse two of the bridges. An advantage of pseudo-static analysis over more complicated modelling methods is that it uses conventional geotechnical data in its inputs, such as SPT blowcount and CPT cone resistance and local friction. Pseudo-static analysis can also be applied without excessive computational power or specialised knowledge, yet it has been shown to capture the basic mechanisms of pile behaviour. Single pile and whole bridge models were constructed for each bridge, and both cyclic and lateral spreading phases of loading were investigated. Parametric studies were carried out which varied the values of key parameters to identify their influence on pile response, and computed displacements and damages were compared with observations made in the field. It was shown that pseudo-static analysis was able to capture the characteristic damage mechanisms observed in the field, however the treatment of key parameters affecting pile response is of primary importance. Recommendations were made concerning the treatment of these governing parameters controlling pile response. In this way the future application of pseudo-static analysis as a tool for analysing and designing bridge pile foundations in liquefying and laterally spreading soils is enhanced.

Acknowledgements

I would first and foremost like to thank my supervisor, Prof. Misko Cubrinovski, for his help and guidance throughout my project; his experience and contributions were extremely valuable and appreciated. My co-supervisors, Dr. Brendon Bradley and Dr. Alessandro Palermo also provided me with guidance at certain points throughout my research and my thanks go out to them. Financial support from the University of Canterbury and the EQC was also gratefully received.

Following the 22nd February earthquake, detailed bridge reconnaissance work was carried out by myself, in conjunction with several other researchers. Particular acknowledgement is paid to Jenny Haskell, a former University of Canterbury student. Her amazingly detailed sketches of bridge damages were true works of art! Other contributors to these bridge inspections include Kelly Robinson, Kun Ma and Duncan Henderson, all fellow postgraduate students at the University of Canterbury, thank you for that. In particular, thanks to Kelly for the lateral spreading transect data provided, and for all those little extras that really mean so much!

I also want to thank Dr. Liam Wotherspoon (University of Auckland) for supplying additional photos and bridge details; namely site investigation data and bridge construction drawings.

I wish to give a massive thanks to my parents, Shayne and Greg, and to my grandfather, Ross, for supporting me throughout my University studies. Without you I would not be where I am today, and your belief in me is truly appreciated and beyond words. Thanks Mum for being the pedantic grammarian that you are and proof-reading my work, even though at times you must have found it as dry as a piece of stale bread!

Finally, to my boyfriend Jeff, thank you for being there throughout these last few years. From proof-reading my work to helping me through minor meltdowns, you pretty much covered all the bases! Thank you so much.

Contents

List of Figures

List of Tables

1 Introduction

1.1 Christchurch earthquakes

On the 4th of September 2010 the M_w 7.1 Darfield earthquake struck the Canterbury region, marking the start of an earthquake sequence which, to date, has included more than twelve events with M_w > 5.0. The most devastating of these events was the M_w 6.2 Christchurch earthquake on the 22nd of February 2011, which was generated by the Port Hills fault line less than 10 km south of Christchurch city centre and resulted in 185 fatalities. Ground accelerations induced by this event were amongst the highest ever recorded in an urban area, and extensive damage was caused to buildings, bridges and other infrastructure. Perhaps the most distinctive feature of the Christchurch earthquake was the extensive soil liquefaction which occurred throughout Christchurch's eastern suburbs and parts of its CBD, particularly pronounced along the Avon River.

1.2 Liquefaction and lateral spreading-induced bridge damage

The surficial soils in eastern Christchurch along the Avon River are predominantly young (loosely deposited) sands, silts, clays and peat, with a huge amount of variability over short length scales and a relatively shallow groundwater table. As such, liquefaction susceptibility is high.

Where liquefaction occurs on sloping ground, or where there is a free-face condition, e.g. a river bank, a typical consequence is lateral spreading of the surrounding ground. Following the 22nd February 2011 earthquake, lateral spreading along the Avon River was substantial, with permanent ground displacements at the river banks ranging from several centimetres to more than two metres. This spreading was particularly damaging to bridges, infrastructure, houses and other buildings near the river banks.

The focus of this research is on the effects of liquefaction and subsequent lateral spreading on road bridges across the Avon River. Following the Christchurch earthquake detailed bridge reconnaissance work was carried out by the author and others on nine bridges; 3 in Christchurch CBD on shallow foundations, and 6 east of the CBD on pile foundations. These bridges are typically short-mid length reinforced concrete structures, with high stiffness in the longitudinal direction. In general, bridges performed better than other engineered structures in the Christchurch earthquakes; there were no collapses, and most bridges were back in service within a couple of days.

In spite of this, significant damages did occur to some bridges, with the most commonly observed, spreading-induced deformation mechanism being that of deck-pinning and abutment back-rotation. This is where the stiff deck provides restraint against lateral ground movements, and subsequently back-rotation of abutments is forced to occur consistent with the direction of ground flow. This can result in large pile deformations and damages, as well as significant slumping of approaches.

1.3 Pseudo-static analysis

Pseudo-static analysis is a relatively simple, seismic modelling tool in which an equivalent static analysis is used to estimate the dynamic earthquake response. It is attractive to practicing engineers in that it uses conventional geotechnical data as inputs (e.g. SPT blowcount) and can be applied without excessive computational power or specialised knowledge, yet it still captures the basic mechanisms of pile behaviour. However, since an equivalent static analysis is being used to represent a highly complex dynamic soil-structure-interaction problem, there exist considerable uncertainties which must be dealt with in a sensible manner. The pseudo-static approach used in this research in based on a finite element beam-spring model in which structural elements (e.g. piles, abutments, bridge deck) are represented by beam elements and springs represent the horizontal stiffness of the soil. The effects of horizontal ground displacements and seismic motions can be allowed for by applying static soil displacements to the ends of the soil springs and/or inertial forces to the pile heads.

1.4 Thesis objectives

The two key objectives of this research are to:

1. Summarise the performance of pile-supported bridges in the 22nd February earthquake. This will be done by:
    - Quantifying the damages observed.
    - Assessing the severity of liquefaction and lateral spreading at the sites and looking at how these affect bridge performance.
    - Correlating bridge damage with land damage.
    - Identifying typical modes of deformation and loads associated with lateral spreading.

2. Enhance the use of pseudo-static analysis. This will be done by:
    - Performing pseudo-static analyses and parametric studies on two case study bridges to look at pile response characteristics and expected damages.
    - Establishing the sensitivity of the pile response to the model parameters.
    - Making recommendations for future application of the model in the analysis and design of bridge foundations.

1.5 Thesis organisation

Chapter 2 presents a literature review which summarises case histories, experimental tests, analytical methods and current design recommendations for piles in laterally spreading soils. Chapter 3 looks at the details of the 2010-2011 Canterbury earthquake sequence and summarises the performance of 9 case-study bridges. In chapter 4 the pseudo-static analysis method of Cubrinovski *et al*. (2009a), which is later used to analyse 2 of the case study bridges, is described and compared with 3 other methods. Chapter 5 presents the pseudo-static analysis results of the ANZAC and Dallington Bridges and looks at the effects of key parameters controlling system response.

2 Literature Review

2.1 Introduction

Pile foundations are typically designed to transfer vertical loads from a superstructure onto a deeper bearing stratum. As a result, they are particularly susceptible to the application of lateral loads throughout their depths (such as those imposed on them by the ground during earthquakes). When liquefaction occurs, piles can lose almost all lateral support in a liquefied layer due to the soil's loss of strength and stiffness.

Several complex mechanisms are involved in soil-pile interaction in liquefying soils. Rapid changes in strength, stiffness, loading and other characteristics make their analysis inherently complicated. One way to clarify different mechanisms is to define two separate loading phases, which are typically considered separately when performing seismic analyses on piles:

1. **Cyclic loading phase** – this occurs during the earthquake shaking. Before the onset of liquefaction, the key loads acting on piles are the inertial loads from the superstructure (Case I in Figure 2-1). With the development of liquefaction, large cyclic shear strains build up resulting in (potentially large) cyclic ground displacements. At this stage, kinematic forces from the ground displacement are acting in conjunction with the inertial loads (Case II).
2. **Lateral spreading phase** – once shaking has ceased inertial loads from the superstructure are no longer significant, however a residual shear strain component may accumulate. The result of this is permanent horizontal ground displacement, or lateral spreading. Case III-a in Figure 2-1 shows the case where residual displacement is small and Case III-b is an example of lateral spreading, where residual deformations can be quite large. Kinematic forces due to soil movement are dominant here.

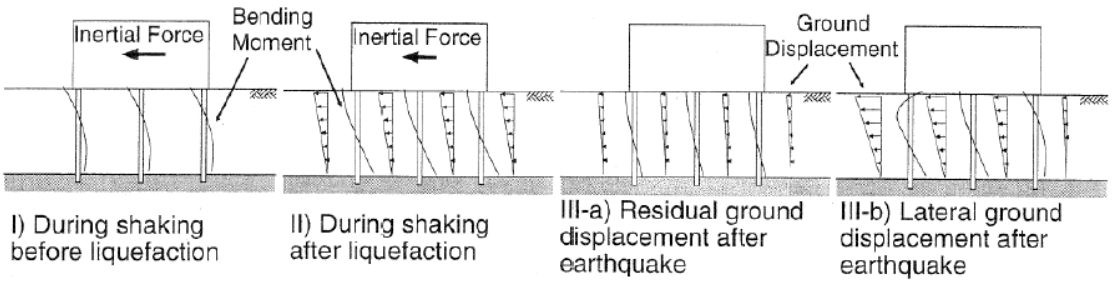

Figure 2-1: Different stages of loading considered in soil-pile interaction analyses (Tokimatsu and Asaka 1998)

Where bridges are concerned, superstructure mass is typically relatively low (in comparison with buildings for example), and those which cross rivers in liquefiable soils are highly susceptible to lateral spreading from the free-face condition at the river banks. For these reasons the governing loading phase on bridges is more likely to be the lateral spreading phase, although it is important to check the cyclic phase also. This chapter summarises some observations from case histories of pile performance in liquefying and laterally spreading soils, experimental tests, analysis methods and current design recommendations.

2.2 Case histories of pile and bridge performance in laterally spreading soils

Case histories provide a tangible way of assessing the effects of an earthquake first hand. By observing damages sustained during past earthquakes, the engineering community can learn from them for the future, and establish better construction codes and techniques. This section looks at the past performance of piles and bridges in several earthquakes.

2.2.1 Kobe earthquake, 1995, Japan

The Kobe (Hyogoken-Nambu) earthquake of January 17th, 1995, caused significant liquefaction of reclaimed fills in the port area of Kobe city. Lateral spreading of the quay walls occurred with a magnitude of 1-4 m (Cubrinovski and Ishihara 2003), causing substantial damages to pile foundations in the waterfront area.

Particularly notable were the regions of maximum damage to piles; Horikoshi *et al.* (2000) stated that almost all piles were significantly damaged (i.e. sustained major cracking) at depths where a reclaimed soil layer existed. Cubrinovski and Ishihara (2003) noted that damage was largest at greater depths, at the interface between the liquefied and non-liquefied layers, which they attributed to the large lateral ground displacements. Tokimatsu and Asaka (1998) also noted high levels of damage at the interface between the liquefied and non-liquefied layers, as well as at the pile heads, stating that the damage at the pile heads was more pronounced in heavier structures. This indicates that the inertial forces created damage in this zone. Finn *et al.* (1996) described how lateral spreading imposed unidirectional forces on bridge pile foundations resulting in significant pier tilt and the subsequent dropping of some girders.

2.2.2 Niigata earthquake, 1964, Japan

In the 1964 Niigata earthquake, the Showa Bridge underwent a catastrophic collapse, as shown in Figure 2-2, where the simply-supported spans fell from their supports into the river. Hamada and O'Rourke (1992) and Berrill and Yasuda (2002) proposed that the bridge failure was due to a 10 metre thick layer of liquefied soil laterally displacing into the river about one minute after the earthquake had stopped (from eye-witness reports), indicating that it was a post-liquefaction failure. Bhattacharya and Madabhushi (2008), on the other hand, proposed that the failure was due to a buckling mechanism induced by instability in the piles from the lack of strength in their surrounding liquefied soils. Upon inspection of piles after their withdrawal from the ground, it was noted that large rotations had occurred at the interface between the liquefied and base soil layers. The deformed S-shape of the piles (see Figure 2-3) makes it clear that laterally-spreading soil caused this deformation, not inertial forces from the superstructure.

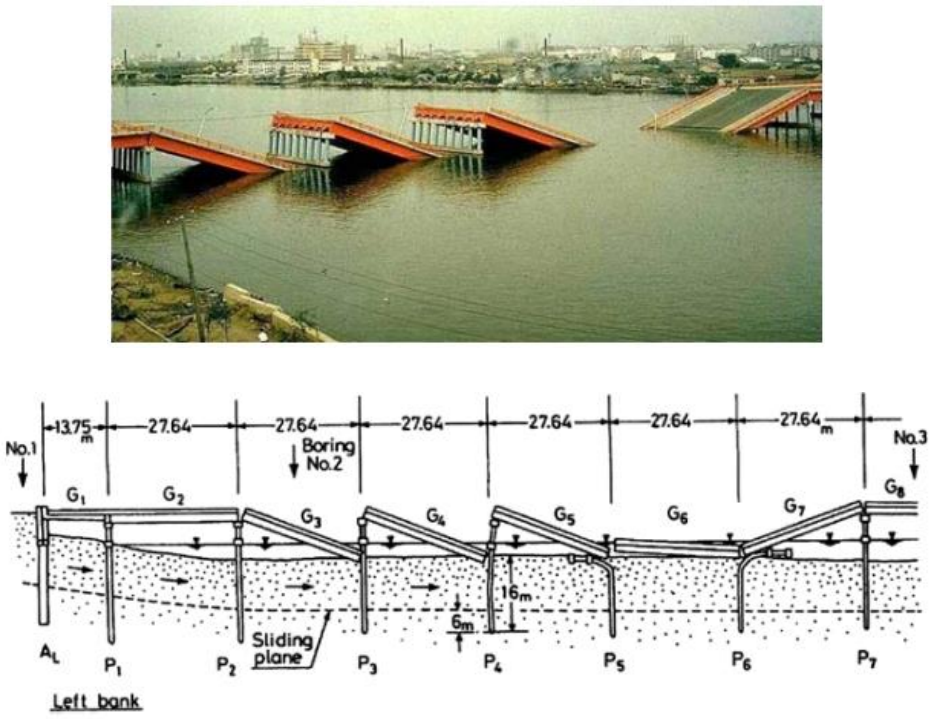

Figure 2-2: Collapse of the Showa Bridge in the 1964 Niigata earthquake (Takata et al., 1965)

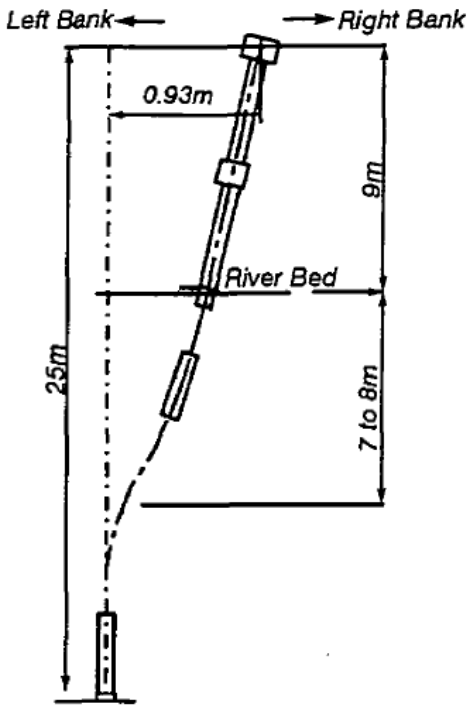

Figure 2-3: Deformed pile extracted from the Showa Bridge after the 1964 Niigata earthquake (Takata et al., 1965)

Another bridge damaged in the Niigata earthquake was the Yachiyo Bridge, a 14-span structure with a simply-supported pre-stressed concrete deck. Liquefaction-induced lateral spreading was in the order of 4 metres on both river banks (Hamada and O'Rourke 1992), and the pile-supported abutments and piers suffered substantial damage, as can be seen in Figure 2-4. The foundation piles themselves also sustained severe damages at the interface between the liquefied and non-liquefied layers (Hamada and O'Rourke 1992), and horizontal cracks were found throughout the piles indicating large bending moment demands. The large unilateral ground displacements towards the river pushed the bases of the piers in that direction, however their movement at the top was restrained by the stiffness of the bridge deck. This induced large pier back-rotations; the horizontal differential movement between the top and bottom of one pier was measured to be 1.1 m.

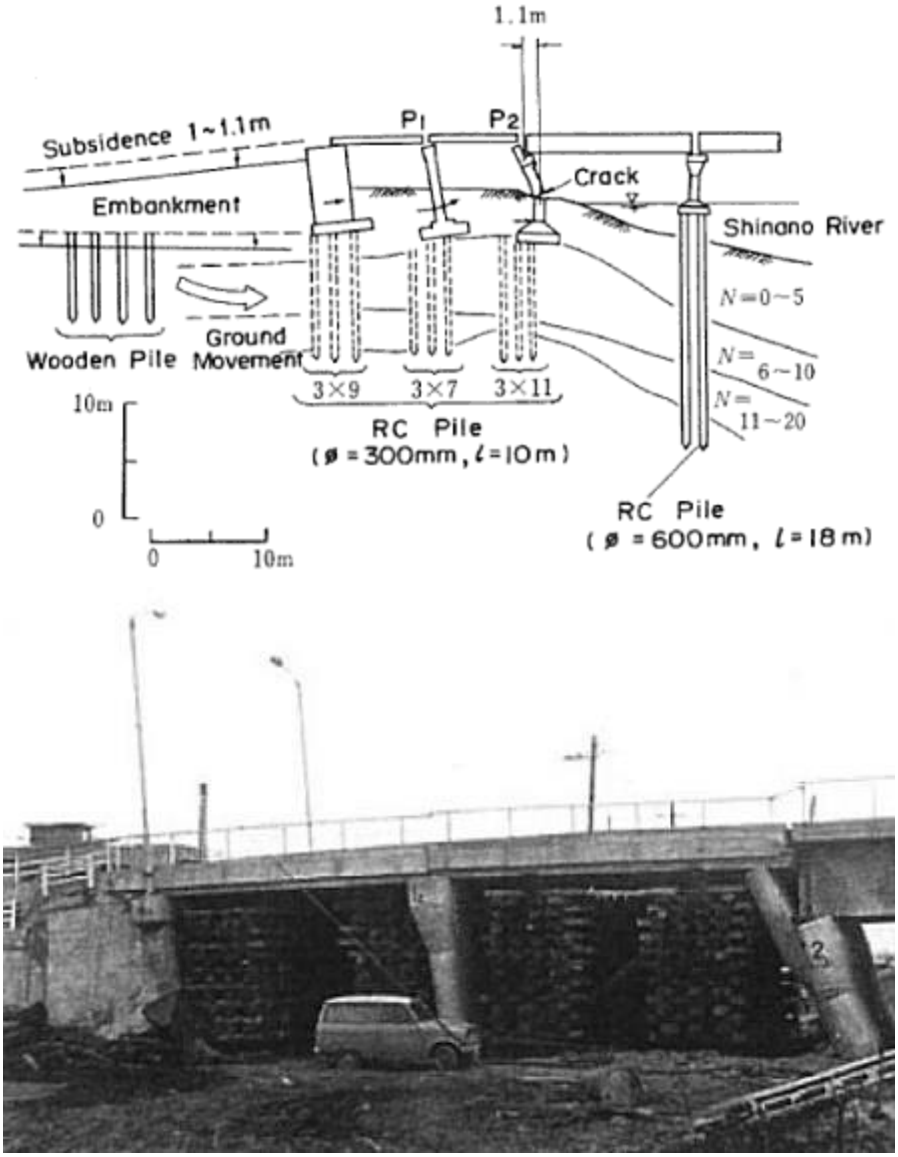

Figure 2-4: Damage to the abutments and piers of Yachiyo Bridge (Hamada and O'Rourke 1992)

2.2.3 Edgecumbe earthquake, 1987, New Zealand

Immediately following the Edgecumbe earthquake, lateral spreading occurred at the Landing Road Bridge in Whakatane. A layer of soil 4 metres thick liquefied and moved 1.5 – 2 m towards the Whakatane River. Berrill *et al.* (2001) identified that spreading towards the river channel in direct alignment with the bridge was significantly impeded by the four or five northern-most piers of the bridge. After the earthquake, soil was mounded up behind these piers, and gaps of up to 0.6 m were measured on the river side, indicating a passive failure mode in the non-liquefied crust layer. According to Berrill *et al.'s* calculations, these passive forces were estimated to be approximately

1 MN per pier (approximately 20 times greater than the drag forces in the liquefied sand), indicating that these are the dominant lateral forces on foundations undergoing lateral spreading. As a result, the importance of non-liquefied crustal layers being carried along with underlying liquefied layers is seen (Berrill and Yasuda, 2002).

2.2.4 Costa Rica earthquake, 1991

The magnitude 7.5 Costa Rican earthquake of 1991 caused extensive lateral spreading damage to bridges in the highway and railway systems. At least 7 bridges collapsed as a result, and many others were severely damaged (Youd *et al.* 1992).

The Rio Bananito Railway Bridge is a single-truss structure 50 metres long supported by elliptical, steel-encased, concrete caissons. In the earthquake, ground displacements caused by liquefaction and lateral spreading pushed the caissons out from under the seating plates on both ends of the bridge, which caused the truss to tilt downstream by about 15 degrees (Youd *et al.* 1992). This can be seen in Figure 2-5. The tops of the caissons had displaced between 1.9 and 5.7 metres towards the river, and were inclined between 7 and 37 degrees. Estimates of the permanent lateral ground displacements at the river banks were between 1 and 2.5 metres.

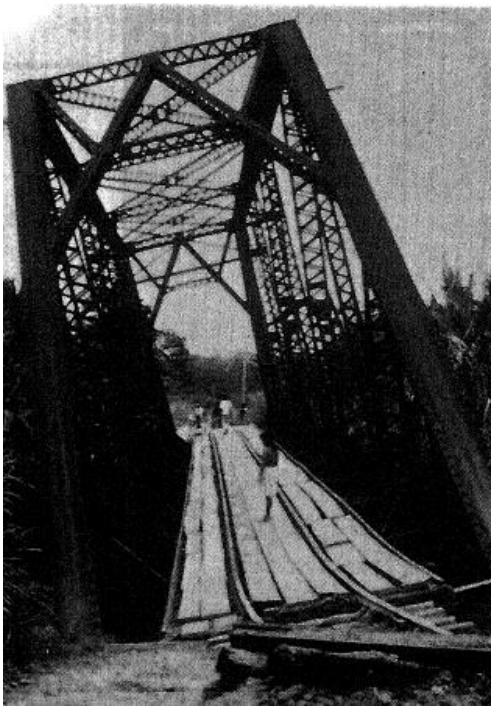

Figure 2-5: Tilting of Rio Bananito Railway Bridge due to caissons being pushed out from under bridge seatings (Youd et al. 1992)

The Rio Estrella Highway Bridge, composed of two 75 metre long trusses and a 25 metre long plate girder section, suffered severe damage as a result of liquefaction-induced lateral spreading. The ends of the two truss sections fell from their common support, as can be seen in Figure 2-6, and concrete spalling was observed at the tops of the north abutment piles. Approximately two metres of settlement occurred in the fill behind the south abutment and as a result the roadway approach on this side of the river settled, broke up and spread laterally (Youd *et al.* 1992). Lateral spreading displacements on this side of the river were estimated to be up to 2 metres. It is interesting to note that the southern abutment was sufficiently strong to resist the large lateral (and vertical) ground displacements imposed on it, and it remained rigid and in place.

Figure 2-6: Rio Estrella Highway Bridge - collapse of truss sections from central pier (Youd et al. 1992)

2.3 Experimental Studies

Many researchers (Cubrinovski *et al.* (1999), Brandenberg *et al.* (2007), Brandenberg *et al.* (2005) and Abdoun *et al.* (2003) to name but a few) have carried out major experimental tests on piles in liquefying soils using either centrifuge models or large-scale shake tables. The main advantages of experimental studies over field studies are that the experimental conditions can be controlled and pile responses can be accurately measured and observed. Input motions are known, soil conditions are more uniform, and other variables can be set so as to isolate parameters of interest. While experiments will never be able to fully capture the behaviour of real life soil-structure interactions in earthquakes, they play a critical role in enhancing the understanding of the response features of piles in liquefying and laterally spreading soils.

In general, findings confirm observations from gathered field data in that the zones of largest damage to piles tend to be concentrated at the pile head (for fixed head condition) and at the interface between the liquefied and non-liquefied layers. The marked changes in stiffness between each successive layer as well as the large displacements in the liquefied layer contribute to the development of large bending moments at these interfaces.

2.3.1 Cyclic phase

Cubrinovski *et al.* (1999) carried out large-scale shake table testing on 5 metre long, 20 centimetre diameter PHC piles in saturated sand. The tests were designed to look at the cyclic phase of loading and investigate the effects of both pile head fixity and the magnitude of cyclic ground displacements. It was found that larger damages occurred to the fixed-head piles over the pinned-head piles, with the influence being not only on the extent of the damage but also on its distribution. The fixed-head piles had reached yielding level at the pile tip and cracks were observed at the pile head, whereas the pinned-head piles suffered damage only at the pile tip. The maximum lateral displacements of the piles indicate that the peak displacements of the pinned-head pile-tops were either similar to or slightly smaller than the peak displacements of the ground surface. On the other hand, the fixed-head pile-tops' peak displacements were 25-30% smaller than the ground surface displacements. As expected, the effect of applied cyclic ground displacements meant that the damages observed in the higher amplitude shaking tests were greater than those observed in the lower amplitude shaking.

Tokimatsu *et al*. (2005) carried out large-scale shake table tests on soil-pile-structure systems to investigate the effects of inertial and kinematic forces qualitatively. Both dry and liquefiable deposits were considered. Their primary findings from the tests in saturated sand were:

- That before liquefaction was induced, the inertial and kinematics loads acted in opposite directions, decreasing the forces transmitted to the pile (Figure 2-7a).
- That after liquefaction, the inertial force and the earth pressures act in the same direction, increasing the shear forces transmitted to the piles (Figure 2-7b). This indicates that the inertial and kinematic forces act in phase with each other, and therefore piles in liquefiable soils should be designed considering both the inertial and kinematic loads at the same time.

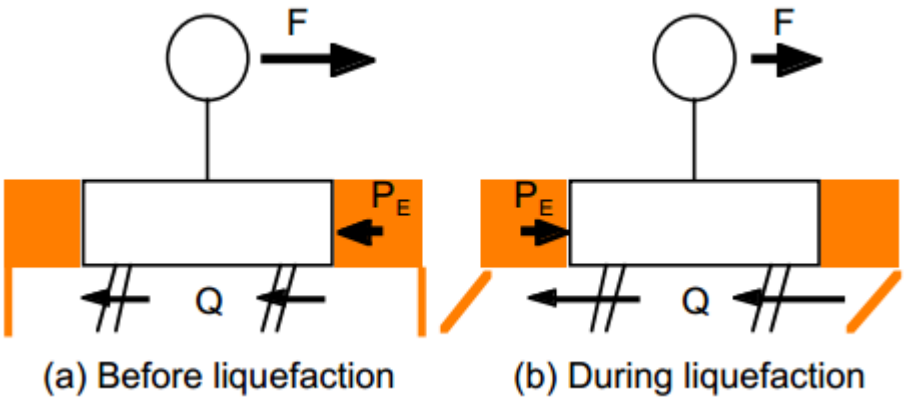

Figure 2-7: Change of action in earth pressure before and during liquefaction (Tokimatsu et al. 2005)

2.3.2 Lateral spreading phase

Brandenberg *et al.* (2005) investigated the behaviour of pile foundations in liquefying and laterally spreading ground using a series of dynamic centrifuge tests. Single piles and pile groups were embedded in a soil deposit consisting of a gently-sloping non-liquefiable crust overlying liquefiable loose sand over dense sand. The layers sloped gently towards a river channel carved in the crust at one end of the model. The systems were then subjected to a series of realistic earthquake motions applied to the base of each of the models. In all experiments, significant strains developed in the liquefiable sand, and the laterally spreading crust displaced more than the liquefied layer. It was shown that the direction of loading in the liquefied sand can be explained by the relative displacements between the piles and the liquefiable sand layer during the critical loading cycles. Figure 2-8 summarises the 3 generalised loading cases observed in the centrifuge tests. Case A is where the pile is stiff enough to resist the imposed loads from the crust layer and displaces less than

the soil in the liquefied layer. As such, it attracts loads from the liquefied layer in the downslope direction, as well as those from the crust. In Case B, the pile displaces more than the liquefied layer and the foundation is stiff enough to resist the load from the crust. Hence, it attracts loads from the liquefied layer in the upslope direction (i.e. resisting downslope movement). Case C is where the pile is too weak to mobilise the full downslope passive pressure in the crust, and in this case the pile head displacement is larger than the ground surface displacement. Ultimately, the stiffness of the piles relative to the soil profile is believed to be the main factor controlling the direction of loading from the liquefied layer, due to relative displacements between soil and pile.

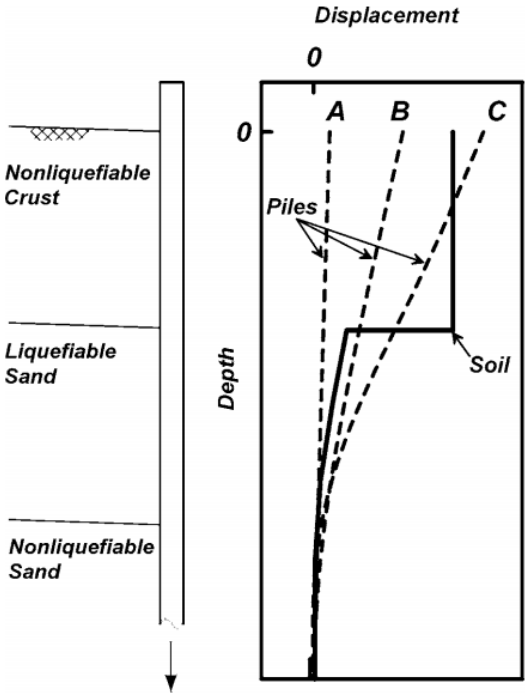

Figure 2-8: Schematic of soil and pile displacements for different cases of pile behaviour during lateral loading (Brandenberg et al. 2005)

Cubrinovski *et al.* (2006a) carried out large-scale shake table testing on stiff and flexible piles in a three-layered deposit, where the liquefied layer is sandwiched between non-liquefied crust and base layers. In these experiments the effects of pile stiffness, liquefied soil stiffness, and the lateral loads from the non-liquefied crust layer were investigated.

The experiment consisted of one stiff steel pile and one flexible PHC pile embedded in a laminar box filled with saturated sand and a crust layer of sand above the water table. The piles were 4.9 m long, fixed at the base and free at the top, and installed at such a spacing so as to avoid interaction effects. The experiments were conducted in two phases; the first a dynamic excitation phase to induce liquefaction, and the second a lateral loading phase to simulate lateral spreading of the soil. The lateral loading was applied by pushing the side of the laminar box at a rate of 4.1 cm/s up to a total displacement at the surface of 84 cm (as can be seen in Figure 2-9); this was initiated about 6 seconds after the end of the cyclic phase. Both piles remained purely elastic during shaking, and the response of both piles in the lateral spreading phase is shown in Figure 2-10.

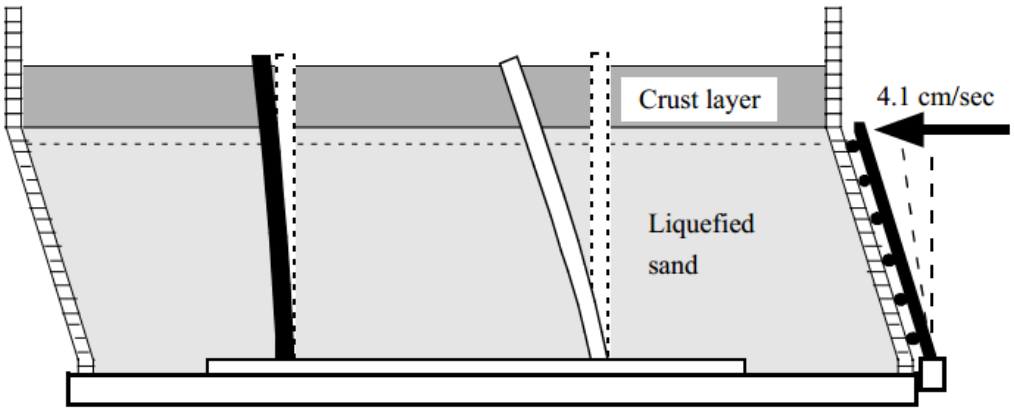

Figure 2-9: Lateral spreading phase, loading of large-scale shake table test (Cubrinovski et al. 2006a)

As can be seen in Figure 2-10, the flexible PHC pile practically followed the ground movement, and ultimate moment was reached at a ground displacement of about 9 cm. On the other hand, the stiff steel pile exhibited much larger lateral resistance, increasing in the initial stages of loading to around 5 cm then remaining constant throughout the rest of the test. Likewise, the pattern observed in the bending moments increased to around 60% of the yield moment and then remained constant. These responses were affected by the combined effects of both the liquefied soil movements and the lateral pressure from the non-liquefied crust; these were then evaluated separately in order to gain further insights into the soil-pile interaction.

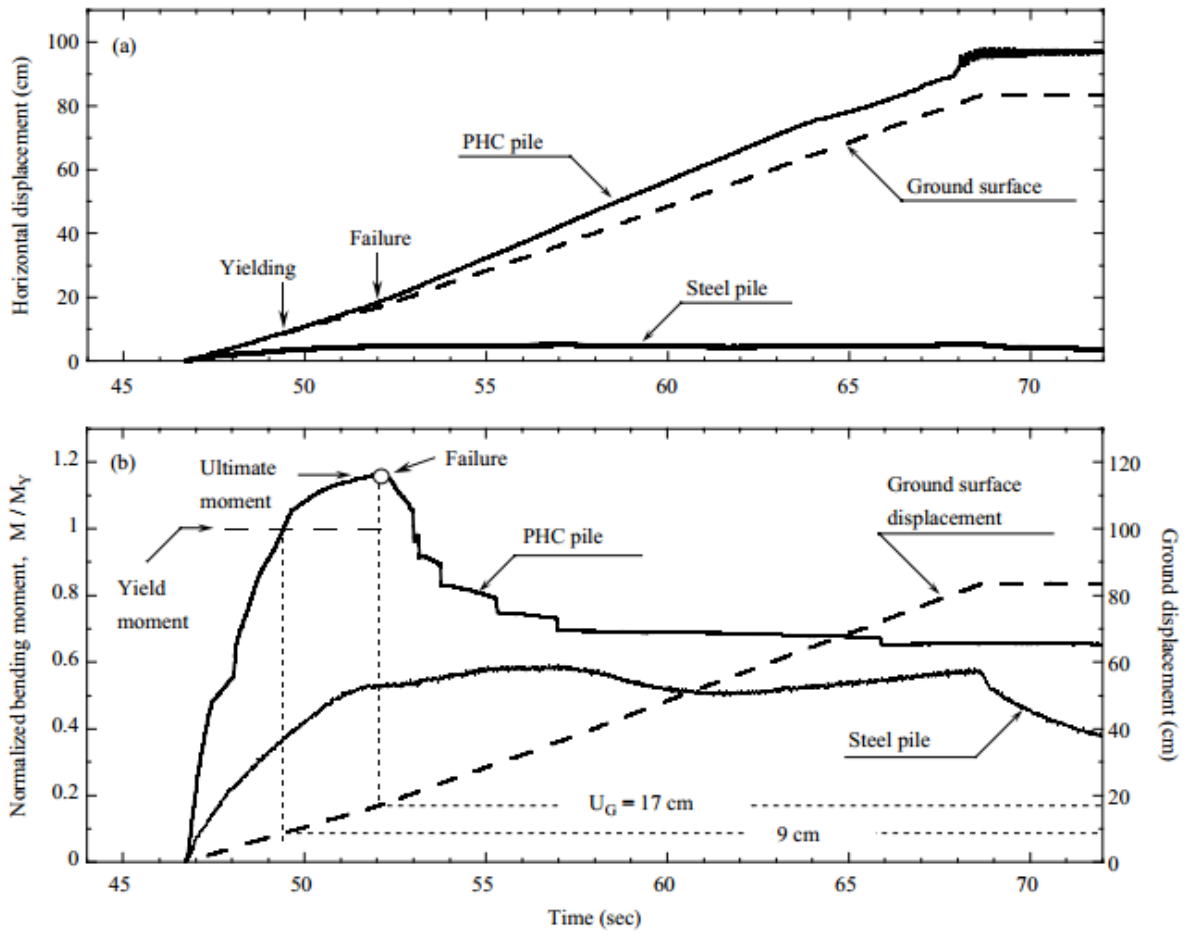

Figure 2-10: Measured displacements and bending moments in piles during lateral spreading phase, (a) displacement at pile head, (b) maximum bending moment near base of pile (Cubrinovski et al. 2006a)

Crust layer

The lateral pressure from the non-liquefied surface layer was found to increase sharply with relative displacement between the soil and the pile, until eventually it was fully mobilised at around 12-15 cm as can be seen in Figure 2-11. The lateral pressure per unit width acting on a single pile is larger than that on an equivalent continuous wall due to shearing resistance in the vertical sides of the failure wedge in the soil. In this experiment, the ultimate lateral pressure from the crust on the steel pile was found to be about 4.5 times the Rankine passive pressure. Once this pressure had been mobilised it remained virtually unchanged despite the subsequent significant increases in lateral soil displacements. This indicates that the lateral load from the surface layer was the key factor influencing the response of the steel pile.

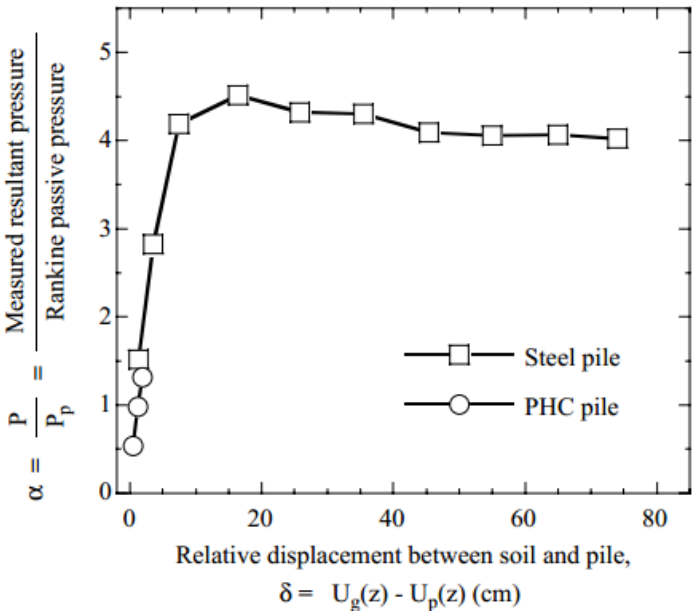

Figure 2-11: Measured pressure-displacement relationship in crust layer in terms of resultant pressure per unit width normalised to Rankine passive pressure (Cubrinovski et al. 2006a)

It is important to distinguish between active and passive modes of pile loading when considering the lateral loads applied to piles. The passive mode of pile loading is that which is representative of piles subjected to lateral spreading. As such, the passive pressures mobilised provide the driving force for pile deformation. Figure 2-12 shows a summary of data from several investigations regarding the shape factor, $\alpha = p_u/p_p$, for both active and passive piles. It can be seen that for passive piles, a reasonable range for α is between 4 and 5.

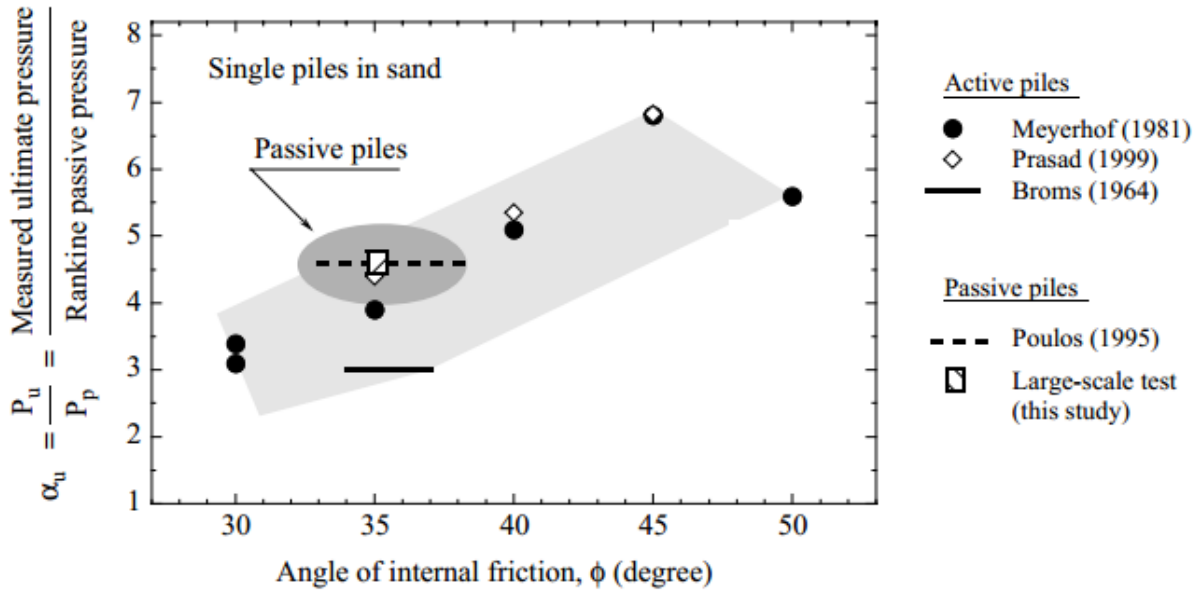

Figure 2-12: Ratio of measured ultimate lateral pressure to Rankine passive pressure as a function of angle of internal friction; summary of data from several experimental studies (Cubrinovski et al. 2006a)

As was shown in Figure 2-11, ultimate lateral pressure on the pile gradually increases with the increase in relative displacement between the pile and the soil. In the case of the steel pile, a relative displacement of 12-15 cm was needed to mobilise passive pressure, while the passive pressure on the PHC pile was never fully mobilised before its failure. Figure 2-13 shows a summary of data collected from several experimental tests on sands which were performed to evaluate the relative displacements required to develop the passive pressure. The relative displacement (δ_u) required is presented, normalised by the height of the wall or pile cap considered (H), as a function of the relative density in the crust layer. It is evident that larger displacements are required to mobilise passive pressures in loose sands than in dense sands.

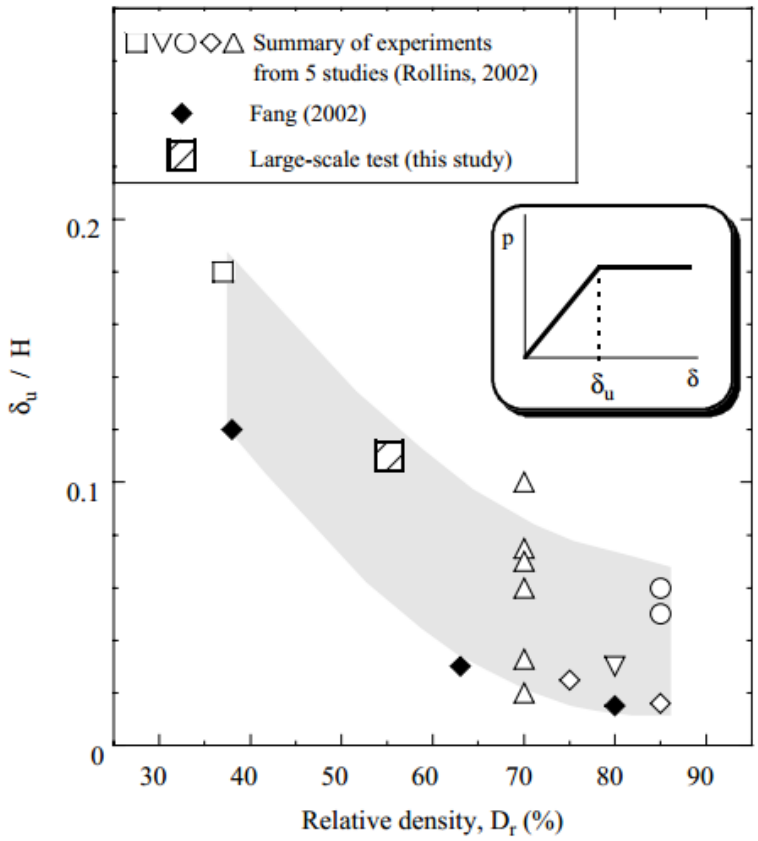

Figure 2-13: Relative displacement required to mobilise passive pressure as a function of density of sand; summary of data from experimental studies (Cubrinovski et al. 2006a)

Liquefied layer

The effect of liquefaction on soil stiffness was evaluated by performing back-calculations from the test result. The stiffness of the soil springs in the liquefied layer are considered to be β*k*, where *k* is directly proportional to the horizontal subgrade reaction coefficient and represents initial stiffness. The values of β which best represent pile response were then back-calculated for different ground displacements; the results of which can be seen in Figure 2-14. It can be seen that the best fit value for β is generally between 1/30 and 1/80, and gradually decreases with increasing ground displacement.

Note that β incorporates the effects from both the reduction in effective stress level as well as non-linear effects due to ground deformation.

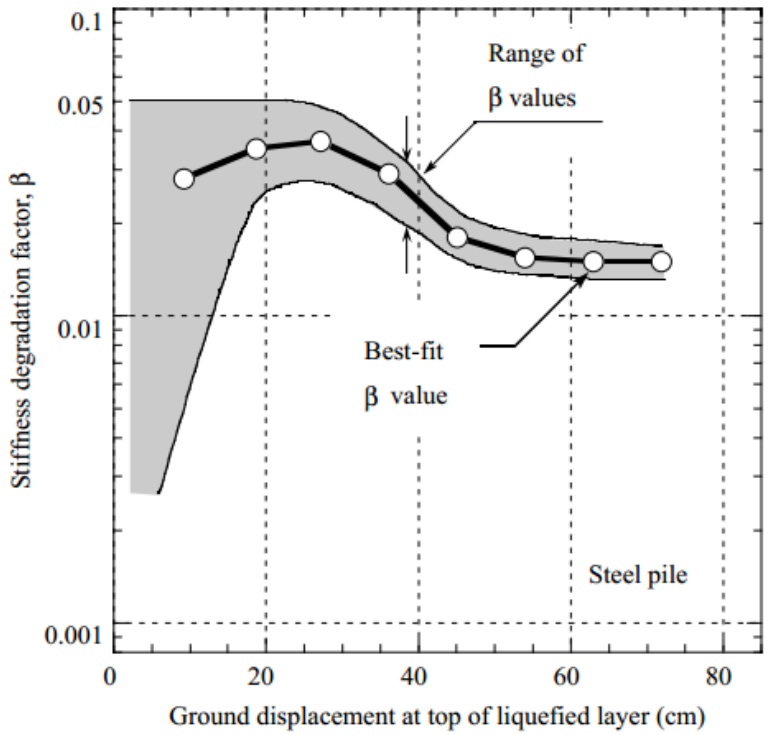

Figure 2-14: Back-calculated stiffness degradation factor as a function of lateral ground displacement (Cubrinovski et al. 2006a)

2.4 Analysis of piles in liquefying and laterally spreading soils

Computational methods for the assessment and analysis of soil-structure systems in earthquakes have evolved significantly over the past few decades, in parallel with better understanding of the physical mechanisms at play.

The assessment of seismic performance of geotechnical structures is inherently complicated by uncertainties and unknowns in (amongst other things) ground motion characteristics, deformations, strength/stiffness degradations, soil-structure interaction effects, input loadings, representative soil profiles and in-situ stress-strain relationships.

There are several methods available for analysing piles in liquefying soils, ranging from sophisticated, dynamic analyses (based on the effective stress principle or similar) to simplified hand-calculation methods. These approaches differ greatly at a theoretical level, as well as at an implementation level (Tokimatsu and Asaka 1998; Cubrinovski and Ishihara 2004; Conte and Zhang 2007; Cubrinovski *et al.* 2008; Cubrinovski 2011). The simplest models available are based on a pseudo-static

approach, in which an equivalent static analysis is used to estimate the dynamic earthquake response. Their simplicity makes them easy to implement, design-oriented and relatively easy to understand in terms of their handling of conventional data and engineering concepts. For this reason, pseudo-static models are commonly adopted in design guidelines worldwide (Cubrinovski and Bradley 2009). Conversely, effective-stress analyses make use of a more rigorous analysis procedure which incorporates the complex dynamic effects of excess pore water pressure generation and subsequent changes in stress-strain response over a period of time (Cubrinovski, 2011). Consequently, these are less frequently used in common practice, however have been used to analyse seismic performance of important structures.

In essence, all analysis methods have the same objective; to assess the seismic performance of a piled foundation by evaluating pile deformations and damage to piles. However, different methods focus on different aspects of the problem presented and each has different merits and drawbacks. In order to illustrate some of these differences, three methods along with their pros and cons are briefly summarised below in Table 2-1.

It is important to understand that use of each model requires complete understanding of the workings of the model on the user's part. If this is not the case, one may not be able to recognise when data outputs are nonsensical or be able to analyse what mechanisms are being considered.

Table 2-1: Methods used for assessment of seismic performance of soil-structure systems

Assessment Method	Key features	Advantages	Disadvantages
Pseudo-static analysis	- Converts dynamic actions and response into equivalent static actions/response (therefore user must consider cyclic phase and lateral spreading phase separately) - Typically uses beam-spring representation of pile-soil relationship	- Simple/practical - Uses conventional geotechnical data and engineering properties as inputs	- Does not consider response of entire soil-structure system - Simple models limited to 2-D analysis - Parametric evaluations are needed
Seismic effective stress analysis	- Can dynamically model the effects of pore-pressure buildup and resulting changes in stress-strain relationship of soil - Realistically simulates ground response and soil-structure interaction in a time-history analysis	- Detailed time-history response incorporates dynamic effects - Good assessment of behaviour of entire soil-foundation-structure system	- Does not take into account uncertainties associated with ground motion and numerical model - Large number of inputs needed, specialist knowledge required
Probabilistic performance-based-earthquake-engineering (PBEE) framework	- Addresses uncertainties associated with ground motion characteristics and numerical model on a site-specific basis - Quantifies seismic risk - Considers all earthquake scenarios and likelihoods	- Provides engineering outputs (e.g. response and damages) as well as economic outputs (e.g. risk/losses) - Enhances communication of design outside profession	- Probabilistic framework means that details of "worst-case" scenario can get lost in output - Large amount of data makes for expensive computational effort - Specialist knowledge required

2.5 Pseudo-static analysis

As mentioned previously, pseudo-static analysis is a relatively simple yet practical tool used in seismic modelling based on conventional geotechnical data (e.g. SPT blowcount) and routine computations. It can be applied without excessive computational power or specialised knowledge, yet it still captures the basic mechanisms of pile behaviour. The application of this method to piles in liquefying soils, however, still retains uncertainties associated with the capture of significant dynamic spatial and temporal changes in a static analysis. Typically, pseudo-static models rely on the assumption of two-dimensional plane-strain.

Pseudo-static models are normally constructed by means of a beam-spring approximation, whereby piles are represented by vertically-placed beam elements and horizontal springs represent the lateral stiffness of the surrounding soil. The effects of horizontal seismic motions can be allowed for by incorporating a horizontal force at the pile head corresponding to the inertial force from the superstructure. The effects of ground movements as external actions on piles can be allowed for by applying a static soil displacement function to the ends of the soil springs.

Typically, a three-layer soil profile is modelled consisting of a liquefied layer sandwiched between non-liquefied crust and base layers. It is normally assumed the non-liquefied crust gets carried along with the liquefied layer. In doing so, it can impose large lateral loads on the head of the pile, significantly greater than passive earth pressures, in the direction of ground flow (Berrill and Yasuda, 2002).

Pseudo-static analysis allows non-linearity in the soil-pile system to be modelled, meaning that inelastic modes of deformation typically caused by strong earthquakes are considered.

More details concerning pseudo-static analysis are covered in chapter 4.

2.6 Previous verifications of pseudo-static analysis

The 1995 Hyogoken-Nambu (Kobe) earthquake contributed to a much-improved understanding of the behaviour of piles in liquefying soils. The extensive records and rich data set provided by this event allowed, in turn, the use of pseudo-static analysis to be verified and calibrated for several piled structures (Cubrinovski and Ishihara 2003; Tokimatsu and Asaka 1998). In general, relatively good correlations have been achieved between computed and observed results when appropriate choices of model input parameters were made. This can be seen in the Figures 2-15 and 2-16, where

predicted and observed displacements can be seen to match, and bending moments greater than the cracking moment of the pile occur in the region of visible cracking:

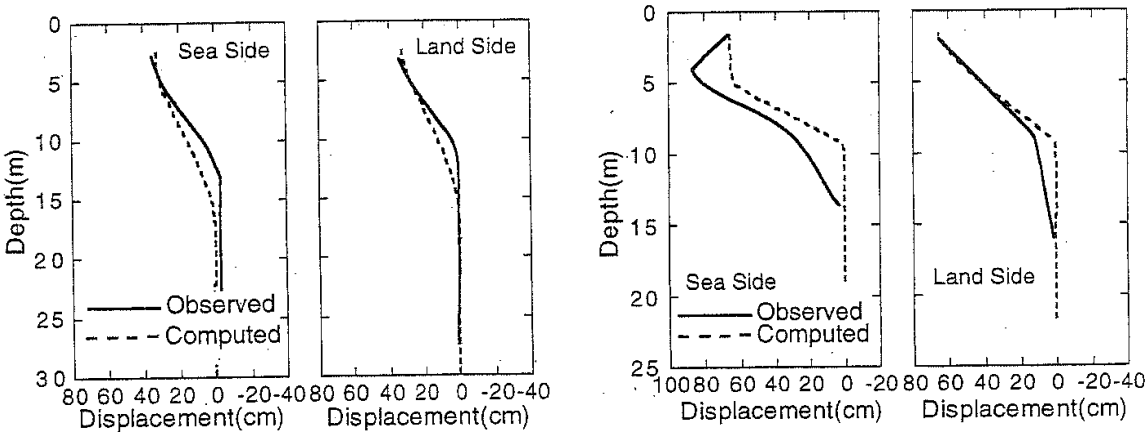

Figure 2-15: Computed vs observed pile displacements undergoing lateral spreading during the Kobe earthquake. Left = steel piles of a 2-storey building situated 100m away from a quay wall, Right = precast concrete piles of a 3-storey building situated 6m away from a quay wall (Tokimatsu and Asaka 1998)

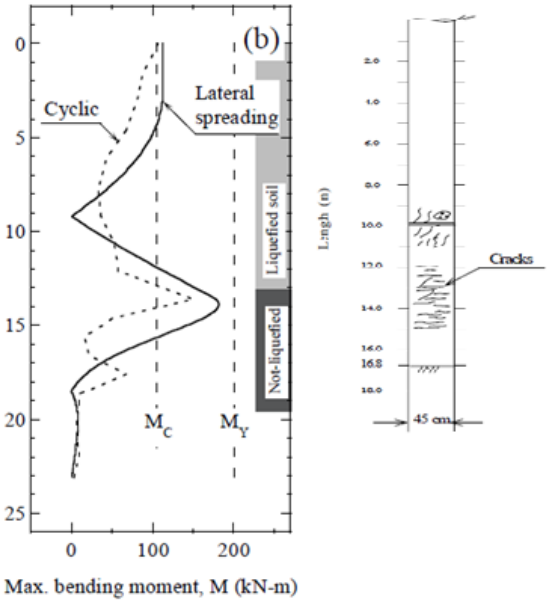

Figure 2-16: Computed bending moments (note that only the solid line is by pseudo-static analysis) of piles in Kobe Tank Farm TA72 matched with visible damages (Cubrinovski and Ishihara 2003)

2.7 Current design recommendations

Several current design recommendations exist worldwide which give some guidance on how best to design piled structures (bridges in particular) to be able to resist lateral spreading loads. Three of these are briefly described below.

2.7.1 Ashford *et al.* 2011 – PEER Report

This report was produced for the Pacific Earthquake Engineering Research Centre and presents recommended procedures and practices for the design (and performance evaluation) of pile foundations for bridges in laterally spreading areas. It aims to develop a set of recommended procedures for analysis and design that are based on research findings, where available, and on the professional opinions of the authors where supporting research is lacking. The three main steps for the design or performance evaluation of piles are deemed to be:

- Design the piles for the inertia loading that would occur in the absence of liquefaction.
- Estimate liquefaction potential, and quantify any expected lateral and vertical ground displacements.
- Design piles for the lateral spreading and inertia demands that would occur if liquefaction is triggered.

It is recommended that the effects of liquefaction on a bridge system are first evaluated for the local subsystems (e.g. pile groups, piled abutments), and then for the global bridge system. The analysis methods used to analyse the pile foundations for liquefaction effects may include nonlinear equivalent static analyses or nonlinear dynamic analyses. Linear elastic analyses are not appropriate for analysing piles in liquefied ground.

Liquefaction potential should be quantified by first performing a site characterisation analysis (e.g. *in situ* ground testing, assessment of geological setting). Then, the potential for liquefaction triggering can be evaluated using a procedure such as that documented in Youd and Idriss (2001). Potential ground deformations due to liquefaction (both vertical and horizontal) should then be assessed, and several empirical methods are presented. The large inherent uncertainties associated with each of these methods should be acknowledged.

Next, it is stated that the response of piles to lateral spreading is best analysed using a beam on nonlinear Winkler foundation (BNWF) approach, where the estimated free-field soil displacements are applied to the support ends of the *p-y* springs. Inertial loads can be applied at the same time,

and in either direction. *p-y* models for liquefied sand can be approximately constructed by applying strength and stiffness degradation factors (p-multipliers) to the initial *p-y* resistances (such as those proposed by Brandenberg 2005), or by using the sand's estimated residual strength along with an appropriate relationship for the undrained behaviour of clay (e.g. Matlock 1970). At the present time, there is not sufficient information available to determine whether either of these techniques is more accurate than the other. The loads from the non-liquefied crusts can also be considered using *p-y* springs, and passive pressures can be estimated using conventional earth pressure theories.

It is stated that group effects should not be used in liquefied ground, as the liquefied soil is weak, but should be considered for deeper nonliquefied layers. They should also not be used in laterally spreading nonliquefied crusts for design purposes, as this would constitute an unconservative reduction in lateral spreading forces.

Also included are recommended procedures for dealing with pile pinning effects. These "pinning" forces are used in the assessment of local abutment/pile systems, and occur when embankment soils spread longitudinally; the piles and bridge superstructure can develop reaction forces which are significant relative to the inertia forces driving displacements of a finite-width embankment. Pinning effects reduce embankment displacements in comparison with those which would occur in the absence of any pinning force. This creates a coupled system, where demands on the bridge are dependent on embankment displacements, which in turn depend on the degree to which the bridge superstructure and piles pin the embankment. This indicates that in a non-coupled simplified pile analysis, where pinning forces are potentially significant (i.e. in the case of short, stiff bridge decks) it would be overly conservative to use free-field lateral displacements to estimate pile response.

It is also recommended that global bridge analyses be carried out in addition to those of local systems, as they can provide a more realistic evaluation of system response, and the distribution of force and displacement demands throughout the structure.

2.7.2 Japanese design specifications for the seismic design of highway bridges

The first design requirements for highway bridges for soil liquefaction were introduced into the *Seismic Design Guidelines for Highway Bridges in Japan* in 1971. Since this time, they have been improved upon and revised many times thanks to on-going research efforts, particularly in the wake of large earthquake events (Tamura 2013). The most recent revisions were made in 2012, following the devastating earthquake off Japan's eastern coast in 2011.

It is stated that in liquefied level ground, the design of the pile foundation against lateral loading is to be considered by the seismic coefficient method, with a coefficient of subgrade reaction which reflects the effects of soil liquefaction, but which does not take into account the influence of ground deformation due to liquefaction. The reduction in subgrade reaction coefficient due to liquefaction is defined as a function of the factor of safety against liquefaction triggering, the liquefaction strength ratio, the depth of the ground considered, and the level of earthquake (Uchida and Tokimatsu 2005).

In laterally spreading ground, on the other hand, the earth pressure is to be applied directly to the pile foundation without inertial forces. The earth pressure used for design is taken to be about 30% of the total vertical stress in the liquefiable layer, and equal to the passive earth pressure in the non-liquefied crust layer (Uchida and Tokimatsu 2005). This is, in effect, a force-based method rather than a displacement-based method.

The Architectural Institute of Japan (AIJ, 2001) recommendations for the design of building foundations, on the other hand, state that design of the pile foundation should be conducted by the seismic deformation method (i.e. displacement-based approach). In this approach, the inertial force of the superstructure can be applied as a direct force at the pile tops, while the ground deformations due to lateral spreading are applied directly to soil springs throughout depth. The stiffness of these soil springs is proportional to the subgrade reaction coefficient, which can then be degraded as a function of SPT blowcount and depth to account for the effects of liquefaction (Uchida and Tokimatsu 2005).

2.7.3 Recommended NCHRP design approach (Project 12-49)

The National Cooperative Highway Research Programme (NCHRP) design approach is the result of a joint venture between the Applied Technology Council (ATC) and the Multidisciplinary Centre for Earthquake Engineering Research (MCEER), and aims to develop a “next generation” set of seismic design guidelines for new bridges. One amongst the set of documents to come out of this venture is the liquefaction study report from the *Recommended LRFD Guidelines for the Seismic Design of Highway Bridges* (MCEER/ATC 49-1 2003). These guidelines are summarised below.

The NCHRP methodology involves four basic steps (Martin *et al.* 2002):

1. Slope stability analyses are conducted to determine the minimum yield acceleration and associated failure surface.

2. Newmark sliding-block analyses are performed to estimate displacements of the soil-pile system.
3. The passive force that can ultimately develop against a pile or foundation due to soil movement is estimated.
4. The likely plastic mechanisms that may develop in the foundations and substructure due to lateral spreading are evaluated.

The rationale behind this approach is to determine the ability of the structure to both accommodate this movement and/or potentially limit the movement. A proposed systematic framework based on the above concepts, adopted in the LRFD guidelines, is outlined below:

- Step 1: Identify soil layers that are likely to liquefy.
- Step 2: Assign residual undrained shear strengths to liquefiable layers, and conduct pseudo-static analyses to determine the likelihood and extent of any soil movements in a failure block.
- Step 3: Estimate the maximum lateral spreading displacement of the soil using Newmark displacement charts or a site-specific time history analysis.
- Step 4: Assess whether the soil will flow around the foundation or whether movement of the foundation will occur. This requires a comparison between the estimated passive soil pressures that can be exerted on the foundation (e.g. from a crust layer) and the ultimate resistance that can be developed in the structure.
- Step 5: If it is assessed in step 4 that flow is likely to occur, then the foundation should be designed for these forces. The induced forces will likely be the largest that the structure will experience, and thus is a conservative design.
- Step 6: If it is assessed in step 4 that foundation movement is likely to occur, then the structure must be evaluated for integrity at the maximum expected displacement.
- Step 7: If the deformations computed in step 6 are not acceptable, then there are two options available. The first is to design or retrofit the foundations to resist the forces accompanying passive soil flow around them (i.e. step 5), and the second is to limit ground movements by providing either structural or ground remediation.
- Step 8: The plastic mechanism likely to occur in the presence of lateral spreading is developed, e.g. hinging in the stable soil zones directly above or below the liquefiable layer.
- Step 9: Assess the system for a prescribed displacement field to represent the likely soil spreading deformation. From this, an estimate of the likely shear resistance provided by the foundation can be determined, and this can be incorporated back into the stability analysis.

- Step 10: If substantial resistance is provided, then its effect of limiting the movement of the soil block should be accounted for.
- Steps 11 and 12: Recalculate the overall displacement on the basis of the revised resistance levels. The foundation and structural system can then be reassessed for this movement. Plastic rotations may be allowed to occur in the foundation under such conditions.
- Step 13: If the structure's behaviour is acceptable, then liquefaction design is complete. If not, the designer must reassess whether to provide adequacy by providing additional piles or by improving ground conditions. The process is then repeated by returning to step 8 and modifying the available resistances until the slope is stabilised and adequacy achieved.

2.8 Summary

Damages to piles and bridges due to liquefaction-induced lateral spreading have occurred in many previous earthquakes. Researchers have examined the key characteristics and failure mechanisms of piles in liquefiable soils by looking at case histories, conducting experimental tests and developing analytical models to predict pile response. Design codes and guidelines worldwide provide recommendations for designers on how to best design for the effects of liquefaction and lateral spreading on bridge pile foundations. Some key findings from this literature review include:

- Piles in liquefiable and laterally spreading soils are subjected to two distinct phases of earthquake loading; the cyclic phase and the lateral spreading phase.
- Case studies of piles and bridges in liquefying and laterally spreading soils show that pile damages are most pronounced at the interface between the liquefied and non-liquefied base layer, as well as at the pile head where fixity is significant.
- Liquefaction and lateral spreading can lead to significant abutment and pier rotations, and in extreme cases can cause collapse of bridge girders.
- Passive failure modes due to lateral spreading in the non-liquefied crust can attract significant forces on abutments and piles, often much greater than the drag forces in the liquefied layer.
- Cyclic ground displacements can impose significant loads on piles. In particular, in liquefied soils the interaction of inertial and kinematic loads tends to be in phase, and creates an additive effect in terms of the shear forces to which the piles are subjected.

- In the lateral spreading phase, the liquefied soil has very little stiffness and large unilateral ground displacements occur. Inertial loads are negligible during this phase, as earthquake shaking has ceased or is negligible.
- Pile behaviour depends on the relative stiffness of the pile and the soil; flexible piles tend to move with the ground whereas stiff piles tend to resist ground movements.
- The ultimate lateral pressure from the crust layer in the lateral spreading phase is taken to be a function of the Rankine passive pressure, and must be increased by a shape factor, α, to account for the difference in pressure on a single pile versus that on an equivalent wall.
- This passive pressure is not mobilised until relative displacements in the order of at least several centimetres are achieved between the soil and the pile.
- The effect of stiffness degradation in the liquefied layer can be accounted for by applying a stiffness degradation factor to the soil springs in this layer.
- Many computational methods for the assessment and analysis of soil-pile systems in liquefying and laterally spreading soils exist.
- Simplified methods, such as pseudo-static analysis, are easy to implement, design-oriented, and are commonly used in practice. They can capture the behavioural features of piles in liquefiable soils without excessive computational effort. Large uncertainties exist, consistent with the capturing of a complicated dynamic problem by an equivalent static analysis, and as such they must be handled in a sensible manner.
- Further details around pseudo-static analysis are given in chapter 4.
- More complicated methods, such as dynamic effective-stress analysis, can capture temporal effects such as pore water pressure generation and stress-strain system response. However, the computational effort required for such analyses is large, and specialised user knowledge is needed.
- Current design codes and guidelines exist worldwide which recommend different methods for analysing and designing piles in liquefying and laterally spreading soils.
- Despite significant advances in this field being made over the last couple of decades, there is still no one right or wrong method; rather within each set of guidelines there exist many references to other literature and recommendations. In the end it is up to the professional judgment of the designer to assess which software or calculations to use, which *p-y* soil relationships to use, and which critical loads from liquefied soils and non-liquefied crust layers to apply.

3 Liquefaction, lateral spreading and associated bridge damage in the 2010-2011 Canterbury earthquake sequence

3.1 Introduction

On the 4th of September 2010 the moment magnitude (M_w) 7.1 Darfield earthquake struck the Canterbury region, marking the beginning of an earthquake sequence which, to date, has included more than twelve events with $M_w > 5.0$. Many of these events generated significant ground motions and caused widespread damage throughout Christchurch city.

Of particular note is the devastating M_w 6.2 22nd February 2011 Christchurch earthquake which killed 185 people and caused extensive damage to buildings, bridges and other infrastructure. This earthquake was generated by the Port Hills fault line less than 10 km south of the city centre and induced ground accelerations amongst the highest ever recorded in an urban area. Liquefaction was widespread causing sand boils, ground settlements and lateral spreading.

This work looks at how nine case-study bridges, all along the Avon River, performed as a result of these earthquakes and focusses primarily on their performance in the February 2011 Christchurch earthquake; however where possible, considerations are made for damages sustained during the September event. Aspects of performance associated with the phenomena of liquefaction and lateral spreading are of particular focus.

In this chapter a brief overview of the phenomena of liquefaction and lateral spreading is first presented, and general features of Christchurch's local geology are outlined. This is followed by outlining the ground motion characteristics and details of the seismic demand, liquefaction and lateral spreading observed during the Christchurch earthquakes. Finally, the performance of nine case-study bridges is documented and a characteristic damage mechanism associated with short-span bridges subjected to lateral spreading is identified and discussed.

3.2 Liquefaction and lateral spreading

Liquefaction is a phenomenon which effectively transforms a saturated granular material from a solid to a liquefied state. This is a result of the losses in shear strength and stiffness which occur in saturated, cohesionless soils when subjected to cyclic shaking.

Liquefaction is most likely to occur in loose, non-plastic sandy or silty soils of a relatively young deposition age (typically less than 10,000 years old). Deposits which typically fit these criteria tend to be areas found near past or present riverbeds, swamps, beaches and sand dunes.

The manifestations of liquefaction can take several forms including sand boils, settlements (global and differential), ground distortions, buoyancy effects and ground cracking/lateral spreading. The latter is the effect most pertinent to this study. Lateral spreading occurs in gently sloping ground or where there is a free-face condition (e.g. a river bank) under which static shear stresses exist in the ground. The loss of strength in liquefied soil can induce a sliding mechanism, whereby inertial forces induced by the earthquake overcome the static equilibrium, essentially forcing a crust layer to "slide" over a liquefied layer. This can lead to very significant lateral ground displacements, with recorded measurements showing these can be in the order of several metres (Ishihara and Cubrinovski 1998, Robinson *et al.* 2011).

All the effects described above can have potentially serious consequences for engineered structures, lifelines and infrastructural services.

3.3 Geological context

The global and local contexts of New Zealand, Canterbury and Christchurch can be seen in Figure 3-1. This shows a progression of maps, each more magnified on one area than the last, such that various geographical features mentioned in the following section can be identified in both a global and local sense. The first map (Figure 3-1a) shows New Zealand as a whole, in particular indicating the Southern Alps, and the next (Figure 3-1b) shows more clearly the greater Canterbury region including the Southern Alps, Canterbury Plains, Banks Peninsula and Pegasus Bay. Figure 3-1c shows the Waimakariri and Rakaia Rivers as well as the location of the causative faults and epicentres of the 2010 Darfield and 2011 Christchurch earthquakes and Figure 3-1d shows the greater Christchurch region. Figure 3-1e shows Christchurch's central and eastern suburbs as well as highlighting the locations of the Avon and Heathcote Rivers with distinctive river loops noted.

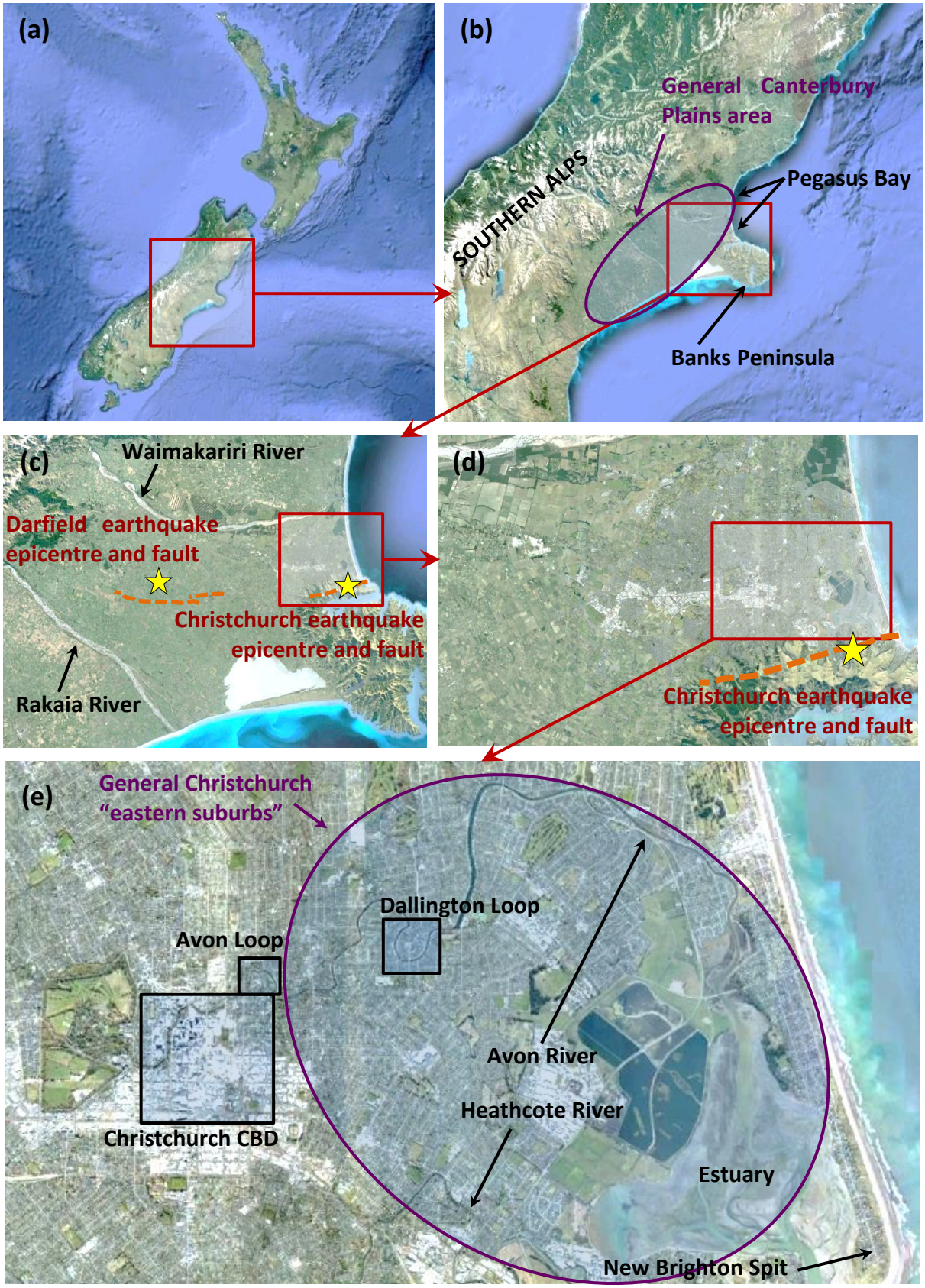

Figure 3-1: Progression of maps showing locations of (a) New Zealand including Southern Alps and greater Canterbury Region, (b) Southern Alps, Banks peninsula, outer Canterbury region, (c) Waimakariri and Rakaia Rivers, earthquake origins, (d) Christchurch region (e) Christchurch CBD, rivers and eastern suburbs (images from Google Earth 2013)

3.3.1 Regional geomorphology

The greater Christchurch City area is located on Holocene deposits at the Pegasus Bay coast of the Canterbury Plains and on the northern slopes of the Port Hills of Banks Peninsula. The shoreline of this region has fluctuated by several kilometres over the last 10,000 years throughout glacial and interglacial periods. Radiocarbon ages of shell materials indicate that about 6,000-6,500 years ago the sea extended inland as far as present-day Kaiapoi, Belfast, Papanui, Riccarton, Spreydon and Beckenham (Brown and Weeber 1992).

The Canterbury Plains are alluvial floodplains, deposited by rivers flowing eastward from the Southern Alps towards the Pacific Ocean, which cover an area approximately 50 km wide by 160 km long. In the Christchurch area, surface sediments are between 15 and 40 metres thick, underlain by 300-500 metre thick gravel formations interwoven by sand, silt, clay and peat layers (Brown and Weeber 1992). These complex inter-layered formations make up a system of fine-grained aquicludes and aquitards separating gravel aquifers with artesian groundwater pressures.

Two rivers meander eastward through Christchurch city: the Avon through the centre and north-east, and the Heathcote to the south. These originate from springs in western Christchurch and eventually flow out to the sea past the New Brighton Spit. North of the city, the Waimakariri River frequently flooded a large area (including Christchurch city) until its stopbanks were erected in the 1920s. The combination of these flooding episodes with the continual movements of the Avon and Heathcote serve to characterise the present-day surficial soils of Christchurch.

Prior to European settlement in the 1850s large reaches of the present-day city area, in particular those flanking the Avon River, were *raupo* (reeds) swampland. This can be seen in Figure 3-2, a compilation of early European settlers' survey maps, which is focussed in on the central and eastern parts of Christchurch. As part of the settlement and expansion of Christchurch city, extensive drainage and infilling of these swamps was undertaken (Brown and Weeber 1992). In the west of the city, the present-day surface sediments are typically fluvial gravels, sands and silts while to the east of the city, coastal swamp deposits such as sand, silt, clay and peat predominate. The near-surface soil deposits show a huge amount of variability over short length scales (i.e. < 10 m) both horizontally and vertically. Figure 3-3 illustrates the dominant near-surface materials of the greater Christchurch area.

An important consequence of the abundant water supply throughout Christchurch from streams, rivers, springs, and active groundwater flows as well as the low-lying coastal land, is that the groundwater level across the city is relatively high. In the western suburbs the water table is

approximately 5 metres deep, becoming progressively shallower tracking eastwards, to around 1 – 2 metres in most of the eastern suburbs.

All bridges documented in this study are located on the Avon River either in or east of the central business district (CBD) and as a result are typically founded in deep, saturated, recent alluvial soils with high liquefaction potential.

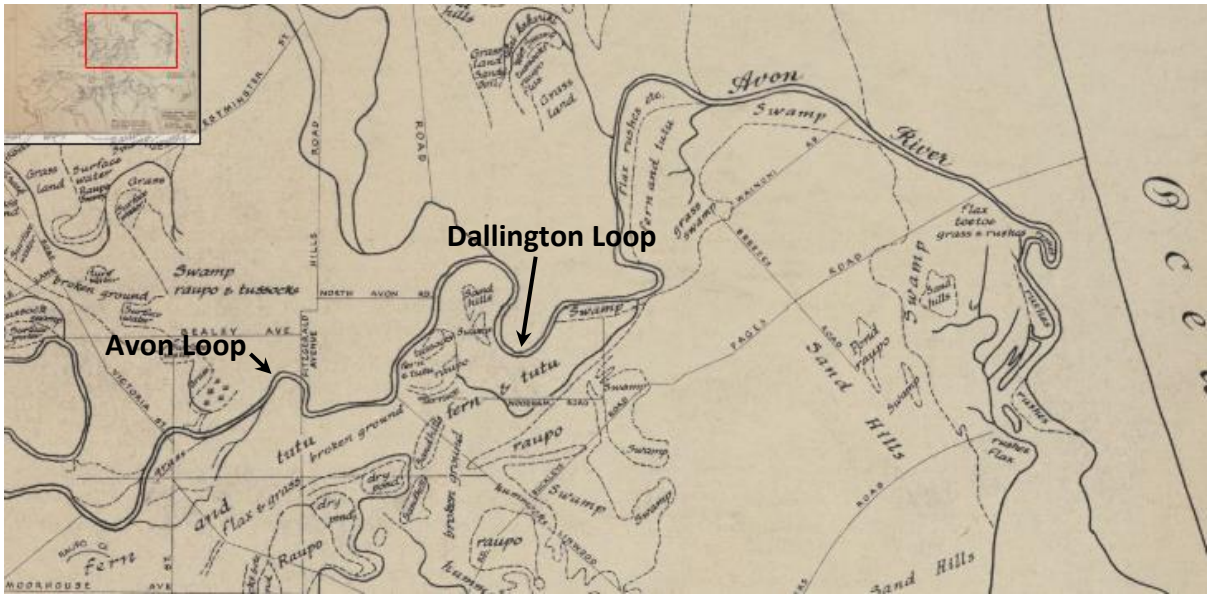

Figure 3-2: Christchurch area, showing swamps and vegetation cover. Distinctive river loops noted for reference. Compiled from "Black Maps" of 1856 (http://christchurchcitylibraries.com/Heritage/Maps/433589.asp)

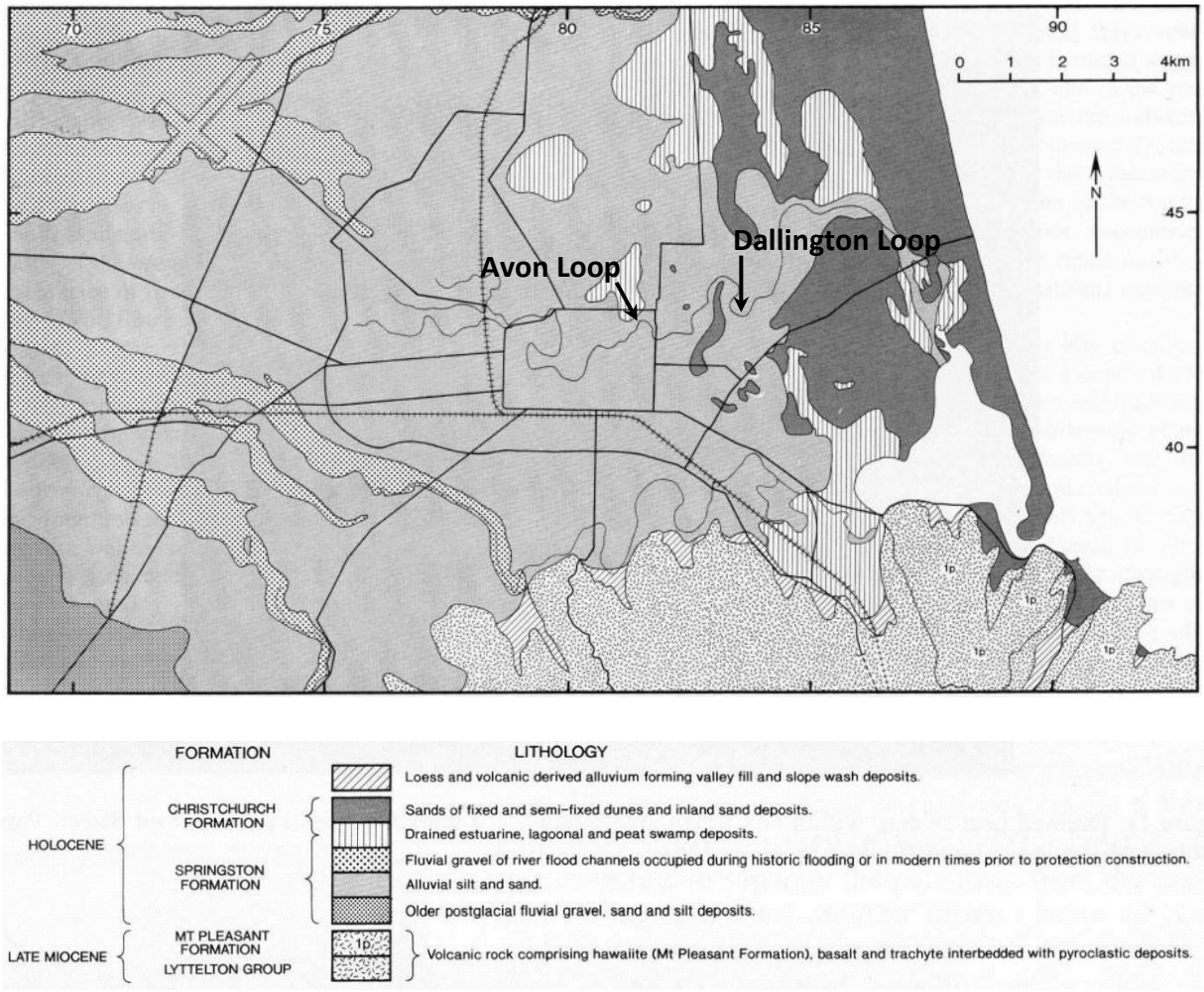

Figure 3-3: Dominant surface or near-surface materials. Distinctive river loops noted for reference (Brown et al. 1995)

3.3.2 Regional tectonics

New Zealand straddles the boundary of the Australian and Pacific tectonic plates, where subduction of the Pacific plate beneath the Australian plate is occurring in the north, and vice versa to the south. The Southern Alps have formed in the transition zone, where relative plate movement is obliquely convergent at a rate of approximately 40 mm per year (Norris and Cooper 2001) as can be seen in Figure 3-4a. As a result of this complex faulting, New Zealand is a region of distributed seismicity, meaning that the relative plate movement is accommodated by many faults over a wide zone (> 100 km), each with their own capability of generating large earthquakes (Figure 3-4b).

Approximately 70% of the slip motion on the plate boundary is accommodated by the Alpine Fault, with the remaining 30% accommodated by a series of faults throughout the Southern Alps and

Canterbury Plains (Norris and Cooper 2001). Many of these faults are well known and documented (for example Porter's Pass fault, Hope fault, Ashley fault) however, as was made clear with the recent sequence of earthquakes in Canterbury, large numbers of fault structures exist underneath the alluvial fans that were previously unknown and unmapped.

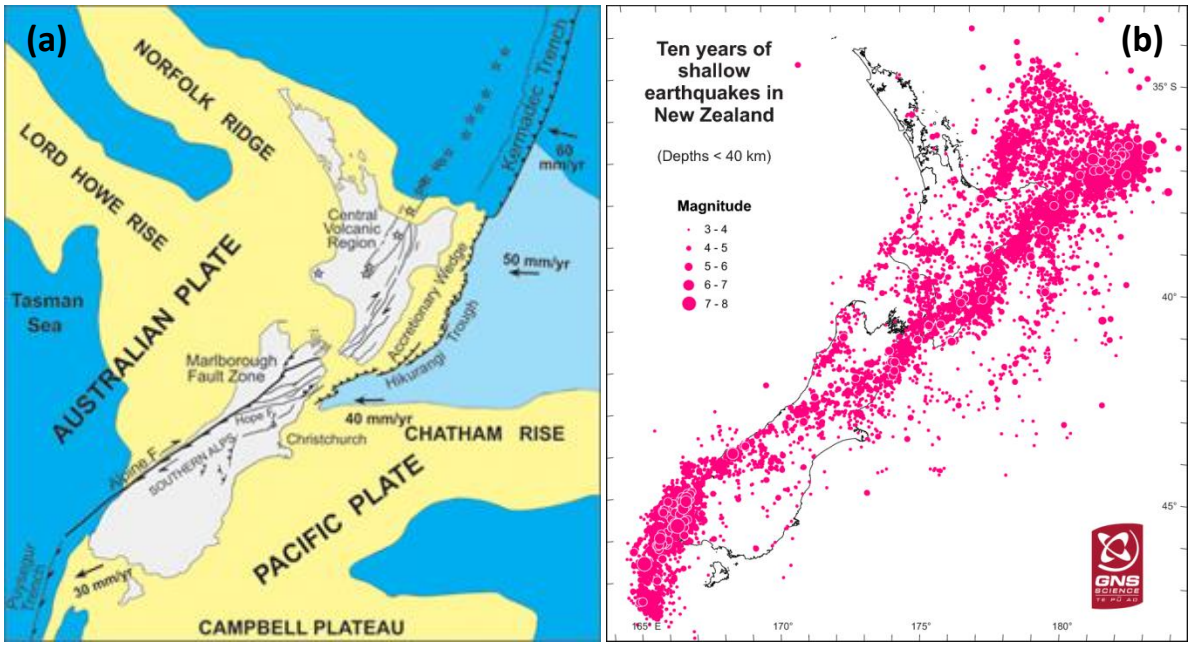

Figure 3-4: (a) New Zealand tectonic plate movements (http://www.geol.canterbury.ac.nz/earthquake/), (b) Ten years of shallow earthquakes in New Zealand (GNS Science: pre-2010/2011 Canterbury earthquake sequence)

3.4 Ground motion characteristics

The 4th September Darfield ("DAR") earthquake occurred 40 km west of Christchurch CBD on a series of faults, the largest of which was the Greendale fault, a structure previously unrecognised before this event. The highest recorded ground motions (measured by strong-motion stations) were near the epicentre, with a maximum horizontal peak ground acceleration (PGA) of 0.76 g and vertical accelerations in excess of gravity (1 g). (Note: from hereon the stated horizontal PGA values will refer to the geometric mean of the recorded horizontal components.) In the Christchurch CBD the recorded horizontal PGAs ranged from 0.15 to 0.25 g, and in the eastern suburbs along the Avon River the accelerations were approximately 0.15 to 0.21 g.

The 22nd February Christchurch ("CHC") earthquake also occurred on a previously unrecognised fault, the Port Hills fault centred approximately 8 km south-east of Christchurch CBD. The shallow focal depth (5 km, with fault rupture propagating to within 2 km of the ground surface) and proximity of this event meant that the intensity of shaking in Christchurch was much higher than that recorded in the September event. Vertical accelerations, in particular, were extremely high, with the highest vertical PGA being 2.21 g recorded at Heathcote Valley School, near the epicentre. This is a result of the steeply dipping fault orientation as well as the large up-dip component of slip. In Christchurch CBD horizontal PGAs of between 0.37 and 0.52 g were recorded, and vertical PGAs of between 0.37 and 0.79 g. To the east of the CBD near the Avon River the PGAs recorded were between 0.49 and 1.88 g (vertical) and 0.22 and 0.67 g (horizontal) (Bradley and Cubrinovski 2011). Figure 3-5 summarises the horizontal PGAs recorded at the central and eastern Christchurch strong-motion (SGM) stations during both the Darfield and Christchurch earthquakes, as well as showing the locations of the nine case-study Avon River bridges.

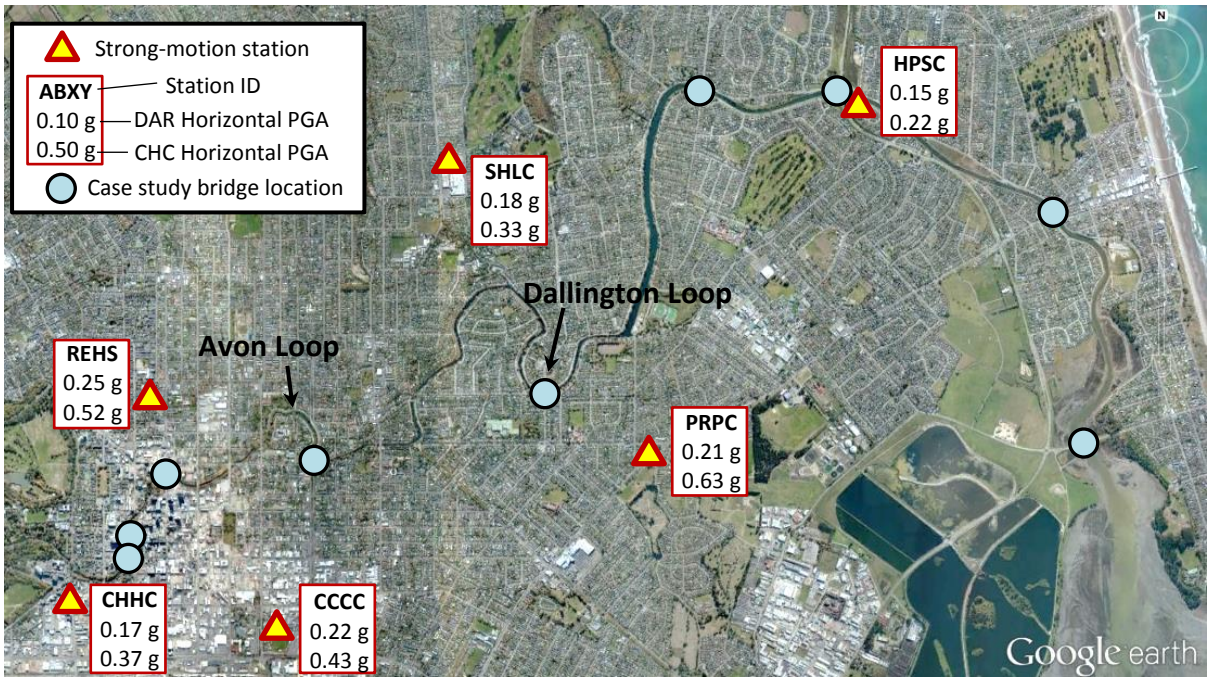

Figure 3-5: Horizontal PGAs recorded at Christchurch strong-motion stations during the Darfield and Christchurch earthquakes and the locations of the case study bridges

The horizontal acceleration response spectra from the SGM stations shown above are plotted in Figure 3-6 and compared with the NZS 1170.5:2004 (Standards New Zealand) design response spectrum for a 500-year return period earthquake in Christchurch on site subsoil class D (NZS 1170.5:2004). Since the Christchurch bridges are typically short-mid span, it can be assumed that their natural periods of vibration, both longitudinally and transversely, will be less than 1 second. Figure 3-6a shows that during the Darfield event the spectral acceleration values in this range were generally less than the pre-earthquake design levels (although older bridges would have been designed to lower design levels). The Christchurch event, on the other hand (Figure 3-6b), generated spectral accelerations in excess of pre-earthquake design levels over the entire period range at almost every SGM station in Christchurch's central and eastern suburbs. In spite of this, bridges experienced minimal damage due to ground shaking alone and were much more affected by liquefaction and subsequent lateral spreading movements.

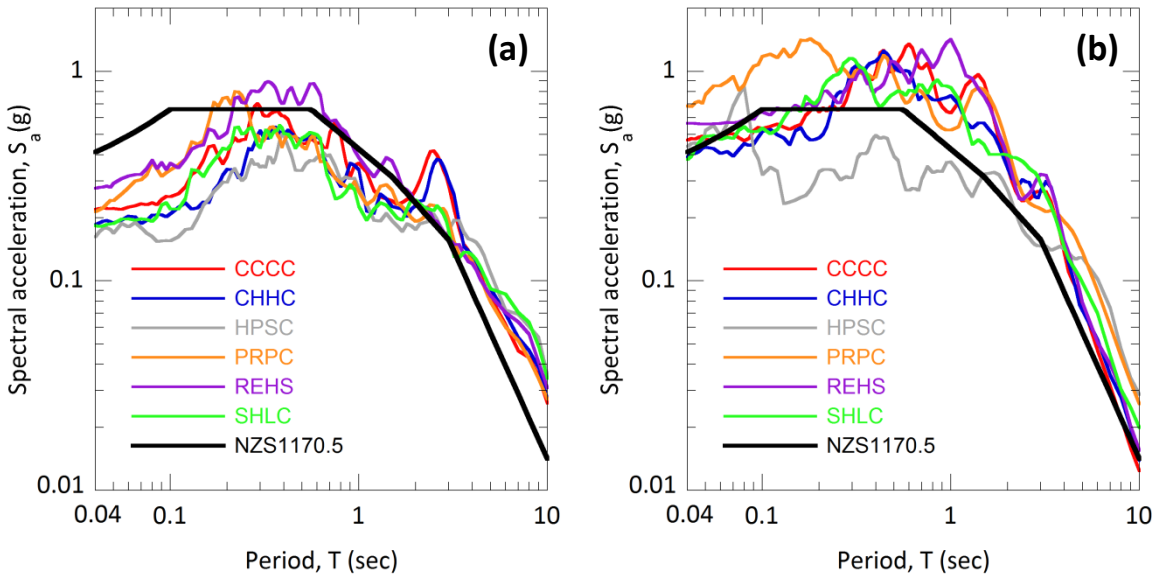

Figure 3-6: Horizontal acceleration response spectra of the central and eastern Christchurch SGM stations in the (a) Darfield and (b) Christchurch earthquakes compared with NZS 1170.5:2004 500-year return period design spectrum on site subsoil class D (data freely available from GNS Science at www.geonet.org.nz)

3.5 Seismic demand

Using the New Zealand-specific ground motion prediction equations developed and codified by Bradley (2010), the PGAs (and their uncertainties) at each bridge site east of the CBD were calculated assuming subsoil site class D at all bridges (NZS 1170.5:2004). In a conventional liquefaction evaluation seismic demand is represented by the cyclic stress ratio (CSR) which is directly proportional to PGA in the portion of a soil profile above the water table. This CSR is then adjusted by magnitude scaling factors (MSF) and converted to $CSR_{7.5}$, for a reference M_w 7.5 earthquake. $CSR_{7.5}$ at shallow depths and above the water table is given by the following equation (Youd and Idriss 2001):

$$CSR_{7.5} = 0.65 \frac{PGA}{g} \frac{1}{MSF} \quad (3\text{-}1)$$

Using this approach with revised Idriss MSF values (Youd and Idriss 2001), ground-surface $CSR_{7.5}$ values were found at each of the eastern bridge sites for both the September and February earthquakes and are summarised in Table 3-1:

Table 3-1: Calculated PGAs, standard deviations and $CSR_{7.5}$ at case study bridge sites during Darfield and Christchurch earthquakes

	Darfield earthquake			Christchurch earthquake		
Bridge	Conditional median PGA (g)	Conditional standard deviation (in PGA)	Conditional median $CSR_{7.5}$	Conditional median PGA (g)	Conditional standard deviation (in PGA)	Conditional median $CSR_{7.5}$
South Brighton Bridge	0.191	0.375	0.108	0.615	0.393	0.245
Pages Rd Bridge	0.182	0.335	0.103	0.525	0.353	0.209
ANZAC Bridge	0.158	0.149	0.089	0.280	0.158	0.112
Avondale Rd Bridge	0.177	0.309	0.100	0.351	0.330	0.140
Dallington Bridge	0.206	0.291	0.116	0.503	0.310	0.201
Fitzgerald Ave Bridge	0.215	0.293	0.121	0.456	0.314	0.182

Looking at the values above it is apparent that the seismic demand of the Christchurch earthquake was much greater than that of the Darfield earthquake; at most of the bridge sites approximately 1.5 to 2 times as much.

3.6 Liquefaction and lateral spreading in the Canterbury earthquakes

The 2010 – 2011 earthquake sequence triggered widespread liquefaction throughout Christchurch's eastern suburbs and parts of the CBD. Figure 3-7 shows the extent and severity of liquefaction in three events; the September 4th and February 22nd earthquakes as well the M_w 6.0 13th June 2011 event. The white contoured areas represent the 4th September event, the black contours represent the 13th June event and the red (moderate to severe liquefaction), pink (moderate liquefaction) and yellow (low to moderate liquefaction) represent the 22nd February event. Note that this map shows the observed liquefaction features over large areas and as such is generalised, whereas in reality the extent and severity of liquefaction within each zone was variable. It is apparent that the 22nd February Christchurch earthquake triggered the largest amount of liquefaction, a direct result of the higher seismic demand it induced in Christchurch city than the Darfield event.

Since the 4th of September 2010, over 500,000 tonnes of liquefaction ejecta have been removed from Christchurch streets and properties, the majority of this attributed to the 22nd February event (Villemure *et al.* 2012). This is arguably one of the most extensive and severe liquefaction events ever observed in native soils on record, with some sites liquefying three or more times in the 2010-2011 earthquake sequence.

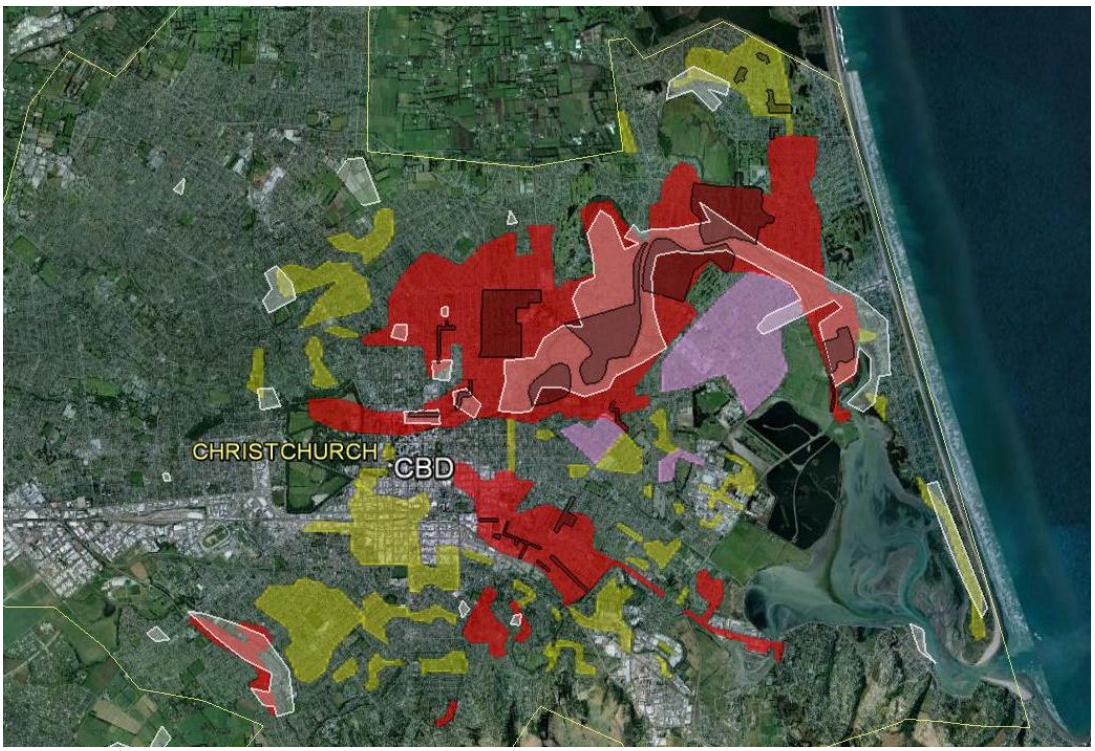

Figure 3-7: Liquefaction map showing areas of observed liquefaction during the Darfield, Christchurch and 13 June 2011 earthquakes (Cubrinovski et al. 2013)

Liquefaction was particularly pronounced along the Avon River, from the CBD to the estuary, a distance along-river of approximately 12 km (or linearly west-east of approximately 7 km). In many places this was accompanied by lateral spreading of the river banks, causing displacements ranging from several centimetres to more than two metres. This lateral spreading was particularly damaging to bridges, infrastructure, houses and other buildings near the river banks.

Following the Darfield and Christchurch earthquakes, extensive field investigations were undertaken to investigate the extent and severity of lateral spreading (led by Kelly Robinson, PhD candidate, University of Canterbury). Approximately 150 lateral spreading transect surveys were carried out, at around 120 separate locations. The method of ground surveying used is described in Robinson *et al.* 2011, and consists of recording ground crack dimensions and distance from the waterway in a straight line oriented perpendicular to the direction of spreading. In this way, a relationship between lateral ground displacement, U_g, and distance from the waterway, L, can be obtained by summing the widths of the cracks measured along a particular transect alignment. This cumulative effect of the ground cracks therefore gives the total displacement of the free face (e.g. river bank) relative to a distant point inland where displacement is taken to be zero.

In general, lateral spreading displacements and the size of the zones (i.e. distance inland from the river) which they affected increased with distance downstream on the Avon River. As can be seen in Figure 3-8, in the CBD the maximum lateral spreading displacements were in the order of 0.1 – 0.7 m, and confined within a distance of 40 – 50 m from the river. In the north-eastern corner of the CBD the first more substantial lateral spreads were measured in the Avon Loop (the meandering loop just before Fitzgerald Bridge) to be over 1.0 m. Further downstream, the Dallington Loop was subjected to significant lateral spreading displacements in the order of 1 – 2 m in places, extending inland as far as 200 m. The largest measured permanent lateral displacement of nearly 3 m was measured near the Pleasant Point Yacht Club, immediately to the south of the South Brighton Bridge where the Avon River discharges into the estuary (Cubrinovski *et al.* 2014).

It is important to note the significant variability in both the magnitude of lateral displacements and the pattern of spreading within any given area. This just serves to highlight the complex mechanisms affecting lateral spreading, ranging from soil variability and site topography to soil-structure interaction. Typically, the spreading was more pronounced on the inner banks of meandering loops in the river (point-bar deposits) than the outer cut-banks. This is due to the continual erosion-deposition processes occurring as the water flow erodes the outer bank and deposits sediments on the inner bank. As a result, the inner banks tend to be composed of less dense material and as such are weaker and hence more susceptible to liquefaction.

In addition to the lateral spreading transects carried out by the University of Canterbury research team, NZ Aerial Mapping (NZAM) collected LiDAR (light detection and ranging) data subsequent to both the Darfield and Christchurch earthquakes. Essentially, LiDAR data is used to create a digital representation of the ground surface based on a set of discrete data points, and can pick up changes in elevation and other topographical features. As such, it can be used to estimate lateral spreading measurements in addition to global ground settlements and more. In the following sections, reference will be made to both the lateral spreading measurements made by the method of ground surveying as well as those made by LiDAR.

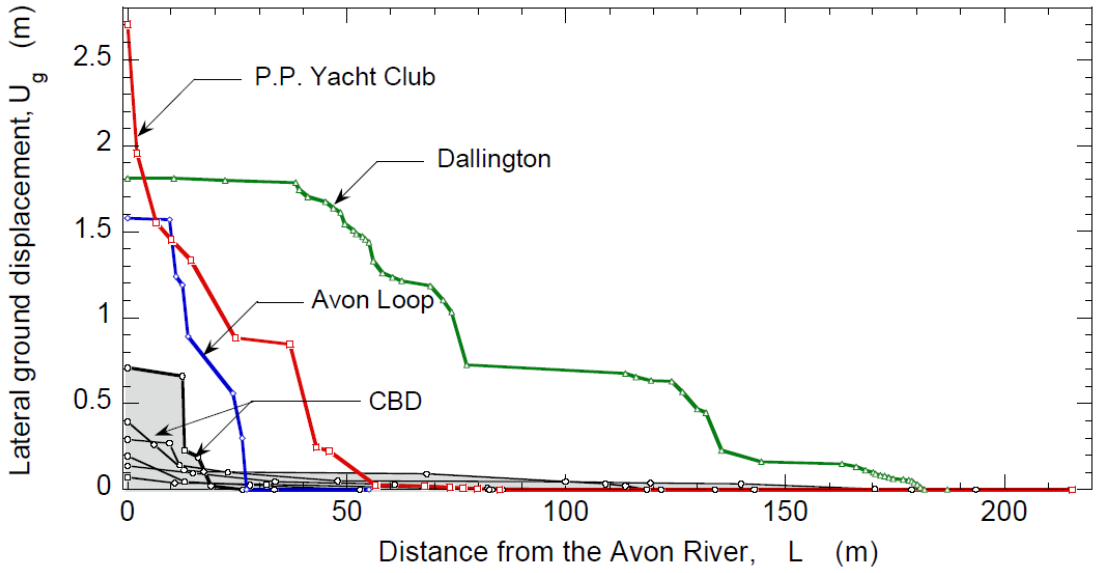

Figure 3-8: Lateral spreading displacements measured along the Avon River after the 22nd February earthquake (from Cubrinovski et al. 2014)

3.7 Overview of bridge performance

In the Canterbury region there are more than 800 road, rail and pedestrian bridges. In general, bridges performed relatively well in the earthquake sequence and suffered less damage than other engineered structures and infrastructure (Cubrinovski *et al.* 2013). The subjects of this research, road bridges in Christchurch city, are typically one to three span short-mid length reinforced concrete structures. After each significant earthquake event all of these types of bridges (bar one) were either immediately in service or reopened within a week. The majority of these short term

closures happened as a result of damage to the approaches, rather than the structure itself, i.e. liquefaction, settlement and lateral spreading in the approach fills or side embankments.

In this section, damage to bridges in non-liquefied areas will be covered briefly, followed by damage to bridges in liquefied areas. The performance of the case study bridges is then presented.

3.7.1 Damage to bridges in non-liquefied areas

The Darfield earthquake did not cause any significant damage to bridges in non-liquefied areas in the Christchurch region, including two long-span bridges across the Rakaia River in close proximity to the fault rupture. A handful of bridges outside liquefied areas sustained some damage in the Christchurch earthquake.

Moorhouse Avenue Overpass, an eleven-span reinforced concrete structure running east-west on the southern boundary of Christchurch's CBD, was the most significantly damaged bridge outside of liquefied areas in the Christchurch earthquake. This bridge was not damaged during the Darfield earthquake, however as a result of the damage it sustained in the Christchurch earthquake the bridge was out of service for more than 5 weeks while strengthening works were undertaken (Palermo *et al.* 2011). The bridge was constructed in three separate sections linked by expansion joints, and later steel rod linkages were installed across the western expansion joint effectively tying together the western and central portions of the bridge. This meant that, during the earthquake, the bridges transverse response was irregular and as such the displacement demand at the eastern expansion joint was excessive. This resulted in the significant shear cracking and flexural-buckling failure of the piers at the eastern expansion joint, putting the central bridge span at risk of collapse and forcing the closure of the bridge until remedial works had been carried out (Palermo *et al.* 2011).

Horotane Valley Overpass, a three-span bridge located within 2 km of the Port Hills Fault, sustained abutment damage as a result of slope failure in the embankment fill. Minor cracking also occurred in the lower halves of all piers, and the ties between spans and at the abutments had elongated and pulled out (Wotherspoon *et al.* 2011). Port Hills Overpass, a six-span twin bridge very close to the Horotane Valley Overpass suffered flexural cracking in the lower halves of the majority of its pier stems; the central pier formed a plastic hinge at its base and buckling of corner reinforcing bars was observed over a length of 150 mm (Wotherspoon *et al.* 2011). The damages to both these bridges were a direct result of the intense ground shaking experienced at a site so close to the earthquakes epicentre, however both were able to service traffic soon after the earthquake.

3.7.2 Liquefaction and lateral spreading–induced damage to bridges

The majority of bridge damage in Christchurch was due to liquefaction in the foundation soils and associated lateral spreading of the river banks. Most of the bridges affected by lateral spreading were designed and constructed at a time when liquefaction and its effects were not well understood, therefore the loads they were subjected to from high backfill pressures were much higher than they would have been designed to withstand. In spite of this, bridges as a group performed significantly better than other engineered structures. One major contributing factor to this is that Christchurch bridges are typically short to moderate in length; as such they exhibit a sturdy seismic response due to their relatively high stiffness and strength, limited reactive mass and geometrical symmetry (Palermo *et al.* 2010). Some structural forms performed better than others and this will be covered in more detail in the following sections.

Inside the CBD, lateral spreading displacements were relatively small, and accordingly bridge damage was minor. The first bridge downstream of the Avon Loop (the area where the first lateral spreading displacements greater than 1 metre were measured), Fitzgerald Avenue Bridge, is the farthest upstream bridge significantly affected by spreading. Nearly all bridges downstream from here along the Avon River were affected by substantial lateral spreading.

Typically, the road bridges spanning the Avon are one to three span short-mid length reinforced concrete bridges. The older bridges tend to be integral monolithic structures (continuous, cast *in situ*) while the newer bridges tend to be constructed from precast concrete components (often simply-supported). Regardless of construction type, all the bridges studied have considerable strength and stiffness in the longitudinal direction provided by the bridge deck which, in most cases, restrained movement at the top of the abutments, forcing back rotation of the abutments to occur consistent with the direction of lateral ground flow. As a result, significant abutment pile deformations were observed in some circumstances, and slumping of the approaches also led to vertical offsets between the approaches and bridge deck. This type of bridge-strut or deck-pinning mechanism (see Figure 3-9) also tended to cause compression buckling across the roadway (parallel to the river) inducing severe damage not only to the road surface but also to buried pipes (Le Heux *et al.* 2011; Palermo *et al.* 2010). In general, there was little bridge superstructure damage observed and in the cases where serviceability was affected this was mainly due to the settlement and spreading of bridge approaches.

It is interesting to note that the characteristic deformation mechanism described above is highly dependent on having a stiff deck, and, where deck stiffness is not sufficient to resist lateral spreading loads then buckling in the bridge deck itself can occur. Le Heux *et al.* (2011) analysed the

Dallington pedestrian bridge under lateral spreading loads, and due to it being a relatively slender bridge, a plastic hinge formed in compression at the apex of the bridge which would have influenced further bridge response.

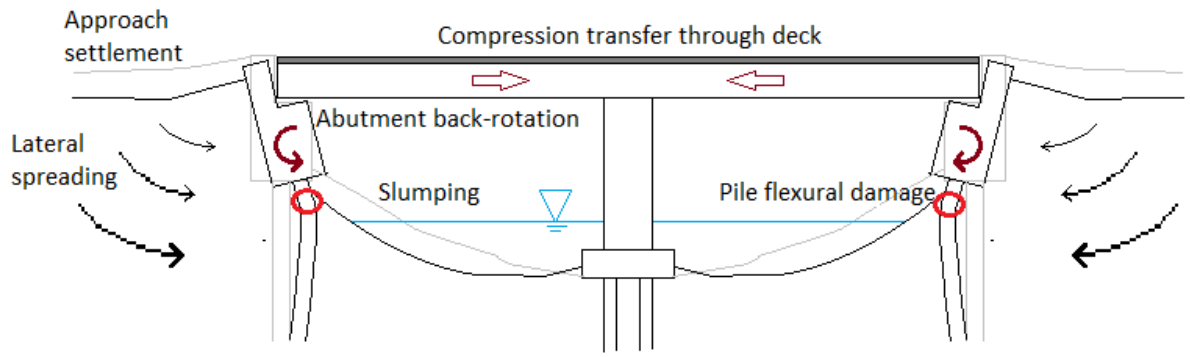

Figure 3-9: Diagram showing the characteristic lateral spreading-induced bridge damage mechanism to short-span bridges; deck-pinning, abutment back-rotation, abutment pile damage, slumping and spreading of approaches

Bridges along the Heathcote River, to the south of the city, suffered much less damage than those along the Avon, despite their being much closer to the causative fault of the Christchurch earthquake. With the exception of the Ferrymead Bridge, located at the point where the Heathcote discharges into the estuary, only 3-4 Heathcote bridges sustained moderate approach damage and any associated abutment and/or structural damage was minor (Cubrinovski *et al.* 2014*)*. Lateral spreading displacements along the Heathcote were much smaller than those along the Avon and the extent of other visible manifestations of liquefaction less pronounced; as such the demands on the bridges from kinematic soil loads were not as significant. Typical Heathcote flow rates are also less than half that of the Avon (McKerchar, 2001) and as a result the river channel is smaller, meaning bridge spans are also smaller. The combination of these factors (reduced lateral displacements and smaller bridge spans) has contributed to the fact that the performance of Heathcote bridges was much better than those of the Avon bridges.

3.7.3 Bridge inspection methodology

Following the 22nd February Christchurch earthquake, detailed bridge reconnaissance work was carried out on several case-study bridges by the author in conjunction with several other researchers. During these investigations, photos were taken and notes/sketches were made

regarding all relevant aspects of bridge structural damages, paying particular attention to any visible abutment/foundation damages. Key measurements that were taken included:

- Tilt angles of abutments and, where possible, piles (using an electronic level)
- Widths/lengths and patterns of any visible concrete cracking (or reinforcing exposure/hinging) in abutments, piles, and piers
- Visible ground settlements or differential movements
- Any gaps or offsets that are not part of the intended bridge design
- Relative displacements between piles/abutments and ground
- General modes of deformation/failure

In addition to structural inspections, ground damage at the case study bridges was noted. Lateral spreading transects were performed (as described previously and in Robinson *et al.* 2011), and notes, photos and sketches were also made of the bridges' surroundings. In particular, other manifestations of liquefaction were recorded such as sand boils, settlement or damage to surrounding structures, uplift of manholes and ground cracking that wasn't encompassed by the lateral spreading survey.

Due to the fact that the evidence was gathered after the 22nd February earthquake it includes the damages of both the September and February events, though, unless stated otherwise, the February event was considered the principal contributor to the damage.

3.7.4 Collection of site investigation and bridge construction data

Christchurch City Council drawings were made available for several of the bridges investigated. Also, all available site investigation data was collected from a range of sources; *Project Orbit*, design drawings, and additional tests commissioned by the Universities of Auckland and Canterbury.

3.7.5 Case-study bridges

The nine bridges that were investigated in detail can be grouped into two categories: integral monolithic bridges (concrete cast-in-place, typically pre-1960s) and segmental precast concrete bridges (post-1960s). They are all located on the Avon River in central and eastern Christchurch and have been chosen in order to represent a wide range of construction types/eras and categories of land damage. The bridges are listed in Table 3-2:

Table 3-2: Selected case-study bridges divided by construction types and years of construction

Integral Monolithic Bridges		Precast Concrete Bridges	
Bridge	**Year**	**Bridge**	**Year**
Bridge of Remembrance (Cashel Street)	1924	Avondale Road Bridge	1961
Pages Road Bridge	1931	Fitzgerald Avenue Twin Bridges	1964
Colombo Street Bridge	1930[1]	South Brighton Bridge (Bridge Street)	1980
Hereford Street Bridge	1938	ANZAC Drive Bridge	2000
Dallington Bridge (Gayhurst Road)	1954		

The bridges will be presented in geographical order from furthest upstream to furthest downstream, beginning with the three bridges in Christchurch's CBD followed by the six to the east and north-east of the CBD (locations were shown previously in Figure 3-5).

Unless referenced otherwise, the observations and photos at each of the bridge sites presented herein come from the inspection data collected by the members of the bridge reconnaissance team mentioned previously.

3.7.6 Christchurch CBD Bridges

Overall, bridges in Christchurch's CBD performed well, with only minor damages observed resulting from lateral spreading, such as abutment cracking and slumping and compression cracking in approach material. All CBD bridges are single span structures and remained serviceable after the Christchurch earthquake (note that while most were not open to the public, this is due to the cordon erected around the CBD, not due to their being unsafe). Their locations are shown in Figure 3-10. The three bridges discussed below are all founded on shallow foundations.

[1] Original construction was 1902 however significant additions to it were made in 1930

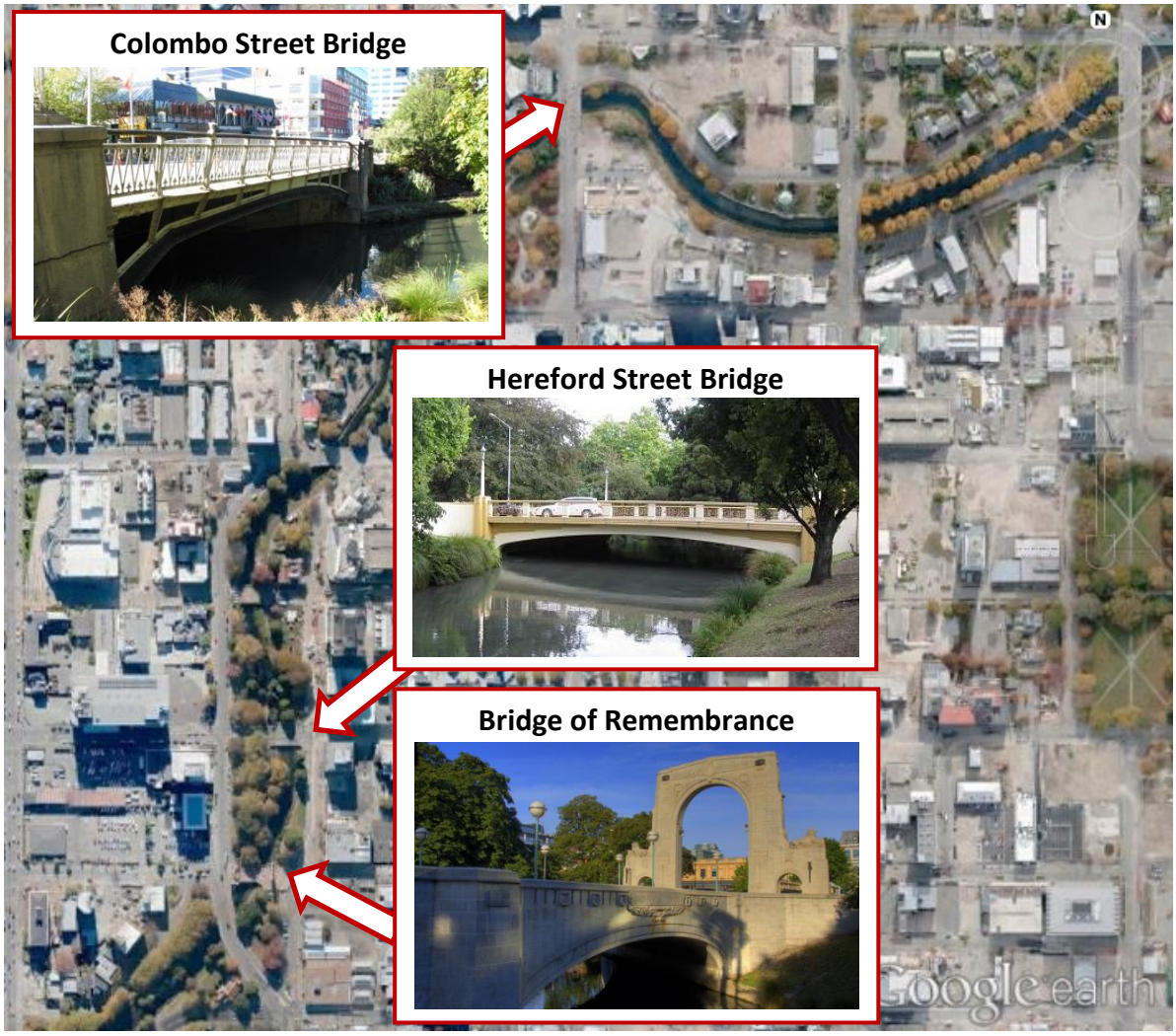

Figure 3-10: Aerial photo of Christchurch CBD showing the locations of the three CBD case-study bridges

3.7.6.1 Bridge of Remembrance (Cashel Street)

The Bridge of Remembrance was constructed in 1924 and is an integral, single-span stone-faced reinforced concrete arch structure on Cashel Street running east-west across the Avon River in central Christchurch. The arch spans into abutments founded on shallow stepped foundations, as can be seen in Figure 3-11.

Land Damage

Very little land damage was observed in proximity to this bridge and visible lateral spreading cracks were not apparent on either side of the bridge.

Bridge Damage

Although no visible spreading was observed, there must have been some degree of movement of the river banks towards the river. This is inferred from the compression pavement damage observed at the bridge/approach interfaces on both sides of the river, however this damage is not significant. A small (< 100 mm) pavement compression overlap was measured at the base of the stairs on the southern side of the bridges western approach; at the eastern end of the bridge an overlap in the order of 10-50 mm was seen (seen Figure 3-12a and b). It is probable that some settlement of surrounding ground occurred, particularly on the south-western side, where a 110 mm vertical drop was measured at the base of the stairs leading up to the bridge deck (Figure 3-12d).

Large vertical cracking was observed on all wingwalls (see Figure 3-12c) and cracks were also seen along the full length of the base of both parapets and in places along the buttress of the arch. It is difficult to tell whether these cracks are merely superficial or whether they might hide any deeper structural issues, however one can safely assume that the cracking in the wingwalls is not critical as they are structurally independent of the main bridge. The cracking of the parapets may indicate minor hogging of the bridge but this is unlikely to significantly affect the bridge's load-carrying capacity, especially given that it is primarily a pedestrian bridge. Christchurch City Council is currently planning to begin repair works on the triumphal arch (the vertical structure seen in Figure 3-12b) in mid-2013. This arch was badly damaged and will be repaired by adding additional vertical reinforcement, the addition of horizontal post-tensioning and the improvement of its foundations so that it will behave in a rocking manner in future seismic events (Christchurch City Council, 2013).

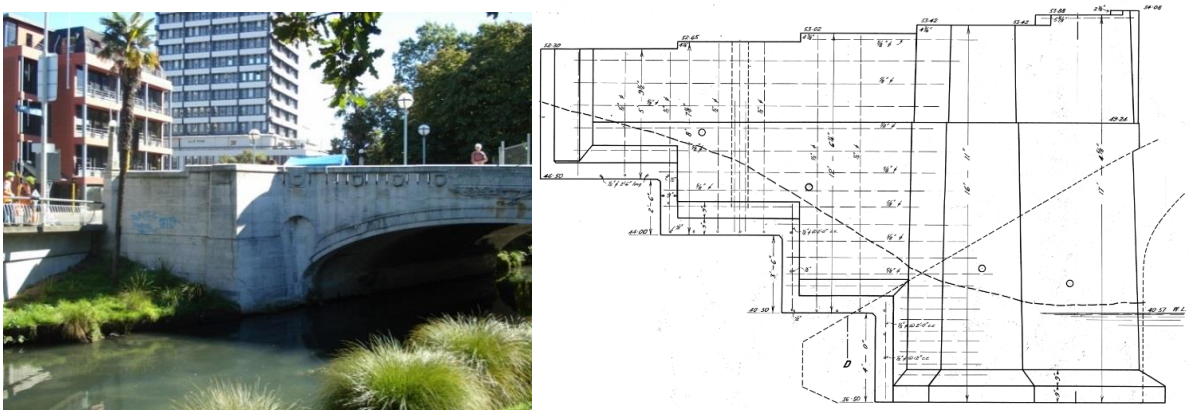

Figure 3-11: Remembrance Bridge arch structure and abutment/foundation plan

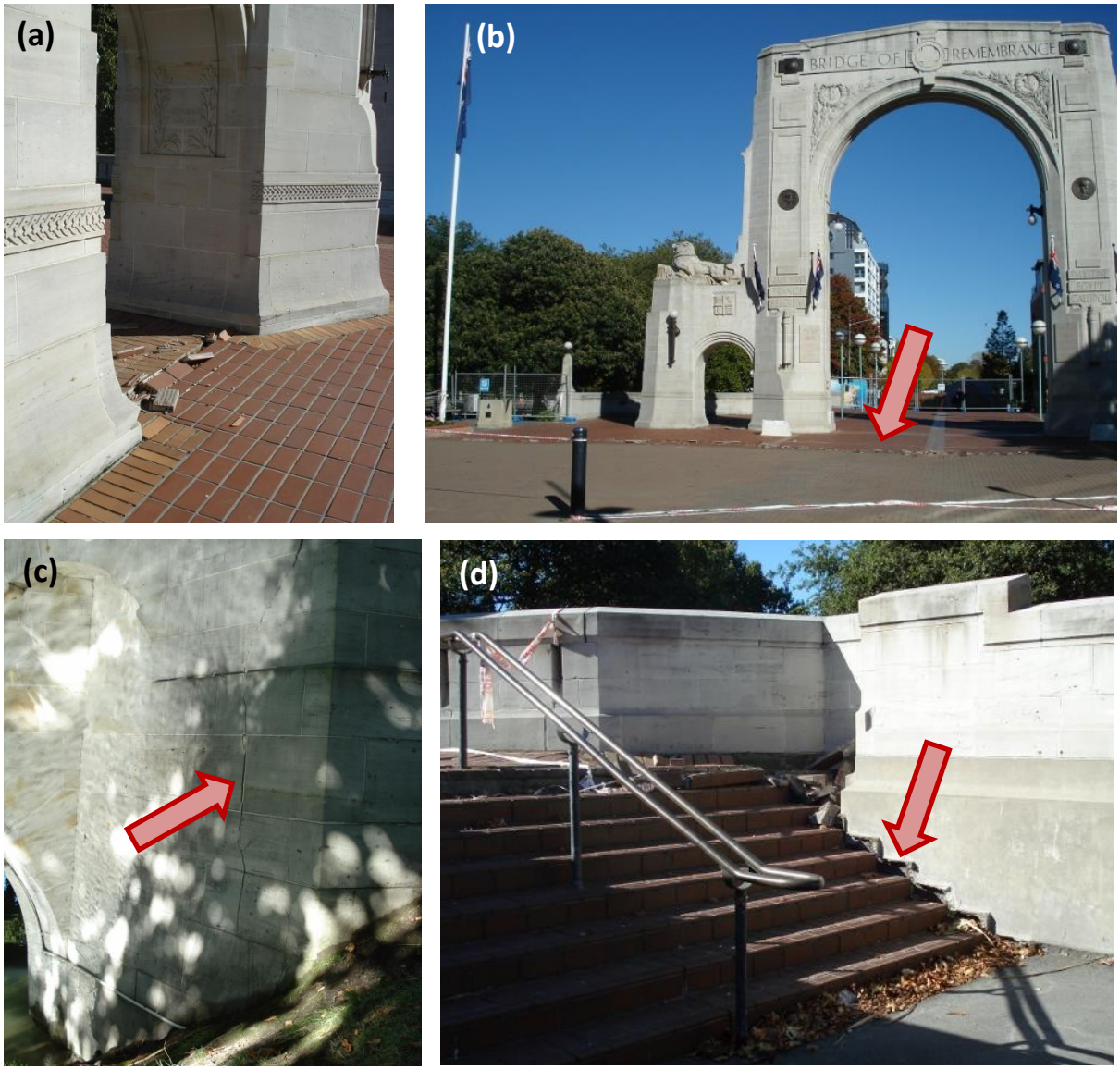

Figure 3-12: Observed damages to the Bridge of Remembrance following 22nd February earthquake: (a) compression cracking in pavement underneath Triumphal Arch, (b) compression cracking in pavement at eastern bridge/approach interface, (c) vertical cracking of wingwall, (d) vertical settlement of western approach visible at stairs

3.7.6.2 Hereford Street Bridge

Hereford Street Bridge, constructed in 1938 and situated less than 100 m north of the Bridge of Remembrance, is an integral, single-span bridge which carries four traffic lanes and two pedestrian lanes east-west across the Avon River. The reinforced concrete bridge is founded on shallow pad footings directly supported on river gravels.

Land Damage

As with the Bridge of Remembrance, no visible signs of lateral spreading were apparent in the immediate area surrounding the bridge. Some indicators of ground settlement were visible, with ground-stain markings seen on the wingwalls and abutments between 10 and 50 mm high.

Bridge Damage

Surface damage of both approaches was observed consistent with there having been some degree of lateral spreading. Minor compression cracking of the roadway occurred on both approach/bridge interfaces as can be seen in Figure 3-13a, more pronounced on the western bank than the eastern (up to 200 mm in places). Significant cracking was observed in all wingwalls, but this is not pertinent to the bridge's structural performance. Vertical hairline cracking was visible in the underside of the decking beams, and small horizontal cracks appeared to propagate from the abutment towards the centre of the bridge along the decking beam on all four corners of the bridge. As can be seen in Figures 3-13b and c, a small amount of back rotation of the abutments occurred, resulting in the separation of the wingwall from the abutment and causing concrete cracking and spalling down this connection. The measured back rotations of the integral abutments ranged from 0.6 degrees (south-eastern corner) to 1.8 degrees (south-western corner).

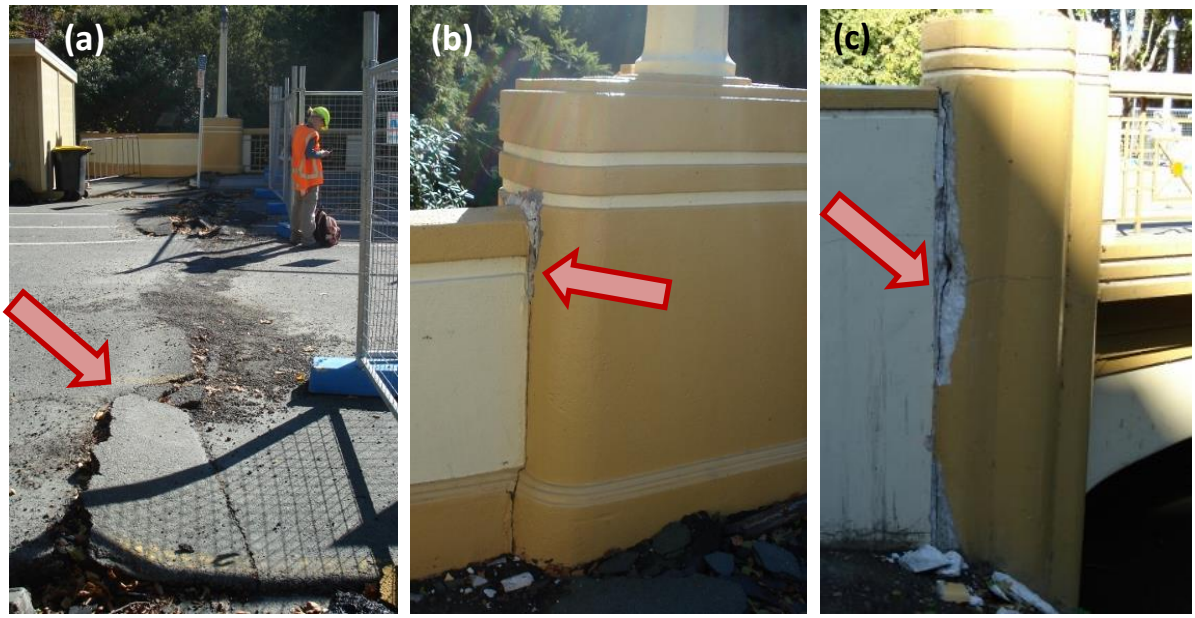

Figure 3-13: Hereford Street Bridge observed damages: (a) compression damage to western road approach, (b) separation of wingwall from bridge structure, (c) cracking between wingwall and bridge structure

3.7.6.3 Colombo Street Bridge

Colombo Street Bridge, originally constructed in 1902, was altered in 1930 (when extra width was added) and again in 1963 (when the timber deck was replaced with a concrete one). The bridge runs north-south across the Avon River and is comprised of arched steel riveted girders on its outside and constant depth riveted steel I beams over its internal portions. The steel beams span into reinforced concrete abutments which are supported on shallow foundations underlain by river gravels. The western elevation of the bridge is shown in Figure 3-14.

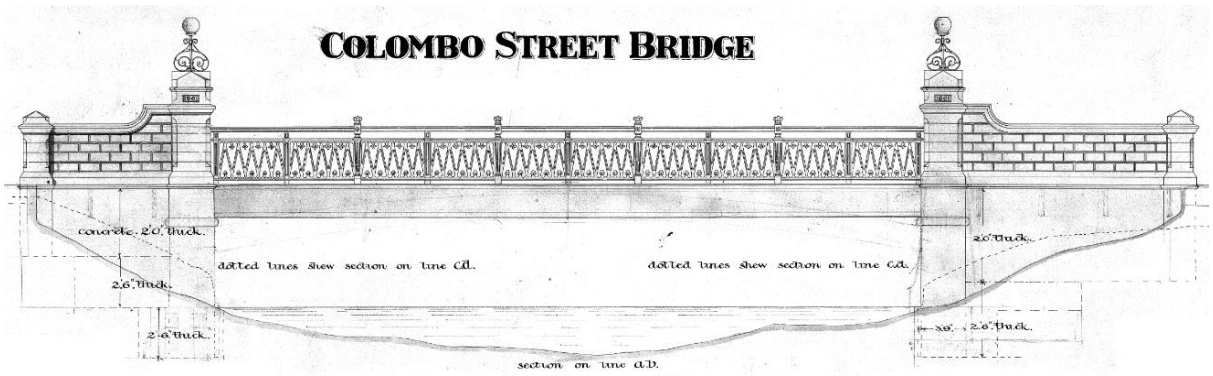

Figure 3-14: West elevation of Colombo Bridge

Land Damage

Following the Christchurch earthquake there was clear evidence of liquefaction and lateral spreading in the vicinity of Colombo Bridge on both river banks. Ground cracks measured to the west of the northern abutment (outer bank of the river) were in the order of 300 mm, while those to its east were in the order of 30 – 100 mm. On the southern side, small ground cracking was visible, as well as localised ground subsidence (holes), some of them infilled with liquefaction ejecta.

Bridge Damage

Abutment wall rotation was observed on both sides of the bridge but was more pronounced on the northern side. The bridge deck appears to have restrained movement of the tops of the abutments and they have undergone back rotations of 2.1 – 3.0 degrees on the northern side and 0.2 – 1.0 degrees on the southern side. Cracking in both concrete abutments was observed and appeared to be mainly vertical along the river-facing segments and hairline multi-directional in the end faces perpendicular to the river. Compression from the lateral spreading of the river banks led to the

severe buckling of the slender exterior steel bridge arches on both the upstream and downstream sides of the bridge, as demonstrated in Figure 3-15a, however the interior steel girders remained structurally sound. Figure 3-15b shows the compression damage observed in the roadway approach on the northern side of the bridge and illustrates the magnitude of the lateral spreading movement.

Figure 3-15: Colombo Street Bridge observed earthquake damages: (a) severe buckling of steel bridge arch, (b) compression damage to roadway approach

3.7.7 Bridges east and northeast (downstream) of Christchurch CBD

The bridges along the Avon River downstream of Christchurch CBD were the most affected by liquefaction and lateral spreading. The poor soil conditions and high levels of ground shaking resulted in severe liquefaction, which in turn produced large ground settlements and lateral soil displacements. The restraint provided by the bridges' stiff superstructures prevented ground movement in the longitudinal direction at the top of these bridges, resulting in the back-rotations of abutments up to the order of several degrees. This abutment rotation and lateral soil movements placed extremely large curvature demands on abutment piles. Piers and pier piles, too, were susceptible to rotation due to the liquefaction and lateral spreading of their underlying soil layers. The bridges discussed in this section are all founded on piles, therefore they did not settle much (if anything) in comparison with the settlement of the liquefied soils and slumping of approaches.

Structural damage did not restrict the use of these bridges post-earthquake, but temporary repairs were typically necessary in order to make the approaches serviceable (i.e. infilling of lateral spreading cracks and regrading of approaches which had subsided relative to the bridge deck). Most

of these repairs were carried out in a number of hours, however the essential services carried by bridges (water, electricity, etc) were often severely damaged and out of service for several weeks.

In this section a group of bridges in eastern Christchurch have been identified which cover a wide age range and demonstrate the performance of different structural systems. Most importantly, they highlight the typical deformation mechanisms and damages associated with liquefaction and lateral spreading, however additional behaviour details are also examined. The bridges, identified in Figure 3-16, are presented in the order of furthest upstream (Fitzgerald Avenue Bridges) to furthest downstream (South Brighton Bridge).

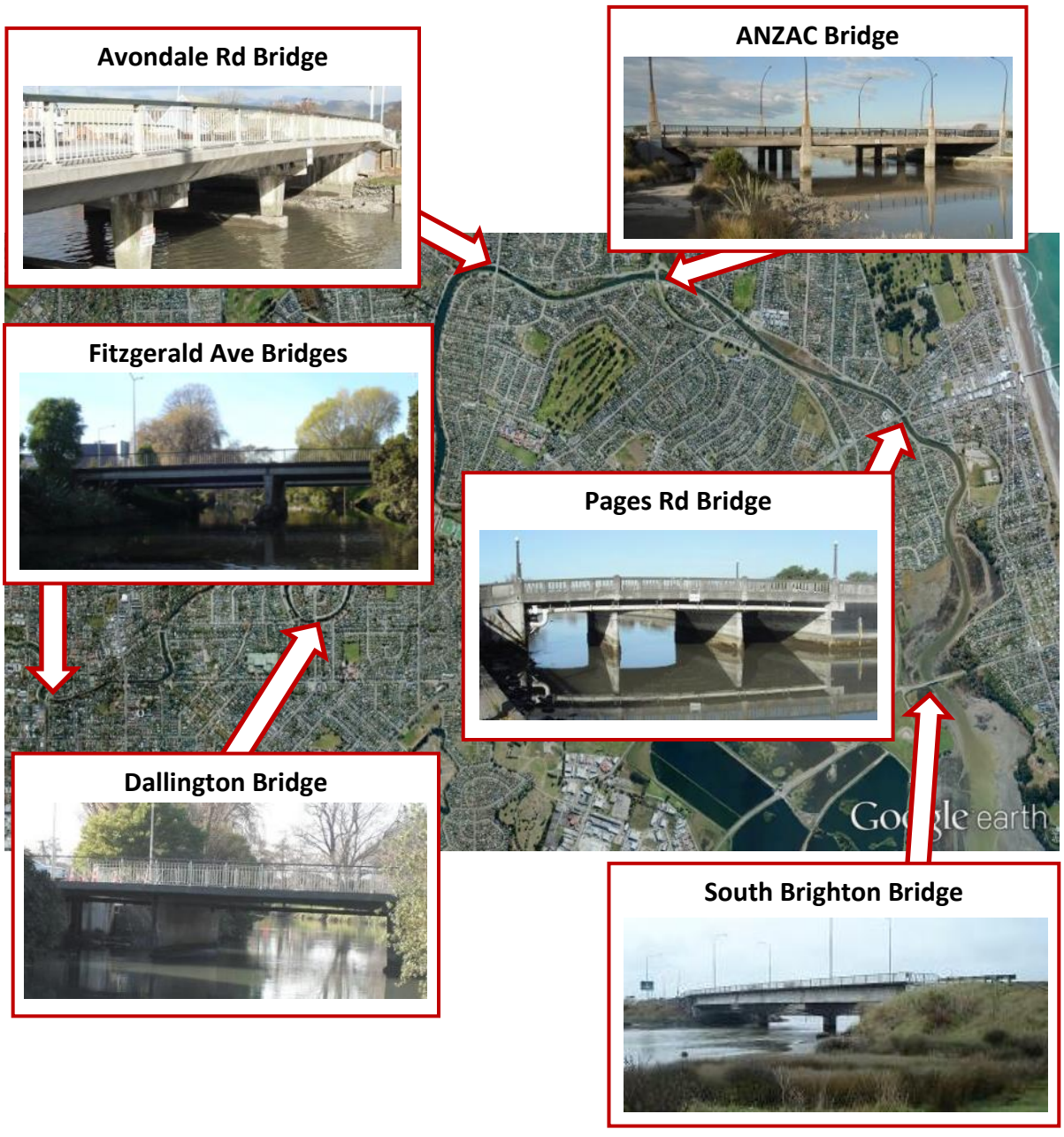

Figure 3-16: Aerial photo of eastern Christchurch showing the locations of the eastern and north-eastern case-study bridges

3.7.7.1 Fitzgerald Avenue Twin Bridges

The two-span Fitzgerald Avenue Bridges run approximately north-south across the Avon River to the immediate northeast of Christchurch CBD. They are located on one of the four main arterial roads surrounding Christchurch's centre, and are considered to be *National Strategic Bridges* by the New Zealand Transport Association as they are a critical link in the transport network. The western bridge carries two northbound lanes and a footpath, the east bridge two southbound lanes and a footpath.

The 28 metre long twin bridges were originally constructed in 1964 but recently (pre-earthquakes) underwent retrofitting. The original construction was segmental in nature and consists of double-span precast concrete girders supported by a pile-supported single wall pier and pile-supported concrete abutments on each bridge. The recent retrofit involved the tying of the pier and abutments to the deck using steel brackets in an attempt to create an integral system. All piles are reinforced concrete, octagonal in cross-section, 0.4 m in diameter and 9 m long. At each pier they are vertical and at the abutments they are both vertical and raked, as can be seen in Figure 3-17.

The northern abutment of the bridges is on the inner bend of the river bank, the southern abutment on the outer bend. The results of several SPT and CPT tests carried out at the site in the late 1990s show that, in general the soil layers that exist down to a depth of 30 m are sandy silt, silty sand, sand and gravelly sand. Overall, the soil on the north bank is looser and more susceptible to liquefaction than the soil on the south bank, consistent with it being a point-bar deposit (the looser fine-grained soil deposited by the river on the inside of a river bend). The worst soil conditions exist in the northeast corner, where a sandy layer 15 metres thick is deemed to be liquefiable (Bowen 2007, Bowen and Cubrinovski 2008).

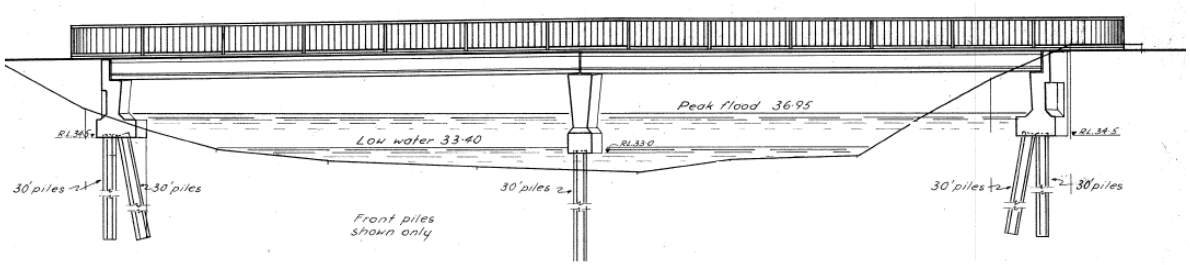

Figure 3-17: Elevation of Fitzgerald Bridge

Land Damage

Following the Darfield earthquake, no evidence of liquefaction was observed on either side of the bridge. However, during the Christchurch earthquake, significant lateral spreading was measured on the east side of the north abutment and moderate displacements were measured on the southern abutment. The locations and results of the lateral spreading transect surveys carried out and LiDAR data are shown in Figure 3-18. These indicate that total cumulative lateral spreading towards the river at the bridge in the order of 0.9 m occurred on the northern bank, while displacements of around 0.25 m occurred on the southern bank. In addition to ground cracking and spreading, settlements of around 0.5 m were also measured on the northern approach, as can be seen in Figure 3-20a. The area circled in green and corresponding arrows in Figure 3-18 indicate the direction of lateral spreading to the immediate northwest of the bridge. Here, large sections of the roadway slumped into the river, and this road was closed for several weeks until while reconstruction works were undertaken.

Figure 3-19 shows the distribution of lateral ground displacements with distance from the river bank of the two transects performed in line with the bridge ((a) and (b) in Figure 3-18). This demonstrates that the extent of lateral spreading on the north bank, although large in nature, only extended back about 25 m from the river meaning that large cracks were observed relatively close to the river bank (shown by the steep slope in Figure 3-19a). On the south bank, however, the shallow slope in Figure 3-19b represents an accumulation of smaller cracks extending back as far as 65 m from the river bank.

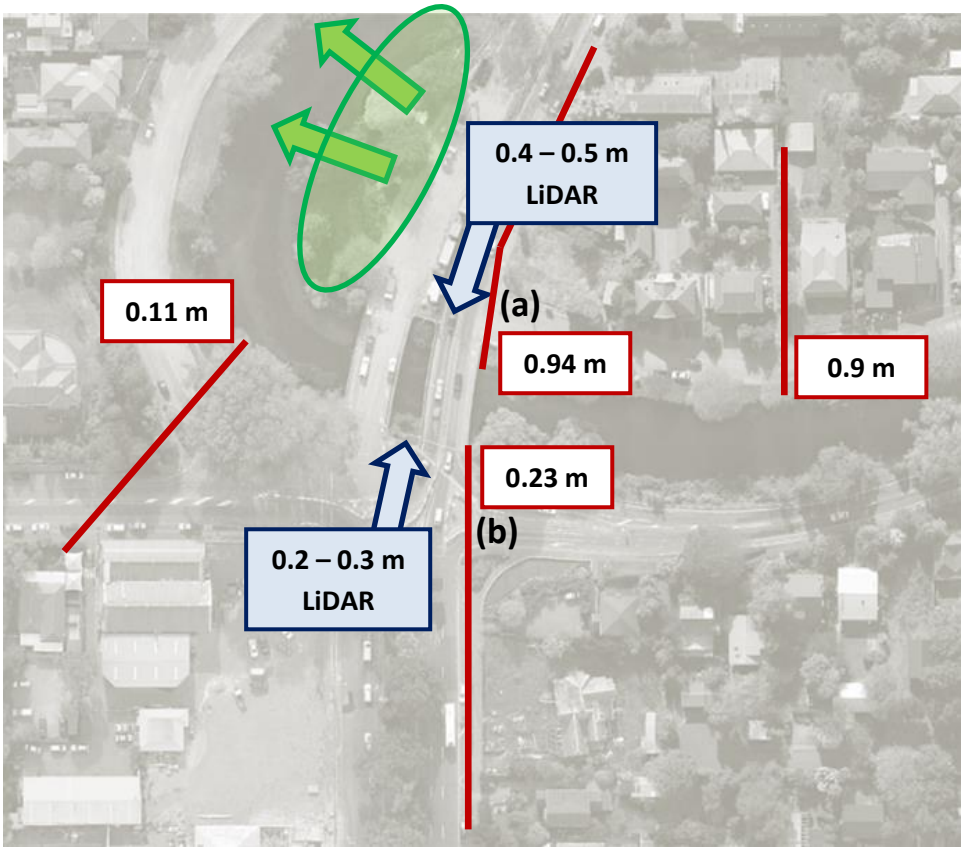

Figure 3-18: Aerial view of Fitzgerald Bridge showing location of lateral spreading transects and cumulative measured displacements at the river banks, LiDAR measurements are also included

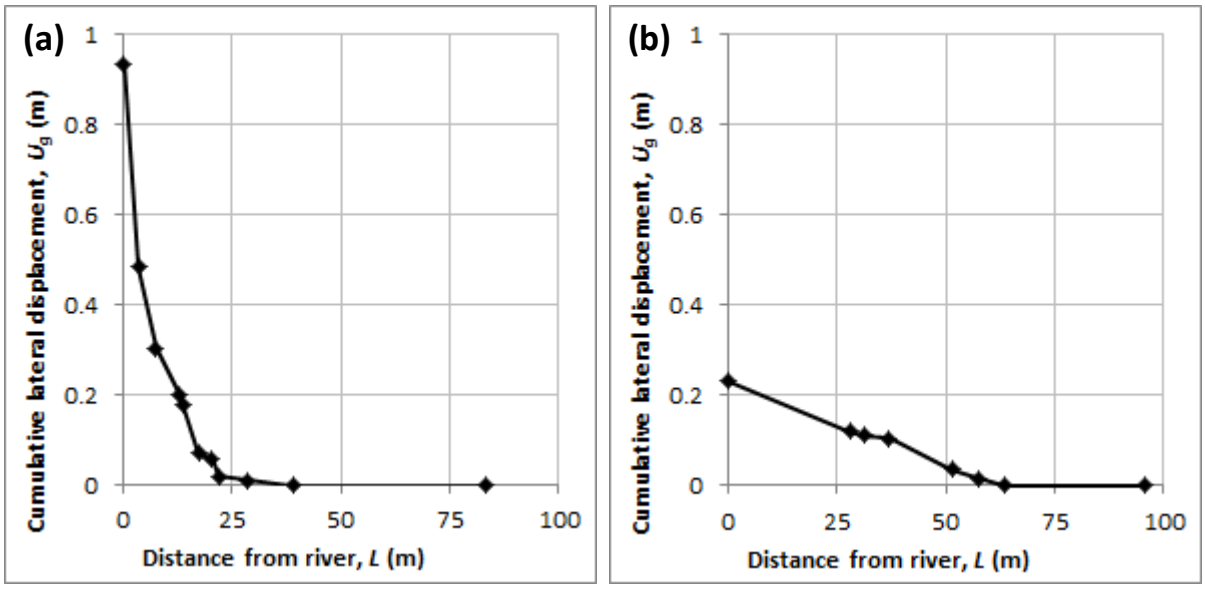

Figure 3-19: Distribution of permanent lateral displacement with distance from the river banks at Fitzgerald Avenue Bridge, (a) north bank, (b) south bank

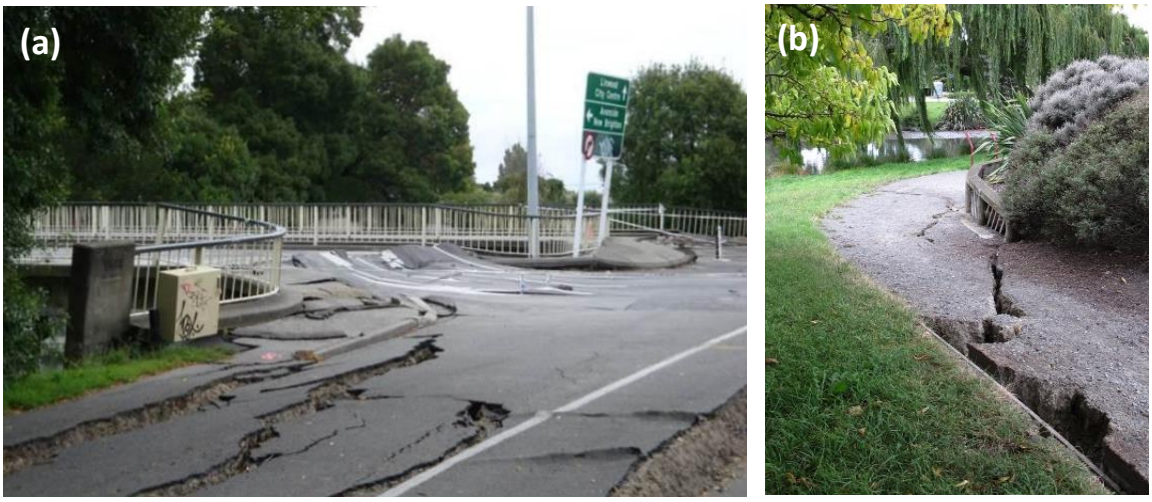

Figure 3-20: Land damage observed in the vicinity of Fitzgerald Ave Bridge, (a) significant cracking and slumping of northern approach, (b) lateral spreading cracks to the immediate west of the north abutment

Bridge Damage

Consistent with the lack of land damage following the Darfield earthquake, the bridge remained unaffected by this event. Thus the damages described below are due solely to the Christchurch earthquake. The north abutments were the most heavily affected in the Christchurch earthquake and underwent significant back-rotations, 5° on the eastern bridge and 3.5° on the western bridge. The wingwalls separated themselves from the abutment ends and underwent independent further back-rotations, measured to be 10° on the east end of the eastern bridge and 5° on the west end of the western bridge. This can be seen in Figure 3-21a, where a gap of 60 mm can be seen between the top of the abutment and the wingwall. The wingwalls also appeared to rotate outwards from the bridge, with a 70 mm sideways offset measured between the easternmost wingwall and the bridge deck. The abutment rotations measured on the southern side of both bridges were all smaller than 1°.

On the northern abutment, the large rotations combined with the settlement and lateral soil displacements towards the river meant that the tops of the abutment piles were exposed. The easternmost pile on the eastern bridge failed in shear and tension, with a crack between 10 and 30 mm in width opening up across the entire tension face of the section (Figure 3-21b). Additional tension cracks ranging from 0.1 to 1.5 mm in width were measured on the river-facing side of all northern piles.

Minor concrete loss (spalling) was observed on the edges of the bottom flanges of the deck girders immediately butting into the north abutments as a result of the deck compression forces due to abutment back-rotation, causing rebar to be exposed in some places (Figure 3-21c). Minor horizontal and vertical cracks were also observed in the river-facing walls of both northern and southern abutments. The steel seating brackets added as part of the retrofit performed relatively well under the large lateral spreading loads and helped prevent the simply supported deck spans from unseating. However, as can be seen in Figure 3-21d, there was some degree of separation observed between the seating brackets and the deck caused by the excessive rotation of the abutments.

Figure 3-22 shows the spreading and settlement immediately under the northern abutments of both bridges. It is clear that significantly more settlement occurred on the eastern bridge (~0.3-0.5 m visible), while horizontal gapping between the piles and soil on the river-facing side due to lateral spreading was similar on both (0.2 – 0.3 m).

Opus International Consultants Ltd, acting on behalf of Christchurch City Council and NZTA, performed preliminary calculations which indicated that the piles supporting each bridge still had the capacity to support Class 1 (legal) live loading (this corresponds to the heaviest vehicles that can legally be registered for road use). Also, despite being prone to further abutment rotation, the collapse mechanism is considered to be ductile and progressive with minimal risk to road users. As such, the bridges were reopened to traffic prior to permanent repairs (or replacement options) being designed and carried out (Waldin *et al.* 2012).

Figure 3-21: Fitzgerald Avenue eastern bridge north abutment, (a) abutment and wingwall back rotation, (b) tension failure of abutment pile, exposure of reinforcement, (c) spalling of bottom flange of deck girder, (d) gapping between steel brackets and bridge deck due to rotation of abutment

Figure 3-22: Fitzgerald Bridge north abutments, (a) western bridge, (b) eastern bridge

3.7.7.2 Dallington Bridge (Gayhurst Road)

Dallington Bridge (sometimes referred to as Gayhurst Road Bridge) was constructed in 1954 and is oriented in the north-south direction across the Avon River. The north abutment sits on the inner bank of the river (point-bar deposit) and the outer cut-bank on the south; it occupies the southernmost point of where the Avon River in the vicinity meanders around the area known as the Dallington Loop. The bridge itself is a three-span integral concrete structure, 26.8 m in length, with one traffic and one pedestrian lane in each direction (see Figure 3-23). The continuous reinforced concrete deck is supported on wall piers and abutments, both of which are supported by driven square reinforced concrete piles 10.4 m in length and 0.35 m wide. Concrete wingwalls exist on either side of each abutment. Prior to the Canterbury earthquake sequence the south approach was approximately level with the bridge deck, as part of the natural level of the river banks, while the north bank was slightly below the level of the bridge deck.

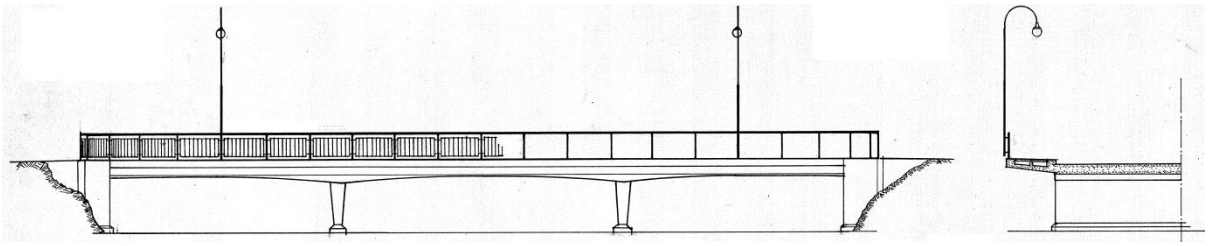

Figure 3-23: Dallington Bridge elevation

Site investigations at Dallington Bridge consist of one SPT borehole at each abutment and several CPTs on the north abutment. The borehole on the southern abutment indicates that the soils consist of sandy silt and silt in the upper three metres. Below this lies medium dense to dense sand and gravelly sand to 6 metres depth, then dense fine sand to 16 metres depth. This is the bearing stratum of the bridge abutment piles. The northern abutment soils, on the other hand, are comprised of much looser materials; the upper 2.5 metres being sandy silt and silt with some peat. Below this, from 2.5 to 15 metres depth, a layer of fine sand exists, loose from 2.5 to 9 m (CPT tip resistance q_c = 3 – 8 MPa, SPT blowcount N = 5 – 15), and medium dense to dense below this extending into the pile bearing stratum. The layer between 2.5 and 9 metres depth is particularly susceptible to liquefaction due to its grain composition and relatively loose materials.

Land Damage

Following the 2010 Darfield earthquake significant liquefaction occurred on the northern inner bank of the river. As a result, ground settlement in the order of half a metre and significant lateral spreading occurred throughout the entire "tongue" of land surrounded by the Dallington Loop. Figure 3-24 shows the magnitude of lateral spreading measured following both the Darfield and Christchurch earthquakes; note that the values in brackets are those measured in late 2010 (i.e. post Darfield) and those not in brackets were measured in late February/March 2011 (i.e. post Christchurch). It is apparent from general observations, lateral spreading transects and LiDAR data that negligible land damage occurred on the south abutment in either event, however both events caused substantial damage on the northern side of the bridge. Following the Darfield event lateral spreading transects on the north abutment measured cumulative free-field ground displacements towards the river to be between 0.6 and 1.0 m (see Figure 3-24).

The Christchurch event caused additional and substantial land damage to the north of the bridge, and the cumulative effects of both events led to more than half a metre of ground settlement. This is clearly visible in Figure 3-26, where the approach road, which was once almost level with the bridge deck, is significantly steepened. To the west of the north abutment, the lateral spreading transect labelled (b) in Figure 3-24 was performed after both the Darfield and Christchurch earthquakes and Figure 3-25b shows the increase in spreading that occurred as a result of the latter event (approximately 25%). The transect labelled (a) in Figure 3-24 was performed after the February event only and the distribution of ground displacement U_g, with distance from the river bank, L, can be seen in Figure 3-25a. This indicates that the cumulative width of ground cracks from the reference "zero displacement" point up to the bridge is 0.2 m. However, immediately at the bridge, the wingwalls had moved independently of the bridge structure towards the river by an additional 0.4-0.7 m. This will be further discussed in the following section, however the general effect can be seen in Figure 3-27, where the bridge deck has clearly restrained the lateral movement of the soils immediately behind it, and the measured displacement at the bridge deck of 0.2-0.35 m is significantly smaller than the free-field displacement of 0.7-0.9 m measured 30 m either side of the bridge.

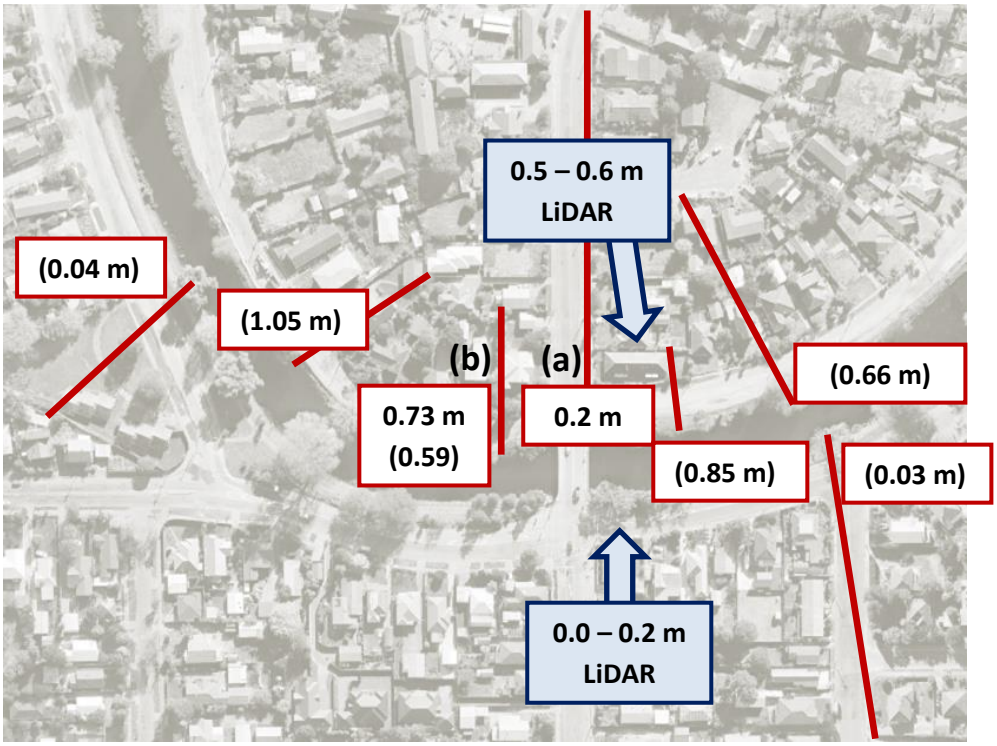

Figure 3-24: Aerial view of Dallington Bridge showing location of lateral spreading transects and cumulative measured displacements at the river banks (note that values in brackets are those measured after the September 2010 earthquake), LiDAR measurements are also included

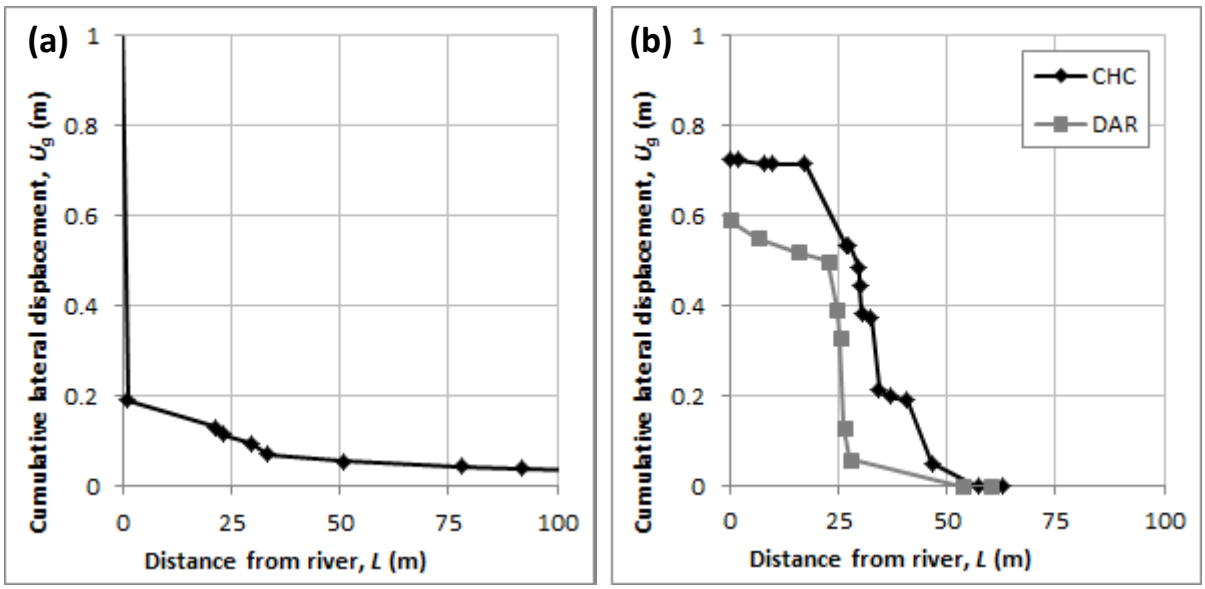

Figure 3-25: Distribution of permanent lateral displacement with distance from the river banks at Dallington Bridge, (a) north bank, directly in line with bridge, (b) north bank, 25 m west of bridge (both significant earthquake events shown)

Figure 3-26: Settlement of northern approach of Dallington Bridge, resulting in steepening of approach road.

Bridge Damage

Minor to moderate bridge damage was initiated during the Darfield event, with further damages occurring as a result of the Christchurch event (Wotherspoon *et al.* 2011). What is described below is the cumulative effects of these two earthquakes, as inspections were carried out by the University of Canterbury reconnaissance team following the February event only. The southern bridge approach suffered negligible damage throughout the earthquake sequence and as such there were no visible signs of distress to the southern abutment, wingwalls or even to the southern pier. However, as can be seen in Figures 3-27 to 3-29, significant damage occurred to the northern end of the bridge and its surroundings. Figures 3-27a and b highlight the significant vertical offset between the bridge deck and approach as a result of ground settlement. The services supported by the bridge seen on either side were severely damaged and remained exposed until the regrading of the approach had been carried out. The separation of the wingwalls from the bridge deck can be seen in both figures, however it is clearer in Figure 3-27b. This shows the independent lateral movement of the wingwalls towards the river bank as well as the outwards rotation and translation of the wingwalls away from the bridge, highlighting the stiffness of the bridge superstructure in its lack of appreciable longitudinal movement.

Although Dallington Bridge is an integral structure, some back-rotation of the northern abutment wall was measured, although much smaller than was seen in the abutments of some of the precast bridges (e.g. ANZAC Bridge, South Brighton Bridge). Figure 3-28a shows a large (~40 mm wide) vertical crack on the eastern side of the north abutment wall; "inside" this crack (i.e. towards the centre of the bridge) a back-rotation of 2.2° was measured, while "outside" the crack a back-rotation of 0.8° was measured[2]. Extensive cracking along the northern abutment wall was evident, and the reinforcing connecting the wingwalls to the abutment was completely exposed. Pile investigations carried out by Dr. Liam Wotherspoon (University of Auckland) at the northern abutment also indicated that severe flexural cracking had occurred in the river-facing sides of some piles immediately beneath the abutment-pile interface, to the point where transverse reinforcing was exposed and confinement lost (Figure 3-28b). This is an expected result of the large displacement and rotation demand imposed on the piles at this critical connection.

Figure 3-29 shows a single horizontal crack along the north face of the northern pier wall, consistent with the rotation of the bottom of the pier towards the centre of the river. Horizontal cracking through the deck soffit can also be seen, however this is not considered to be critical to the load-carrying capacity of the bridge.

Dallington Bridge was proof-loaded in February 2011 to confirm that it could safely support traffic prior to permanent repairs being undertaken. It was deemed to still have the residual capacity to support Class 1 (legal) live loading, however was restricted to a gross vehicle weight of 3,500 kg in order to protect the substructure from any further damage (Waldin *et al.* 2012). Also, despite the northern abutment still being prone to further rotation, the collapse mechanism was determined to be ductile with minimal risk to road users, so the bridge was reopened to traffic prior to permanent repairs (or replacement options) being designed and implemented.

[2] Note that there are discrepancies in these values between those stated in GEER 2011 and Wotherspoon *et al.* 2011 versus those stated here. The values stated in this thesis have been verified by the author and are correctly reported here.

Figure 3-27: North abutment, Dallington Bridge looking south, (a) eastern side showing settlement of approach from bridge deck and exposed services, (b) western side showing translation and rotation of wingwall, settlement of approach and exposure of services.

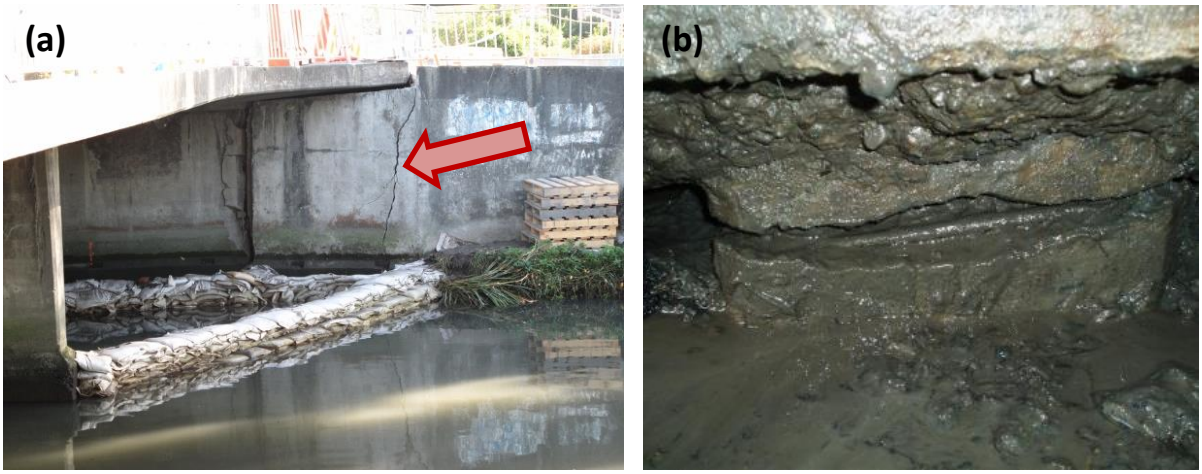

Figure 3-28: Dallington Bridge, north abutment, (a) vertical cracking in abutment wall, (b) cracking of abutment pile and exposure of transverse reinforcing.

Figure 3-29: Dallington Bridge, looking south, horizontal cracking in northern pier, horizontal cracking on underside of pedestrian cantilever.

3.7.7.3 Avondale Road Bridge

Avondale Road Bridge, constructed in 1961, is a simply-supported bridge running approximately north-south across the Avon River. The bridge consists of a 37 m long three-span precast concrete girder supported on two three-column bents and seat-type abutment walls with wingwalls (an elevation of the bridge can be seen in Figure 3-30). The piers are each founded on 8 14-metre long 0.4 m square reinforced concrete piles, and the abutments are founded on 7 12-metre long 0.4 m square reinforced concrete piles, alternately raked and vertical (see Figure 3-31). Like the Fitzgerald Avenue Bridges, Avondale Rd Bridge underwent recent retrofitting (pre-earthquakes) which utilised bolted steel brackets to tie the piers and abutments to the bridge deck in an attempt to create an integral system. The north abutment sits on the outer cut bank of the river and the south abutment on the inner bank.

Site investigations show that the soils on the northern side of the bridge consist of sand to 2 metres depth underlain by a layer of silt to 3.5 m depth. Below this, a layer of silt exists down to at least 16 metres depth; medium dense from 4-7 m and dense below this. On the southern side of the bridge a 2.5 m thick sand layer overlies 1 metre of silty sand and then over 20 metres of sand. At 3.5 m depth this is relatively loose (CPT tip resistance, q_c = 4 MPa), gradually increasing in density to q_c = 20

MPa (and SPT blowcount, *N* = 25) in the bearing stratum of the piles. In general, the southern side of the river consists of looser soils and thus is more susceptible to liquefaction.

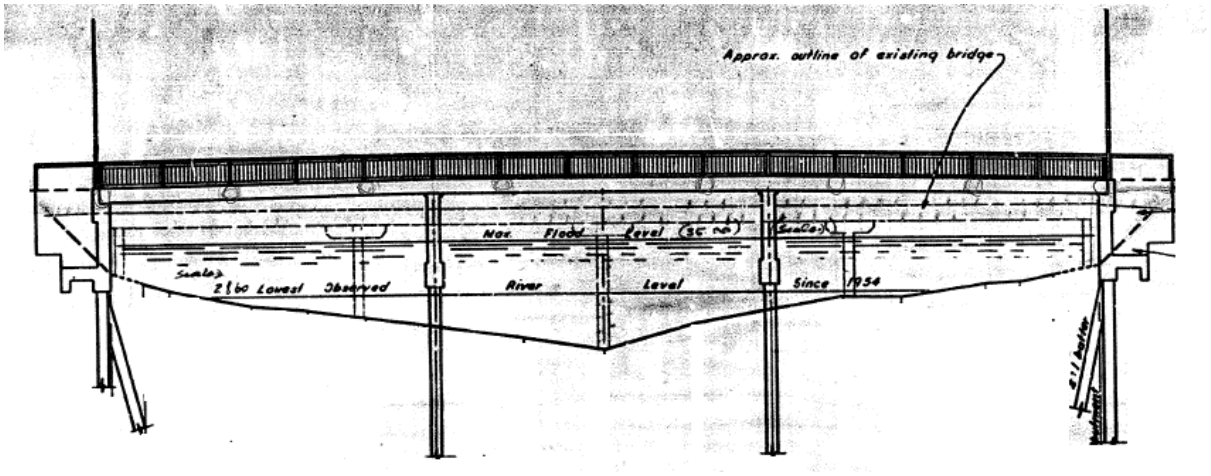

Figure 3-30: Avondale Bridge, elevation

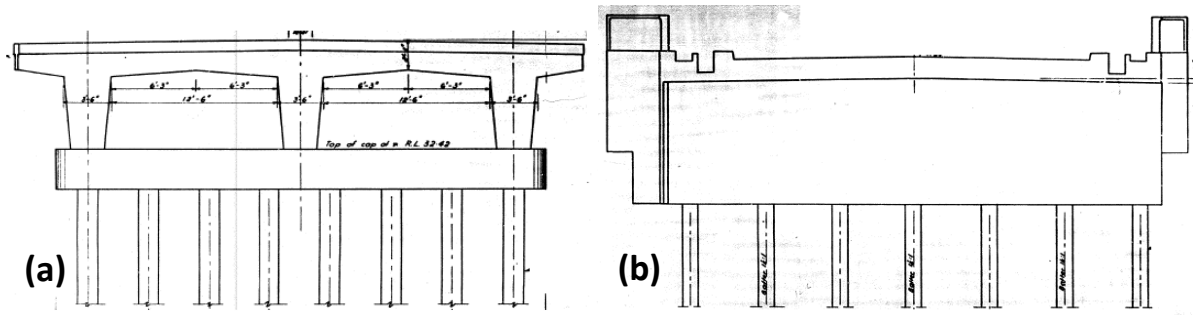

Figure 3-31: Avondale Bridge pile layouts, (a) pier piles, (b) abutment piles

Land Damage

Following the Darfield earthquake the area north of the bridge showed no evidence of liquefaction. To the south of the bridge, minor to moderate levels of liquefaction ejecta were observed, with the severity increasing towards the southwest, however the bridge was not at all affected in this event (Wotherspoon *et al.* 2011). Liquefaction and lateral spreading were more severe during the Christchurch earthquake, with large volumes of ejecta on the south side of the bridge and significant lateral spreading on either side of the abutment (Figure 3-34b). On the north side of the bridge

there were minor amounts of liquefaction ejecta and moderate spreading ~50 m upstream of the bridge. Two lateral spreading transects were carried out following the Christchurch earthquake, both on the southern side of the river; one immediately west of the bridge ((a) in Figures 3-32 and 3-33) and one 300 m east of the bridge ((b) in Figures 3-32 and 3-33). The steep initial slope in Figure 3-33a indicates that approximately two-thirds of the total lateral displacement of the free face was manifested in the form of three large cracks within 10 metres of the river bank, while the remaining third of the total displacement was accommodated by a series of smaller cracks extending as far back as 100 m from the river. Figure 3-33b shows that, further downstream, the lateral spreading cracks are smaller and evenly distributed with distance from the river.

The northern bridge approach showed little indication of lateral ground movement or settlement, while settlement of the south approach was in the order of half a metre (Figure 3-34a).

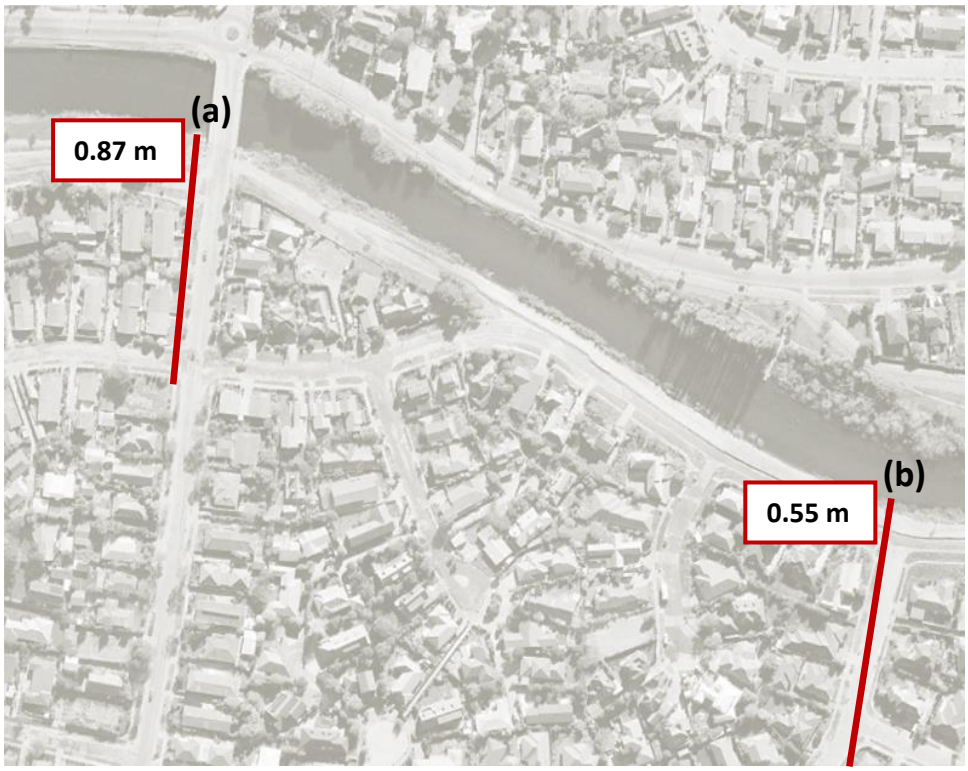

Figure 3-32: Aerial view of Avondale Rd Bridge showing location of lateral spreading transects and cumulative measured displacements at the river banks

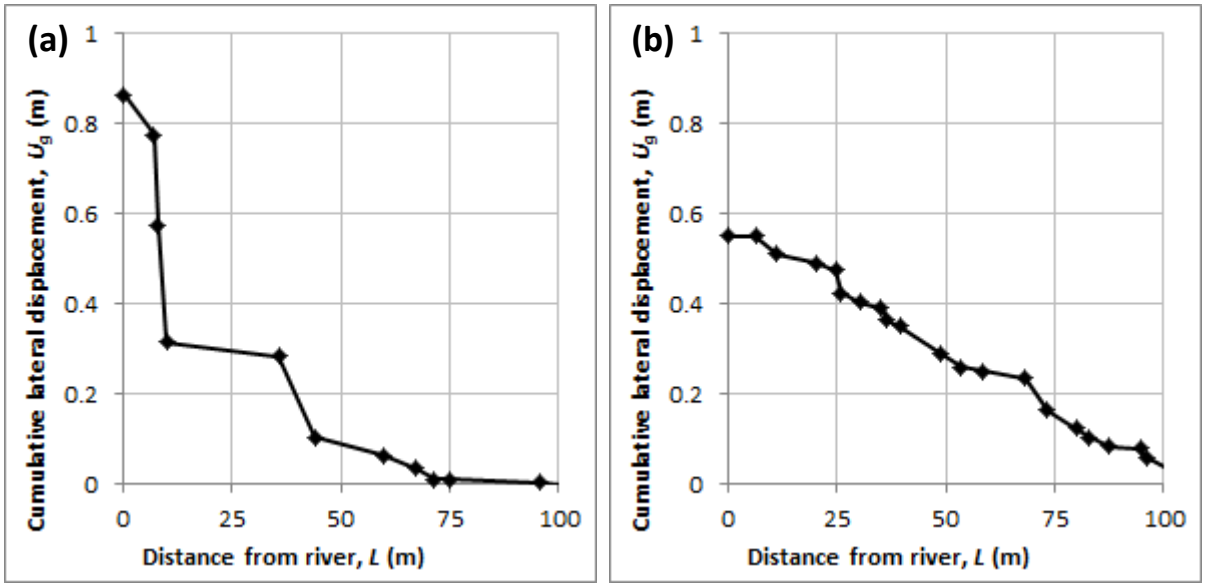

Figure 3-33: Distribution of permanent lateral displacement with distance from the river banks at Avondale Bridge, (a) south bank, immediately to west of bridge, (b) south bank, 350 m east of bridge

Figure 3-34: Avondale Road Bridge south abutment, (a) observed ground settlement leading to steepening of approach road, (b) lateral spreading cracks observed immediately to the east of the south abutment.

Bridge Damage

All the damages detailed here occurred as a result of the February 2011 event. Avondale Road Bridge was a good demonstration of the typical deck-pinning, abutment back-rotation mechanism associated with lateral spreading of the river banks. Despite there being minimal land and roadway damage on the northern side of the bridge, this abutment still underwent a 1.5-3° (west face – east face) back-rotation. A 25 mm gap was apparent in the footpath pavement surface between the bridge deck and approach as a result of this rotation. On the west side minor concrete spalling was visible on the bottom of the deck girder close to the abutment, exposing some reinforcing.

In accordance with the increased level of land damage on the southern side of the bridge, the back-rotation of the south abutment wall was 7-8°. As can be seen in Figure 3-35a, a vertical offset between the bridge deck and immediate approach was measured to be 100 mm, with a horizontal gap of 70 mm. Concrete spalling was also visible on the western face and underside of the deck girder close to the abutment. As with the Fitzgerald Avenue Bridge, gapping was observed between the retrofitted steel seating brackets and bridge deck as a result of excessive abutment rotation (Figure 3-35b). This has since been regrouted to restore bearing. No superstructure or pier damage was noted.

Avondale Road Bridge was periodically closed following the February 2011 earthquake until the piles were inspected and repairs were made to those damaged (in particular those on the southern abutment). The bridge is currently considered to be earthquake prone with very little capacity to resist further lateral spreading loads on the abutments (Christchurch City Council 2011a), however it still has adequate live load capacity for normal traffic. A 30 km/h heavy vehicle speed limit restriction has been in place since the Christchurch earthquake and the bridge is open to traffic until permanent repairs (or replacements) will be carried out.

Figure 3-35: Avondale Road Bridge south abutment, (a) back rotation of abutment, (b) observed gapping between steel bracket and bridge deck.

3.7.7.4 ANZAC Bridge (ANZAC Drive)

ANZAC Bridge is located on State Highway 74 north-east of Christchurch's Central Business District. The four-lane bridge spans approximately north-south across the Avon River and was constructed in the year 2000 to form part of the Christchurch eastern ring road (Burwood Expressway). SH 74 is classified by the NZ Transport Agency as a *National Strategic highway*, meaning that ANZAC Bridge plays a valuable and integral role in both Canterbury's and New Zealand's transport network. The north abutment sits on the outer cut-bank of the river and southern abutment on point-bar deposits of the inner bank. A roundabout exists on the northern approach to the bridge and beyond this lies a swampy wetland area.

ANZAC Bridge is a three-span reinforced concrete structure 48.4 metres in length with a 13° skew in plan. There are two traffic lanes in each direction and a footpath on the western side. The bridge deck consists of precast concrete double core units and is supported by two central 4-column bents and concrete abutments. The piers were cast *in situ* and founded on steel-encased reinforced concrete piles. The concrete abutments were also cast *in situ* on top of embankment fill and driven

steel H piles. Pedestrian underpasses are provided on both sides of the river and are effectively independent of the bridge structure, being attached only superficially to the bottom of each abutment. An elevation of ANZAC Bridge can be seen in Figure 3-36.

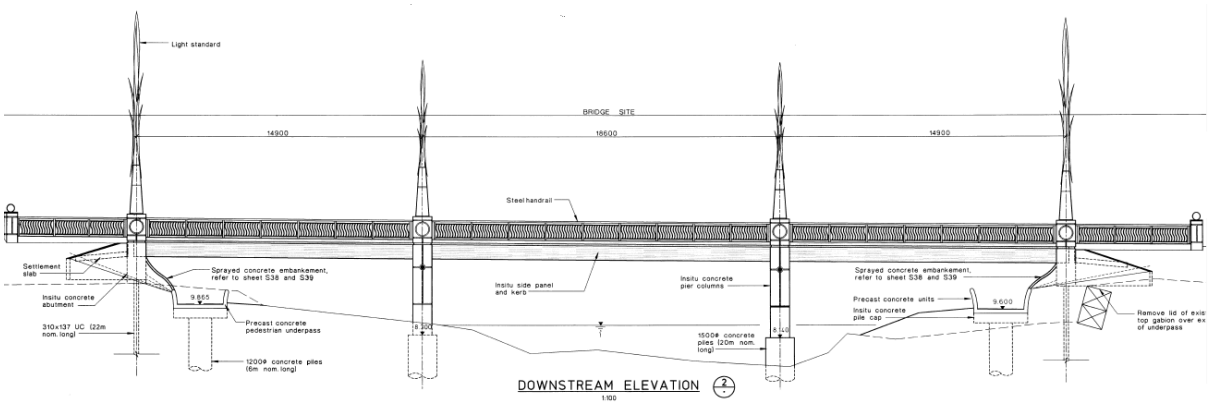

Figure 3-36: ANZAC Bridge, elevation

Site investigations at ANZAC bridge consist of one SPT and one CPT at each abutment. The borehole on the northern abutment indicates that the soils consist of a mixture of gravel, topsoil, silt and sand in the top metre overlaying 2 metres of coarse sand with some small gravel. From 3 to 15 metres depth the profile is deemed to be a relatively uniform medium dense sand, below this the profile varies between denser sand and silty sand. The soils on the southern abutment are sands in the upper 1.5 metres overlaying a thin peat layer and another 1.5 metres of silty sand. From around 3.5 metres to 30 metres depth the material present ranges from fine to coarse medium dense sand, increasing in density at around 15 metres depth.

Land Damage

Marginal liquefaction and lateral spreading occurred in the area of the bridge during the Darfield earthquake, such that the bridge and its functionality were not at all affected (Wotherspoon *et al* 2011). The Christchurch earthquake, on the other hand, saw significant liquefaction and lateral spreading occur at the bridge site. Figure 3-37 shows the extent of liquefaction ejecta, clearly more severe on the south bank than the north.

Figure 3-37: Aerial view of ANZAC bridge (looking towards the north-east) subsequent to the Christchurch earthquake (Becker-Fraser photos)

There were a significant number of sand boils observed in the grassy areas on either side of the southern bridge approach and large lateral spreading fissures were observed running parallel to the river-bank (see Figure 3-38). Lateral spreading transects performed near the bridge indicate that the free-field displacement of the ground towards the river ranges between 0.9–1.1 m (see Figure 3-41). These values were also confirmed by LiDAR measurements. Figure 3-42b shows the distribution of cracks with distance from the river as measured in the transect performed immediately to the west of the abutment. This indicates one large crack (~0.5 m wide) 8 metres from the river bank, followed by a succession of cracks gradually decreasing in width and increasing in spacing extending back further than 100 m from the river bank. Ground settlement led to steepening of the approach road and, as can be seen in Figure 3-39, induced severe pavement compression cracking at the deck/approach interface. Smaller pavement and ground cracks were also apparent running perpendicular to the river on both sides of the approach suggesting that the approach fill slumped away from the roadway as well as towards the river.

Figure 3-38: Ground cracking and slumping in direction of river, southern abutment, ANZAC Bridge (a) looking east, (b) looking west from the bridge

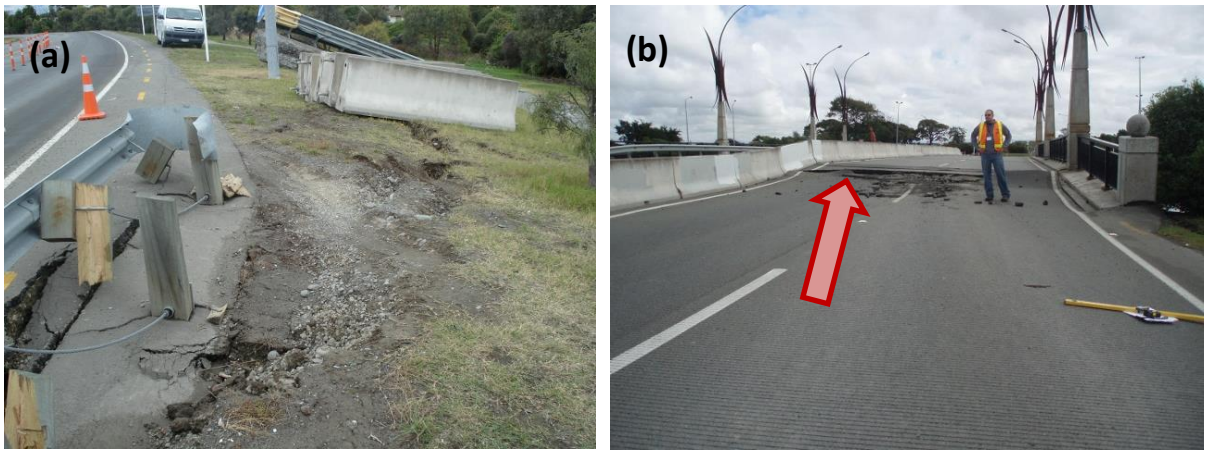

Figure 3-39: (a) lateral cracking/slumping of southern approach, ANZAC Bridge, (b) steepening and pavement compression of southern approach, ANZAC Bridge

The roundabout just to the north of the northern abutment is an important feature in that it significantly affected the observed behaviour on this side of the river. Because it is a local point of high ground, complex visible cracking patterns reflect this, with radial as well as lateral cracks appearing to stem from here. The lateral spreading transect performed on this side of the river ((a) in Figure 3-41) indicated that the cumulative width of ground cracks from the highest point of the roundabout to the river bank is approximately 0.4 m; while ground cracking from the highest point of the roundabout tracking north appears to be in the direction of the swampy area. The distribution of measured cracks can be seen in Figure 3-42a, a plot of U_g vs L. In general, liquefaction

and lateral spreading were less pronounced in the vicinity on this side of the river, however as mentioned previously the roundabout may have affected this both by obscuring the evidence of sand ejecta or similar and by increasing the local stiffness of the ground. Ground settlement was also less pronounced than the southern abutment, however slumping appeared to be mainly in the direction of the river and not pronounced in the perpendicular direction. As can be seen in Figure 3-40, moderate pavement damage to the road occurred at the bridge/approach interface and more severe cracking and slumping was visible in the footpaths running parallel to the river.

Figure 3-40: Pavement damage and ground settlement, northern abutment, ANZAC Bridge, (a) liquefaction damage in footpath immediately to the west of abutment, (b) footpath damage, photo taken from bridge looking west, (c) compression pavement damage at approach/deck interface

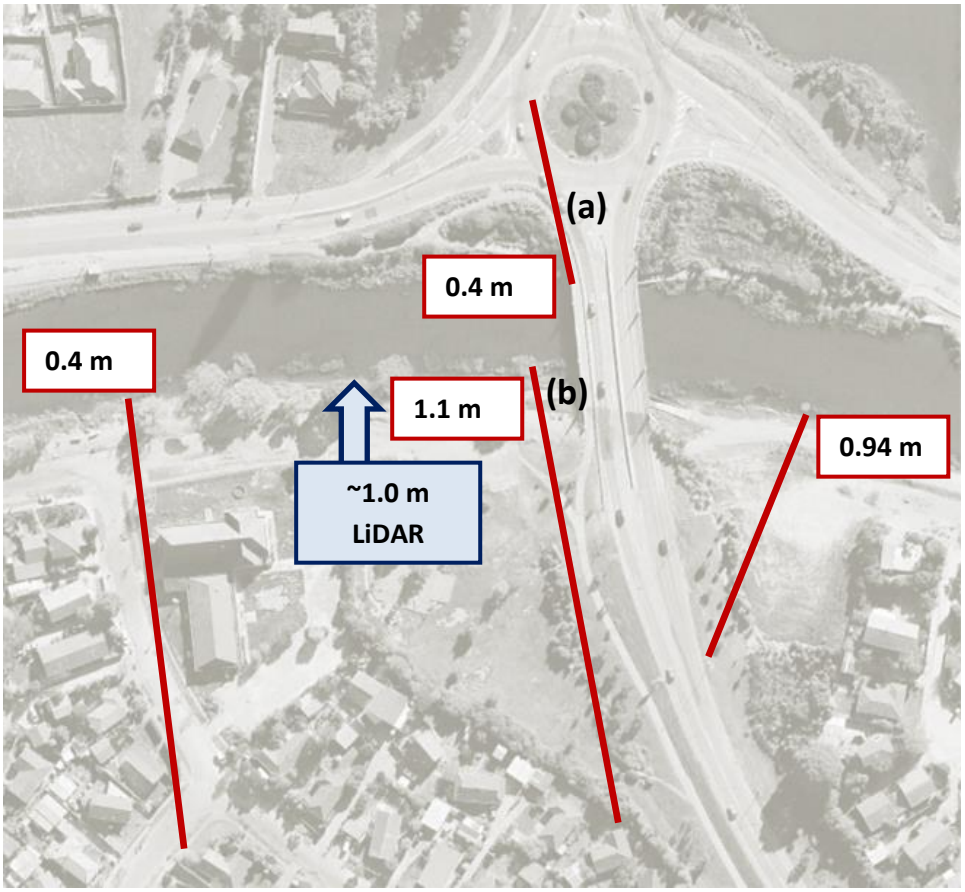

Figure 3-41: Aerial view of ANZAC Bridge showing location of lateral spreading transects and cumulative measured displacements at the river banks, LiDAR measurements are also included

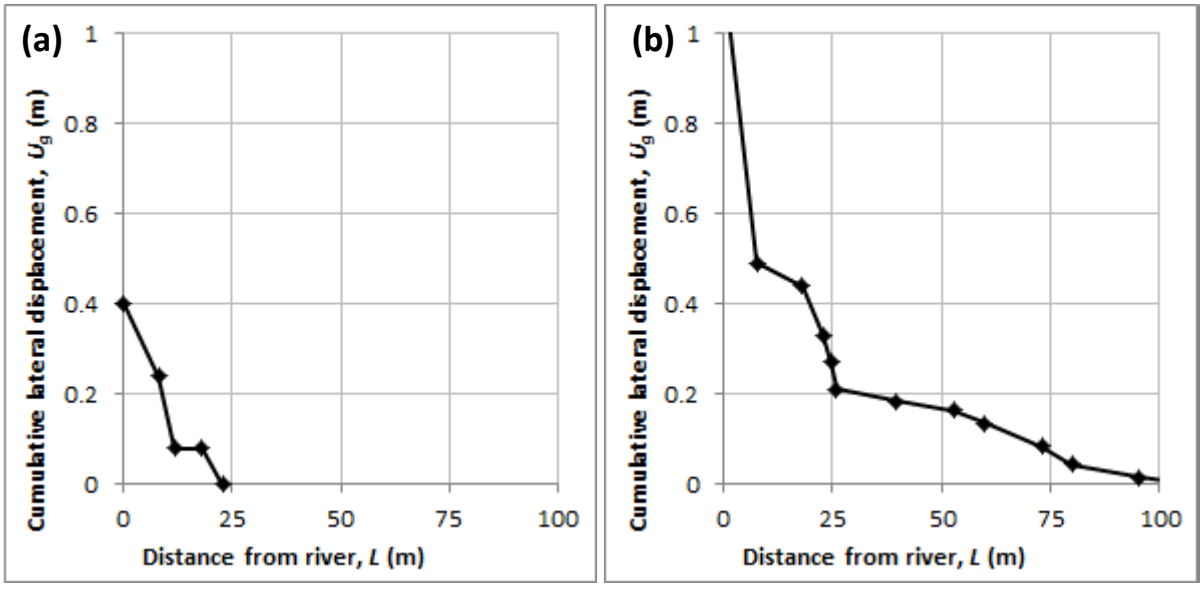

Figure 3-42: Distribution of permanent lateral displacement with distance from the river banks at ANZAC Bridge, (a) north bank, immediately to west of bridge, (b) south bank, 20 m west of bridge

Bridge Damage

The dominant spreading-induced damage mechanism involved deck-pinning and abutment back-rotation, shown below in Figure 3-43. The south abutment back-rotated to a permanent tilt of about 6 degrees, while the north abutment reached a permanent tilt of 4-5 degrees.

Figure 3-43: ANZAC Bridge, 24 February 2011, showing elevated water levels and spreading-induced damage mechanism

As can be seen in Figure 3-44, abutment back-rotation was accompanied by the independent lateral displacement of the pedestrian underpass resulting in the separation of these two elements. On the south abutment the relative lateral displacement between underpass and abutment toe ranged from 400 to 650 mm with a vertical offset of 150 to 250 mm. Since the piles of the underpasses are founded in the liquefying layer it can be inferred that they effectively floated with the lateral ground movement and as such are representative of the total foundation displacement (Cubrinovski *et al.* 2013). Multiplying the back rotation of the abutment by its lever arm gives a displacement due to

rotation of 150 mm. By adding this to the assumed displacement required to close the gap between the deck-beam and abutment (30 mm) and the lateral offset between underpass and abutment it can be calculated that the permanent lateral displacement of the foundation soils on the southern abutment was between 0.5 and 0.8 m. Note that these values are considerably less than the lateral displacements measured in the free-field immediately adjacent to the bridge.

As a result of the large gap created between the abutment toe and the underpass the tops of the steel H-piles supporting each abutment were clearly visible from the underpass. Rubber tyres and other rubbly fill in this area were also exposed.

Figure 3-44: ANZAC Bridge south abutment (a) back-rotation of abutment, (b) separation of underpass from abutment

On the northern abutment (Figure 3-45) the measured lateral offset between the underpass and the abutment toe ranged from 240 to 380 mm, while the displacement due to abutment rotation was calculated to be 100-120 mm. This implies that the permanent lateral displacement of the foundation soils was between 0.3 and 0.5 m.

Figure 3-45: ANZAC Bridge north abutment (a) back-rotation of abutment, (b) separation of underpass from abutment

Both of the bridge pier column-bents sustained visible damage, particularly pronounced at the pier-beam connections. Concrete spalling due to excessive compressive forces appeared to be concentrated at the corners of each pier, as can be seen in Figure 3-46a, however further inspections of all piers showed that the cracks extended only as far as the cover concrete and therefore structural integrity remained. The southern pier group was on a lean consistent with the direction of the south abutment back-rotation (Figure 3-46b), however given access constraints this angle was unable to be measured. Decking rebar was exposed at the external deck-abutment interfaces however this damage was not deemed serious and the bridge remained in service after each earthquake. At the time of writing, vehicle restrictions on the bridge are still in place which limit its use for oversize and non-standard vehicles without appropriate permits. Current repair plans for ANZAC Bridge involve the temporary removal of the spans supported by the abutments while the abutments and abutment piles are demolished. These will be replaced with new abutments supported by substantial piles, and ground improvements will be carried out in the area to minimise the impacts of any future occurrences of liquefaction and lateral spreading (Cubrinovski *et al.* 2014).

Figure 3-46: ANZAC bridge pier damage, (a) concrete spalling on southern pier column, (b) back-rotation of southern pier group

3.7.7.5 Pages Road Bridge

Pages Road Bridge (sometimes referred to as New Brighton Bridge), constructed in 1931, is a cast *in situ* monolithic structure running approximately east-west across the Avon River. The 23 metre long three-span deck is supported by concrete abutments and two wall piers, each founded on 14 driven, 350 mm diameter, octagonal concrete piles. The pier caps and abutments are skewed 6° in plan relative to the axis of the bridge. Arched beams, cast integral with the piers and abutments, run longitudinally along each span. A bridge elevation can be seen in Figure 3-47. Each abutment has wingwalls although they are different at either end of the bridge; the west abutment has a sloped rock façade while the east abutment has curved concrete walls. The west abutment lies on the inner point-bar deposit river bank while the east abutments lies on the outer cut-bank of the river bend.

The soils on the west abutment comprise a layer of fine sand to 2 metres depth, then a layer of silt to 3 metres depth. Below this, medium to fine sand exists to at least 25 metres depth. The upper three metres of the thick sand layer (3 – 6 m depth) are loose to medium dense (SPT blowcount N = 2-12) and as such are susceptible to liquefaction. The deeper layers are medium dense to dense. On the east abutment a 1.5 m thick layer of fill overlies fine to medium sand to a depth of at least 20 metres. Up to 7 metres depth the sand is medium dense (SPT blowcount N = 9-14), becoming dense below this point (N > 22).

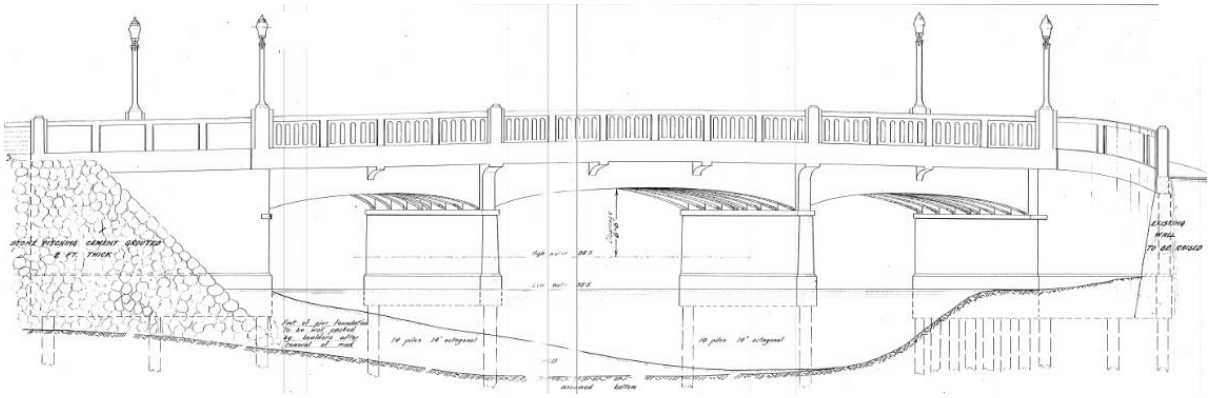

Figure 3-47: Pages Road Bridge, elevation

Land Damage

Some liquefaction occurred in the vicinity of the bridge during the Darfield earthquake, but the bridge itself remained unaffected (Palermo *et al.* 2011). Damage to the surrounding area was exacerbated following the Christchurch earthquake, and moderate lateral spreading was evident both to the northwest and southeast of the bridge. While lateral spreading transects were not carried out here by the University of Canterbury team, LiDAR measurements indicate that the cumulative displacement of the ground towards the river on the eastern bank was between 0.3 and 0.4 m (Figure 3-48). Figure 3-49 shows ground cracking and slumping on both sides of the river; (a) on the west abutment looking northwest and (b) on the east abutment looking southeast. It was noted that the magnitude of land damage on either side of the river was similar, although the presence of the roundabout on the eastern side may have prevented some of the typical manifestations of liquefaction from being visible. Ground settlement in the order of half a metre was apparent on both bridge approaches.

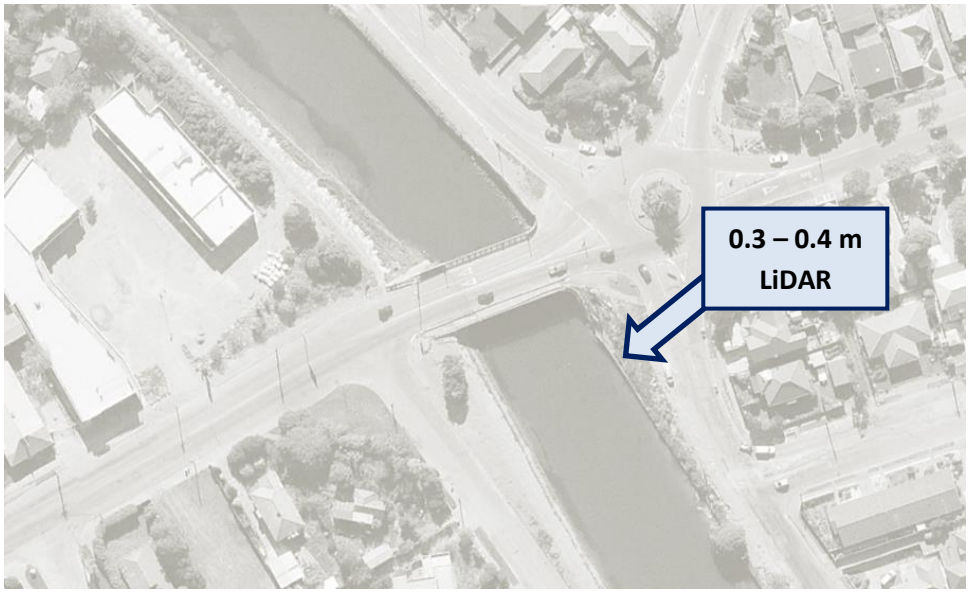

Figure 3-48: Aerial view of Pages Rd Bridge showing LiDAR measurements of lateral spreading.

Figure 3-49: Pages Rd Bridge, (a) west abutment looking north-west, spreading/slumping cracking of river bank, (b) east abutment looking south-east, spreading/slumping cracking of river bank.

Bridge Damage

Cracking and settlement of the approaches developed on both abutments as a result of lateral spreading and ground slumping (Figure 3-50a). Although both abutments and the eastern pier

suffered minor rotation and cracking, the overall performance of the structure remained good. Moderate damage occurred to the services (water and power cables) running along the bridges underside, with one water pipe broken and the exposure of power cables underneath the deck. All wingwalls rotated independently of the bridge structure, and cracking was visible in the rock façades of both western wingwalls (Figure 3-50b). Concrete cracking was also visible in the eastern wingwalls. Remedial works have been undertaken to stitch the wingwalls to the abutments to prevent any further separation from occurring.

The abutments are prone to additional rotation in the event of further liquefaction and lateral spreading, however the bridge remains open and serviceable with a live load-carrying capacity above Class 1 (the heaviest class of road-using vehicles) and no significant reduction in as-built capacity of the structure from earthquake damage (Christchurch City Council 2011b). Permanent recovery works are currently in the process of being designed.

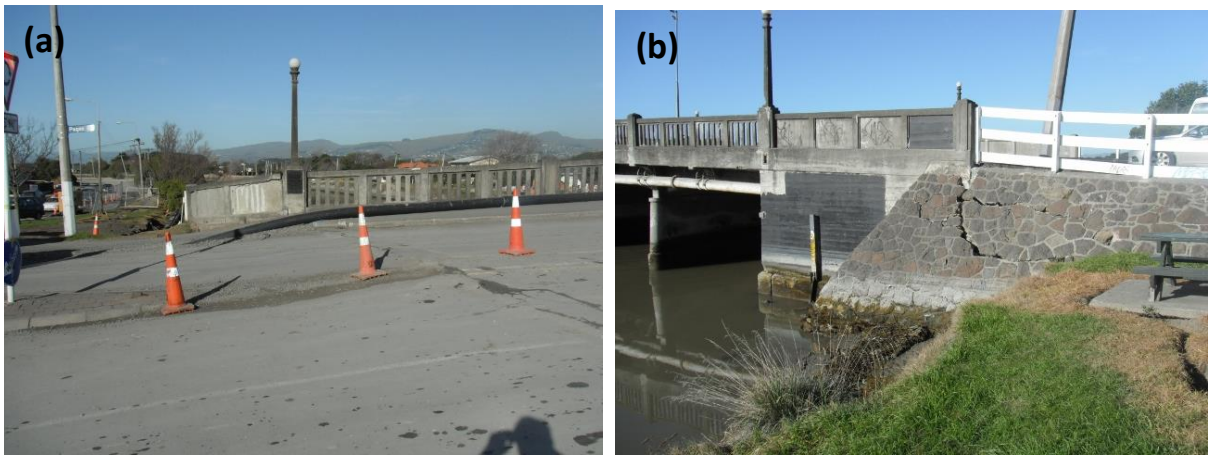

Figure 3-50: Pages Road Bridge, (a) east abutment approach settlement, (b) west abutment settlement and cracking through rock façade.

3.7.7.6 South Brighton Bridge (Bridge Street)

South Brighton Bridge (otherwise known as Bridge Street Bridge) was constructed in 1980 and runs approximately east-west across the mouth of the Avon River where it discharges into the estuary. The three-span bridge is 65 metres long with a 25° skew in plan and supports one traffic and one pedestrian lane in each direction. The bridge superstructure consists of a continuous *in situ*

reinforced concrete deck on top of precast, post-tensioned concrete I beams supported by two octagonal "hammerhead" reinforced concrete piers and seat-type concrete abutments (Figure 3-52). The two octagonal piers are supported by twelve raked 13.3 metre long piles, while the abutments are each supported by ten raked 18.7 metre long piles, all octagonal in shape, 450 mm diameter precast reinforced concrete (Figure 3-53). Prior to the Darfield earthquake there were elastomeric bearing pads at the abutment-bridge deck connections, however as a result of damage induced by this event these were removed, and in their place temporary hardwood packing was present when the Christchurch earthquake occurred (Palermo *et al.* 2011). In the pier caps steel shear keys link the superstructure rigidly to the piers.

Prior to bridge construction the site was originally a wetland, typical of a highly liquefaction-prone area. As a result, extensive infilling was required such that approach embankments were constructed on both sides of the river extending inland up to 200 metres on either side. At the river banks this approach fill is approximately 4 metres high. On either side of both approach embankments swampland still predominates as can be seen below in Figure 3-51.

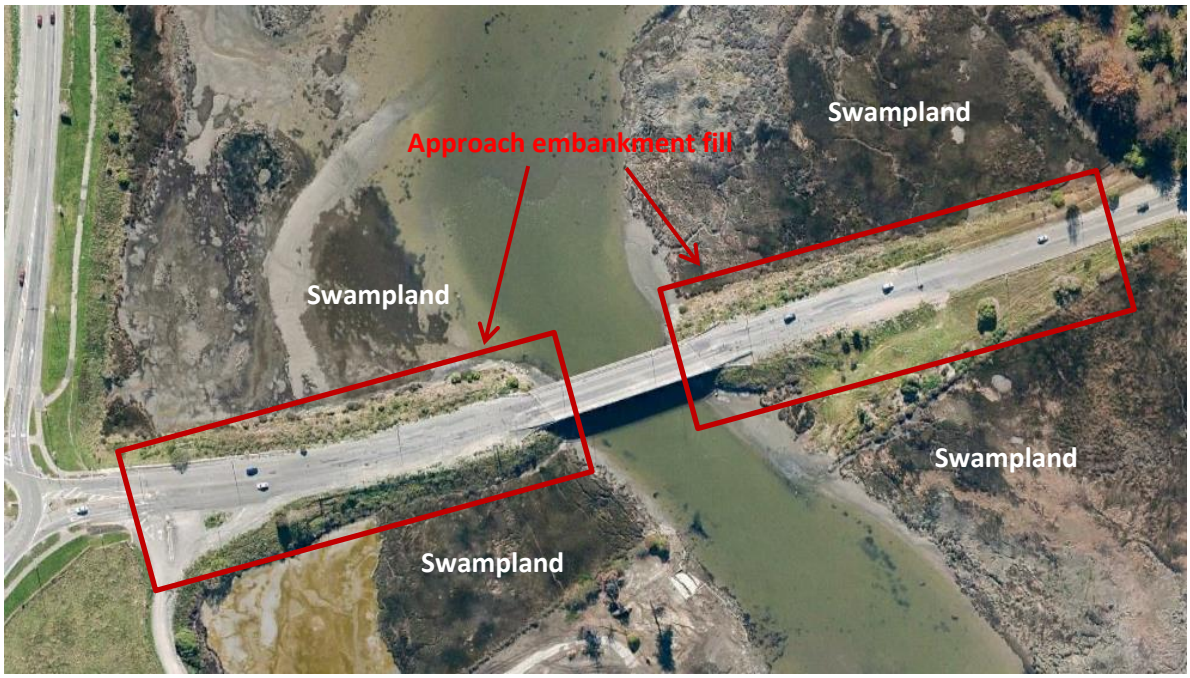

Figure 3-51: South Brighton Bridge and surroundings, highlighted are the constructed fill embankments and natural swampland on all sides

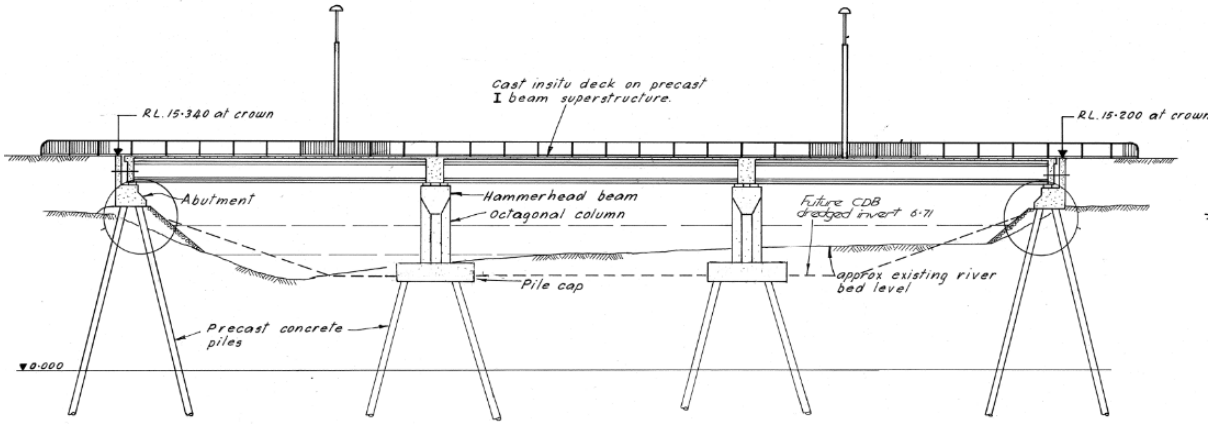

Figure 3-52: South Brighton Bridge, elevation

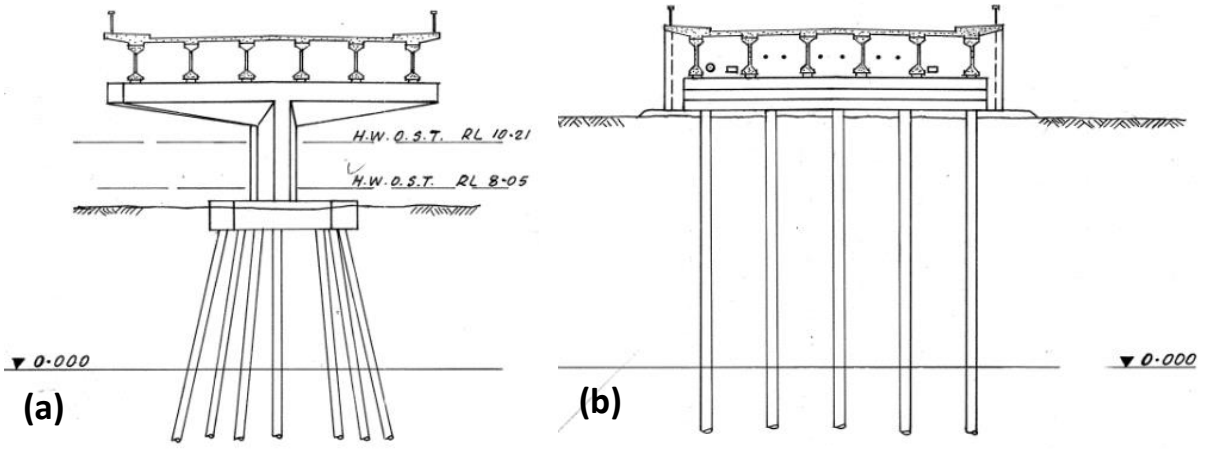

Figure 3-53: South Brighton Bridge sections, (a) pier and pier piles, (b) abutment piles

Geotechnical site investigations carried out on each side of the bridge indicate that the west abutment consists of, first, 4 metres of uncontrolled fill material. Beneath this, in the native soils, from 4 to 6 metres depth is a layer of loose fine to medium sand followed by a layer of medium-coarse gravel to 8 metres depth. Below this fine to medium sand exists down to a depth of at least 30 metres. From 8 to 13 metres depth this sand is medium dense (SPT blowcount N = 10-15) and below 13 metres the density is much higher, with N > 23 extending into and below the bearing stratum of the piles. On the eastern side of the bridge the upper 4 metres are also an uncontrolled fill material; beneath this to 6 metres depth there is sandy gravel, sandy silt and fine sand, relatively loose. From 6 metres depth to more than 25 metres depth is a layer of fine to medium sand, medium dense from 6 to 11 metres depth (SPT blowcount N = 8-19, CPT tip resistance q_c = 7-12 MPa) and denser below this (N > 20, $q_c \approx$ 15 MPa).

Land Damage

Following the Darfield earthquake significant cracking of the approach embankments (parallel to the roadway) on both sides of the bridge occurred. This was due to slumping of material immediately adjacent to the abutments occurring as a result of lateral ground movement towards the river. Lateral spreading transects measured to the south of the western abutment indicate that free-field displacement of the swampy ground in this vicinity was in the order of 1 metre (see Figure 3-54, where the values in brackets are those measured following the Darfield earthquake). Liquefaction ejecta was evident in the area surrounding both approaches and lateral spreading was apparent in the native swampland soils on either side of both approaches.

Following the Christchurch earthquake even more liquefaction, approach slumping and lateral spreading occurred, severe on both sides of the bridge. The lateral spreading transects performed in the swampland immediately to the south of the west abutment indicated that free field displacements towards the river were in the order of 2-3 metres (see Figure 3-54), an increase of approximately 100-200% on the Darfield event. The surveys labelled (a) and (b) in Figure 3-54 are plotted in more detail in Figure 3-55, where it can be seen that the cracking consists mainly of several large cracks, demonstrated by the steep slopes in both plots. The zone over which these cracks extend inland is approximately 50 metres, however it should be noted that transect (a) was halted around 40 metres from the river due to increasingly wet and difficult ground conditions, so more cracks may well have been present beyond this point. Figure 3-56a shows the terrain and cracks in which this transect was performed; it is a view looking southeast from the west abutment.

Figures 3-56b and c show the extent of the sideways slumping and cracking of the approach fill material parallel to the roadway; this resulted in large settlement of the approaches and vertical offsets between the bridge deck and embankment approach being observed. Unlike the unconstrained spreading of the river banks either side of the bridge, the deformations observed in the embankments themselves were significantly affected by the bridge structure. Lateral spreading of the embankments towards the bridge was restrained by the stiff bridge deck and the combination of this with the 25° skewed geometry of the bridge led to a bias in the imposed kinematic loads and constraints. As is illustrated in Figure 3-57, this caused the east abutment approach to displace towards the north (relative to the bridge deck) by 250 mm, while the west abutment approach moved relatively to the south by 230 mm. This effect can also be seen in Figure 3-59c.

The southern sides of both embankments performed worse than the northern sides; on the west abutment there was more global ground settlement than the east, possibly due the larger lateral spreading cracks visible to the immediate south of the west abutment. On the other hand, the east

abutment performed worse than the west in terms of local slumping, with larger ground displacements towards the south creating significant cracks in the direction parallel to the roadway.

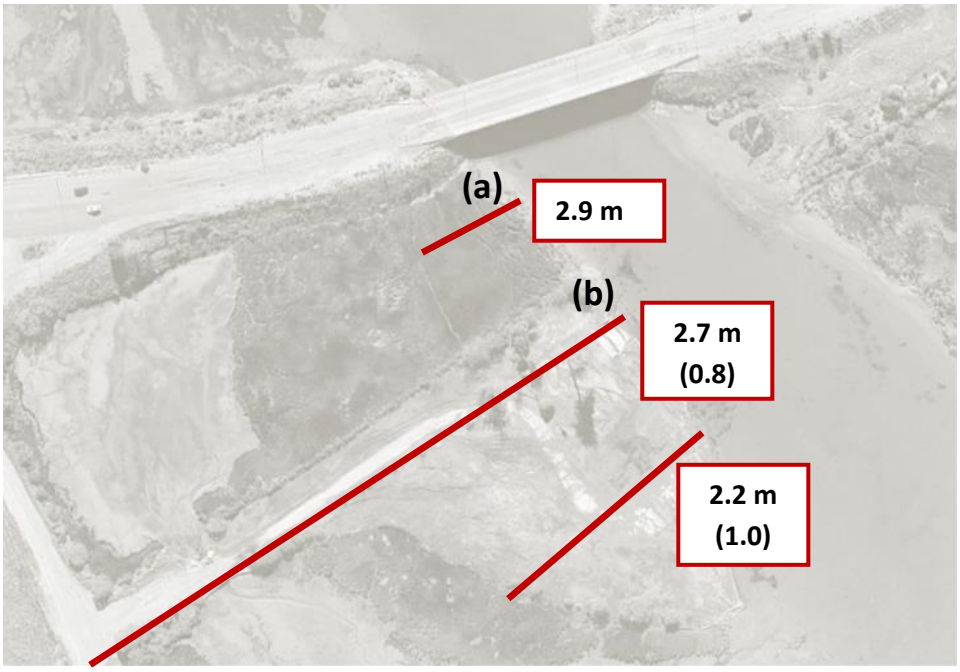

Figure 3-54: Aerial view of South Brighton Bridge showing location of lateral spreading transects and cumulative measured displacements at the river banks (note that values in brackets are those measured after the September 2010 earthquake)

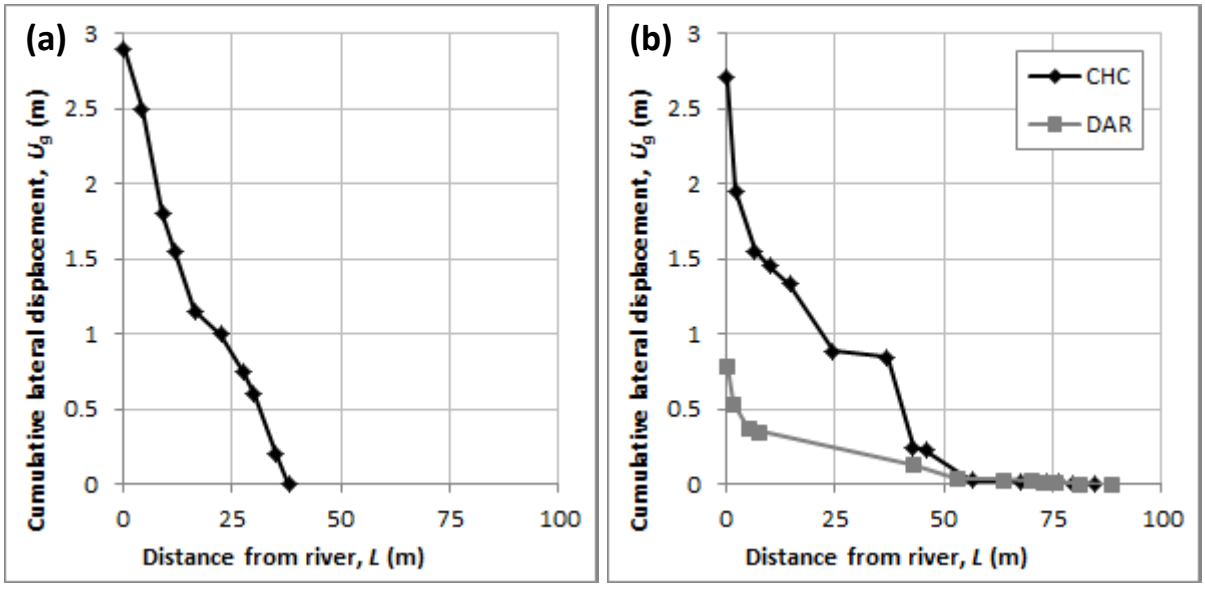

Figure 3-55: Distribution of permanent lateral displacement with distance from the river banks at South Brighton Bridge, (a) west bank, 30 m south bridge, (b) west bank, 80 m south of bridge (both significant earthquake events shown)

Figure 3-56: Land damage in vicinity of South Brighton Bridge, (a) lateral spreading cracks through swampland to immediate south of west abutment, (b) sideways slumping/cracking of fill material, north side of west abutment, (c) sideways cracking/slumping of fill approach material, south side of east abutment.

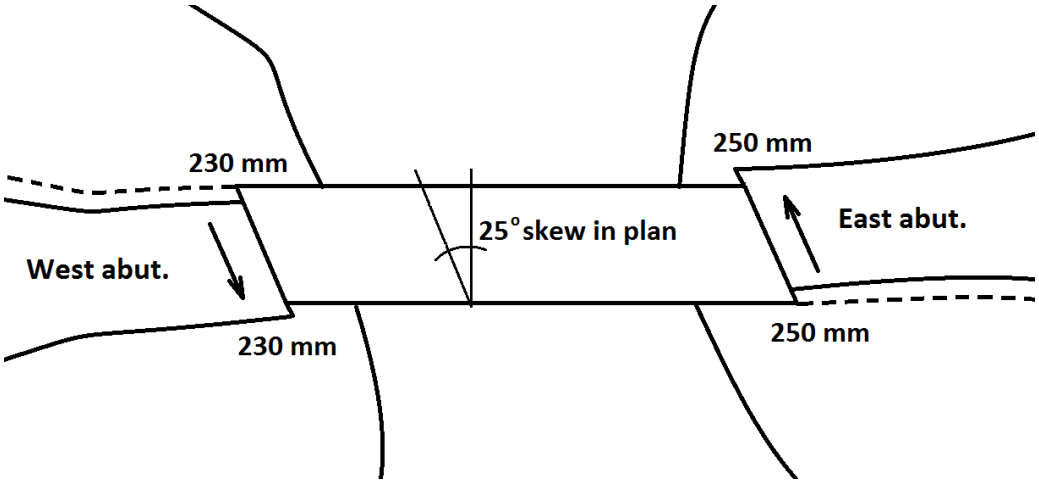

Figure 3-57: Schematic view of South Brighton Bridge showing the 25° skew in plan, as well as the relative horizontal offsets between bridge deck and approaches measured as a result of the kinematic constraints imposed by the geometry of the superstructure.

Bridge Damage

South Brighton Bridge demonstrated the typical spreading-induced deck-pinning/abutment back-rotation mechanism and associated damages. Some damages were initiated following the Darfield earthquake, however presented below are the cumulative effects of both the Darfield and Christchurch events combined, due to reconnaissance works being undertaken following the Christchurch earthquake. Figure 3-58 below, photos taken by members of the GEER reconnaissance team following the Darfield and Christchurch events, shows a comparison of the soil displacements observed under the east abutment as a result of these two significant events. It can be seen that, even though approach settlement and lateral displacement was initiated in the Darfield event, the ground movements after the Christchurch event were much larger both in magnitude and severity.

Figure 3-58: South Brighton Bridge east abutment, comparison of the soil displacement under east abutment after the (a) Darfield and (b) Christchurch earthquakes (GEER 2011).

The back-rotations of both the west and east abutments were measured to be 7-8° (west abutment is shown in Figure 3-59a), and settlement and spreading of the underlying embankment soils exposed the abutment piles (Figure 3-59b). These piles rotated along with the abutment structure and clear evidence of tensile cracking was visible in the river-facing sides of both the front and back rows of piles (Figure 3-60c). Conversely, concrete spalling and crushing was more prevalent on the land-facing sides of the piles as can be seen in Figure 3-60b. Figure 3-60a shows flow of liquefaction ejecta around the base of an abutment pile. Some minor concrete cracking between the abutment and the wingwalls was visible, and in general the rotation of the wingwalls was approximately 1 degree more than that of the abutments themselves.

There was no appreciable damage to the bridge superstructure, apart from some minor spalling at the deck girder ends due to pounding between the deck and abutment seat. The bridge abutments are vulnerable to further rotation in future seismic events, however there is low risk to road users due to the robust nature of the bridge with the abutments remaining well connected and propped apart by the superstructure. Following temporary approach repairs and infilling of offsets between the bridge deck and approach, the bridge was back in service nearly immediately after each event. Permanent recovery works are currently being detailed (Christchurch City Council 2011c).

Figure 3-59: South Brighton Bridge abutment back-rotation, (a) west abutment (north face), (b) east abutment looking southeast, noticeable land cracks shown, (c) skewed movement of southwestern approach relative to bridge deck.

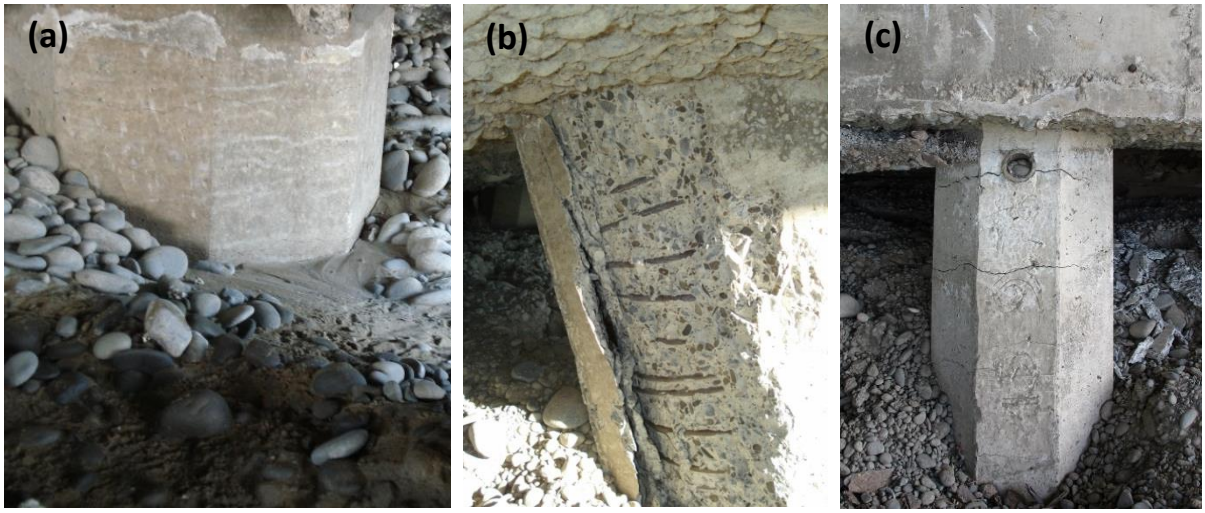

Figure 3-60: South Brighton Bridge observed pile damages, (a) flow of liquefaction sand ejecta around pile, (b) concrete spalling and exposure of transverse reinforcing, (c) flexural cracking in the river-facing side.

3.8 Summary

The 2010-2011 Canterbury earthquakes, in particular that of February 22nd 2011, caused widespread liquefaction throughout Christchurch's eastern suburbs and parts of the CBD. Along the Avon River, liquefaction was the cause of substantial lateral spreading which affected all bridges to the east of the CBD. The most commonly observed bridge damage mechanism associated with liquefaction and subsequent lateral spreading was that of deck-pinning and abutment back-rotation. This is a direct result of the short, stiff bridge decks restraining lateral ground movement in the longitudinal direction. Associated damages included substantial approach settlements and pile damages immediately beneath the abutment-pile interfaces.

The key findings at each of the 9 bridges investigated in more detail are summarised in Table 3-3.

Table 3-3: Summary table of damage to investigated bridges, including permanent ground displacements, abutment rotations and dominant damage features

Bridge	Integral/ Segmental structure	Approach settlement (inner/ outer bank)[1]	Free-field lateral spreading displacements (inner/ outer bank)[2]	Foundation soil permanent lateral displacements (inner/ outer bank)[3]	Abutment rotations (inner/ outer bank)[4]	Pile top disp. associated with abutment rotation[5]	General damage features and mechanisms
Remembrance	Int.	Minor/ NS	NS/ NS	NS/ NS	NS/ NS	Not applicable	Wingwall cracking, minor arch hogging, pavement damage
Hereford	Int.	Minor/ NS	Minor/ NS	NS/ NS	1-1.8°/ 0.6-1°	Not applicable	Wingwall cracks, hairline cracking deck beams, pavement damage
Colombo	Int.	NS/ 0.1m	Minor/ 0.1-0.3m	50mm/ 0.1m	0.2-1°/ 2.1-3°	Not applicable	Buckling of exterior steel bridge arch, pavement damage
Fitzgerald	Seg.[6]	0.2-0.5m/ NS	0.4-0.9m/ 0.2-0.25m	0.3-0.5m/ 0.1m	3.5-5°/ <1°	0.1-0.15m/ 50mm	Abutment back rotation, some pile hinging, pavement damage, spalling in deck girders
Dallington	Int.	0.5-1m/ NS	0.5-0.9m/ NS	<0.3m/ NS	0.8-2.2°/ NS	50-120mm/ NS	Approach settlement, pier/abutment cracking, some pile hinging
Avondale	Seg.[6]	~0.5m/ Minor	0.6-0.9m/ Minor	0.2-0.4m/ 0.1m	7-8°/ 1.5-3°	0.2-0.3m/ 50-100mm	Abutment back rotation, spalling in deck beams, approach settlement

ANZAC	Seg.	0.15-0.25m/ 0.1-0.4m	0.9-1.1m/ 0.4m	0.5-0.8m/ 0.2-0.5m	6°/ 4-5°	0.15m/ 0.1-0.12m	Approach settlement, abutment back rotation, pier cracking pavement damage
Pages	Int.	0.3-0.5m/ 0.3-0.5m	NA/ 0.3-0.4m	NA/ NA	NA/ NA	NA/ NA	Approach settlement, abutment/wingwall cracking
South Brighton	Seg.	>0.5m/ >0.5m	NA/ 2-3m	0.3-1m/ 0.3-1m	7-8°/ 7-8°	0.25-0.35m/ 0.25-0.35m	Approach fill slumping, abutment back rotation, sideways/skewed movement, pile cracking

1 - Settlement measured relative to bridge deck
2 - Taken from measured lateral spreading transects, LiDAR, or both where available
3 - Taken as pile top displacement associated with rotation plus any gapping observed between pile fronts and river
4 - Measured on abutment walls
5 - Abutment rotation (tan(angle)) multiplied by lever arm (height of abutment)
6 - With steel brackets used to try and create an integral structure

NA = not available
NS = not significant (i.e. less than 50 mm and/or not in the direction of the river)
"Minor" refers to anything less than, or in the order of, 0.1 m

The following key findings can be taken from the bridge investigations:

- Overall, bridges performed better than other engineered structures in the Canterbury earthquakes; most of the damage was due to liquefaction and associated lateral spreading, not due to the inertial effects of ground shaking. Any prolonged bridge closures were generally due to failures in the approach fill rather than the bridge structures themselves.
- Both integral and segmental bridges on piles exhibited the same deformation mechanism of deck-pinning and abutment back-rotation. Segmental bridges exhibited abutment back-rotations in the order 4-8 degrees, while integral bridges exhibited much smaller rotations, in the order of 1-2 degrees. These back rotations resulted in, sometimes large, permanent displacements of pile tops, and consequent damages in this zone. Where pile tops were visible the most commonly observed damages were cracking along the tension faces (river side) and crushing/spalling along the compression faces (land side). The rigid abutment-pile connections in conjunction with the displacement demands would have caused large bending moments near pile heads.
- The fact that all the bridges considered had relatively short, stiff decks was a major contributing factor to the observed characteristic deformation mechanism. It meant that the lateral spreading displacements imposed on the bridges were restrained by the deck structure. This resulted in the deck-pinning effect and consequent abutment back-rotation about the deck/abutment point of collision because the large lateral movements of the foundation soils were not able to be resisted by the abutment piles.
- The case studies indicate that permanent lateral movements of the foundation soils were larger than the displacements of the abutment pile tops but smaller than the free field lateral spreading displacements. This suggests that using free field lateral spreading displacements to analyse bridge performance may be overly conservative.
- Bridges on pile foundations did not settle appreciably, as such where approaches settled and/or slumped as a result of liquefaction and lateral spreading, large vertical offsets occurred between approaches and bridge decks. This often led to damages to the services carried by bridges, such as water pipes, sewer pipes and communications cables.
- Limited damages were observed in the bridge decks.
- In general, lateral spreading displacements, foundation soil displacements, abutment rotations and approach settlements were larger on the inner banks of meandering river loops. These point-bar deposits are aggraded in the continual erosion-deposition process and as a result are generally composed of looser materials than outer cut-banks, making them more susceptible to liquefaction.

- All the measurements and observations made in this section (unless stated or referenced otherwise) were made by the author and other members of the University of Canterbury reconnaissance team after the 22nd February 2011 earthquake. While certain other papers have been referenced, some discrepancies in measurements have been encountered, and, where this has occurred the values presented herein are those measured by the University of Canterbury reconnaissance team and have been checked to ensure their validity.

In chapter 5, pseudo-static analyses are carried out on the ANZAC and Dallington Bridges. The observations presented in this chapter are used as inputs to the modelling process (i.e. permanent lateral ground displacements) as well as verifications of the outputs of the modelling process (e.g. abutment back-rotations and other observed damages).

4 Pseudo-static analysis

4.1 Introduction

The pseudo-static analysis method of Cubrinovski *et al*. (2009a) is chosen for the analysis of ANZAC and Dallington Bridges, and is outlined in this chapter. Three alternative methods for calculating soil-spring properties are also briefly outlined. Particular focus is given to pseudo-static analysis and the different methods of *p-y* spring construction which exist for liquefying and laterally spreading soils.

4.2 Background

There are many methods available for the analysis of piles in liquefiable soils which range from relatively simple approximate methods to highly complex soil-pile-structure interaction analyses. While the more rigorous methods permit a detailed evaluation of a system's seismic response, they require more geotechnical inputs, computational power and specialised user knowledge to appropriately interpret. As such, for the preliminary design and assessment of design of piles in liquefiable soils, simplified analyses are both attractive and practical.

The pseudo-static method of analysis is a relatively simple, practical engineering approach based on conventional geotechnical data (e.g. SPT blowcount) and routine computations. It can be applied without excessive computational power or specialised knowledge, yet it can capture the basic mechanisms of pile behaviour, hence is a widely adopted approach in current practice and seismic design codes. The application of this method to piles in liquefying soils, however, still retains uncertainties associated with capturing significant dynamic spatial and temporal changes in a static analysis. In order to satisfy the objectives of a seismic performance analysis, it is desirable that the pseudo-static model can:

- Capture the relevant deformation mechanism for piles in liquefying soils
- Permit the estimation of inelastic deformation and damages to piles
- Address the uncertainties associated with seismic behaviour of piles in liquefying soils

Pseudo-static models are typically constructed by means of a beam-spring approximation, whereby piles are represented by vertically-placed beam elements and horizontal springs represent the

lateral stiffness of the surrounding soil. The effects of ground movements as external actions on piles can be allowed for by applying a static soil displacement function to the ends of the soil springs, while the effects of horizontal seismic motions can be allowed for by incorporating a horizontal force at the pile head corresponding to the inertial force from the superstructure.

Since pile foundations are particularly vulnerable to liquefaction and lateral spreading, their analysis is an important issue and is particularly relevant in seismic areas of New Zealand. The phenomena of liquefaction and lateral spreading are inherently complex and are subject to a high level of uncertainty. This may suggest that, when an analysis is carried out, the most important consideration is not the modelling itself, but rather the way in which key uncertainties are handled.

The pseudo-static method of analysis is suited to practical engineering because it is relatively easy to understand and implement despite the complex mechanisms it is modelling. It estimates the peak response of a pile (or pile system), that is maximum curvatures, strains, bending moments or shear forces, which result from earthquake loading. The principal assumption of a pseudo-static analysis (PSA) is that complex dynamic loadings due to earthquake shaking or lateral spreading can be idealised as static actions.

In general engineering practice there are two main approaches used in the PSA of piles subjected to lateral spreading and/or cyclic earthquake loading: force-based methods and displacement-based methods. These approaches differ in the way in which the lateral load on the pile due to ground movement (kinematic load) is treated. Force-based methods represent the pressure from laterally spreading soil against the pile as an equivalent static load on the pile; applied either as discrete forces or as a distributed load along the length of the pile. These loads essentially “push” the pile in the direction of the lateral spreading (see Figure 4-1a). One main drawback of force-based methods is that they do not account for soil and pile interaction; that is to say that they do not consider the dependence of the mobilised lateral soil pressure on the pile’s response. This is a function of the relative displacement between the soil and the pile. Displacement-based methods, on the other hand, do consider the compatibility of the mobilised soil pressure with the relative movement between the soil and pile. Displacement-based approaches work by applying lateral ground displacements to the free ends of soil springs attached to the pile, as is illustrated in Figure 4-1b. In this scenario, the forces that develop in the soil springs are compatible with the relative displacement between soil and pile, thus the induced pile response is compatible with the mobilised lateral soil pressure.

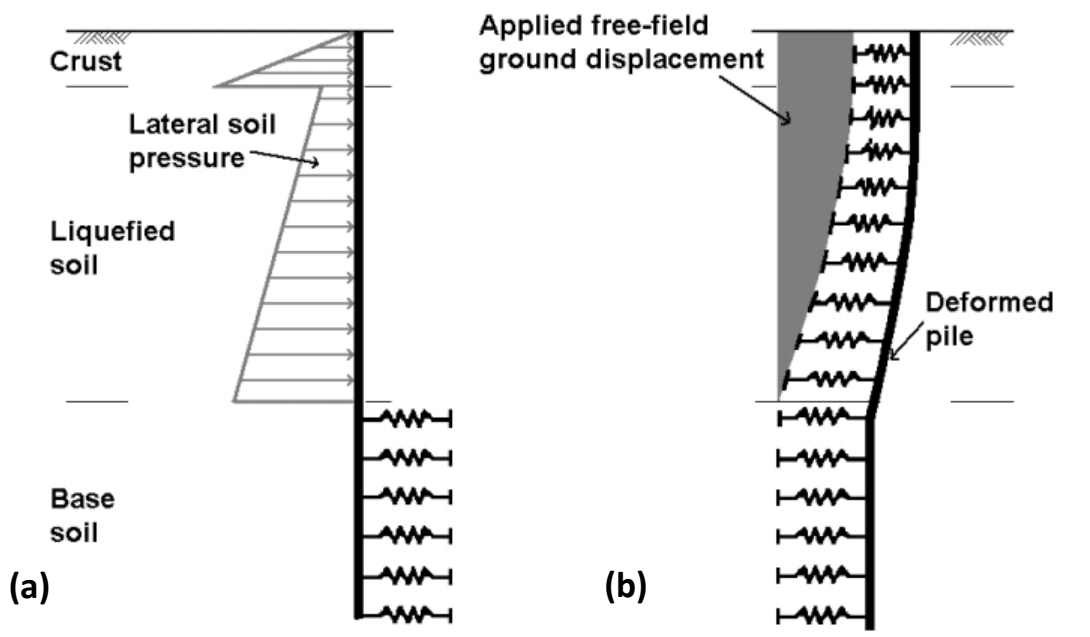

Figure 4-1: Pseudo-static methods for analysis of piles, (a) force-based approach, (b) displacement-based approach (Cubrinovski et al. 2009a)

4.3 PSA method of Cubrinovski et al. (2009a)

The analytical model outlined in Cubrinovski *et al.* (2009a) follows on from the work of Cubrinovski and Ishihara (2004) and is a simplified pseudo-static, displacement-based analysis. The model can account for the two critical stages of earthquake loading; the cyclic loading phase and lateral spreading phase. However, since both the characteristics of the foundation soil and the lateral loads on piles are very different between these phases, they are considered separately in the simplified pseudo-static analysis of piles.

4.3.1 Cyclic loading phase

During the cyclic phase of loading, piles are subjected to cyclic horizontal loads from both the ground displacements and the inertial loads from the superstructure. Within only a few seconds of strong ground shaking, excess pore water pressure in liquefiable soils may reach the level of the effective overburden stress; during this time the soil stiffness reduces towards zero. This reduction in stiffness and strength of liquefied soil is accompanied by cyclic lateral ground displacements and inertial loads from the vibration of the superstructure (Figure 4-2a).

4.3.2 Lateral spreading phase

The lateral spreading phase of loading typically occurs near the end of earthquake shaking or once shaking has ceased. At this point, the primary loads on piles are kinematic loads from the unilateral displacement of the ground, which can be into the order of several metres in the down-slope direction (or towards waterways/a free face), and any inertial loads are comparatively small (Figure 4-2b).

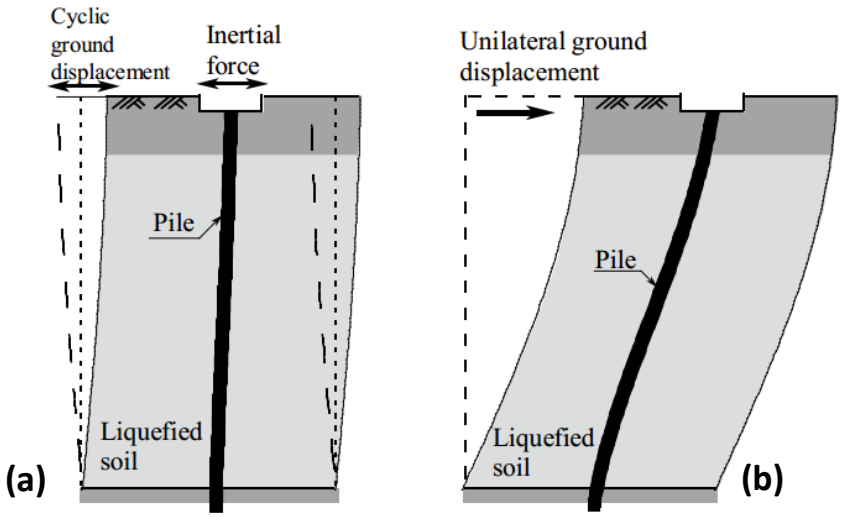

Figure 4-2: (a) loads on pile during strong shaking (cyclic phase), (b) post-liquefaction lateral spreading (Cubrinovski et al. 2012)

4.3.3 Model construction

A finite-element (FE) beam-spring model is described in this approach which represents the pile-soil system. One key requirement of the analysis (as outlined in the introduction) is the estimation of inelastic deformation and damages to piles, so simple but non-linear relationships are used for the components of the soil-pile model. The pile is modelled using a series of beam elements with tri-linear moment-curvature relationships, and the soil is modelled using bi-linear springs. Both the stiffness and strength of these soil springs can be degraded in order to account for the effects of liquefaction (or other non-linear behaviour).

Traditionally, a three-layer model is constructed which consists of a liquefied soil layer sandwiched between non-liquefied crust and base layers. In saying this, however, the model can also easily

incorporate highly stratified deposits, but for the purposes of the explanation to follow the typical three-layer deposit will be that which is referred to. The general model formulation for this type of setup can be seen in Figure 4-3. The following sections will describe the model parameters in more depth.

In the model, equivalent static loads can be applied to the pile: a lateral force at the pile head (*F* in Figure 4-3) which represents the inertial load on the pile from superstructure vibration, and a horizontal ground displacement (U_G in Figure 4-3) applied to the free ends of the soil springs in the liquefied layer and non-liquefied crust, representing the kinematic load on the pile due to lateral ground movement (cyclic or lateral spreading) in the free field. It is assumed that the crust layer gets carried along with the underlying liquefied soil and undergoes that same ground displacement as the top of the liquefied layer, U_G. The effects of axial loads and geometric non-linearity are usually ignored in this approach, but they can be accounted for if such features are available in the finite element software used.

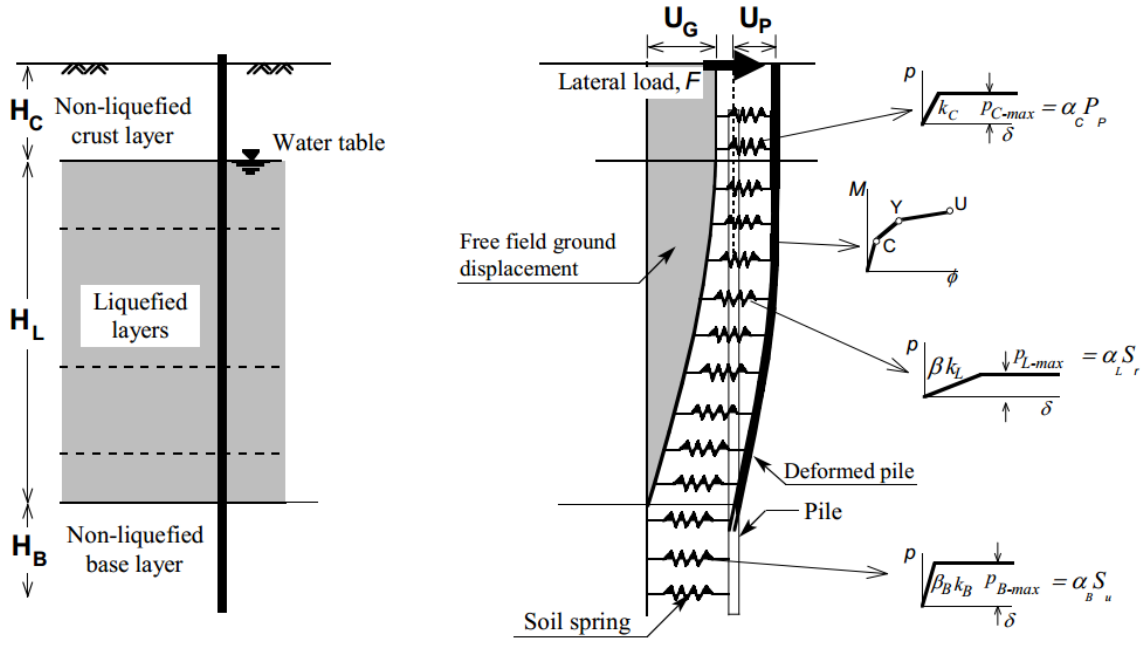

Figure 4-3: Beam-spring model for pseudo-static analysis of piles in liquefying soils; model parameters and characterisation of nonlinear behaviour (Cubrinovski et al. 2012)

4.3.4 Beam elements

In this pseudo-static model a pile (or piles) is represented by beam elements which have tri-linear moment-curvature (M-ϕ) relationships. For a reinforced concrete pile, the three points which define the shape of the M-ϕ plot would correspond to:

1. Cracking (M_c) – the point where tensile stress in the concrete exceeds concrete tensile strength. The initial slope of the M-ϕ plot up to this point is equivalent to the elastic flexural stiffness of the pile (EI).

2. Yielding (M_y) – the point where the yield stress of the reinforcing steel exceeds reinforcing yield strength.

3. Ultimate (M_u) – the point where compressive stress in the concrete exceeds the crushing strength of concrete.

For other sorts of piles, appropriate points of change in slope can also be chosen.

4.3.5 Soil springs

The formulation of this model is such that non-linearity in the soil is approximated by assigning each soil spring a bi-linear load-deformation (p-δ or p-y) relationship. The soil pressure (p) mobilised is a function of the relative displacement reached between the soil and pile (δ or y). For each soil layer (crust, liquefied layer, base layer), and even each soil spring, this p-y relationship differs. Each layer will be dealt with separately below, however it is first useful to explain the basic components which define the formulation of each soil spring. Each spring has an initial spring stiffness, κ [FL^{-1}] up until the soil's yield point (δ_y or δ_u), at which point its ultimate pressure (p_y or p_u) is mobilised. Past this point it is assumed that the soil spring has negligible tangent stiffness and is exerting the ultimate pressure on the pile. Reduced stiffness due to liquefaction can be accounted for by applying a degradation factor β to the initial spring stiffness. In summary the three main factors that influence the shape of the p-y relationships, as illustrated in Figure 4-4 are:

1. Soil ultimate pressure, p_u [FL^{-2}]
2. Soil spring stiffness, κ [FL^{-1}]
3. Degradation factor, β, to account for the loss of soil stiffness due to liquefaction

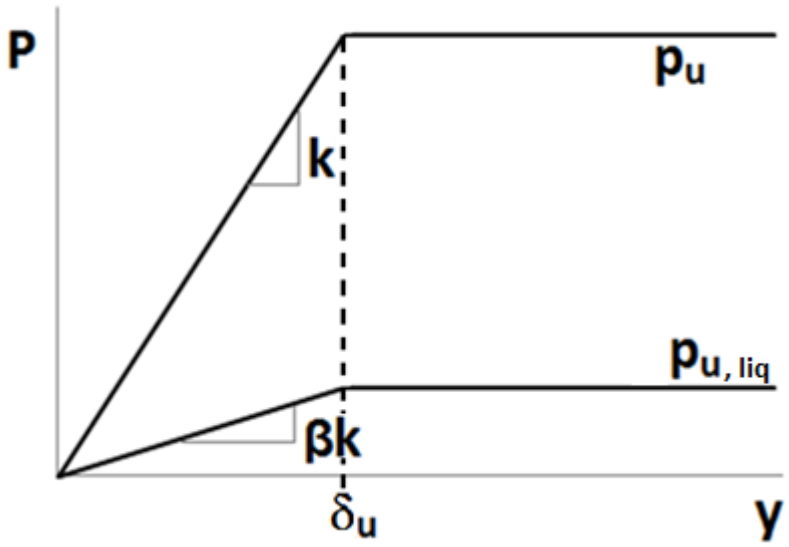

Figure 4-4: Generalised bi-linear soil spring formulation (top = non-liquefied layer, bottom = liquefied layer)

4.3.5.1 Crust layer

The lateral load from the crust layer may often be the critical load governing pile response due to its large magnitude and unfavourable position at the top of the pile. The ultimate pressure exerted by this crust layer on a pile ($p_{u\text{-}crust}$) is taken to be equivalent to the Rankine passive pressure (p_p) multiplied by a scaling factor (α_C) to account for the difference in lateral pressure between a single pile and equivalent wall, i.e.

$$p_{u-crust} = \alpha_C p_p \qquad (4\text{-}1)$$

Figure 4-5 below, constructed from a series of full-scale lateral spreading shake table experiments (Cubrinovski *et al.* 2006a), shows that the range of α remains relatively stable at a value of 4.5 for relative soil-pile displacements of 50 – 700 mm. Data from other experiments suggest that α can realistically range between 3 and 5. Figure 4-6 shows the relative soil-pile displacement (δ_u) which is required to mobilise the ultimate soil pressure in the crust layer as a function of the relative density of the crust. In this plot, *H* denotes the height of the model wall or pile cap used in the test. It is apparent that larger displacements are required to mobilise passive pressures in loose sand than in dense sand, but in any case displacements in the order of at least several centimetres are required to mobilise the maximum pressure from the crust layer on the pile.

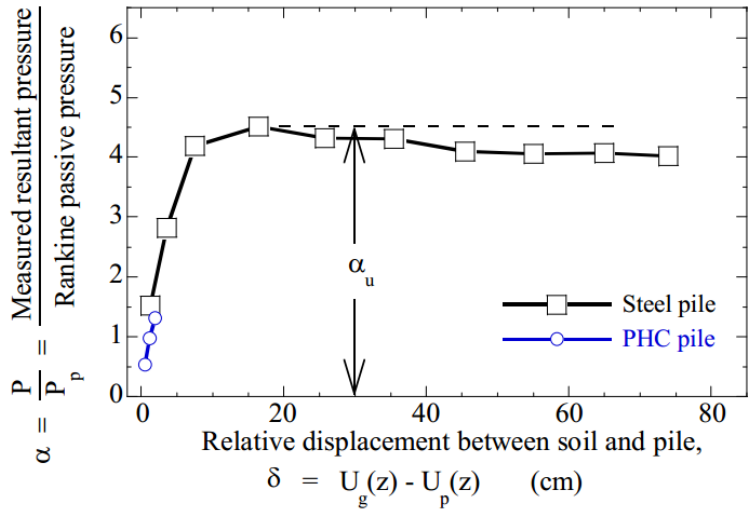

Figure 4-5: Ratio of lateral pressure from crust layer on a single pile to Rankine passive pressure (Cubrinovski et al. 2006a)

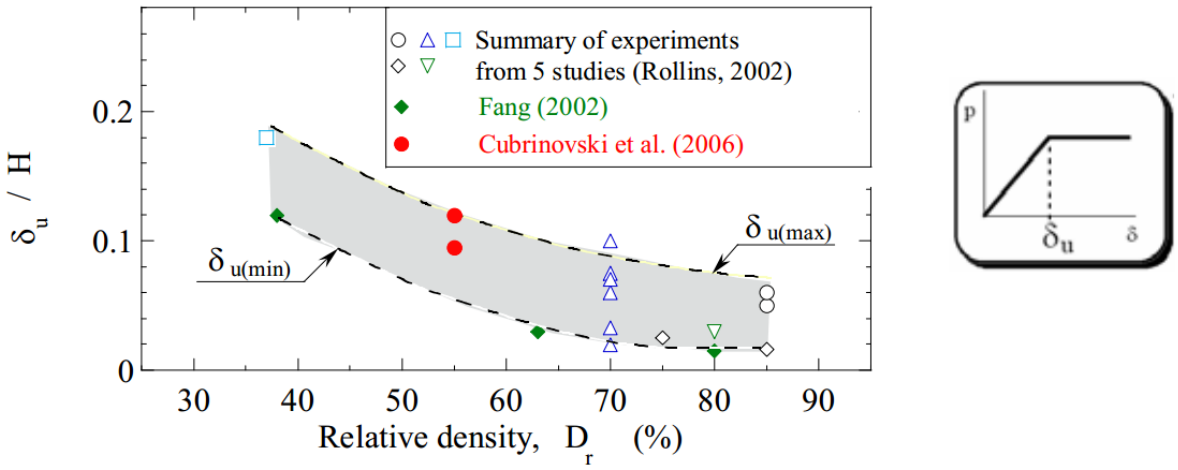

Figure 4-6: Relative displacement required to fully mobilise passive pressure as a function of relative density of sand: summary of data from experimental studies (Cubrinovski et al. 2009a)

4.3.5.2 Liquefied layer(s)

The ultimate lateral load applied to the pile by liquefied layers is considered to be proportional to the residual strength of liquefied soil, S_r, as defined using empirical correlations such as those proposed by Seed and Harder (1990) (see Figure 4-7) which considers residual strength to be a

function of SPT blowcount. The relationship between the ultimate pressure exerted by the liquefied soil and residual strength can be given by the following equation:

$$p_{u-liq} = \alpha_L S_r \quad (4\text{-}2)$$

where α_L is a strength multiplier subject to significant uncertainties, but note that it is different from the corresponding crust parameter, α_c, because the interaction and mobilisation of pressure from soils on piles is different between liquefied and non-liquefied soils.

The initial stiffness of the *p-y* relationship can be defined based on empirical correlations between the subgrade reaction coefficient and SPT blowcount or elastic moduli. This stiffness is then degraded to account for the effects of liquefaction. Figure 4-8 shows the range of spring stiffness degradation factor, β, under lateral spreading conditions, observed from full-scale tests on piles. This illustrates that β is not a constant, and depends on the magnitude of lateral ground displacement. β is also dependent on the level of excess pore water pressure developed, drainage conditions, relative density and rate of ground displacements, however these factors are not individually taken into consideration in this model. Instead, their combined effects lead to the recommendation that β under cyclic loading regimes should range between 1/50 and 1/10, while for lateral spreading β is recommended to range between 1/1000 and 1/50. In general, the quantification of this parameter is very subjective because of the inherent uncertainties associated with the properties of liquefying soils.

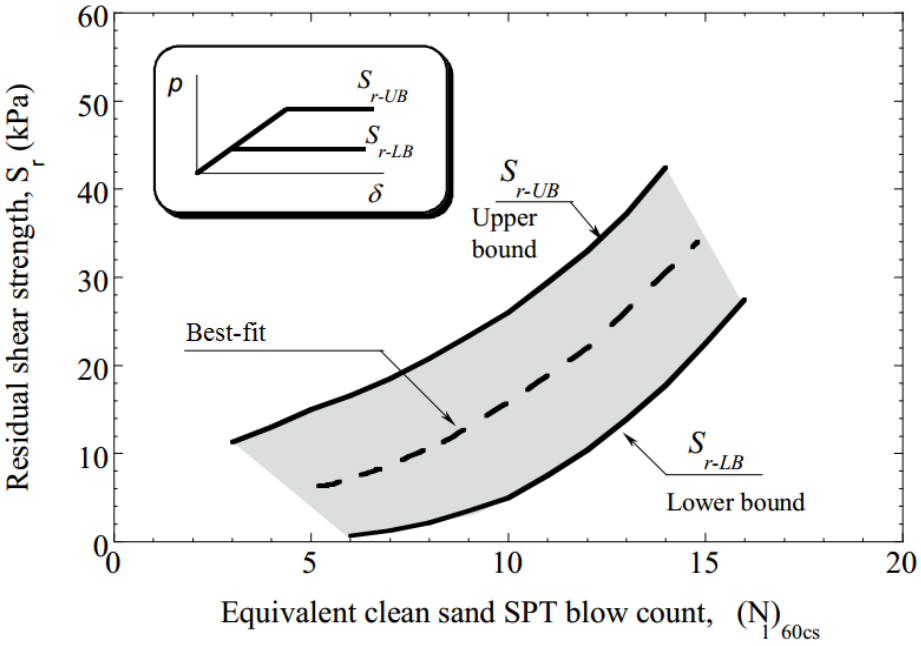

Figure 4-7: Residual strength of liquefied sandy soils back-calculated from case histories (after Seed and Harder 1990, Cubrinovski et al. 2009a)

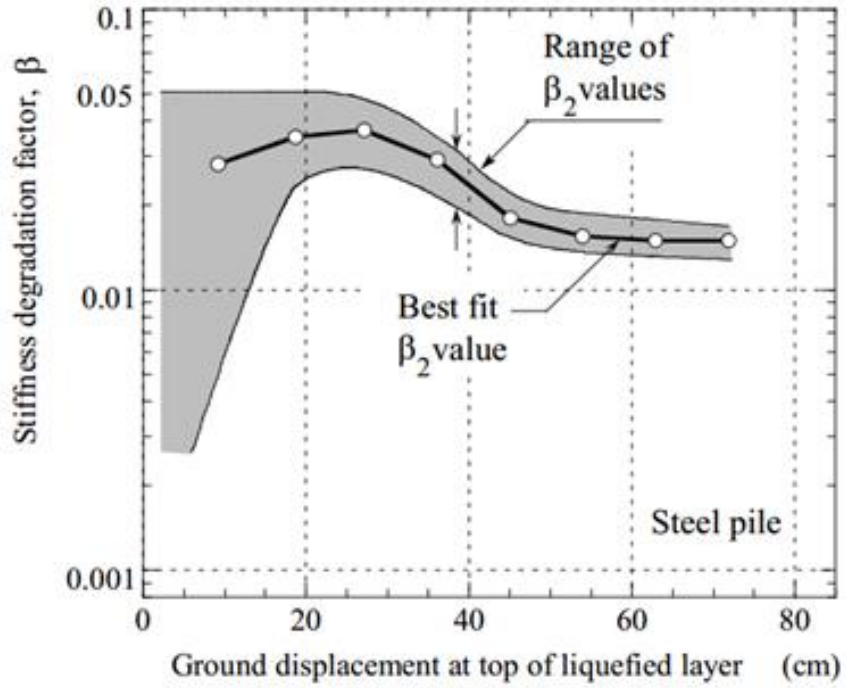

Figure 4-8: Degradation of stiffness in liquefied layer observed in full-scale tests on piles (Cubrinovski et al. 2006a)

4.3.5.3 Base layer

The strength properties of the base layer are defined in a similar way to the non-liquefied crust layer, the only difference being that there is no scaling factor (α) to account for any differences between the pressure exerted on a single pile and that exerted on an equivalent wall. As such, the ultimate pressure, p_u, is taken to be equivalent to the Rankine passive pressure, p_p. Also, the spring stiffness is found from empirical correlations between the subgrade reaction coefficient and SPT blowcount or elastic moduli.

4.3.6 Key uncertainties

As mentioned previously, the behaviour of piles subjected to lateral spreading is very complex and is therefore subject to significant uncertainties. Cubrinovski *et al.* (2009a) identified the following key parameters to be the ones most affecting the pile response:

- Ultimate pressure exerted by the crust layer, $p_{u\text{-}crust}$
- Magnitude of lateral ground displacement, $U_{G,max}$
- Stiffness and strength of the liquefied layers, β and $p_{u\text{-}Liq}$

It is envisaged, therefore, that a range of values for these parameters are considered instead of a uniquely determined set of values.

4.3.7 BS-Pile

BS-Pile (Beam-Spring) is a finite-element (FE) programme developed in-house at the University of Canterbury. While it was used to run the PSA in this research, any suitable finite element software could have been used which allows displacements to be applied directly to the ends of soil springs.

4.4 Soil-spring formulations

The construction of a beam-spring model is a popular approach for computing lateral pile response under earthquake loads; this is commonly referred to as the "Beam on Winkler Foundation" approach. However, there exists a good deal of uncertainty regarding how to properly represent the load-deformation (*p*-*y*) behaviour of liquefied soils. This uncertainty stems not only from the inherent complexities of the phenomenon itself, but also from the large number of proposed models available which have attempted to replicate it. This section outlines the equations (or equivalent

relationships) used to formulate the properties of liquefied soil spring *p-y* relationships using four different proposed methods.

4.4.1 Cubrinovski *et al.* 2009a

4.4.1.1 Ultimate pressure, p_u

This method recommends that empirical relations for residual strength be used to estimate ultimate pressure, p_u. The empirical correlations proposed by Seed and Harder (1990) show residual strength, S_r, as a direct function of SPT blowcount, as can be seen in Figure 4-9a below. Those proposed by Olson and Stark (2003), however, show a relationship between SPT blowcount and residual strength normalised by effective overburden stress, σ'_{vo} as illustrated in Figure 4-9b. Cubrinovski *et al*. (2009b) showed that the effects of shear strength normalisation on pile response can be significant in some situations, while in others they are negligible. The magnitude of normalisation effects is dependent on pile stiffness and thickness of the non-liquefied crust; the more flexible the pile, the smaller the effect of shear strength normalisation, and for crust thicknesses greater than 1.75 m the effects of normalisation are eliminated completely regardless of pile type.

The relationship between the ultimate pressure exerted by the liquefied soil and residual strength can be given by the following equation:

$$p_{u-liq} = \alpha_L S_r \qquad (4\text{-}3)$$

where α_L is a strength multiplier found to vary between 1 and 6, with a typical value of 1.

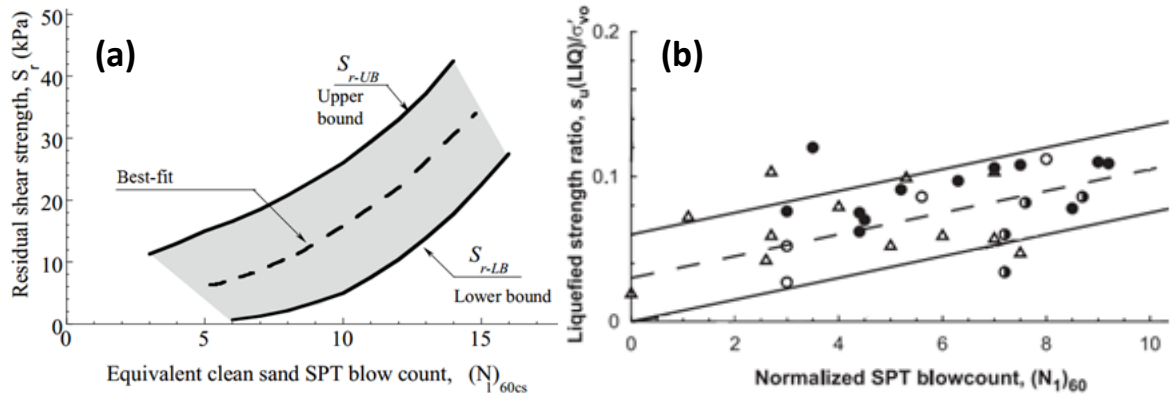

Figure 4-9: Residual strength of liquefied soils as a function of SPT blowcount, (a) after Seed and Harder 1990, (b) after Olson and Stark 2003.

4.4.1.2 Soil spring stiffness, κ

The initial stiffness of the *p-y* relationship is defined based on empirical correlations between the subgrade reaction coefficient and SPT blowcount or elastic moduli. In this instance, spring stiffness can be found by first calculating the subgrade reaction coefficient, *k*, as:

$$k = 56\,N\,D_0^{-3/4} \qquad (MN/m^3) \tag{4-4}$$

where *N* is SPT blowcount (≈ N_{60}), and D_0 is the effective pile diameter (cm). Then, spring stiffness can be found by multiplying the subgrade reaction coefficient by the node spacing in the FE model, l_s (m), and pile diameter, D_0 (m):

$$\kappa = k\,D_o l_s \qquad (MN/m) \tag{4-5}$$

4.4.1.3 Stiffness degradation factor, β

Stiffness degradation in the liquefied layers is applied through a factor β, taken to be between 1/50 and 1/1000 for lateral spreading, and between 1/10 and 1/50 for cyclic loading. This changes the initial spring stiffness such that:

$$\kappa_{degraded} = \beta\,\kappa \qquad (MN/m) \tag{4-6}$$

4.4.2 Architectural Institute of Japan (2001): Recommendations for design of building foundations

4.4.2.1 Ultimate pressure, p_u

In order to evaluate limiting soil pressure, p_u, a function of the Rankine passive pressure is used:

$$p_u = \lambda K_p \sigma'_v(z) \qquad (kN/m^2) \tag{4-7}$$

where λ = 3 for single piles, σ'_v is the vertical effective stress and K_p is the Rankine passive earth pressure coefficient, defined as:

$$K_p = \frac{1 + \sin\varphi'}{1 - \sin\varphi'} \tag{4-8}$$

where the angle of internal friction, φ', is estimated as:

$$\varphi' = 20 + (20(N_1)_{60})^{0.5} \tag{4-9}$$

For liquefied layers, the ultimate soil pressure is reduced by a factor, α:

$$p_{u,liq} = \alpha\, p_u \tag{4-10}$$

In the prescribed code there is no description of this reduction factor for lateral spreading; Uchida and Tokimatsu (2005) recommend that the same degradation value as for liquefaction be used. Thus, in this instance, α = β (described below).

4.4.2.2 Soil spring stiffness, κ

The coefficient of subgrade reaction, k, is evaluated by the following:

$$k = k_{h0}\, y^{-1/2} \qquad (kN/m^3) \tag{4-11}$$

$$k_{h0} = \alpha\, \zeta\, E_0 {D_o}^{-3/4} \qquad (kN/m^3) \tag{4-12}$$

$$E_0 = 700\, N \qquad (kN/m^2) \tag{4-13}$$

where *y i*s the lateral displacement of the pile in cm, α = 80 m^{-1} for sandy soil, ζ is a constant for group piles (1.0 for single pile), E_0 is Young's modulus, N is SPT blowcont, and D_o is the width of the pile in cm.

Then, initial (non-degraded) spring stiffness, κ, can be evaluated by Equation (4-5).

4.4.2.3 Stiffness degradation factor, β

β, the liquefaction stiffness degradation factor is taken to be a function of both the N_a value and depth as can be seen in Figure 4-10 below. N_a is taken to be equivalent to $(N_1)_{60}$. In this case, β is equivalent to α, meaning that both stiffness and strength are reduced by the same factor.

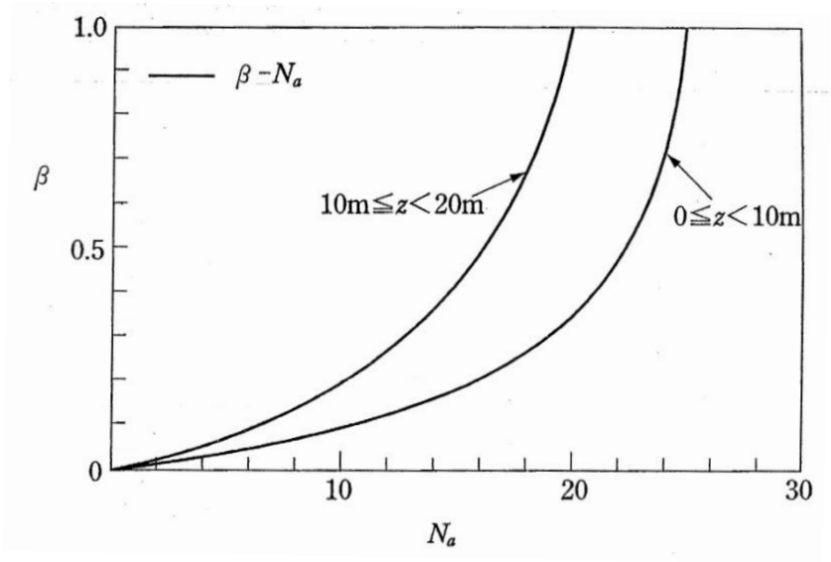

Figure 4-10: Stiffness reduction factor (AIJ 2001)

4.4.3 Ashford *et al.* 2011: Pacific Earthquake Engineering Research (PEER) Centre, Recommended Design Practice for Pile Foundations in Laterally Spreading Ground

This PEER publication presents two different options for the way in which to model the *p-y* behaviour of liquefied sands and lets the designer come to their own conclusions about which of their recommendations are most appropriate to use. The first approach is to use non–liquefied *p-y* curves and then degrade them (stiffness and strength) by some factor, such as the p-multipliers proposed by Brandenberg 2005. The second approach is to use the sand's estimated residual

strength along with an appropriate relationship for the static, undrained behaviour of clay (e.g. Matlock 1970). In this brief comparative study, the first approach is addressed using *p-y* curves taken from Reese and Van Impe (2001) and applying p-multipliers to them, while the second approach will use Matlock 1970's formulations for soft clay.

4.4.4 Reese and Van Impe 2001

In the absence of experimental *p-y* curves for the site of interest, empirical *p-y* curves for sand will be employed based on the method described in Reese and Van Impe (2001). The influence of liquefaction on these curves will be accounted for by applying p-multiplier scaling factors to the *p-y* resistances.

Reese and Van Impe's method is based on case study data from Mustang Island tests (Reese *et al*. 1974) and the characteristic *p-y* shape consists of two straight line segments (p_1 and p_3) joined by a parabolic curve (p_2) and bounded by an ultimate resistance limit (p_4), as can be seen in Figure 4-11.

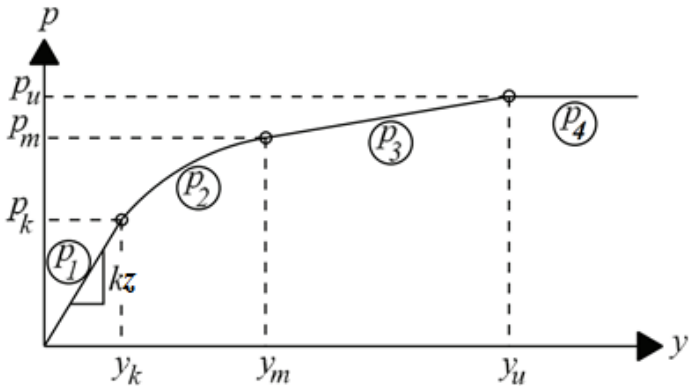

Figure 4-11: p-y curve for sand, after Reese et al. (1974)

4.4.4.1 Ultimate pressure, p_u

The ultimate pressure per unit length of pile, p_u, is determined by assuming a wedge-type failure mechanism for shallow depths and a flow-type mechanism for deeper depths (Figure 4-12). The transition depth between these failure modes occurs where the ultimate resistances based on each failure mode are equal.

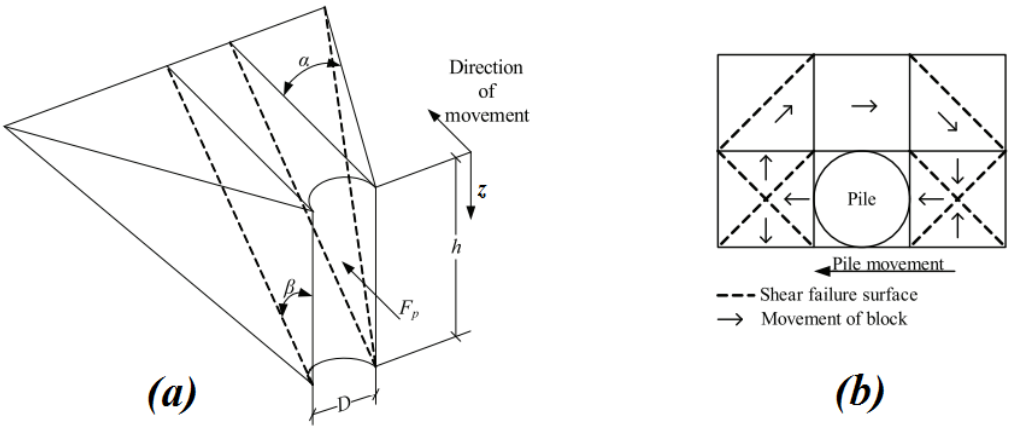

Figure 4-12: Failure modes, after Reese et al. (1974) - (a) shallow mode, (b) deep mode

The theoretical passive ultimate resistance at shallow depths, p_{cs}, is derived to be:

$$p_{cs} = \gamma z \left[\frac{K_0 z \tan\varphi \sin\beta}{\tan(\beta-\varphi)\cos\alpha} + \frac{\tan\beta}{\tan(\beta-\varphi)}(D + z\tan\beta\tan\alpha) + K_0 z \tan\beta(\tan\varphi\sin\beta - \tan\alpha) - K_a D\right] \quad (4\text{-}14)$$

and for deep depths:

$$p_{cd} = K_a D\gamma z(\tan^8\beta - 1) + K_0 D\gamma z \tan\varphi \tan^4\beta \quad (4\text{-}15)$$

where $K_0 = 0.4$, D *is the* pile diameter, z *is the* depth below ground surface, γ *is the* soil unit weight (buoyant unit weight below GWT), and:

$$\alpha = \frac{\varphi}{2} \quad (4\text{-}16)$$

$$\beta = 45 + \frac{\varphi}{2} \quad (4\text{-}17)$$

$$K_a = tan^2(45 - \frac{\varphi}{2}) \quad (4\text{-}18)$$

The theoretical ultimate resistance must be scaled by a factor $\bar{A}$ which is a function of loading type and normalised depth, such that:

$$p_u = \bar{A} p_c \quad (4\text{-}19)$$

Here, the static loading curve is used (Figure 4-13), as Ashford *et al.* 2011 recommend that corrections for the effects of cyclic loading (Matlock 1970) should not be used for piles in liquefying and laterally spreading ground.

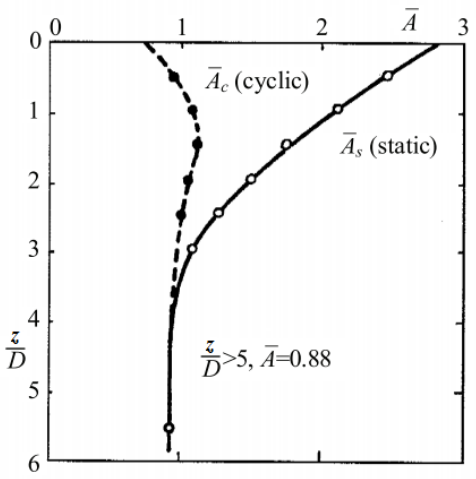

Figure 4-13: Values of scaling coefficients A_c and A_s (Reese et al. 1974)

4.4.4.2 Soil spring stiffness, κ

The subgrade reaction coefficient, *k*, is determined as function of relative density and whether the considered layer is above or below the water table, as summarised in Table 4-1:

Table 4-1: Representative subgrade reaction coefficient values (after Reese et al. 1974)

Relative density	Saturation	Recommended *k* (MN/m^3)
Loose	Above GWT	6.8
ϕ'≤30°	Below GWT	5.4
Medium	Above GWT	24.4
30°<ϕ'≤36°	Below GWT	16.3
Dense	Above GWT	61
ϕ'>36°	Below GWT	34

Then, initial (non-degraded) spring stiffness, κ, can be evaluated by Equation (4-5).

4.4.4.3 Stiffness degradation factor, β

Stiffness degradation, β (in the PEER 2011 document referred to as a p-multiplier, m_p), is to be taken as that proposed by Brandenberg (2005), which is a proposed range of values as a function of the clean sand corrected blowcount as illustrated in Figure 4-14. This is multiplied by the non-degraded stiffness to give degraded stiffness by:

$$\kappa_{degraded} = m_p \, \kappa \tag{4-20}$$

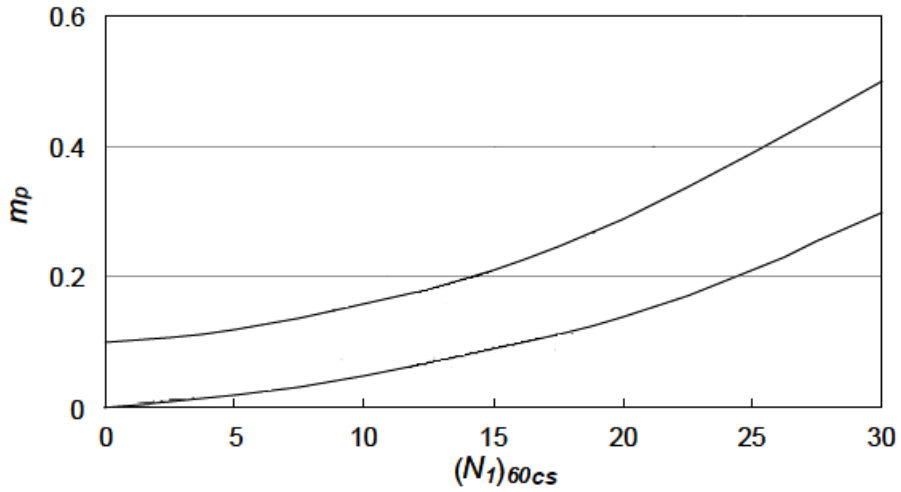

Figure 4-14: p-multiplier as a function of clean sand corrected blowcount, (Brandenberg 2005)

4.4.5 Matlock 1970

A second approach to compute an appropriate *p-y* relation for liquefied sand is to use the sand's estimated residual strength in conjunction with a relation for the undrained behaviour of soft clay (e.g. Matlock, 1970). Matlock's model for soft clay under static loading is shown in Figure 4-15.

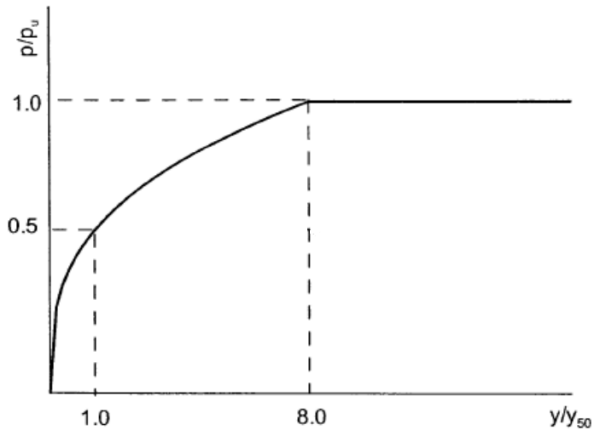

Figure 4-15: Characteristic p-y for soft clay under static loading (after Matlock, 1970)

4.4.5.1 Ultimate pressure, p_u, and degraded stiffness

The bounding ultimate pressure is found by:

$$p_u = \min \begin{cases} \left[3 + \frac{\gamma'}{c} z + \frac{J}{D} z\right] cD \\ 9cD \end{cases} \quad (4\text{-}21)$$

The parabolic curve is represented by:

$$\frac{p}{p_u} = 0.5 \left[\frac{y}{2.5(\varepsilon_{50})D}\right]^{1/3} \quad (4\text{-}22)$$

where D is pile diameter, γ' is the average effective unit weight from the ground surface to the *p-y* curve of interest, J is a model factor equal to 0.5 for a soft clay, ε_{50} is the strain corresponding to half of the maximum principal stress difference (recommended by Wang and Reese (1998) to be 0.05 for liquefied soil), and c is the shear strength at depth z (represented by undrained residual strength S_u in the case of liquefied soil).

4.5 Summary

Pseudo-static analysis, in general, is a simple, useful and practical way of modelling lateral loads on piles in liquefying and laterally spreading soils. There exist many different ways of modelling the *p-y* relationships in liquefying (and non-liquefying) soils, and no one method is more "right" or "wrong" than another, they simply come from different veins of research.

Lateral ground displacements of liquefied soils can be very significant and damaging for piles during both phases of earthquake loading; the cyclic phase and lateral spreading phase. Since soil properties during both these phases differ significantly, they should be considered separately while modelling.

The models presented show the potential for significant uncertainties to exist when dealing with the effects of complicated dynamic phenomena in an equivalent static analysis, and as such it is desirable that the employed pseudo-static model can:

- Capture the relevant deformation mechanism for piles in liquefying soils
- Permit the estimation of inelastic deformation and damages to piles
- Address the uncertainties associated with seismic behaviour of piles in liquefying soils

The proposed Cubrinovski *et al.* (2009a) methodology is capable of satisfying these points, and in the following chapter is further investigated by considering two case studies of bridges in liquefying and laterally spreading soils. It is acknowledged that particular attention should be paid to the parameters known to most affect pile response:

- Ultimate pressure exerted by the crust layer, $p_{u\text{-}crust}$
- Magnitude of lateral ground displacement, $U_{G,max}$
- Stiffness and strength of the liquefied layers, β and $p_{u\text{-}Liq}$

A range of values for these parameters should be considered instead of a uniquely determined set of values.

5 Pseudo-static analysis of ANZAC and Dallington Bridges

5.1 Introduction

In order to further investigate bridge pile response to cyclic and lateral spreading loads, a comprehensive set of pseudo-static analyses (PSA) was carried out on the ANZAC and Dallington Bridges. These two bridges were chosen because they each represent one of the typical construction types (segmented and monolithic respectively), their behaviours were well documented following the Christchurch earthquake, and reasonable site investigation data and good estimates of ground movement were available at both sites.

The pseudo-static approach employed herein consists of a finite element beam-spring model as described in chapter 4 where the bridge structure (abutments/piles/deck) is represented by beam elements and lateral soil stiffness is represented by springs. The analysis is nonlinear and equivalent static, meaning that the effects of soil and pile nonlinearity are accounted for, and dynamic actions are represented as equivalent static ones. Considerable uncertainties exist, arising from the fact that a complex dynamic soil-structure-interaction problem is being modelled by a relatively simple equivalent static analysis, however PSA has proven to be a very useful and effective modelling tool. The model sensitivity to variations in key parameters is examined through a series of parametric analyses, and there is the opportunity to examine the selection of appropriate values for the model parameters via back-calculations. This contributes to the refinement of PSA and its future application as a seismic modelling tool. The method summarised in Cubrinovski *et al.* (2009a) has been used for this research, more details of which were given in the chapter 4.

This chapter first describes the analysis of the site investigation data for liquefaction triggering, followed by model construction details. Both single pile and whole bridge analyses are then performed for each bridge, and the two separate phases of PSA (cyclic loading and lateral spreading) are considered separately. Results are presented and discussed, with the effects of key parameter uncertainties on each model highlighted. The principal objectives of this set of analyses are:

- To identify whether or not the PSA can predict the observed damage mechanism(s)
- To highlight the sensitivity of pile response to key parameters and, if applicable, back-calculate appropriate parameter values

- To see if there are any significant differences between the single pile and whole bridge models, particularly with respect to fixity conditions

5.2 Analysis methodology

For the purposes of this research all available existing geotechnical information for each of the bridge sites was collected from a range of sources. The origins and details of each test used in these analyses are given in the sections specific to each bridge, while the raw data can be found in Appendix A.

The geotechnical site investigations consist of standard penetration and cone penetration tests (SPT and CPT respectively). The data these two tests provide can be analysed to determine the nature and sequence of any subsurface strata including associated physical and mechanical soil properties. Both tests are conducted *in situ* which is particularly advantageous over laboratory testing methods, in particular with regard to the assessment of liquefaction potential. Both SPT and CPT are well-established testing methods, each with their own advantages and disadvantages. In particular, the SPT method allows for the extraction of soil samples where the CPT does not, however the CPT gives measurements continuously throughout a soil's profile where the SPT cannot. It is pertinent at this stage to note the sensitivity that the SPT has to the energy ratio of the specific falling hammer/rod system used. This ratio can range from around 50% to 95% and has a large bearing on the blowcount to be used in further analyses, thus highlighting the importance of knowing the specific calibration of each testing rig.

The site investigation data are first processed to assess liquefaction triggering as shown in the following section. Then, the distribution of displacements throughout depth is established. Finally, representative soil columns to be used in the PSA are constructed.

5.2.1 Liquefaction triggering

In order to develop appropriate soil-springs for each model, it must first be identified which layers are deemed to have liquefied under earthquake loading. In this research the method used to assess liquefaction triggering is the "simplified procedure", as summarised in Youd and Idriss (2001). This method is based on the evolution of more than 25 years of field observations and research. The two basic variables required for evaluating the liquefaction resistance of soils are: the seismic demand on a soil layer, expressed in terms of cyclic stress ratio (CSR); and the capacity that the soil layer has

to resist liquefaction, expressed in terms of cyclic resistance ratio (CRR). These are both described below. In Appendix B, an example spreadsheet is attached (*CPT-2;* the CPT performed on the south bank of ANZAC Bridge) which summarises the results of the liquefaction triggering calculations.

5.2.1.1 Evaluation of CSR

The seismic demand on a soil layer is expressed by the following formulation:

$$CSR = \frac{\tau_{av}}{\sigma'_{vo}} = 0.65 \frac{a_{max}}{g} \frac{\sigma_{vo}}{\sigma'_{vo}} r_d \quad (5\text{-}1)$$

where a_{max} is the peak horizontal ground acceleration at the surface (PGA), g is the acceleration due to gravity, σ_{vo} and σ'_{vo} are the total and effective overburden stresses respectively, and r_d is a stress reduction coefficient. For the purposes of this research, the PGAs calculated by the model of Bradley (2010) are used at each bridge site, and the overburden stresses are calculated assuming dry and saturated unit weights of sand to be 18 and 19 kN/m^3 respectively. The location of the ground water table (GWT) was found using data taken from *Project Orbit* (Tonkin and Taylor database), which assimilated piezometer readings from all over the Christchurch area at the time of each earthquake. The stress reduction coefficient has been calculated using the method of Liao and Whitman (1986) as:

$$r_d = \begin{matrix} 1.0 - 0.00765z & for\ z \leq 9.15\ m \\ 1.174 - 0.0267z & for\ 9.15\ m\ < z \leq 23\ m \end{matrix} \quad (5\text{-}2)$$

5.2.1.2 Evaluation of CRR

The cyclic resistance ratio is calculated differently for CPT and SPT data; each is described below.

CPT

The CRR based on CPT data is established using the methodology of Robertson and Wride (1998). The equations (and process) used are summarised in flowchart form below (Figure 5-1), where the output CRR is $CRR_{7.5}$, that is CRR scaled to a magnitude 7.5 earthquake. The results of this process on *CPT-2* can be seen in Appendix B.

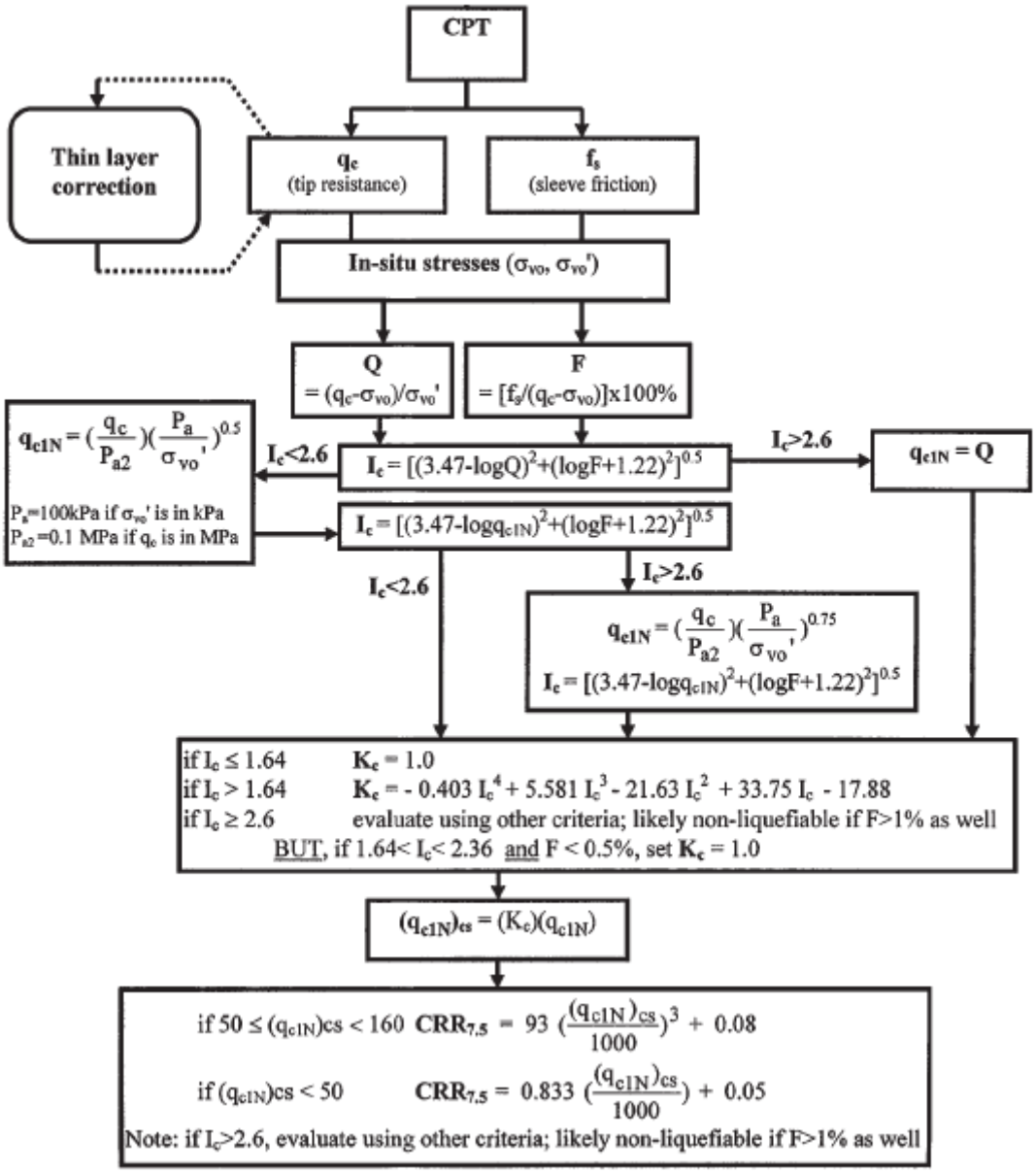

Figure 5-1: Flow chart illustrating the CPT method of evaluating cyclic resistance ratio in sandy soils (Robertson and Wride 1998)

SPT

$CRR_{7.5}$ is established for SPT data using the methodology outlined in Youd and Idriss (2001). Firstly, the measured blowcount must be corrected for overburden stress, energy ratio and rod length:

$$(N_1)_{60} = N_m C_N C_E C_R \quad (5\text{-}3)$$

where C_E corrects the measured blowcount to an energy ratio of 60%. C_R depends on the rod length used in the test and ranges from a value of 0.75 for rod lengths of less than 3 metres, to a value of 1.0 for rod lengths greater than 10 metres. C_N normalises the measured blowcount to a common reference effective overburden stress (here taken as atmospheric pressure, p_a):

$$C_N = \left(\frac{p_a}{\sigma'_{vo}}\right)^{0.5} \leq 1.7 \tag{5-4}$$

Next, the clean sand corrected blowcount is calculated as:

$$(N_1)_{60,cs} = \alpha + \beta(N_1)_{60} \tag{5-5}$$

where

$$\alpha = \begin{cases} 0 & FC \leq 5\% \\ \exp\left[1.76 - \dfrac{190}{FC^2}\right] & 5\% < FC < 35\% \\ 5.0 & FC \geq 35\% \end{cases}$$

$$\beta = \begin{cases} 1.0 & FC \leq 5\% \\ 0.99 + \dfrac{FC^{1.5}}{1000} & 5\% < FC < 35\% \\ 1.2 & FC \geq 35\% \end{cases} \tag{5-6}$$

where the apparent fines content (*FC*) is assumed based on available information; where soil samples are available then particle size analyses can be carried out, or in the cases where a CPT was performed at the same time/location, the corresponding apparent fines content from this can be used for each discrete blowcount measurement. Where these options are not available, or if the borelog results do not correlate well with the CPT results, the soil classification from the borelog is used as the main indicator of fines content.

Now, $CRR_{7.5}$ (for blowcounts less than 30) is calculated as:

$$CRR_{7.5} = \frac{1}{34 - (N_1)_{60,cs}} + \frac{(N_1)_{60,cs}}{135} + \frac{50}{\left[10(N_1)_{60,cs} + 45\right]^2} - \frac{1}{200} \tag{5-7}$$

Sands with blowcounts greater than 30 are deemed too dense to liquefy.

5.2.1.3 Evaluation of factor of safety against liquefaction triggering (FS)

The factor of safety against liquefaction triggering (for both SPT and CPT) is found by:

$$FS = \frac{CRR_{7.5}}{CSR_{7.5}} \cdot K_\sigma = \frac{CRR_{7.5}}{CSR} \cdot MSF \cdot K_\sigma \quad (5\text{-}8)$$

where *MSF* is a magnitude scaling factor which converts CSR into CSR scaled to a magnitude 7.5 earthquake, $CSR_{7.5}$. For this research, the revised Idriss equation is used:

$$MSF = \frac{10^{2.24}}{M_w^{2.56}} \quad (5\text{-}9)$$

For the 4th September 2010 earthquake (DAR), a moment magnitude of 7.1 gives *MSF* = 1.15, and for the 22nd February 2011 earthquake (CHC), a moment magnitude of 6.2 gives *MSF* = 1.63.

K_σ is a correction factor for overburden stress:

$$K_\sigma = \left(\frac{\sigma'_{vo}}{p_a}\right)^{(f-1)} \leq 1.0 \quad (5\text{-}10)$$

where f is an exponent which is a function of site conditions including relative density, stress history, aging and overconsolidation ratio; recommended to be 0.7-0.8 for a relative density of 40-60% and 0.6-0.7 for D_r = 60-80%. For the purposes of this study, f is taken to be 0.7 (corresponding to a relative density of approximately 70%), since K_σ is only in effect at depths greater than approximately 10 metres, where the vertical effective stress is greater than atmospheric pressure, thus density is expected to be relatively high.

5.2.2 Applied soil displacements

Two phases of applied loading are considered; the lateral spreading phase and the cyclic phased. The displacements for each phase are very different and must be treated separately.

5.2.2.1 Lateral spreading

Since the permanent observed ground surface movements at the bridge sites were measured (by lateral spreading transect surveys and LiDAR), it does not make sense to use empirical formulations to calculate the lateral ground displacement at the surface due to spreading, $U_{G\text{-}max}$. However, there does need to be some way to distribute ground displacements to the free ends of the soil springs throughout depth in the PSA. In this research, the method of Zhang *et al.* (2004) was used to determine the lateral displacement index (LDI), which is calculated by integrating the maximum cyclic shear strains in each layer over depth. LDI is then the total integrated value at the ground surface. The shear strains are computed as a function of relative density (D_r) and factor of safety

against liquefaction triggering (*FS*), this is shown in both graphical and equation form in Figure 5-2. Relative density is calculated using the relation of Tatsuoka *et al.* (1990) for CPT data:

$$D_r = -85 + 76\log(q_{c1N}) \tag{5-11}$$

and the modified Meyerhof relation for SPT data:

$$D_r = 14\sqrt{(N_1)_{60}} \tag{5-12}$$

An LDI has units of displacement, however for this research, the LDI profile is scaled to a unitless LDI, i.e. LDI at the ground surface = 1. Then this distribution can be multiplied by the observed lateral spreading displacements and applied to the ends of the soil springs. It is recognised that the method of Zhang *et al.* (2004) does not capture all the mechanisms contributing to lateral spreading (for example the effects of excess pore pressure dissipation, ground settlements, geometric boundaries and more), however for the purposes of this research it is a reasonable approximation and is of lesser significance than the actual magnitude of ground displacement. The results of the LDI calculations for *CPT-2* can be seen in the spreadsheet in Appendix B.

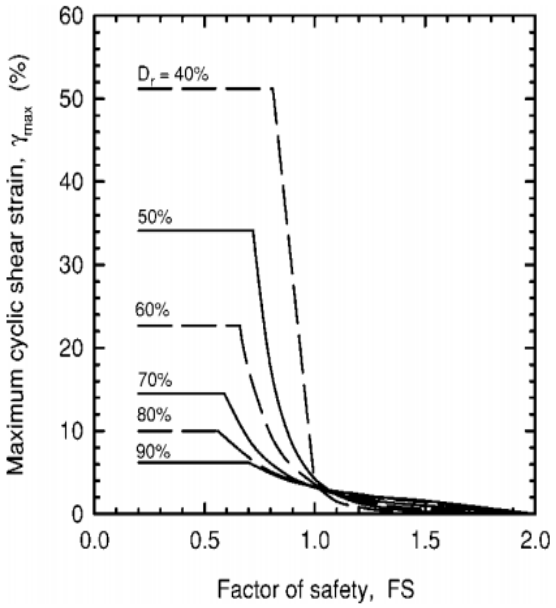

if $D_r = 90\%$, $\gamma_{max} = 3.26(FS)^{-1.80}$ for $0.7 \leq FS \leq 2.0$

if $D_r = 90\%$, $\gamma_{max} = 6.2$ for $FS \leq 0.7$

if $D_r = 80\%$, $\gamma_{max} = 3.22 \cdot (FS)^{-2.08}$ for $0.56 \leq FS \leq 2.0$

if $D_r = 80\%$, $\gamma_{max} = 10$ for $FS \leq 0.56$

if $D_r = 70\%$, $\gamma_{max} = 3.20 \cdot (FS)^{-2.89}$ for $0.59 \leq FS \leq 2.0$

if $D_r = 70\%$, $\gamma_{max} = 14.5$ for $FS \leq 0.59$

if $D_r = 60\%$, $\gamma_{max} = 3.58 \cdot (FS)^{-4.42}$ for $0.66 \leq FS \leq 2.0$

if $D_r = 60\%$, $\gamma_{max} = 22.7$ for $FS \leq 0.66$

if $D_r = 50\%$, $\gamma_{max} = 4.22 \cdot (FS)^{-6.39}$ for $0.72 \leq FS \leq 2.0$

if $D_r = 50\%$, $\gamma_{max} = 34.1$ for $FS \leq 0.72$

if $D_r = 40\%$, $\gamma_{max} = 3.31 \cdot (FS)^{-7.97}$ for $1.0 \leq FS \leq 2.0$

if $D_r = 40\%$, $\gamma_{max} = 250 \cdot (1.0 - FS) + 3.5$ for $0.81 \leq FS \leq 1.0$

if $D_r = 40\%$, $\gamma_{max} = 51.2$ for $FS \leq 0.81$

Figure 5-2: Curves and corresponding equations relative maximum cyclic shear strain to factor of safety and relative density (Zhang et al., 2004)

5.2.2.2 Cyclic displacements

In order to estimate the cyclic ground displacements which occur during earthquake shaking, the simplified method of Tokimatsu and Asaka 1998 is used. This method is based on observations from previous earthquakes, where cyclic shear strains in liquefied soil layers were evaluated from the analysis of strong motion records and detailed surveys of piles in level ground. Knowing the SPT blowcount in each liquefied layer and the cyclic stress ratio (*x* and *y* axes in Figure 5-3), the cyclic shear strain in each layer can be computed using the chart. Then, these strains are integrated throughout depth to obtain a cyclic ground displacement profile.

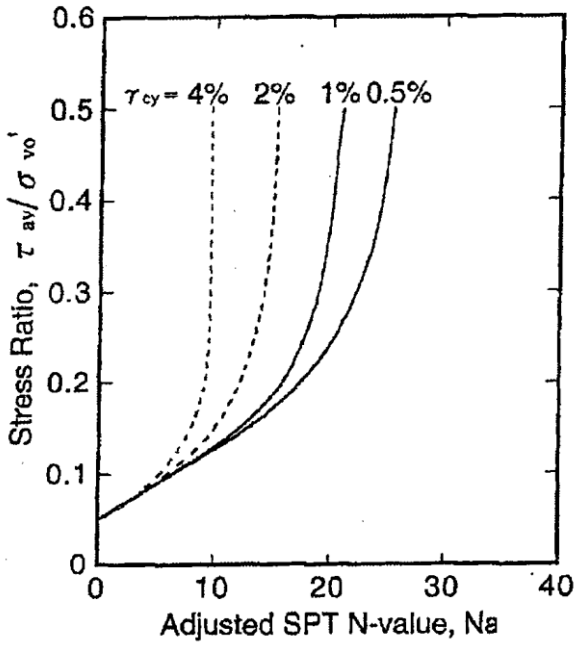

Figure 5-3: Cyclic shear strains as a function of SPT-N and CSR (Tokimatsu and Asaka 1998)

5.2.3 Discretisation of soil layers for model construction

The finite element beam-spring models used in the PSA have nodal spacings of 0.1 m in the vertical direction. Also, the inputting of soil spring parameters into each model is a manual process. As such, it makes sense to discretise an analysed soil column into several layers, each of which is assigned properties deemed to be representative of the soil throughout that layer.

In order to distinguish these discrete soil layers to use in the modelling process, considerations were made relating to penetration resistance, $(N_1)_{60,cs}$ or $q_{c1N,cs}$, soil type (from borelog or behaviour type

index) and factor of safety against liquefaction triggering. Each soil column is divided into several discrete layers based on the interrelations of these properties and is assigned a representative blowcount to use in order to construct each model. The way in which the majority of the soil springs are formulated is such that spring stiffness is directly proportional to an SPT blowcount, equivalent to N_{60}. Thus, CPT penetration resistance, q_c, is converted into an equivalent SPT blowcount using the equation of Jefferies and Davies (1993):

$$N_{60} = \frac{q_c}{p_a} \cdot \frac{1}{8.5\left(1 - \frac{I_c}{4.6}\right)} \tag{5-13}$$

which is valid for values of I_c < 4.06, but since above this range the material present is stiff clays then for the bridge sites considered in Christchurch this equation is relevant.

Similarly to the SPT data, equivalent normalised and clean sand normalised blowcounts are calculated using equations (5-5) and (5-6), where the fines content is estimated by the equation of Robertson and Wride (1998):

$$FC\ (\%) = \begin{matrix} 0 & I_c < 2.6 \\ 1.75I_c^{3.25} - 3.7 & 1.26 \le I_c \le 3.5 \\ 100 & I_c > 3.5 \end{matrix} \tag{5-14}$$

In this way, each layer in the soil model is assigned a representative value of $(N_1)_{60,cs}$, $(N_1)_{60}$ and N, which are all used in the calculation of various soil spring parameters. This can be seen in the spreadsheet and following figures and table in Appendix B.

5.3 Model construction

Two separate types of models are constructed for each bridge; a single-pile model and a whole bridge model. The single pile models represent a single abutment/pile system and are constructed with a node spacing of 0.1 metres. The whole bridge models represent the entire bridge system, including deck, piers and pier piles. Vertical node spacings are 0.1 m for these systems also, while horizontal node spacing along the deck is determined by having 10 beam elements per span. A representative tributary bridge width is chosen for each bridge model (both single pile and whole bridge), based on practical considerations concerning pile spacing.

Two loading phases to apply to each bridge are considered separately; the lateral spreading phase in which kinematic loads from the soil dominate, and the cyclic loading phase in which kinematic loads from the soil are combined with inertial forces from the superstructure.

5.3.1 Parametric studies

Three types of soil layers are considered in the definition of the soil springs; a non-liquefied crust layer, liquefied layers, and deeper non-liquefied layers. The important modelling difference in the crust layer compared with the deeper non-liquefied layers is that the "wedge-effect", represented by α_{Crust}, must be considered to account for increased pressures on a single pile. The important difference in the liquefied layers in comparison with the deeper non-liquefied layers is that both the stiffness and strength of the soil are significantly lower, as defined by the stiffness degradation factor, β, and the residual strength of soil, S_r, respectively.

The method of Cubrinovski *et al.* (2009b) was described in more detail in chapter 4, and Tables 5-1 to 5-3 show a summary of the equations used to calculate each parameter and the variations in key parameter values. The reference value for each parameter is based on median or best estimate values, while the lower bound (LB) and upper bound (UB) values indicate the likely range of that parameter based on previous studies (Cubrinovski *et al*. 2009b, 2009c, 2012). Typically, one parameter at a time is varied while keeping the others at their reference value. In doing so, the sensitivity of the pile response to that particular parameter can be examined. Firstly, a reference model (hereafter referred to as "RM") is constructed which consists of the best estimate/reference values for each parameter. From this, individual parameters are varied between their upper and lower bounds, while all others remained at their reference values. The results of the parametric studies are presented based on the layers in which the parameters are being varied, that is to say that the effects of the crust layer variations, liquefied layer variations and non-liquefied layer variations are examined separately:

Crust layer

Table 5-1: Soil spring parameters and variations used in PSA of ANZAC Bridge – crust layer

Property affected	Parameter [units]	Equation	Ref. Value	LB Value	UB Value	Remarks
Strength	$p_{u\text{-}crust}$ [FL^{-2}]	$p_p \cdot \alpha_{Crust}$	-	-	-	
	α_{Crust} [-]	-	4.5	3	5	
	φ' [deg]	$20 + \sqrt{20(N_1)_{60}}$	Calc.	33°	40°	
Stiffness	κ [FL^{-1}]	$(p_{u-crust}/\delta_u)\, l_s D_o$	-	-	-	[1]
		$\beta_{Crust} l_s D_o 56 N {D_o}^{-3/4}$	-	-	-	[2]
	β_{Crust} [-]	-	-	0.3	1	
	δ_u [L]	-	5% H_a 14% H_a	2% H_a 10% H_a	8% H_a 18% H_a	[3],[4]

Remarks:

[1] Back-calculation of spring stiffness from displacement required to mobilise passive pressures (δ_u) – this reference value is what is used in the RM

[2] Forward-calculation of spring stiffness using subgrade reaction coefficient method – only used for the purposes of parametric variation (not in RM)

[3] See Figure 5-4

[4] H_a refers to height of abutment, the values on the top line refer to ANZAC Bridge, where the crust layer has D_r = 70-80%, the values on the bottom line refer to Dallington Bridge, where the crust layer has D_r = 30-40%.

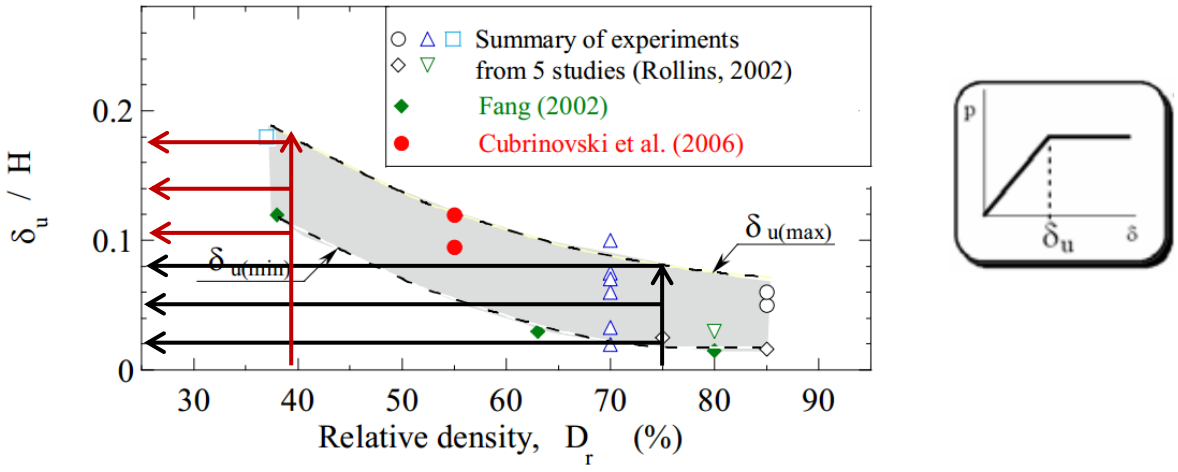

Figure 5-4: Displacement required to mobilise passive pressure as a function of relative density (Cubrinovski et al. 2009a). the black arrows refer to ANZAC Bridge, the red arrows refer to Dallington Bridge.

Liquefied layers

Table 5-2: Soil spring parameters and variations used in PSA of ANZAC Bridge - liquefied layers

Property affected	Parameter [units]	Equation	Ref. Value	LB Value	UB Value	Remarks
Strength	$p_{u\text{-}Liq}$ [FL^{-2}]	$S_r \cdot \alpha_{Liq}$	S_r Med.	S_r LB	S_r UB	[1]
	α_{Liq} [-]	-	1 (3)	1 (1)	6 (6)	[2], [3]
	φ' [deg]	$20 + \sqrt{20(N_1)_{60}}$	Calc.	-	-	
Stiffness	κ [FL^{-1}]	$\beta_{Liq} l_s D_o 56 N {D_o}^{-3/4}$	-	-	-	
	β_{Liq} [-]	-	1/100 (1/20)	1/1000 (1/50)	1/50 (1/10)	[3]

Remarks:

[1] Residual shear strength, S_r, as a function of SPT blowcount, after Seed and Harder (1990)

[2] α_{Liq} is a factor which accounts for the possibility of an increased volume of soil contributing to the generation of soil pressure on a pile

[3] The values in brackets are those used in the cyclic analysis

Non-liquefied deeper layers

Table 5-3: Soil spring parameters and variations used in PSA of ANZAC Bridge - non-liquefied layers

Property affected	Parameter [units]	Equation	Ref. Value	LB Value	UB Value	Remarks
Strength	$p_{u\text{-}NLiq}$ [FL^{-2}]	p_p	-	-	-	
	φ' [deg]	$20 + \sqrt{20(N_1)_{60}}$	Calc.	33°	37°	
Stiffness	κ [FL^{-1}]	$\beta_{Non-Liq} l_s D_o 56 N {D_o}^{-3/4}$	-	-	-	
	$\beta_{Non\text{-}Liq}$ [-]	-	1	0.3	1	

Other variations

Further parametric studies were also carried out which varied the magnitude of ground displacement applied ($U_{G\text{-}max}$). At ANZAC Bridge an additional analysis was carried out which included the effect of having a bridge construction or expansion joint at the bridge deck/abutment connection.

5.4 ANZAC Bridge

This section covers the PSA of ANZAC Bridge.

5.4.1 Bridge structure

ANZAC Bridge is a reinforced concrete structure 48.4 metres in length and 22.5 metres wide at its northern end tapering to 21 metres at the southern end with a 13° skew in plan. There are two traffic lanes in each direction and a footpath on the western side. The bridge consists of three reaches spanning 14.9 m – 18.6 m – 14.9 m, the plan view of which is shown in Figure 5-5.

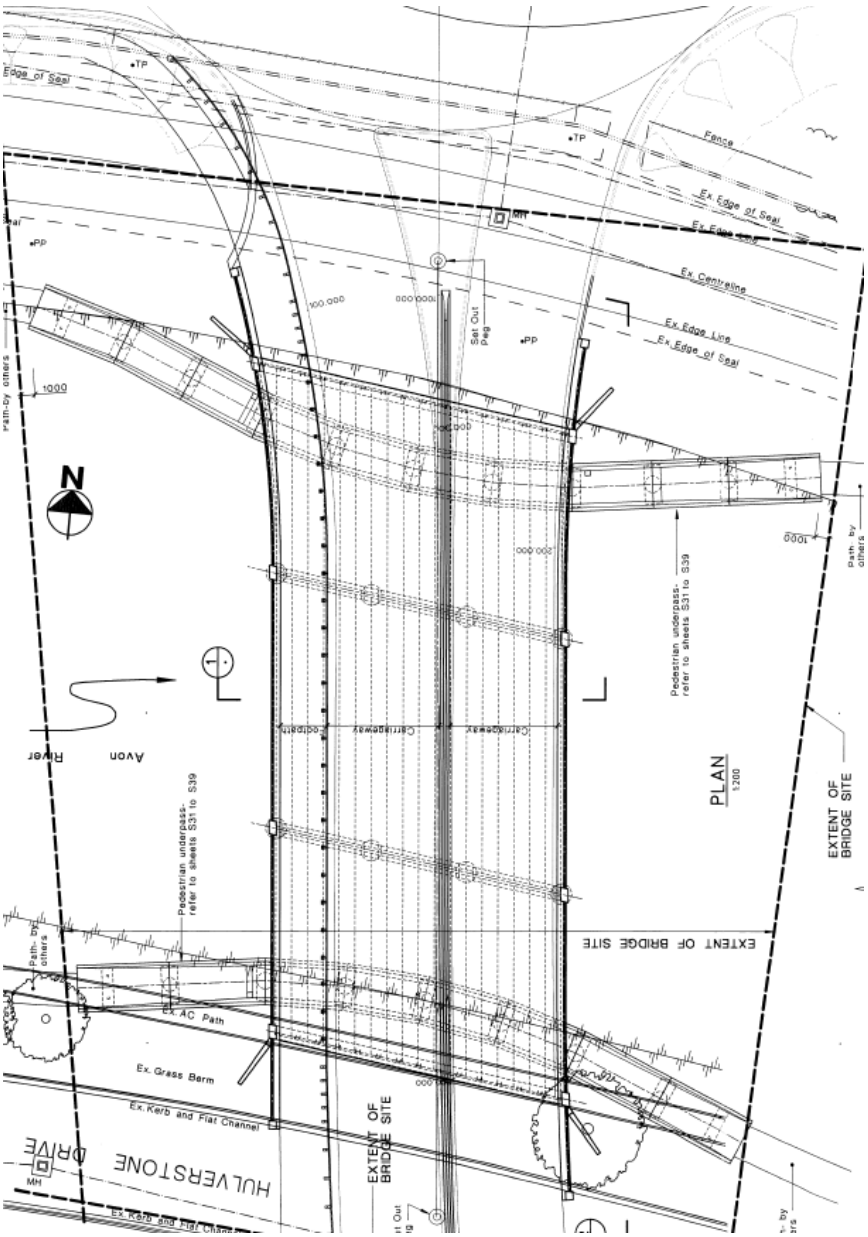

Figure 5-5: Plan view of ANZAC Bridge, Christchurch City Council design drawing

The bridge deck consists of precast concrete double core units and is supported by two central 4-column bents and concrete abutments. The 1 m x 1 m rhomboid piers were cast *in situ* and founded on 1.5 m diameter steel-encased reinforced concrete piles 20 m in length and at *4.6D* spacings. The concrete abutments were also cast *in situ* on top of embankment fill and 15 (south) to 16 (north) driven steel H piles 22 m in length (Grade 300 UC 310 x 137) at *5D* spacings. Figures 5-6 and 5-7 show longitudinal and transverse sections of the bridge.

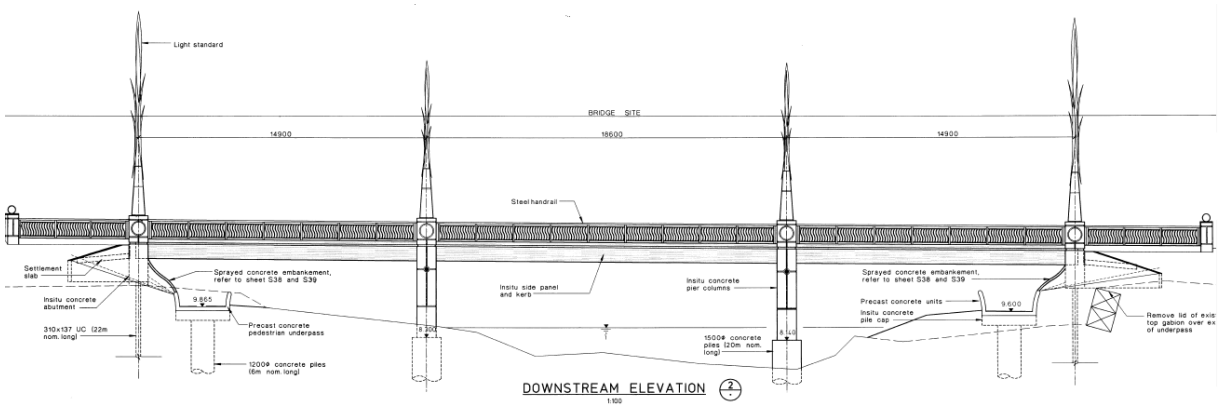

Figure 5-6: ANZAC Bridge downstream elevation, Christchurch City Council design drawing

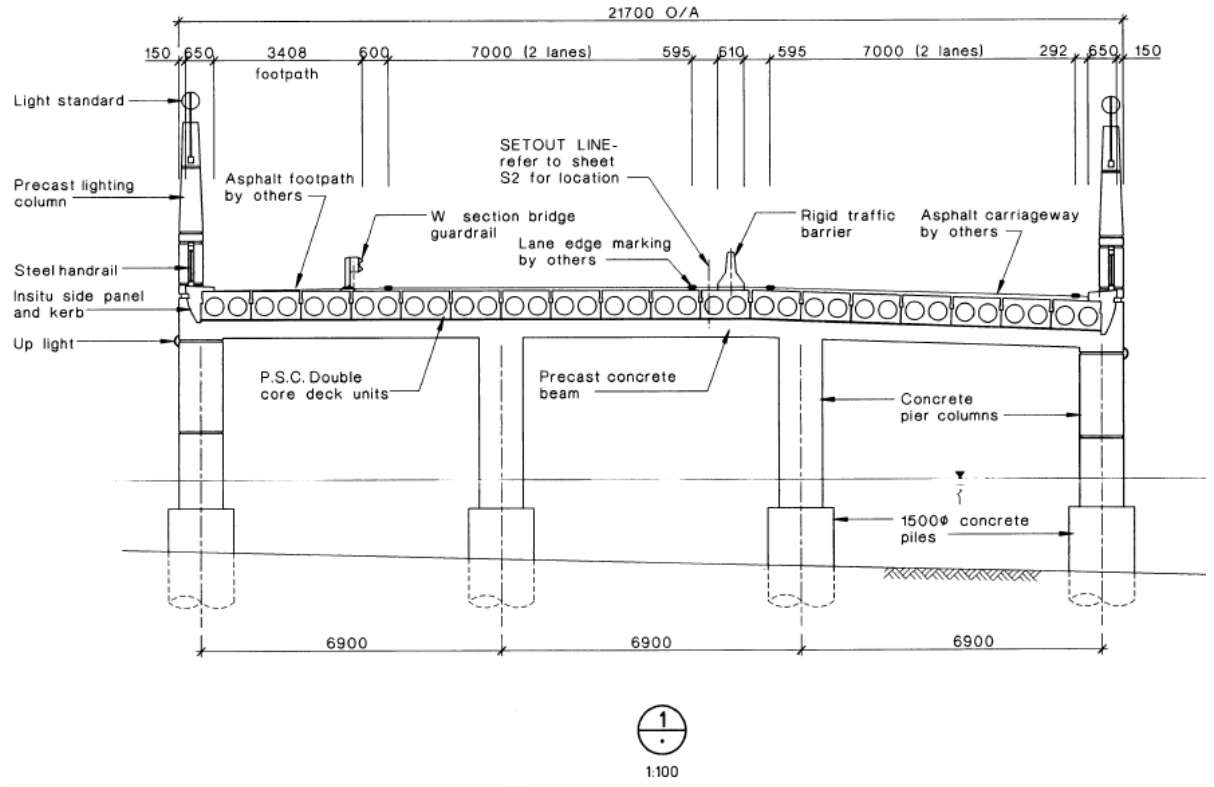

Figure 5-7: ANZAC Bridge transverse section, Christchurch City Council design drawing

Pedestrian underpasses are provided on both sides of the river and are structurally independent of the bridge structure itself. Each of them is founded on 1.2 m diameter 6 m long concrete piles and is attached superficially to the bottom of each abutment.

The southern bridge approach and abutment were constructed on a substantial amount of embankment fill, while the northern abutment required fill only at the abutment due to the remainder of the surrounding grade already being at the same level as the proposed bridge deck.

Details relating to each individual component including material properties can be found in the Christchurch City Council's design drawings for ANZAC Bridge.

5.4.2 Geotechnical site conditions

Prior to the bridge's construction a site investigation was carried out consisting of an SPT and CPT at each abutment (BH1 & 2, CPT1 & 2 in Figure 5-8). Two additional CPTs commissioned by the EQC as part of their greater Christchurch ground investigations are located near ANZAC Bridge (CPT-BUR-70 and CPT-AVD-62), however these were not considered to be of use for this research for two key reasons. First, they were carried out in November 2011 meaning that they are unlikely to be representative of pre-quake conditions due to the area having been disturbed several times in the 2010-2011 earthquake sequence. Secondly, their distance from the bridge itself is quite large (each of them around 50 m) and so due to the large variability in Christchurch soils they are unlikely to encounter strata entirely characteristic of those found at each abutment. CPT-BUR-70 in particular is more likely to be representative of the swamp land found further north of the bridge itself. Table 5-4 summarises the exact locations, dates of testing and other details of the geotechnical site investigations.

Figure 5-8*: ANZAC Bridge site investigation locations (Google Earth image)*

Table 5-4: ANZAC Bridge geotechnical site investigation details

Abutment	Name	Latitude	Longitude	Test date	Performed by/for
North	CPT-1	43°30'2.27"S	172°42'4.02"E	Nov 1994	Avon Bridge - Burwood Expressway SI Report
North	CPT-BUR-70	43°30'1.00"S	172°42'2.00"E	Nov 2011	Perry (for EQC ground investigations)
North	BH2	43°30'1.58"S	172°42'3.96"E	Oct 1994	Dynes Rd Drilling (for Avon Bridge - Burwood Expressway SI Report)
South	CPT-2	43°30'4.36"S	172°42'4.72"E	Nov 1994	Avon Bridge - Burwood Expressway SI Report
South	CPT-AVD-62	43°30'5.00"S	172°42'8.00"E	Nov 2011	Perry (for EQC ground investigations)
South	BH1	43°30'4.32"S	172°42'4.33"E	Oct 1994	Dynes Rd Drilling (for Avon Bridge - Burwood Expressway SI Report)

For the purposes of this research the CPT data (*CPT-1* and *CPT-2*) were used in order to set up and create the PSA models. This is due to the fact that the energy ratio of the SPT hammer is unknown thus the use of the recorded blowcounts in a liquefaction evaluation is inaccurate, however soil types indicated in the borelogs were still of use for identifying strata susceptible to liquefaction. An

additional benefit of using the CPT data is that a continuous profile throughout depth can be evaluated. The original CPT data and SPT borelogs do correlate well with one another and can be seen in Appendix A.

In Figures 5-9 and 5-10 on the following pages the CPT data (both raw and subsequent analysis results) are shown, one at each abutment. These analyses were performed using the methods outlined in sections 5.2 and 5.3, and the adopted profiles used in the PSA are also shown, where the blue layers are those deemed to have liquefied in the 22nd February 2011 earthquake. The upper two metres of both profiles is a fill material, placed at each abutment subsequent to the dates of testing but prior to the bridges construction. Note that this alters the stress state used to calculated seismic demand (as opposed to cyclic resistance). Groundwater levels were identified using data from *Project Orbit* and are deemed to be the best estimates of GWL at the time of the earthquake.

The properties assigned to the fill layer assume a relative density of 70-80% (well-compacted grade). This corresponds to a blowcount of approximately 20 (for clean sands/gravels) using the well-known Meyerhof relation:

$$N = \left(17 + 24\frac{\sigma'_{v0}}{98}\right) D_r^2 \tag{5-15}$$

It can be seen that, at the north abutment (Figure 5-9), the critical layers for liquefaction are from 2 to 4 metres depth, and 13 to 18 metres depth. On the south abutment (Figure 5-10), the critical layers for liquefaction lie between 3 and 14 metres depth.

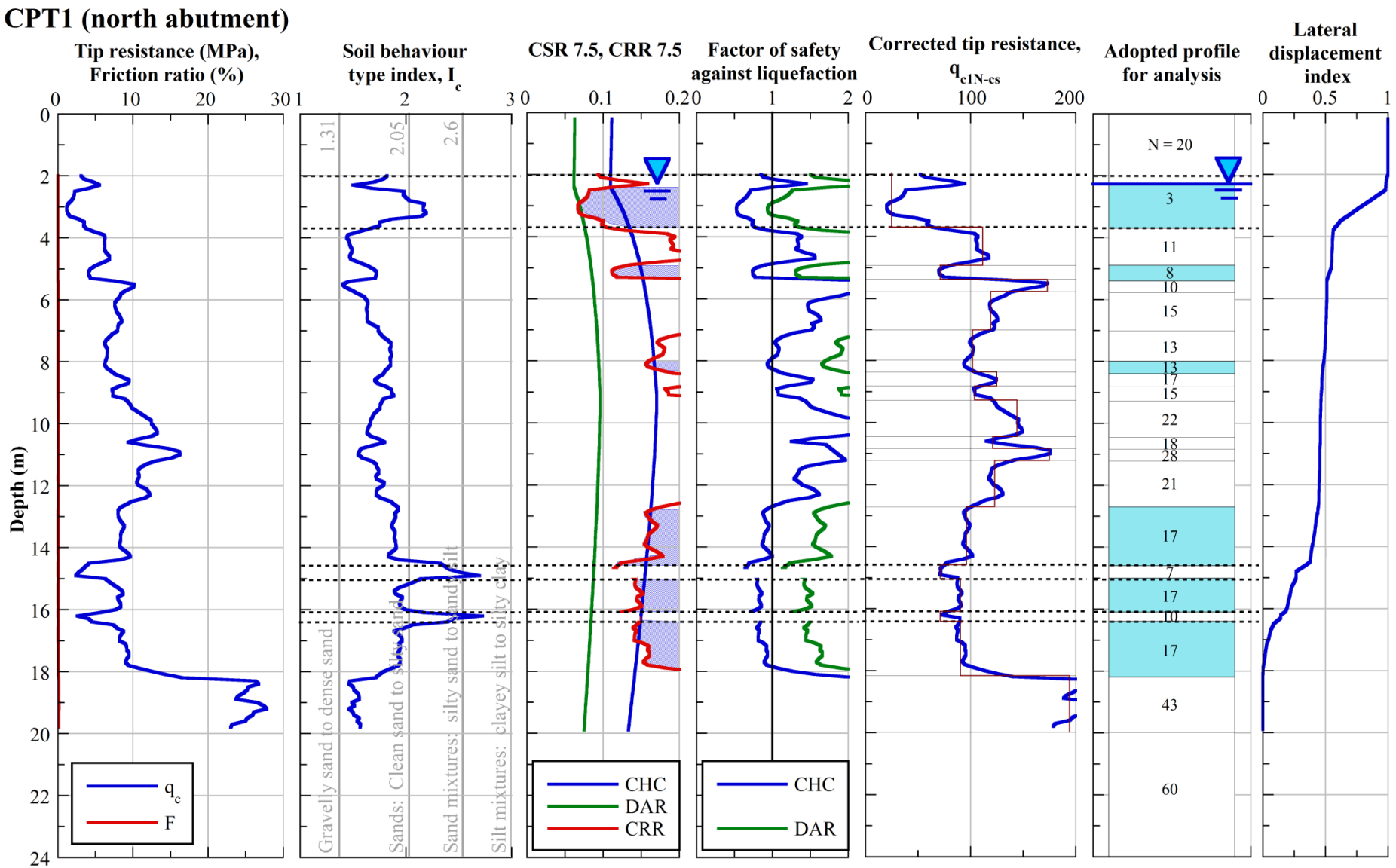

Figure 5-9: ANZAC bridge north abutment CPT data and liquefaction analysis results

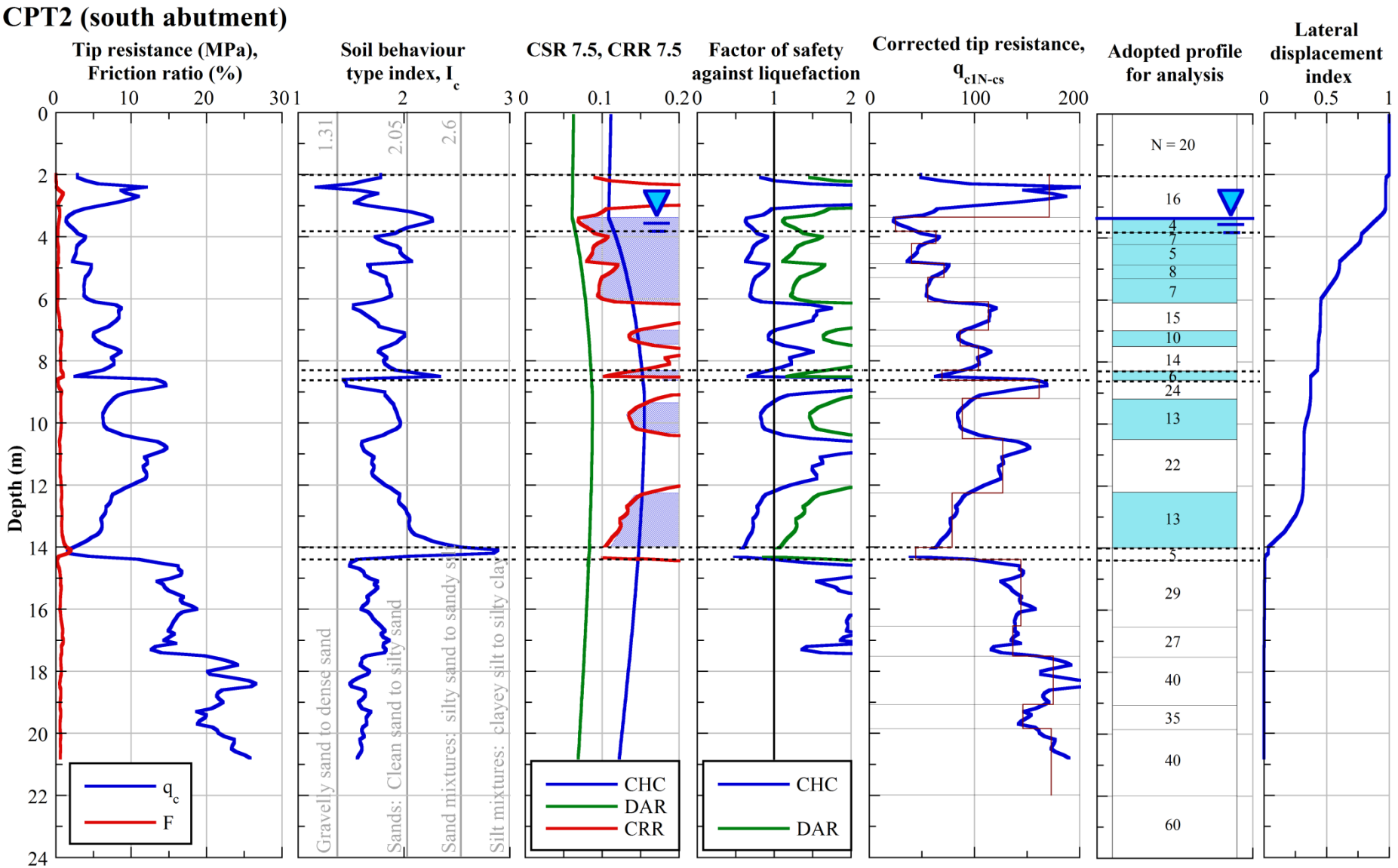

Figure 5-10: ANZAC bridge south abutment CPT data and liquefaction analysis results

5.4.3 Earthquake observations

Subsequent to the Darfield earthquake, marginal liquefaction and lateral spreading occurred in the area of the bridge, such that the bridge and its functionality were not at all affected. This corresponds well with the analysis of the CPT tests shown in Figures 5-9 and 5-10, where *FS* (DAR) > 1 everywhere.

The Christchurch earthquake, on the other hand, caused significant liquefaction and lateral spreading at the bridge site, more severe on the south bank than the north. Lateral spreading (free-field) displacements in the order of 1 m were measured on the south bank, and 0.4 m on the north. The southern approach also slumped away from the roadway as well as towards the river.

The dominant spreading-induced damage mechanism involved deck-pinning and abutment back-rotation; this was measured to be 6 degrees at the south abutment and 4-5 degrees at the north. The point of rotation of the abutment about the bridge deck appeared to be between half and two-thirds of the way down the deck beam (300 – 400 mm from the deck surface). As a result of abutment rotation and the relative movement of the pedestrian underpasses to the abutment toe, the inferred permanent lateral displacements of the foundation soils were found to be ~0.66 m and ~0.36 m at the south and north abutments respectively. Both of the bridge pier column-bents sustained visible cracking damage, particularly pronounced at the pier-beam connections; inspections showed that these cracks extended only as far as the cover concrete.

For more information relating to observed damages to ANZAC Bridge and its surrounds refer to the detailed observations in Section 3.7.7.4.

5.4.4 Pseudo-static analysis

Two separate series of PSAs were performed on ANZAC Bridge; the first to simulate the post-liquefaction lateral spreading phase, and the second to simulate the cyclic loading phase which occurs during earthquake shaking. Within each set of analyses single-pile models were first constructed, followed by a model of the whole structure. All models are based on a representative tributary bridge width of 1.5 metres (centre-to-centre abutment pile spacing), and all beam element and soil-spring properties have been scaled to this accordingly. The model results will be presented systematically. First, the lateral spreading phase of loading is considered and single pile model results are shown followed by the global bridge model. Secondly, the cyclic loading phase is considered again represented first by single pile models followed by the global bridge model. All analyses are based on measurements made following the 22nd February 2011 earthquake.

5.4.4.1 Beam elements

The global bridge model comprises five beam elements which represent the abutments, abutment piles, piers, pier piles and bridge deck respectively. The concrete abutments and bridge deck are assumed to remain in the elastic range and thus have linear moment-curvature relationships with a flexural stiffness (EI) found by multiplying Young's modulus (E) of concrete by each sections second moment of area (I). The steel H-piles beneath each abutment have bi-linear moment-curvature relationships determined by Young's modulus of steel and the sections elastic and plastic second moments of area.

The moment-curvature relationships of the reinforced concrete piers are tri-linear, with the 3 points defined as:

1. Cracking (M_c) – the point where tensile stress in the concrete exceeds concrete tensile strength

2. Yielding (M_y) – the point where the yield stress of the reinforcing steel exceeds reinforcing yield strength

3. Ultimate (M_u) – the point where compressive stress in the concrete exceeds the crushing strength of concrete

The moment-curvature relationships of the pier piles are also tri-linear, however the 3 points are defined differently due to the reinforced concrete piles being encased by an 8 mm thick permanent steel casing. The first point corresponds to the yielding of the casing steel ($M_{y,c}$), then, as above, this is followed by the yielding of the reinforcing ($M_{y,r}$) and finally the crushing of the concrete (M_u).

Knowing each member's cross-section, material properties and other characteristics (i.e. area, dimensions, axial load, position of reinforcement, spacing of transverse reinforcement) the moment-curvature relationships for each element were calculated using *CUMBIA* (Montejo and Kowalsky 2007) and are shown below in Figure 5-11. Note that these have been scaled to be representative of a 1.5 m tributary bridge width (i.e. scaled to the width of the bridge supported by one abutment pile).

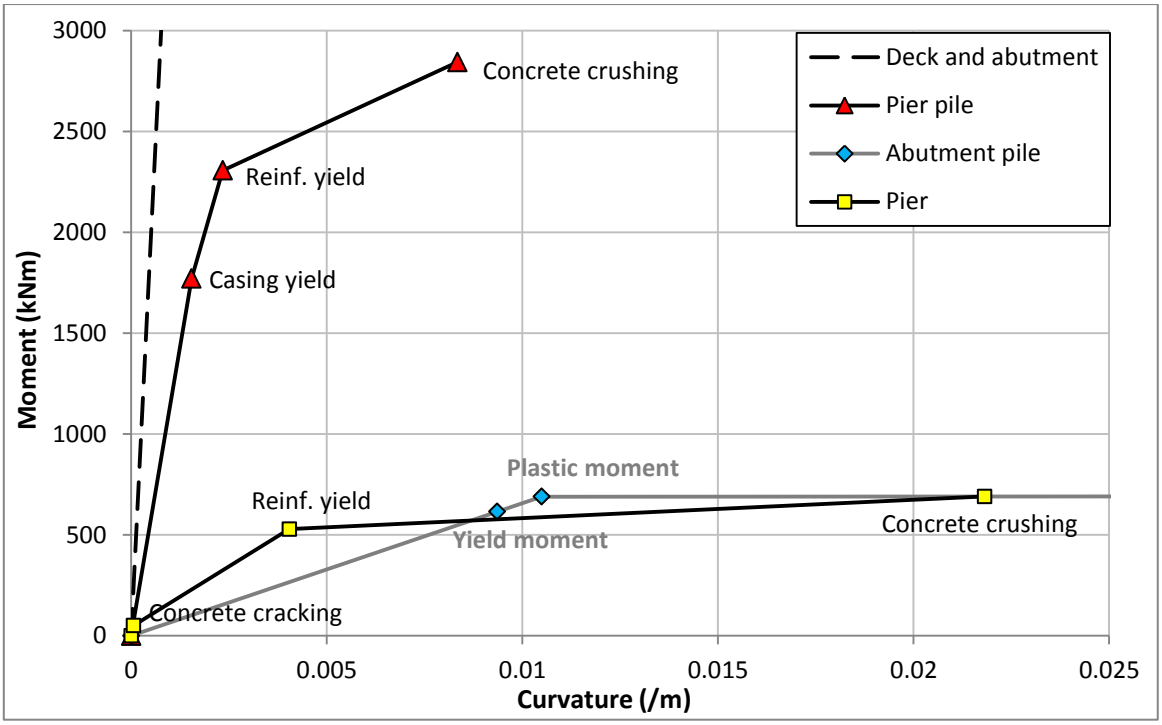

Figure 5-11: Moment-curvature relationships for beam elements, ANZAC Bridge

5.4.4.2 Soil springs

Each soil spring is assigned a bi-linear load-deflection (*p-δ* or *p-y*) relationship in order to account for soil yielding once it reaches its ultimate pressure. Reduced stiffness due to liquefaction or other nonlinearity can be accounted for by applying a degradation factor β to the initial spring stiffness.

The soil springs were divided into layers at each abutment based on the analysis results from the two CPTs as discussed previously. For the purposes of the global bridge model it was necessary to interpolate between these in order to create assumed profiles for the central pier piles. This interpolation is shown in Figure 5-12, where the layers deemed to have liquefied are shaded blue. The exact formulation of each soil spring is treated separately for each of three distinct zones within a soil column; the crust layer, liquefied layers, and deeper non-liquefied layers. In Appendix C is a spreadsheet which shows the results of all the soil-spring calculations (including parametric variations) for the lateral spreading phase using *CPT-2*, the south abutment model of ANZAC Bridge.

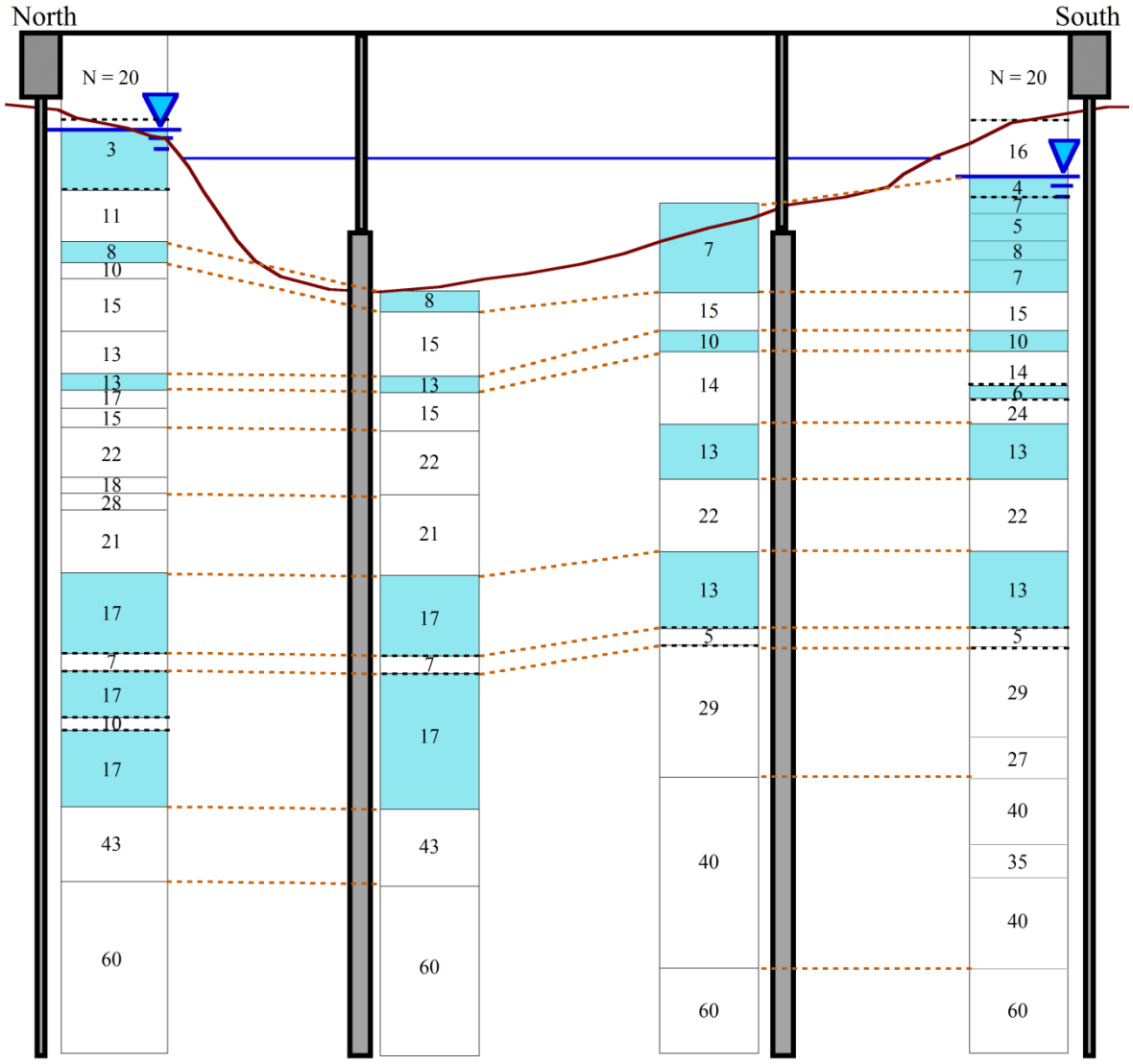

Figure 5-12: ANZAC whole-bridge model assumed soil-spring columns

5.4.4.3 Lateral spreading phase

First, the lateral displacement to apply to each abutment/pile system must be established. Lateral spreading transects in the vicinity of the bridge provided a measure of the total lateral displacement at the ground surface in the "free field". Thus, this displacement is likely to form the upper bound limit on the displacement experienced by the bridge system. A best estimate lateral displacement, smaller than that measured in the free field (due to the fact that a bridge restrains lateral ground movement) is then calculated, where possible, based on observations made relating to the permanent displacements of the foundation soils. A lower bound displacement is then chosen

which would represent the lowest damage scenario. These were found to be 0.4 m, 0.36 m and 0.2 m at the north abutment respectively, and 1.0 m, 0.66 m and 0.4 m at the south abutment.

These values were then multiplied throughout depth based on the lateral displacement index profiles shown in Figures 5-9 and 5-10 and applied to each set of soil springs in the models. The point of "zero depth" shown in the following figures refers not to the ground surface but in fact to the point of rotation occurring between the deck beam and the abutment seat, approximately 400 mm below the approach/deck surface. The top of the abutment is constrained laterally in the single pile model at this point of rotation, corresponding to zero displacement. The results of the parametric study are presented below and the effects of changing different parameters in each layer are examined separately. Horizontal pile displacements and bending moments throughout depth are presented to highlight the response of the system.

Single pile model

Both the north and south abutment-pile systems are modelled separately; the results of the parametric studies are as follows. In the single pile models the point of abutment rotation ("zero depth" in the following figures) is constrained in the lateral direction, hence zero lateral displacement shown, but is free to rotate.

Effect of crust layer

Figures 5-13 and 5-14 display the results of the abutment-pile systems' response to variations in the crust parameters α_{Crust}, β_{Crust}, δ_u and φ'_{Crust}. The response of the north abutment piles (Figure 5-13) shows little sensitivity to the variations in these parameters, aside from small differences in the bending moments in the upper 2 metres of the piles. The results suggest that bending moments close to the yielding moment are reached from approximately 0.5 m to 2.5 m below the pile top, with $M<<M_y$ everywhere else. Back-calculating the induced abutment back-rotation from the computed displacement of 60 mm at the abutment toe gives a rotation angle of 2.5°, just over half of what was observed in the field. This indicates that the model may be slightly under-predicting the systems response in this case.

The south abutments response shows a high sensitivity to the variations in crust parameters. Of particular influence are those parameters affecting the soil-spring strength properties, α_{Crust} and φ'_{Crust}, while the parameters affecting stiffness, β_{Crust} and δ_u, only led to minor variations in pile response. The RM model predicted displacements at the abutment toe of 350 mm, implying a back-rotation of 14°, much greater than the observed 6°. The computed bending moments indicate that

the yield moment was exceeded and plastic moment approached between 0.5 and 1.5 metres below the pile top as well as at the interface between a strong non-liquefied layer and the bottom of the liquefied layer at approximately 15 metres depth.

When the lower bound value of α_{Crust} = 3 was used along with all other parameters at RM the pile head displacement was decreased to around 200 mm, highlighting the sensitivity of the piles response to this parameter. In light of this, an additional analysis was performed which combined the lower bound values of both strength parameters, setting α_{Crust} = 3 and φ'_{Crust} = 33°, with all other values at RM. This combination further reduced abutment toe displacements (and associated bending moments) to approximately 150 mm, i.e. equivalent to the 6° back-rotation observed in the field. This illustrates the high sensitivity of the model to the choice of crust parameters, which, in this case, are clearly dominating the response. It may be argued that one reason for the lower bound strength parameters better matching the observed systems response is that the soils directly behind the abutment did not remain as a rigid block during the earthquake. Substantial slumping of the south approach occurred in the direction parallel to the roadway which would have reduced confining pressures, and hence reduced the ultimate pressure that the backfill soils were applying to the abutment piles in the crust layer.

The primary reason for the difference in the sensitivity of the response between the north and the south is that the effect of the crust thickness on the south is more significant than the north (3.4 m compared with 2.3 m) and highlights the magnitude of the load it applies and hence the governing role that it plays. In recognition of this, a separate analysis on the south abutment was carried out using the same crust thickness as the north and with RM values everywhere else ("NA crust" in Figure 5-14). The resulting response was significantly reduced in comparison to the larger crust thickness, both in terms of computed displacements and induced bending moments, and tended towards the response of the north.

Effect of liquefied layers

Figure 5-15 illustrates that for both the north and south abutments the properties of the liquefied layers have practically no influence whatsoever. Variations in the strength parameters, α_{Liq} and S_r have negligible effect as does the stiffness-affecting parameter, β_{Liq}. Here it is clear that the load from the crust is still dominating the behaviour.

Effect of deeper non-liquefied layers

Figure 5-16 presents the effects that the deeper non-liquefied layers (not including the base layer) have on pile response. These too have little to no consequence on pile response. There is a small reduction in computed bending moment between the depths of about 6 and 14 metres in both

abutments when the lower bound value of $\beta_{Non\text{-}Liq}$ = 0.3 is used to reduce the stiffness of these layers. It is more than likely that some degree of stiffness reduction did occur in these layers as a result of seepage from deeper layers and elevated pore pressures.

Effect of magnitude of ground displacement

In order to investigate the effect that a larger or smaller applied ground displacement has on pile response, the applied displacements at the surface were varied between 0.2 and 0.4 m for the north abutment, and 0.4 and 1.0 m for the south (scaled throughout depth accordingly). Figures 5-17 and 5-18 show the analysis results with these applied displacements as well as the previous "best estimate" displacements, all applied to the RM model. Results using the lower bound crust model with values of α_{Crust} = 3 and φ'_{Crust} = 33° at both abutments are also presented. It is evident that the magnitude of ground displacement has a large effect on both the displacement response and computed bending moments in the piles.

On the north abutment (Figure 5-17), the lower bound applied displacement meant that $M<<M_y$ everywhere and an abutment back-rotation of 1.5° was induced. The upper bound displacement produced results very similar to those of the best estimate results.

The south abutment lower bound displacement models (Figure 5-18) led to computed bending moments reaching plastic moment at approximately 1.5 m below the pile head, with $M<M_y$ everywhere else. The calculated displacements inferred abutment back-rotations of 1.5 – 4 degrees, much smaller than observed. The upper bound displacement of 1 metre, on the other hand, yielded inferred back-rotations of between 10 and 23°, significantly greater than observed, even with the use of the lower bound crust properties. This implies that the use of free-field lateral spreading displacements as an input into this PSA may be overly conservative. The computed bending moments were virtually the same as those produced by the best estimate ground displacement models.

Effect of allowing for a bridge expansion/construction joint

Figure 5-19 shows the effect of allowing for a bridge construction or expansion joint at each abutment/deck connection. Since ANZAC Bridge is a segmental structure it more than likely contains expansion joints at each end which allow for thermal or other similar expansive movements. As such, an extra set of analyses was run which assumed a gap joint size of 30 mm, meaning that the top of the abutment was free to move laterally up to a limit of 30 mm, at which point it was restrained from moving any further. At the north abutment this slightly altered the displacement profile up to a depth of 5 metres and also reduced the induced bending moments near the pile tip to beneath yielding. At the south abutment both RM and LB crust strength models were considered.

In both cases a distinct discontinuity in pile displacement response was observed between 1 and 2 metres beneath the pile top. Computed bending moment response was negligibly affected. The inclusion of this construction gap in the model is only used to illustrate the magnitude of change in the response, and cannot be considered an improvement on the accuracy of the model. The reason for this is that it is not known whether this joint was closed previously as a result of the Darfield earthquake, or perhaps temperature effects meant that it was reduced at the time of the Christchurch earthquake (occurring in the middle of the day in late summer).

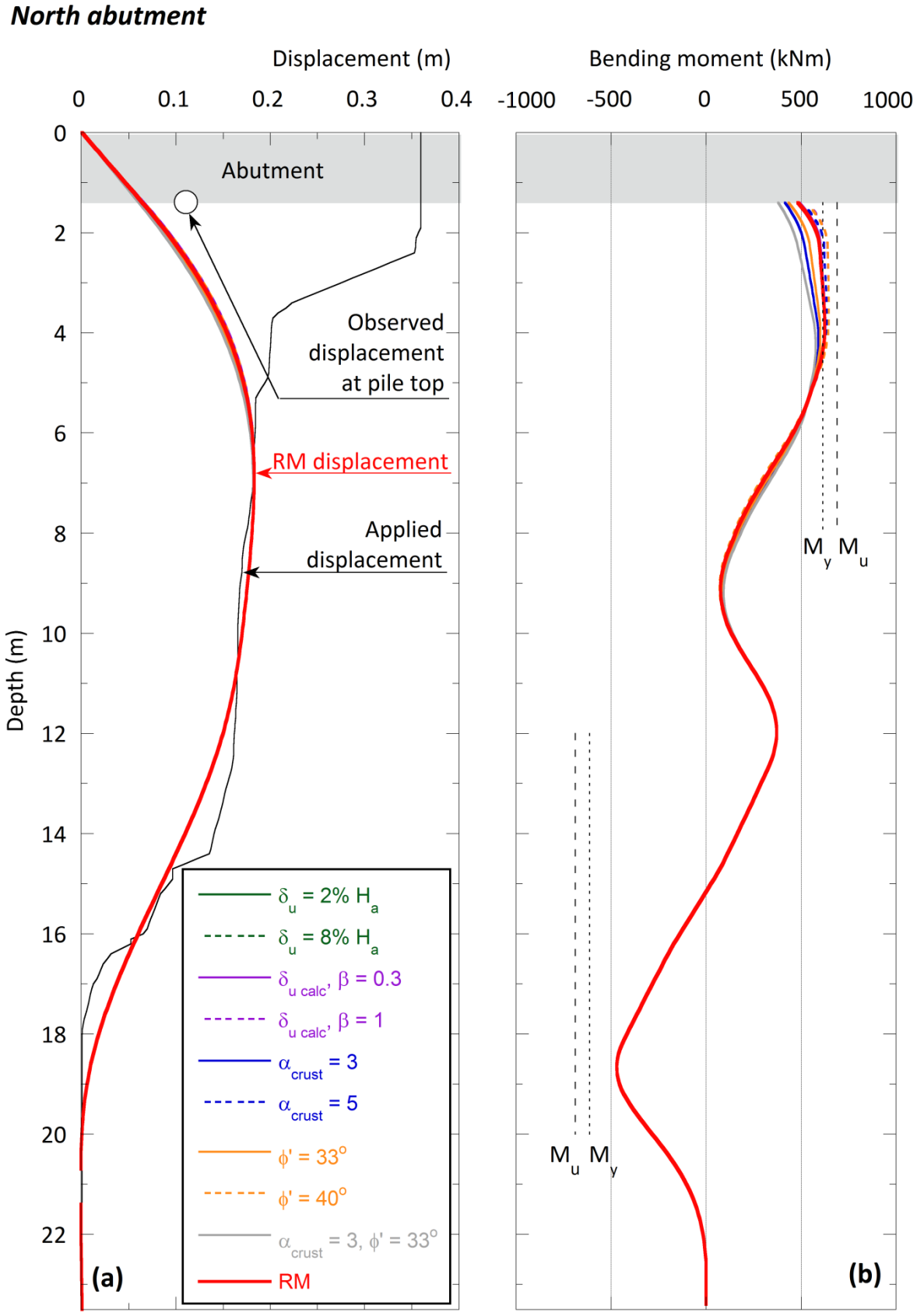

Figure 5-13: Single pile lateral spreading analyses, ANZAC Bridge, effect of crust layer (a) north abutment displacement, (b) north abutment bending moments

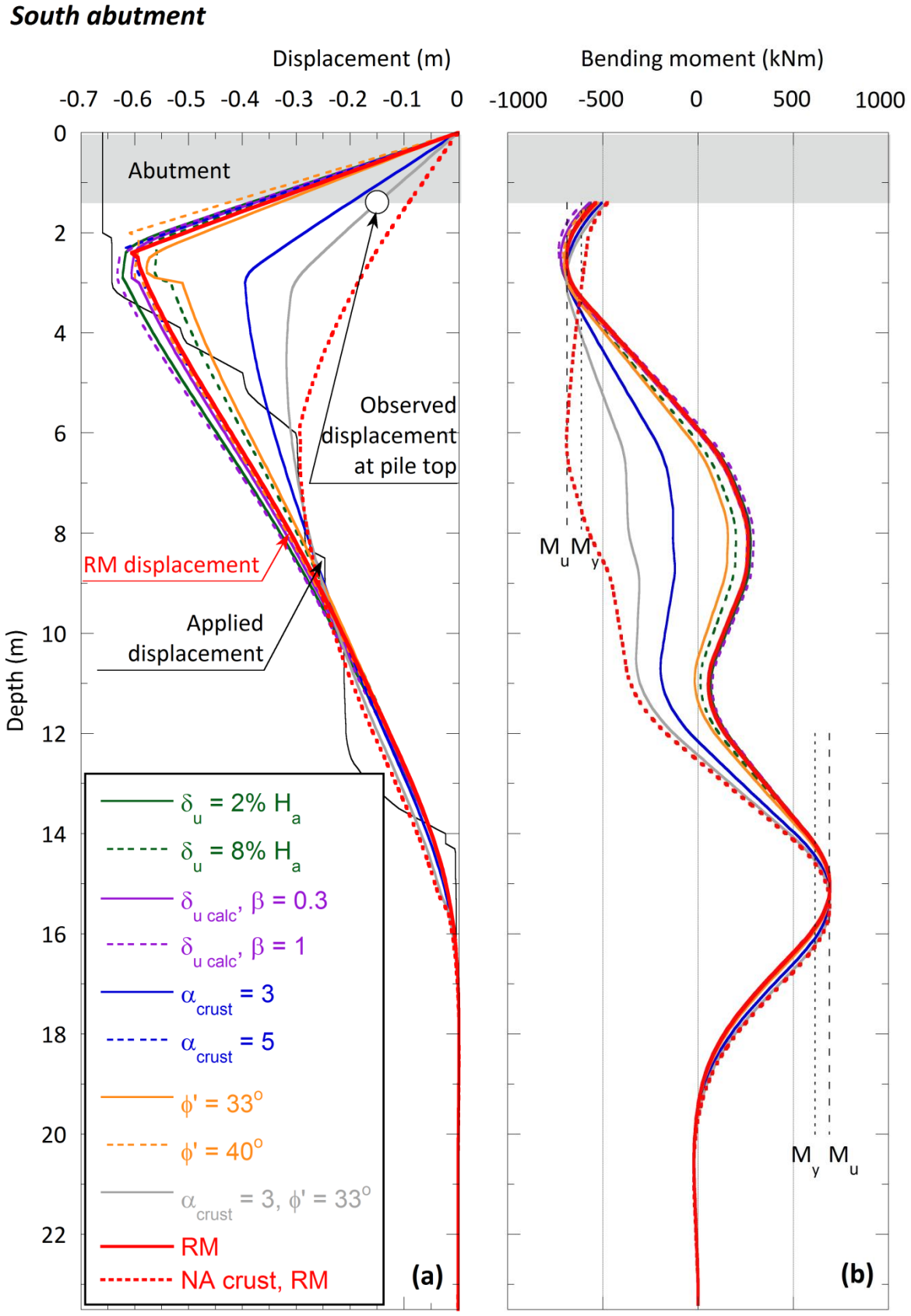

Figure 5-14: Single pile lateral spreading analyses, ANZAC Bridge, effect of crust layer (a) south abutment displacement, (b) south abutment bending moments

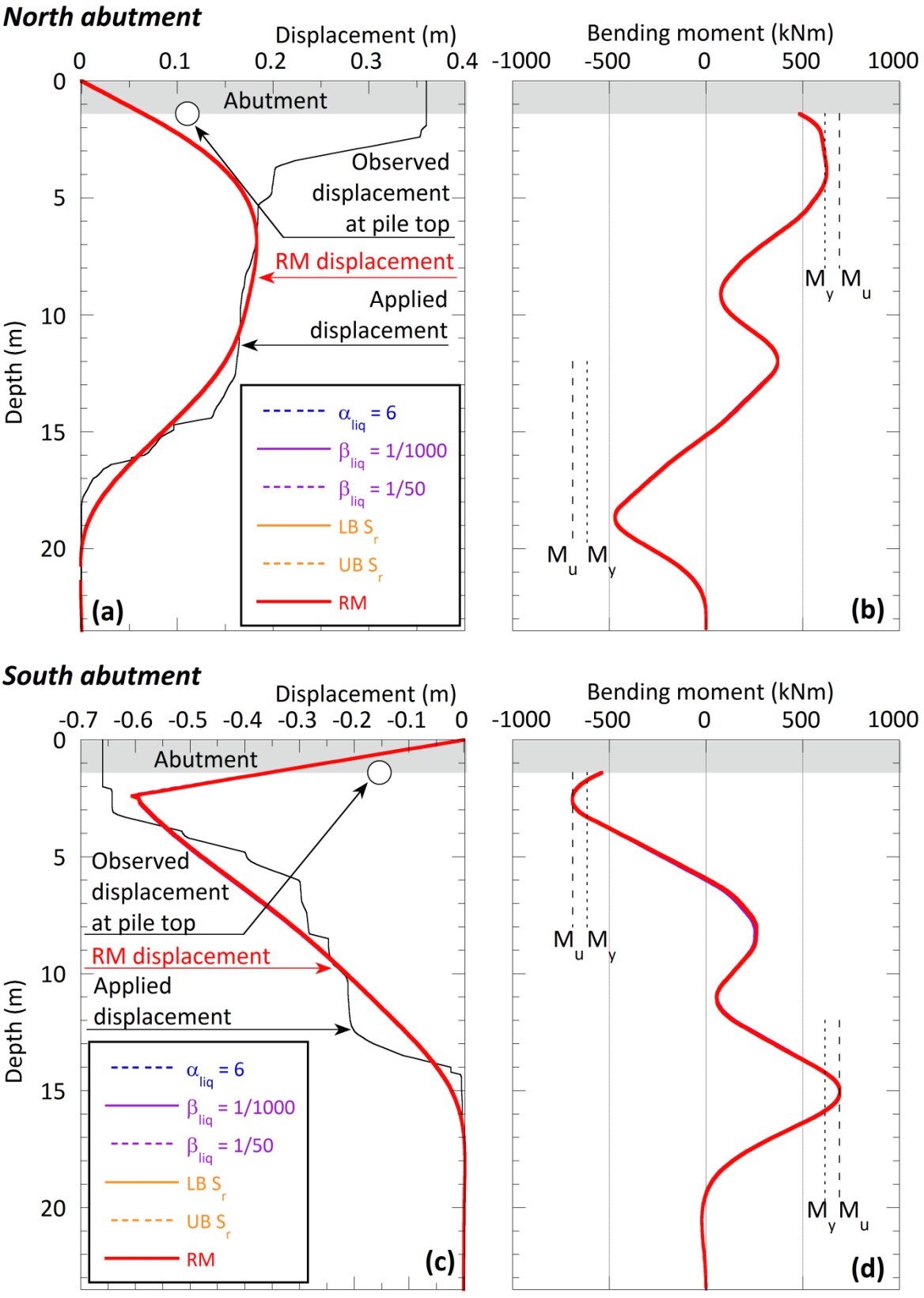

Figure 5-15: Single pile lateral spreading analyses, ANZAC Bridge, effect of liquefied layers, (a) north abutment displacement, (b) north abutment bending moments, (c) south abutment displacement, (d) south abutment bending moments

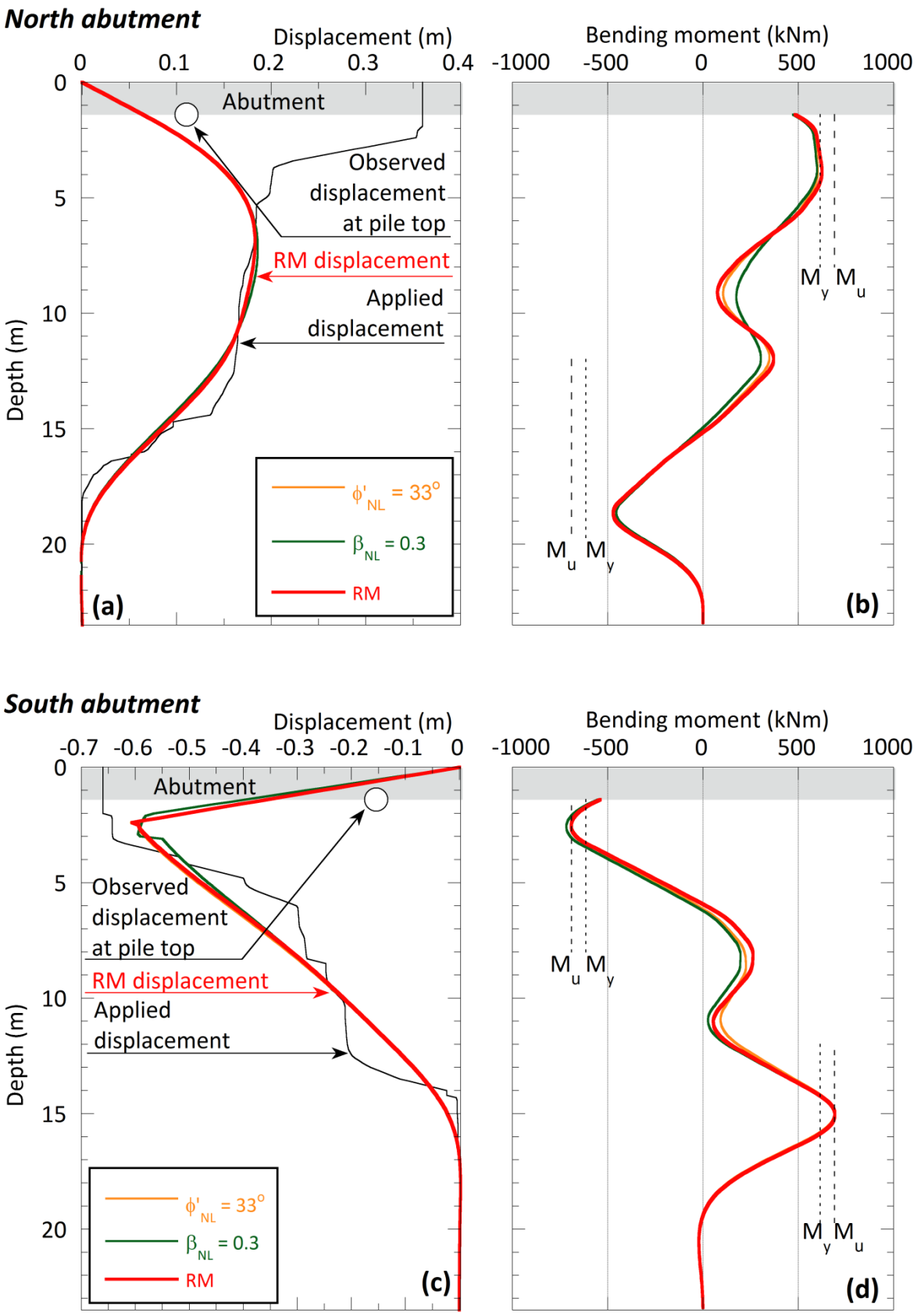

Figure 5-16: Single pile lateral spreading analyses, ANZAC Bridge, effect of deeper non-liquefied layers, (a) north abutment displacement, (b) north abutment bending moments, (c) south abutment displacement, (d) south abutment bending moments

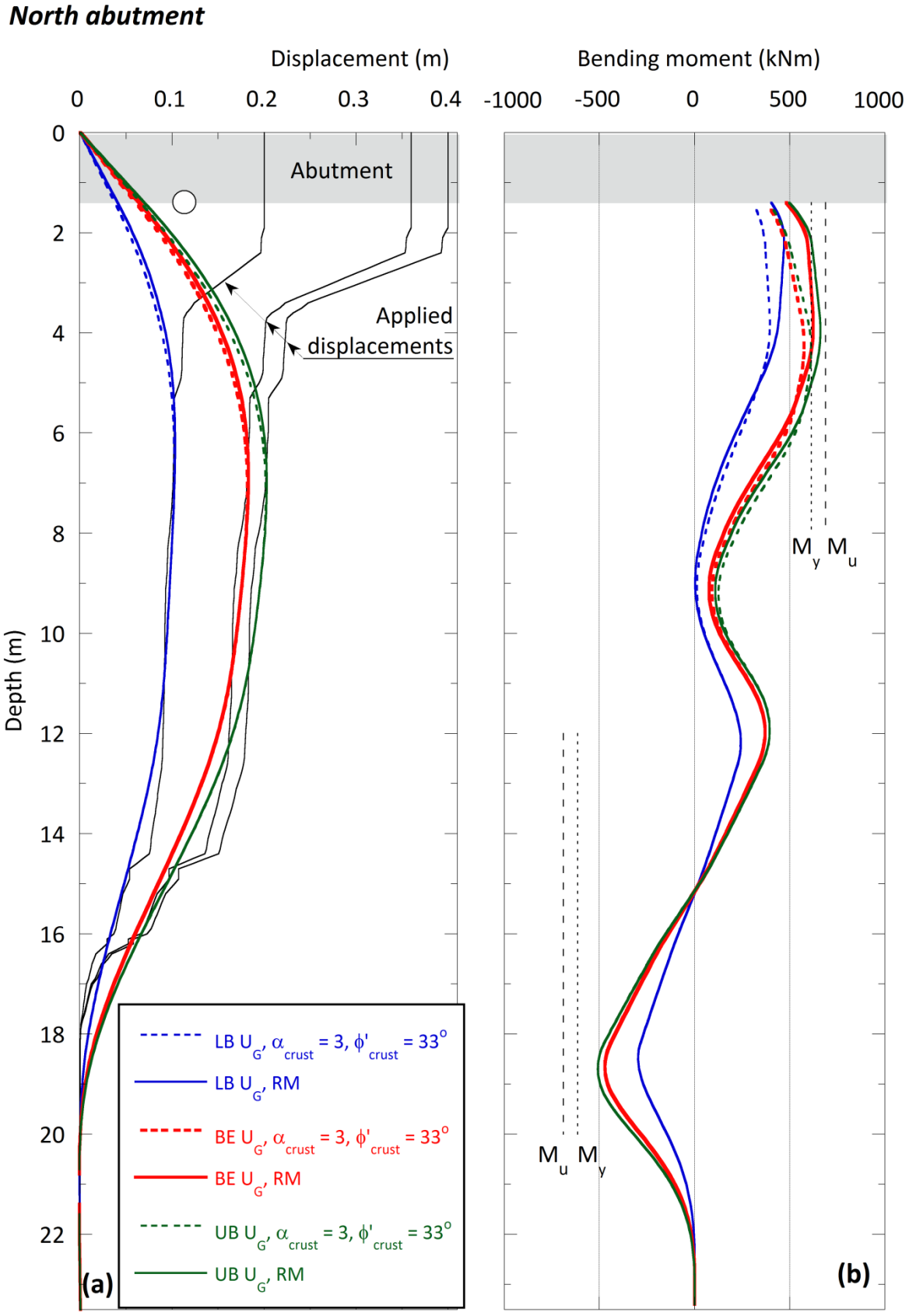

Figure 5-17: Single pile lateral spreading analyses, ANZAC Bridge, effect of magnitude of ground displacement, (a) north abutment displacements, (b) north abutment bending moments

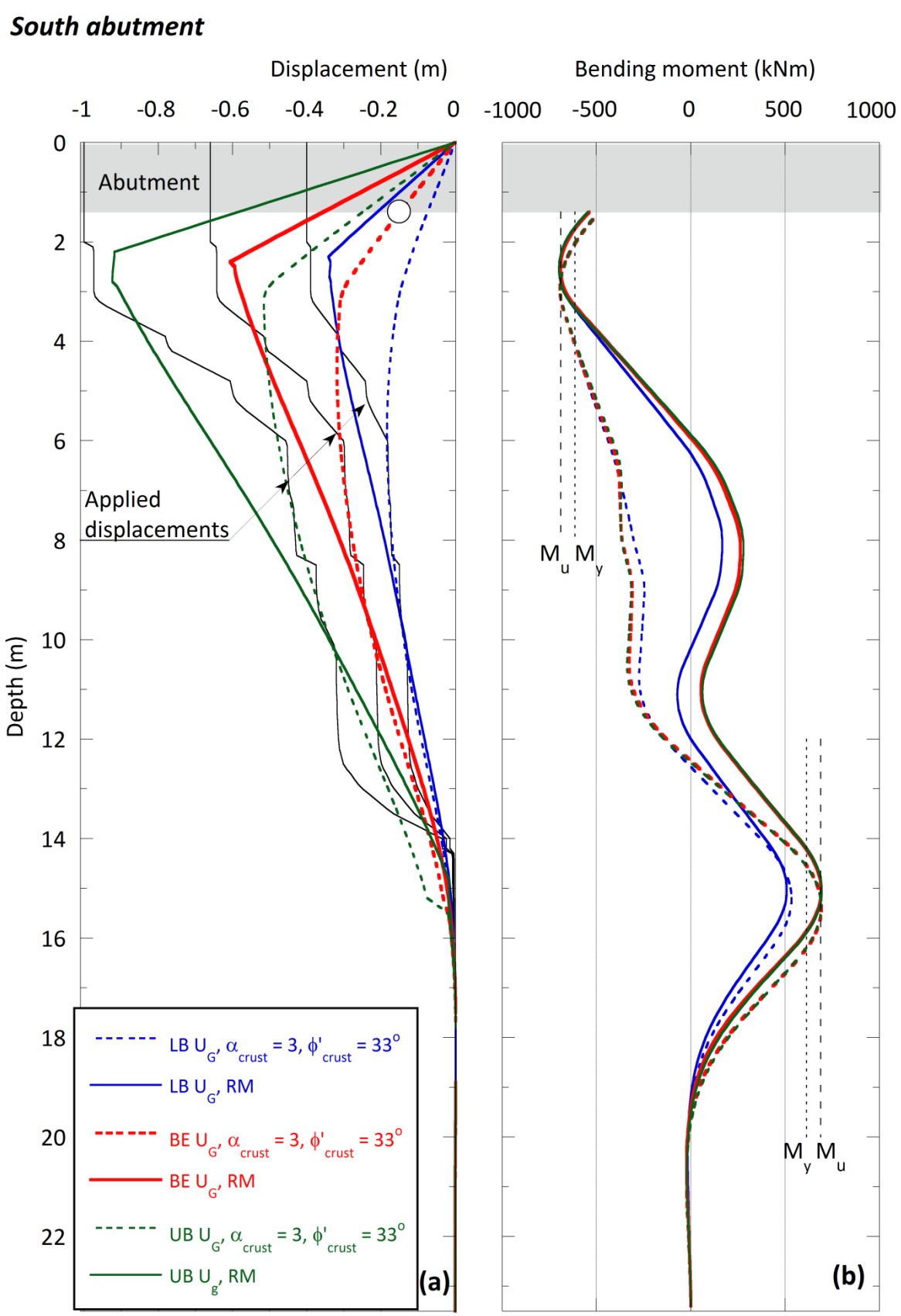

Figure 5-18: Single pile lateral spreading analyses, ANZAC Bridge, effect of magnitude of ground displacement, (a) south abutment displacements, (b) south abutment bending moments

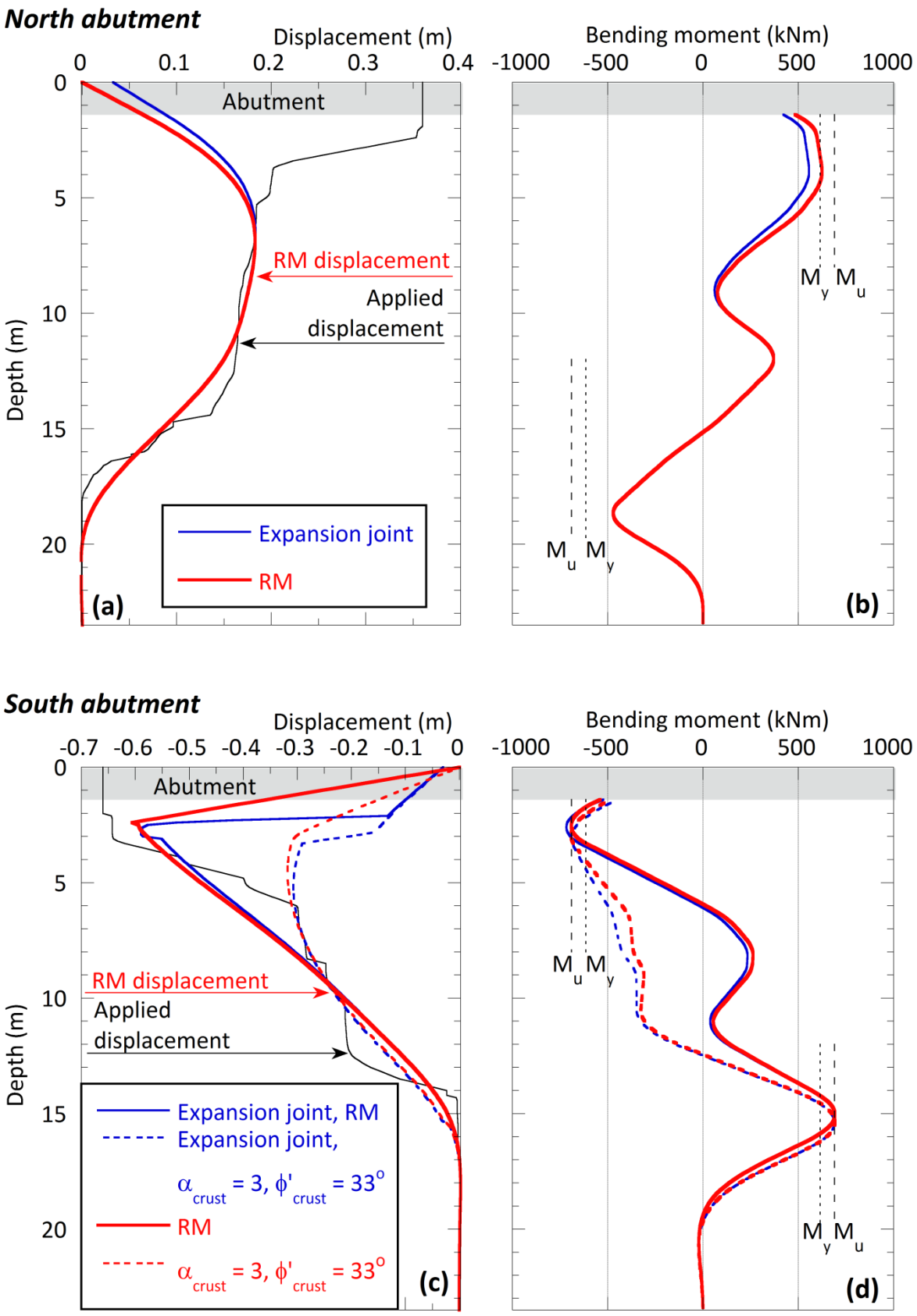

Figure 5-19: Single pile lateral spreading analyses, ANZAC Bridge, effect of expansion/construction joint, (a) north abutment displacements, (b) north abutment bending moments, (c) south abutment displacement, (d) south abutment bending moments

Whole bridge model

One difference between the single pile and whole bridge model is in the fixity conditions imposed on each end of the bridge. At each abutment/deck connection the abutment is considered free to rotate as well as displace laterally up to a limit of 30 mm (using the same expansion joint assumption as mentioned previously). At each pier/deck connection rotation is restrained such that a moment connection is established.

Figure 5-20 gives a schematic view of the global bridge model including applied ground displacements, bridge deformed shape and computed bending moments in the piers and pier piles. First the global bridge model was run by simply applying the best estimate lateral spreading displacements to the end abutment/pile systems to see if the results were comparable to those of the single pile systems ("A" analysis in Figure 5-20). These were shown to be fully consistent. Note that the soil model used at the south abutment for all global analyses was that with the lower bound crust strength parameters of $\alpha_{crust} = 3$ and $\varphi'_{crust} = 33°$.

Next, lateral spreading displacements were applied to the central pier/pile systems in addition to those already on the abutments ("A + P" analyses in Figure 5-20). These displacements are distributed throughout depth in proportion to a lateral displacement index calculated for each central pier/pile soil profile based on the methodology of Zhang *et al.* (2004) described earlier. The displacement at the surface is calculated (at a best estimate) to be some proportion of the displacement at the same horizontal level of the nearest abutment. As a reference value, the surface displacement at each pier/pile was taken to be 50% of the lateral displacement applied at the same elevation of the nearest abutment/pile system. This displacement was varied in order to see what effect it had on system response.

Typically, due to being submerged, the central piers/piles will not have a crust layer as often the top layer being fully saturated and relatively weak or loose will liquefy. For this reason no parametric variations based on a crust layer were carried out for the central piers/piles.

The RM for the liquefied layers in the central piers/piles was the same as described for the single pile systems. However, due to the lack of a crust layer, a significant variation in the properties of the liquefied layers is to use the empirical relationship for residual strength of Olson and Stark (2002). The difference between this method and that proposed by Seed and Harder is that the residual strength is normalised as a function of the effective overburden stress. Cubrinovski *et al.* (2009b) showed that the effects of normalised residual strength on pile response are affected by both the properties of the pile and the thickness of the crust layer. The effects were particularly pronounced when the crust layer was thin (no effect after $H_c > 1.75$ m) and the piles were relatively stiff. For a

thicker crust the crust properties dominate pile response and hence shear strength normalisation of liquefied layers is insignificant. For the central piers/piles one parametric variation is to look at the effect of normalising the residual strength. The strength of deeper non-liquefied layers was also reduced as one parametric variation in order to analyse its effect.

Effect of applied displacement

As can be seen in Figure 5-20, the inclusion of lateral displacements on the pier piles ("A + P") somewhat increased pier displacements over the A-analysis and induced bending moments approaching yield at the top of the northern pier. However, since the uncertainties associated with estimating permanent lateral ground displacements at the piers are significant, additional analyses were performed which further reduced these displacements. Shown in Figure 5-20 is analysis "A + 0.2P", where the displacements at the piers were reduced to 20% of their initial reference value (i.e. they are 10% of the abutment pile displacements at the equivalent elevation); as expected, this reduced bending moments in the piers. In all analyses the bending moments in the pier piles indicate that they did not suffer any damage, while cracking moments were reached substantially throughout the piers.

Effect of liquefied layers

Using the normalised residual strength of liquefied soil, instead of that proposed by Seed and Harder 1990, had negligible effect on the outcome of system response, and for this reason it was not deemed significant to show in Figure 5-20.

Effect of non-liquefied layers

Reducing the strength of non-liquefied layers by 50% in the pier pile soil columns had a similar effect to reducing the displacement applied to the pier piles ("A + P, $\alpha_{NL\text{-}0.5}$" in Figure 5-20). Strength reduction in the non-liquefied layers sandwiched between liquefied layers is likely to occur in the post-shaking lateral spreading phase of ground movement, due to excess pore pressures being elevated and dissipating with time. The results of this analysis indicate no damage to the pier piles and induced cracking in the piers.

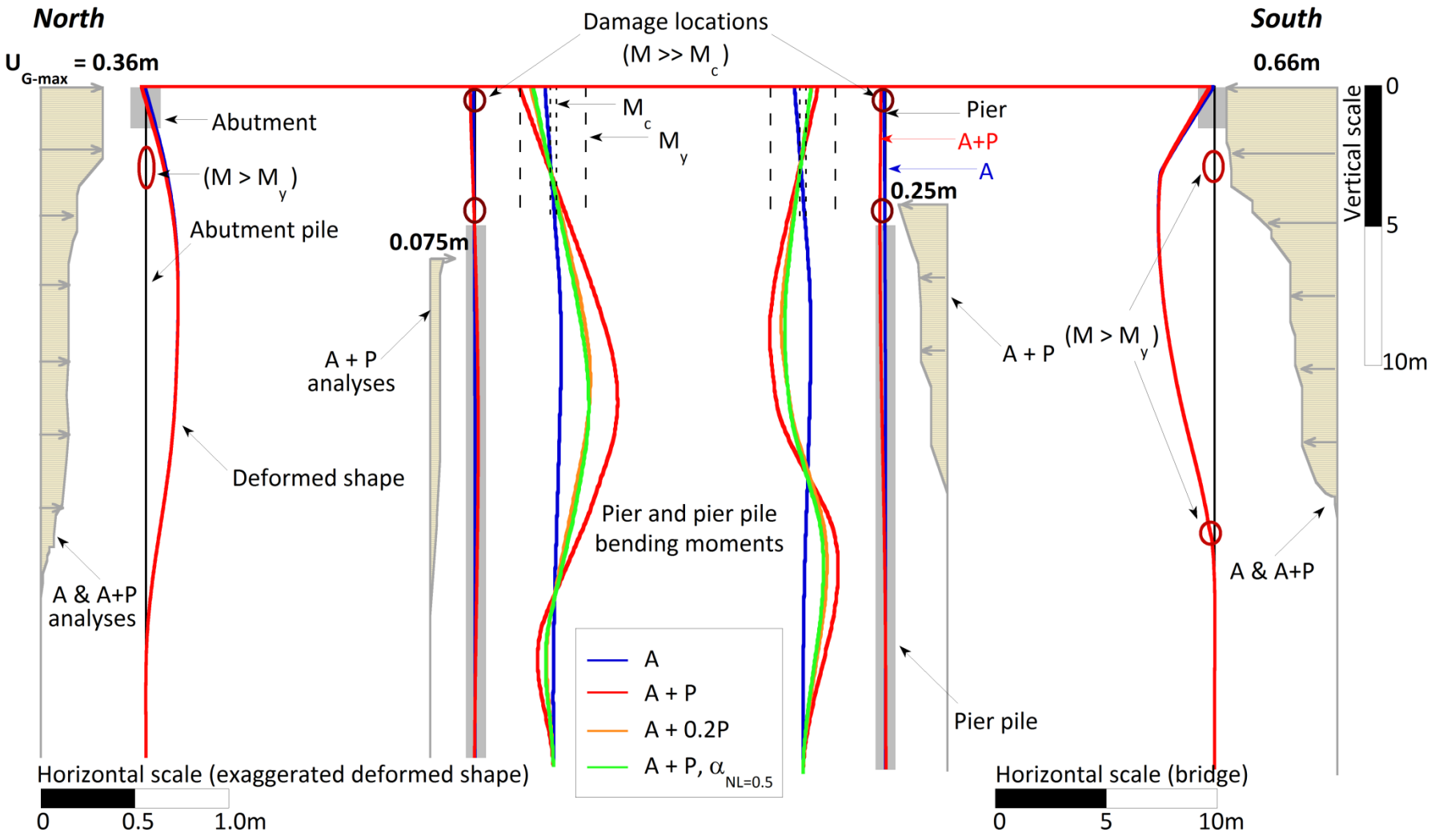

Figure 5-20: Whole bridge lateral spreading analyses, ANZAC Bridge, applied ground displacements, deformed shape and bending moments in piers and pier piles shown

5.4.4.4 Cyclic loading phase

The cyclic loading phase which occurs during earthquake shaking involves the application of cyclic ground displacements to the soil-pile system in conjunction with inertial loads from the vibrating weight of the superstructure. Cyclic ground displacements and their distribution throughout depth were evaluated for all soil columns using the method of Tokimatsu and Asaka (1998). Inertial loads were established by multiplying the axial load (proportional to the tributary width considered) on each component by the PGA. First, a single pile model is considered which includes the effects of ground displacements only, followed by a global bridge model which includes the effects of inertial loads and ground displacements. The computed cyclic ground displacements at the top of each soil column are 0.16, 0.11, 0.14 and 0.17 m for the north abutment, north pier, south pier and south abutment respectively. Cyclic loadings in the longitudinal direction only are considered.

Single pile model

Effect of liquefied layers

Figure 5-21 shows the applied cyclic ground displacements in the downslope direction (towards the river) for the north and south abutment/pile systems. At the north abutment no induced pile damage is computed, and any changes in liquefied layer properties have negligible effect. At the south abutment the parametric variations in liquefied layer properties also have little effect, yet yielding and/or ultimate moment is still reached between 1 and 2 metres below the pile head (depending on crust strength parameters considered). It is likely that this can also be attributed to the large crust thickness; hence this load is still the one which dominates.

Effect of displacement in the opposite direction

Figure 5-22 demonstrates the effect of applying cyclic ground displacements to the abutment piles in the upslope direction (i.e. away from the river). These displacements are only applied from 1.8 m depth and downwards, since the top 300-400 mm of the sides of the piles facing the river are exposed and hence do not have any soil to directly push against them. The magnitudes of the applied displacements are taken to be 50% of those in the downslope direction, this is an assumption made based on the fact that cyclic displacements are likely to be biased in the downslope direction due to gravity effects. At both abutments the resulting bending moments are computed to be well below yield moment everywhere.

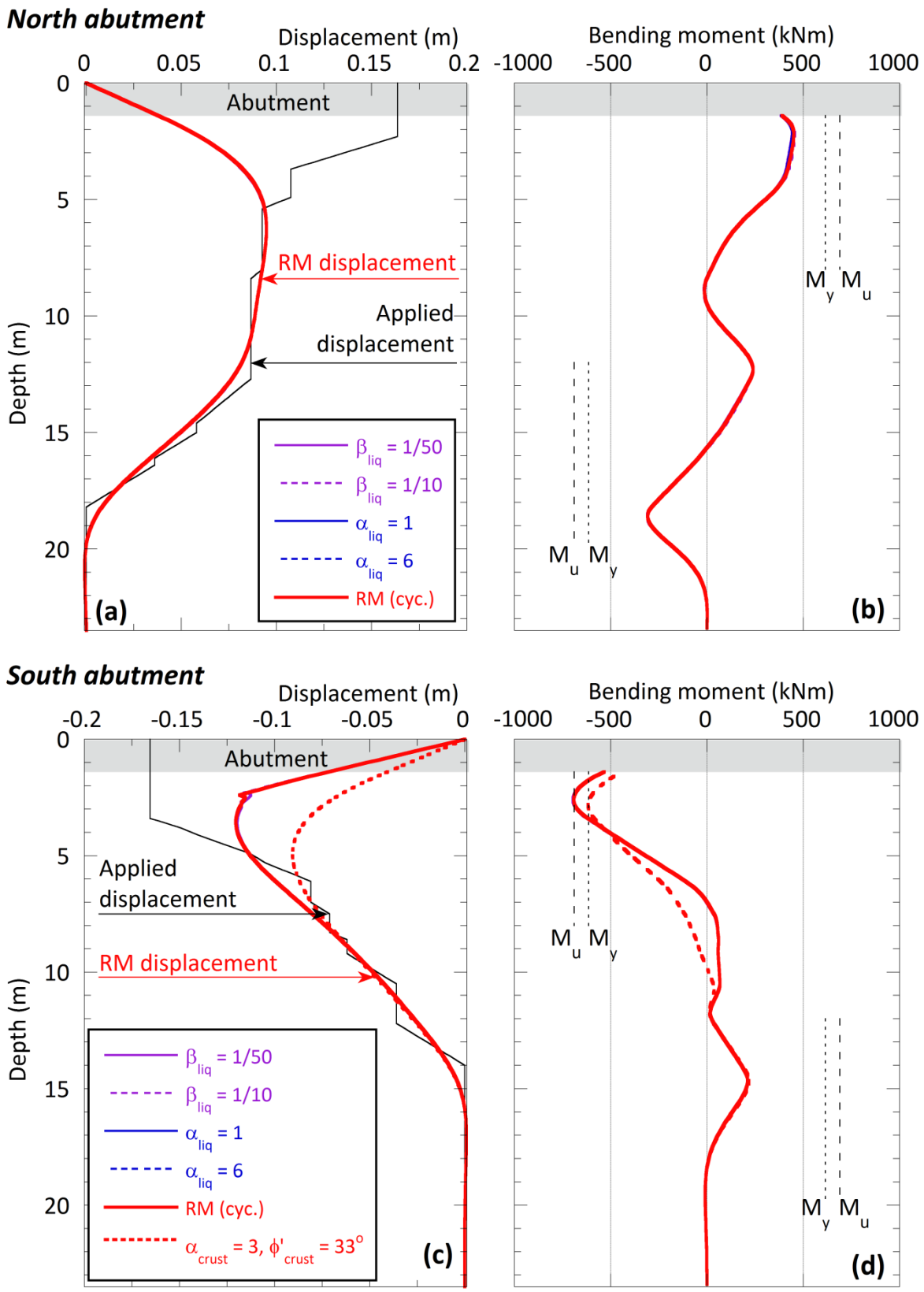

Figure 5-21: Single pile cyclic analyses, ANZAC Bridge, effect of liquefied layers, (a) north abutment displacement, (b) north abutment bending moments, (c) south abutment displacement, (d) south abutment bending moments

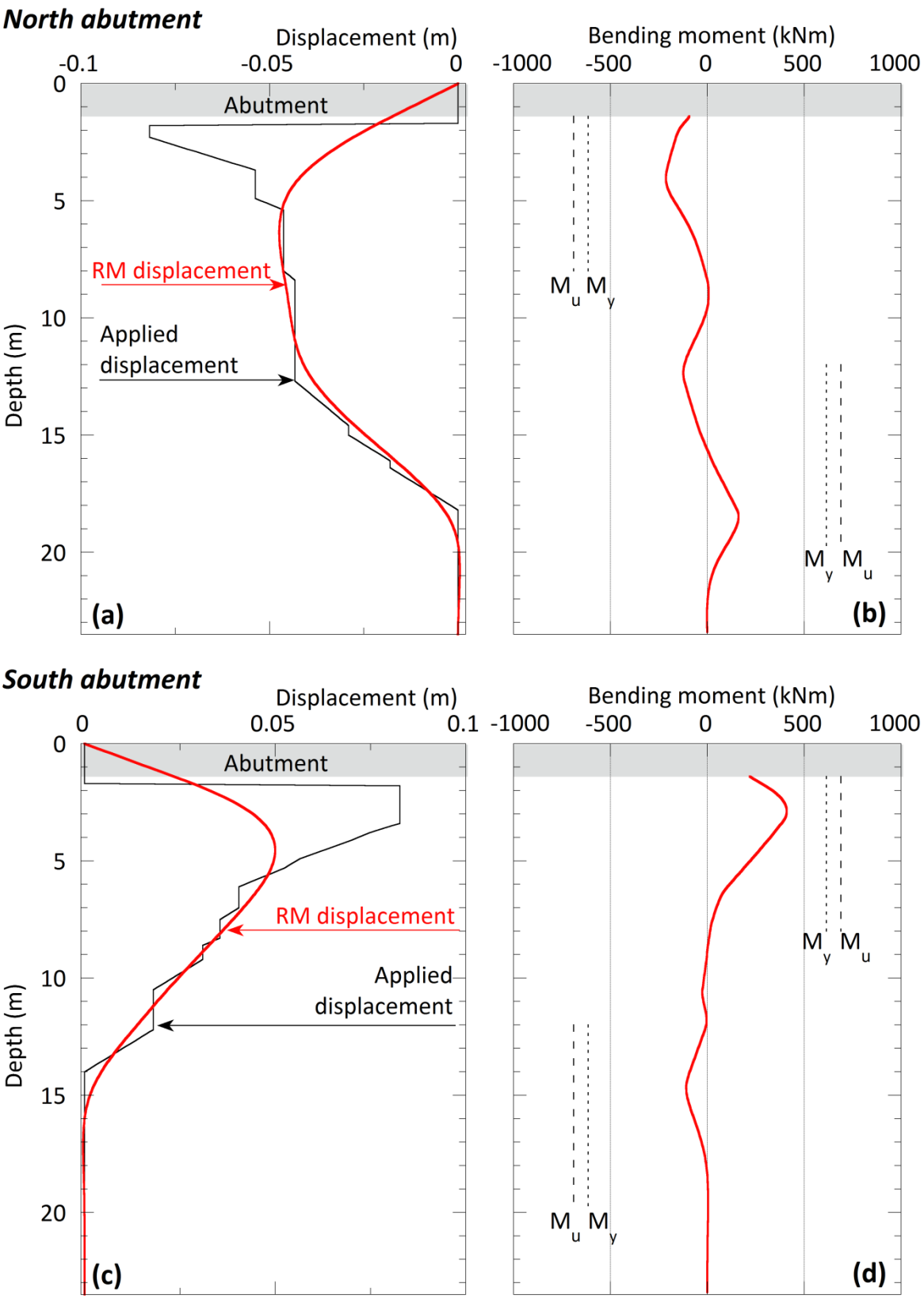

Figure 5-22: Single pile cyclic analyses, ANZAC Bridge, effect of displacement in opposite direction, (a) north abutment displacement, (b) north abutment bending moments, (c) south abutment displacement, (d) south abutment bending moments

Whole bridge model

Cyclic analyses were carried out on the whole bridge model in both longitudinal directions, north to south loading (the schematic of which is shown in Figure 5-23) and south to north (Figure 5-24). In both cases the first analyses were run by applying inertial loads due to the horizontal seismic weight of the superstructure to the tops of the abutments and piers ("I" analyses). Then, cyclic displacements in each direction were considered ("D" analyses). Finally the combined effect of inertial loads plus cyclic displacements was analysed ("I + D" analyses).

Effect of inertial loads

In both directions of loading, inertial loads alone were shown not to induce any damage in the abutment piles. Bending moments at the tops and bottoms of both piers slightly exceeded the cracking moment.

Effect of ground displacements

Applied cyclic ground displacements had a much more significant effect on system response than inertial loads, and in both directions of loading caused bending moments greater than the cracking moment throughout both piers. Figure 5-23 shows that if the full computed cyclic displacement is applied to the southern pier and abutment (in the upslope direction) then yielding would be induced in the southern abutment pile approximately 1.5 metres below its head. In the south to north direction of loading ultimate moment is reached at this point in the southern abutment pile (Figure 5-24). No damage is predicted at the north abutment in either scenario.

Combined effects

In combining the effects of the inertial and displacement loads the inertial loads are rendered insignificant. The I+D-analyses match the D-analyses very closely, and the resulting responses are as described above. The last set of analyses run reduced the applied cyclic displacements on the upslope components of each system by 50% (e.g. for the north to south loading scenario the displacements on the south pier and abutment were reduced) in order to account for gravity-induced biases in the loading ("I + $D_{50\%\ upslope}$" analyses). In the north to south direction of loading (Figure 5-23) it can be seen that the bending moments on the northern abutment pile and pier remain unchanged, but those on the southern pier and abutment pile are reduced. Consistent with the single pile analysis of the south abutment pile, no yielding is predicted in this case. In the south to north direction of loading the moment demands on the northern pier and abutment pile are also reduced.

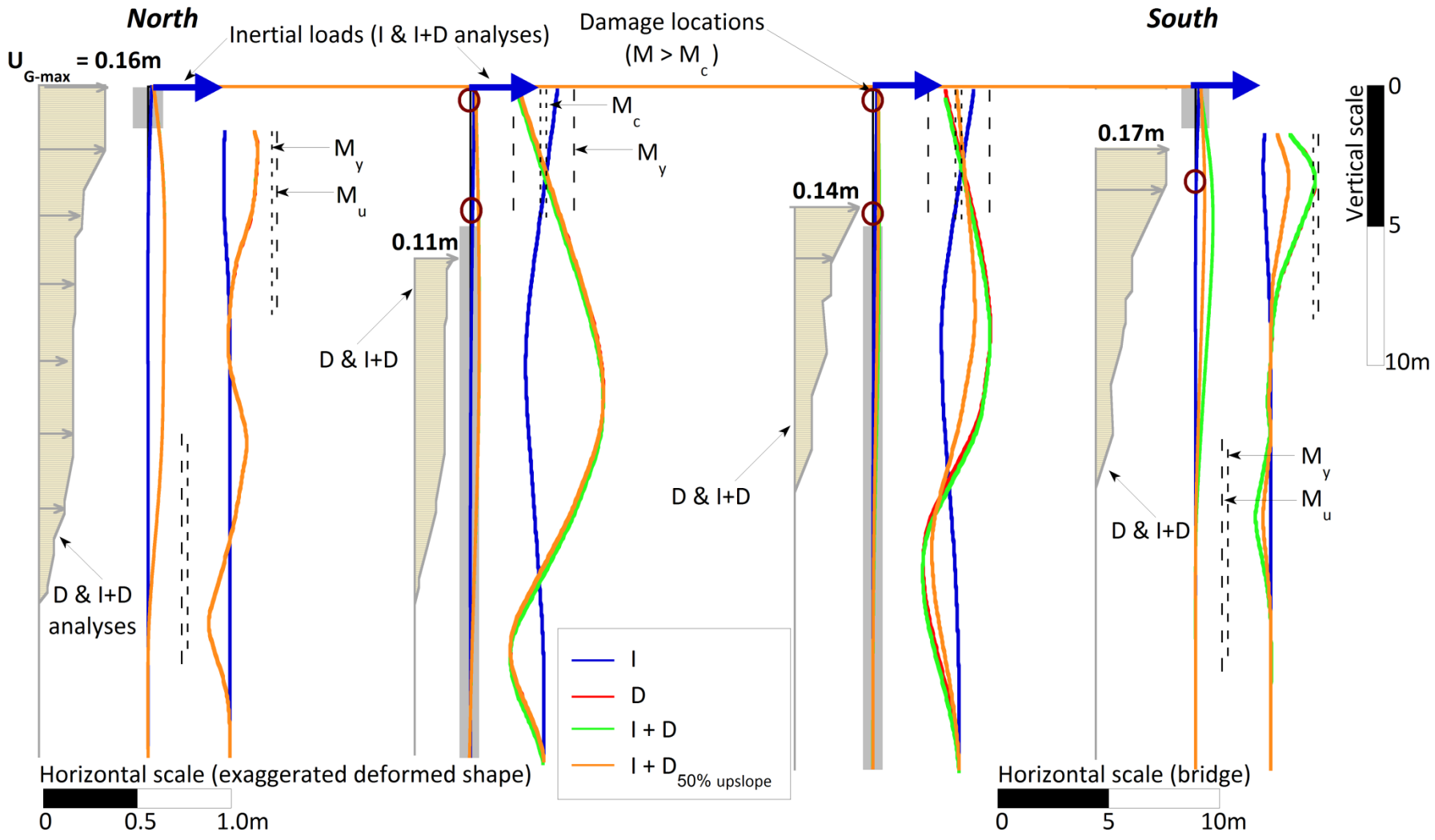

Figure 5-23: Whole bridge cyclic analyses (North to South direction), ANZAC Bridge, applied ground displacements, deformed shape and bending moments in abutment piles, piers and pier piles shown

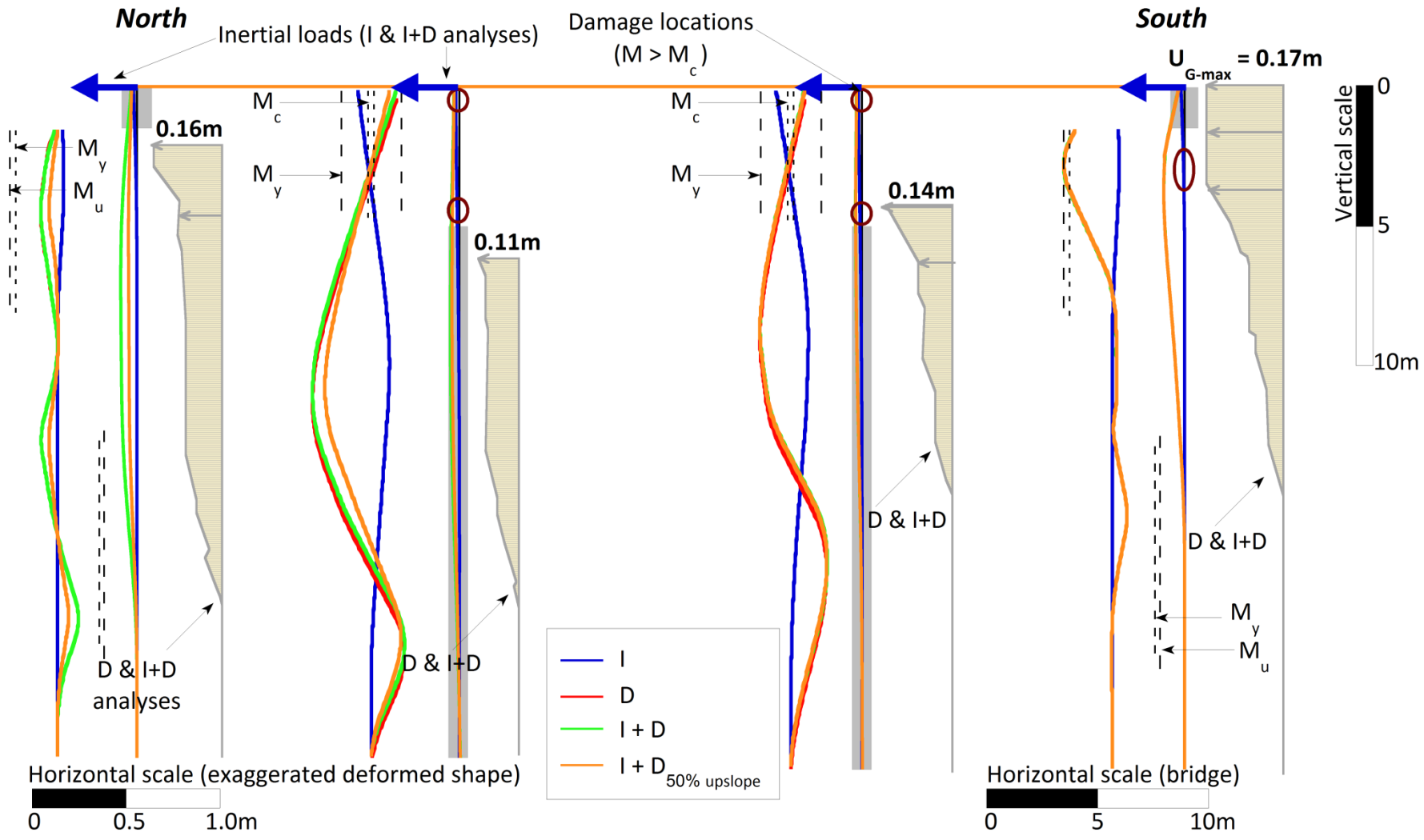

Figure 5-24: Whole bridge cyclic analyses (South to North direction), ANZAC Bridge, applied ground displacements, deformed shape and bending moments in abutment piles, piers and pier piles shown

5.4.4.5 Comparison between PSA model results and observed damages

The single pile and global bridge PSAs produced results consistent with one another in the abutments and abutment piles in both loading phases. By using a boundary condition of constrained translation (but free rotation) at the point of abutment/deck collision in the single pile PSAs, the mechanism of abutment back-rotation was able to be captured, representative of the behaviour observed at the bridge.

The response of the abutment piles in the single pile lateral spreading PSAs was found to be practically governed by the magnitude of applied lateral ground displacement and lateral load from the nonliquefied crust layer. The response of the south abutment was much more sensitive to changes in parameters in the crust layer than the north; this was due to it being approximately 50% larger in thickness. The response of the abutment piles remained virtually insensitive to changes in the properties of the liquefied and deeper nonliquefied layers, indicating that the crust layer was that which was dominating pile response. At the north abutment, yielding is computed to have occurred in the piles between 0.5 and 2.5 m below the pile head. At the south abutment, ultimate moment is computed to have been reached between 0.5 and 1.5 metres below the pile top, as well as just below the interface between the bottom non-liquefied layer and the base layer at approximately 15 metres depth. Abutment rotations were under-predicted by the model at the north abutment, and generally over-predicted by the model at the south abutment. However, when lower bound strength parameters in the crust were applied at the south abutment, the computed abutment rotations was almost identical to that observed in the field. It may be argued that these lower bound strength parameters were more appropriate to use in the model, given the degree of sideways slumping observed in the approach embankment which would have reduced the ultimate pressure capacity of the crust layer.

The global bridge response due to lateral spreading showed a high sensitivity to the effects of lateral spreading displacements to be applied to the piers/pier piles. While no yielding was computed in the piers or pier piles, the degree of cracking moments varied in the piers based on the applied level of ground displacements to the pier piles. Observations of concrete cracking and spalling at the tops of the piers are consistent with the general damages predicted by the model.

In general, the lateral spreading models predicted larger damages than the cyclic loading models. It was found that the inertial loads, on their own, in the cyclic models were of little to no consequence in the response of the abutment piles, but predicted cracking in the piers. The inertial loads were later shown to be insignificant in comparison with the applied cyclic ground displacements, and it was clear that the magnitude of applied ground displacement governed pile response.

5.5 Dallington Bridge

This section covers the PSA of Dallington Bridge.

5.5.1 Bridge structure

Dallington Bridge, sometimes referred to as Gayhurst Road Bridge, is an integral reinforced concrete structure 26.8 m in length and 12.8 m wide. It supports one traffic and one pedestrian lane in each direction and spans north-south across the Avon River at the southernmost point of the Dallington Loop. The bridge deck is a continuous span reaching 8.2 – 10.4 – 8.2 m between abutments and piers, a plan sketch is shown in Figure 5-25 and a side elevation can be seen in Figure 5-26.

The abutments and pier walls are 3.4 m high, supported by 0.365 m square, reinforced concrete piles 10.4 m in length. Six piles at *6D* spacings support each abutment, while 7 piles at *4D* spacings support each pier; their locations are indicated by the red squares in Figure 5-25. The piles beneath the piers are alternately raked at 1:10, as can be seen in Figure 5-27, while those under each abutment are vertical. The level of the river bed is approximately equal with the tops of the piles

Both bridge approaches were constructed on surrounding grade, which was approximately level with the bridge deck on the southern side and slightly below it on the northern side. Curved concrete wingwalls exist on either side of each abutment and are connected to the abutment via nominal reinforcement.

Details relating to each individual component including material properties can be found in the Christchurch City Council's design drawings for Dallington Bridge.

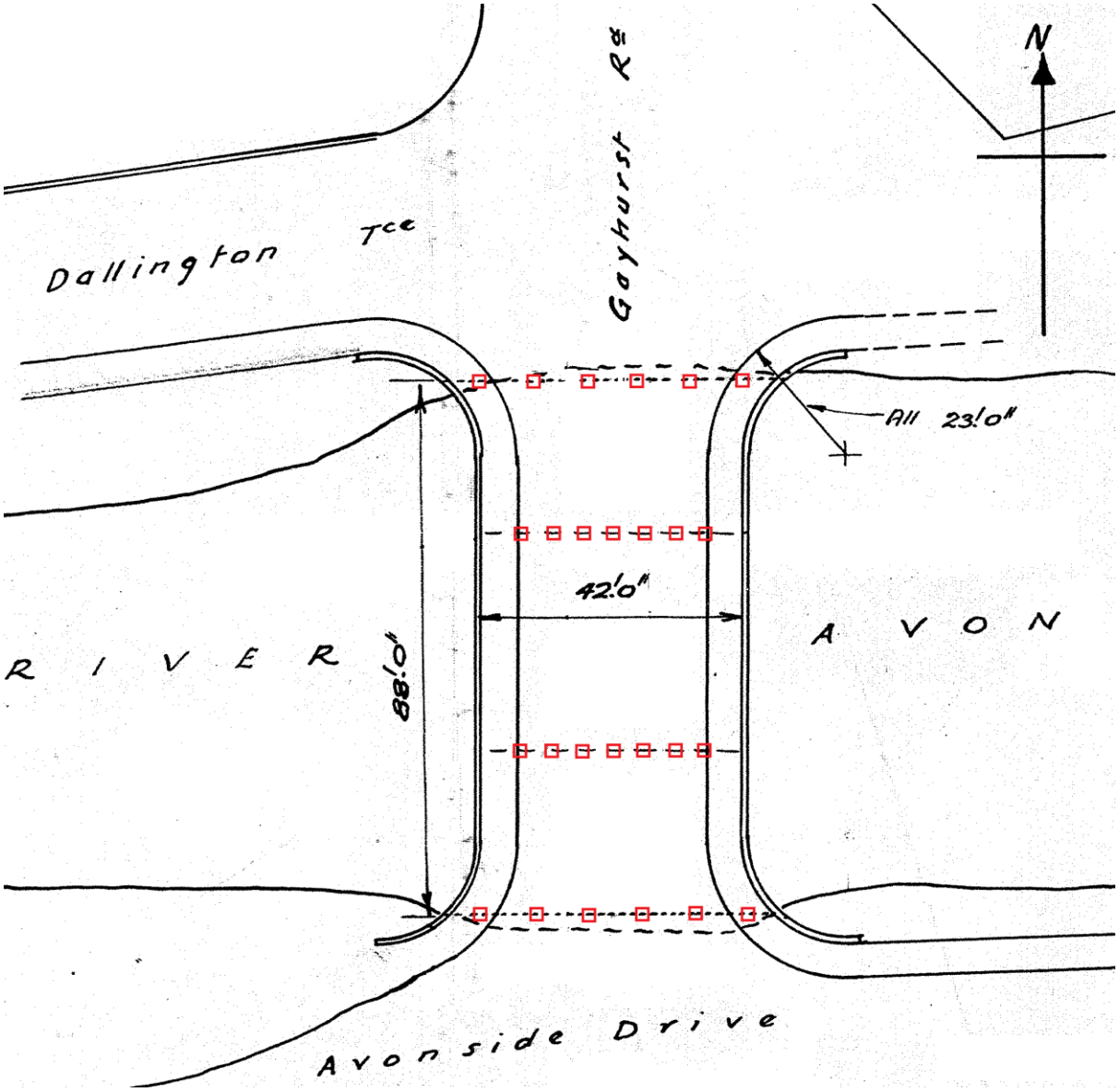

Figure 5-25: Plan view of Dallington Bridge indicating positions of piles beneath each abutment and pier, adapted from Christchurch City Council drawing

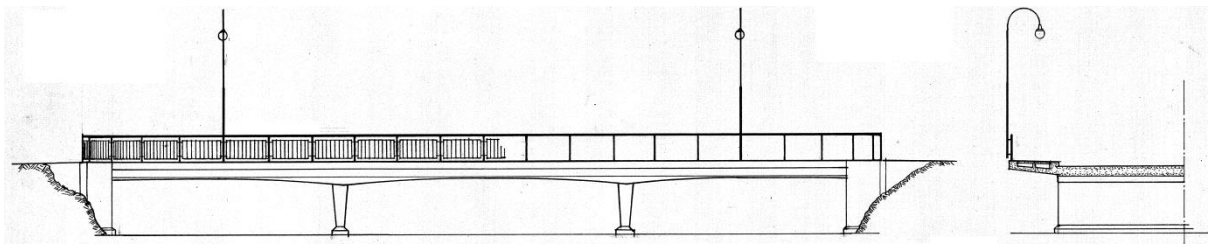

Figure 5-26: Dallington Bridge elevation, Christchurch City Council drawing

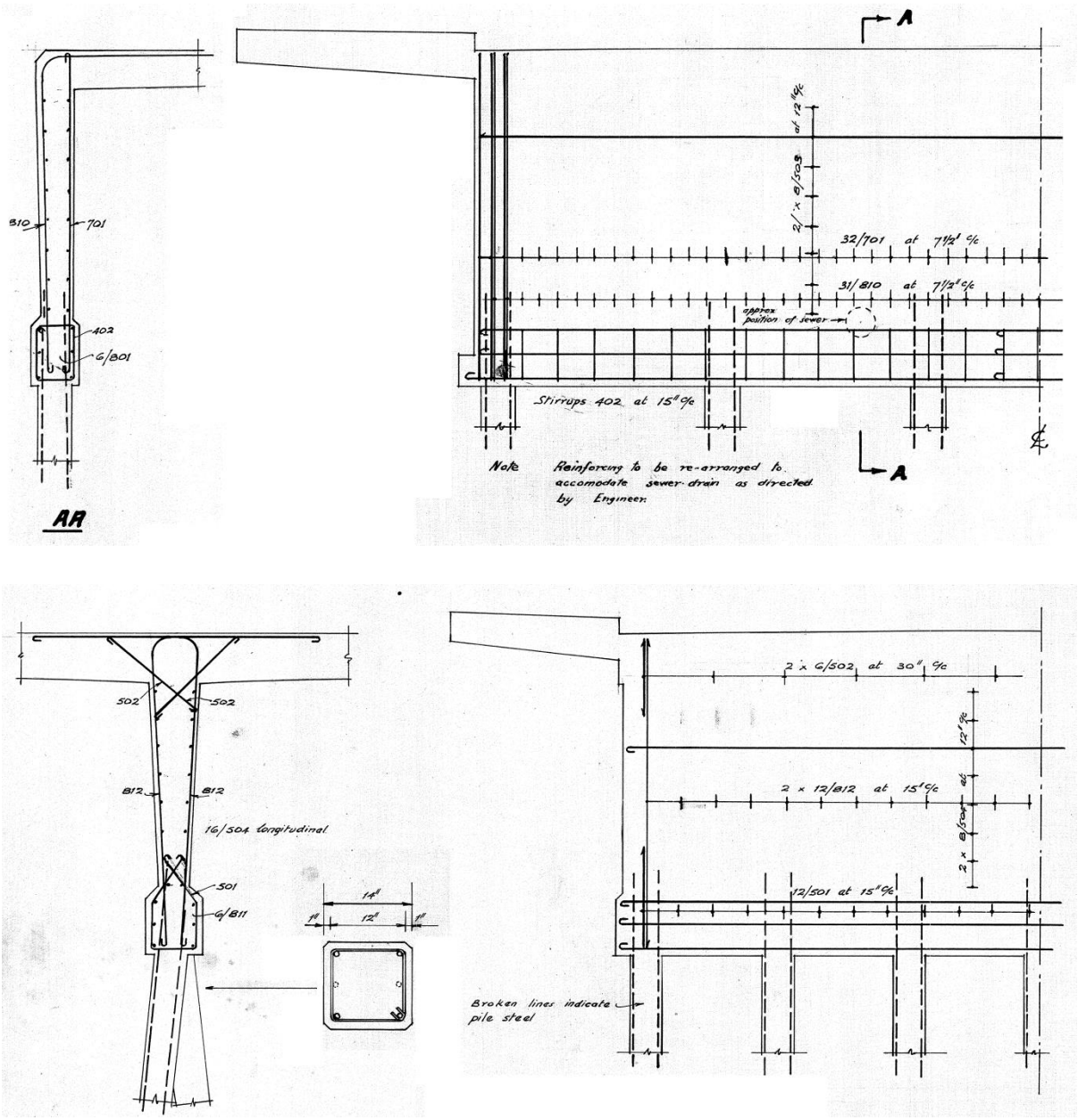

Figure 5-27: Dallington bridge abutment (top) and pier (bottom) transverse half-sections, showing locations of piles

5.5.2 Geotechnical site conditions

Figure 5-28 shows the existing site investigation data in the vicinity of Dallington Bridge. All of the original CPT and SPT data from these can be seen in Appendix A. For the purposes of this research it was decided to use CPT-DAL-07 and BH-GAY-01 to construct the model of the northern abutment, and BH-GAY-02 for the southern abutment. On the northern abutment CPT-DAL001 is of little use due to its maximum penetration depth of 10 m. CPT-DAL-07 and CPT-DAL-49 were both carried out as part of the EQC's greater Christchurch ground investigations following the Darfield earthquake, and correlate well with one another; it was decided to use CPT-DAL-07 because of its proximity to the bridge. BH-GAY-01 and BH-GAY-02 were requisitioned by the Universities of Auckland and Canterbury and carried out in November 2011; equipment calibrations indicate a hammer energy ratio of 85%. Table 5-5 summarises the exact locations, dates of testing and other details of the geotechnical site investigations.

Figure 5-28: Dallington Bridge site investigation locations (Google Earth image)

Table 5-5: Dallington Bridge geotechnical site investigation details

Abutment	Name	Latitude	Longitude	Test date	Performed by/for
North	CPT-DAL001	43°31'16.90"S	172°40'23.41"E	Jun 1997	Soils and Foundations (1997)
North	CPT-DAL-07	43°31'17.04"S	172°40'22.37"E	Nov 2010	Perry (for EQC/T&T ground investigations)
North	CPT-DAL-49	43°31'17.25"S	172°40'20.37"E	Dec 2010	Perry (for EQC/T&T ground investigations)
North	BH-GAY-01	43°31'17.05"S	172°40'22.54"E	Nov 2011	McMillan Drilling (for Universities of Auckland and Canterbury)
South	BH-GAY-02	43°31'17.76"S	172°40'25.88"E	Nov 2011	McMillan Drilling (for Universities of Auckland and Canterbury)

On the following pages Figures 5-29 to 5-31 show the raw CPT and SPT data for CPT-DAL-07, BH-GAY-01 and BH-GAY-02 and the subsequent liquefaction analysis results. These analyses were performed using the methods outlined in the sections 5.2 and 5.3, and the adopted profiles to be used in the PSA are shown, where the layers shaded blue are those deemed to have liquefied in the 22nd February 2011 earthquake. Ground water levels were identified using data from *Project Orbit* and are deemed to be the best estimates of GWL at the time of the earthquake. It should be noted that the author carried out particle size distribution analyses (by means of both sieving and laser diffraction analysis) on soil samples from key strata in BH-GAY-01 and BH-GAY-02. The fines contents from these were used in the liquefaction triggering analysis as part of calculating the corrected clean sand blowcount for establishing CRR (PSD curves can be seen in Appendix D).

It can be seen that, at the north abutment, BH-GAY-01 and CPT-DAL-07 (Figures 5-29 and 5-30) are relatively consistent with one another and that the critical layers for liquefaction in the Christchurch earthquake lie between 2 and 11 metres depth. The analyses also show that some layers between 2 and 8 metres depth likely liquefied in the Darfield event. The model used in the majority of the PSA is based on the CPT data, however one parametric study was carried out using the SPT profile in order to establish what effect this difference had. The bearing stratum for the piles is founded in stronger material deemed too dense to liquefy ($(N_1)_{60,cs} > 30$, $q_{c1N,cs} > 160$).

On the south abutment, BH-GAY-02 (Figure 5-31) indicates that the soil column did not liquefy in either earthquake event. This was reflected in the lack of land damage observed near this abutment.

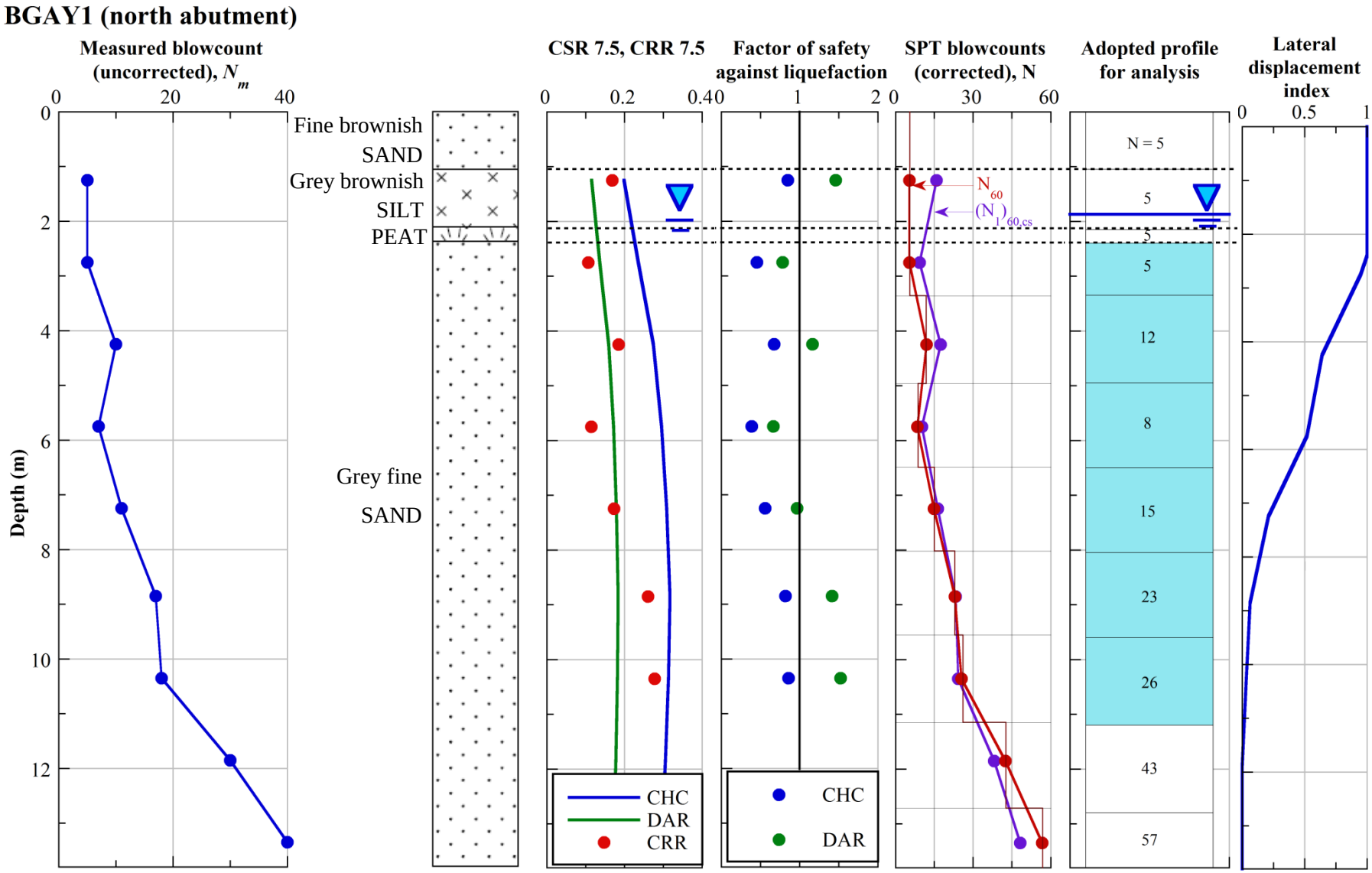

Figure 5-29: Dallington Bridge north abutment SPT data and liquefaction analysis results

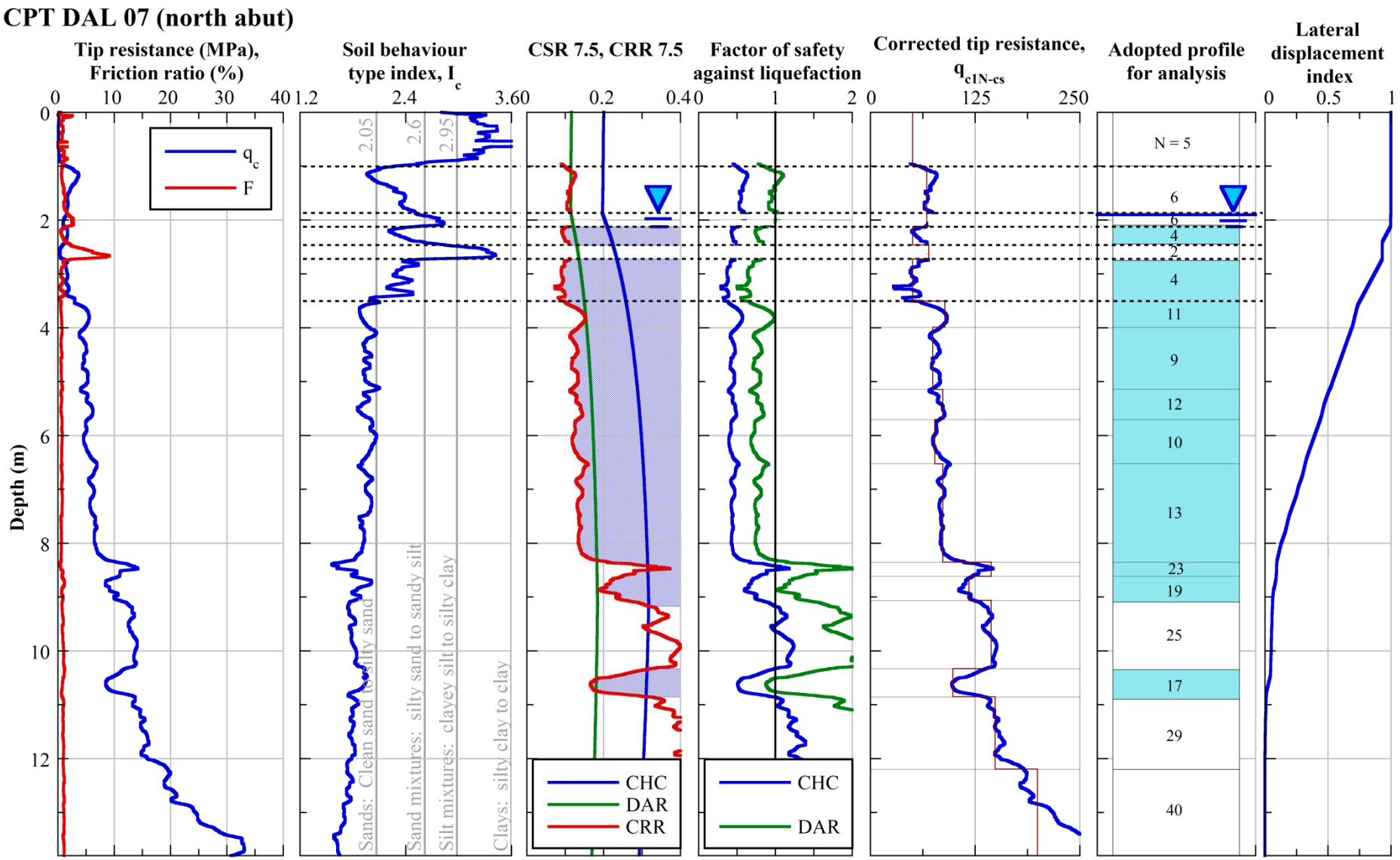

Figure 5-30: Dallington Bridge north abutment CPT data and liquefaction analysis results

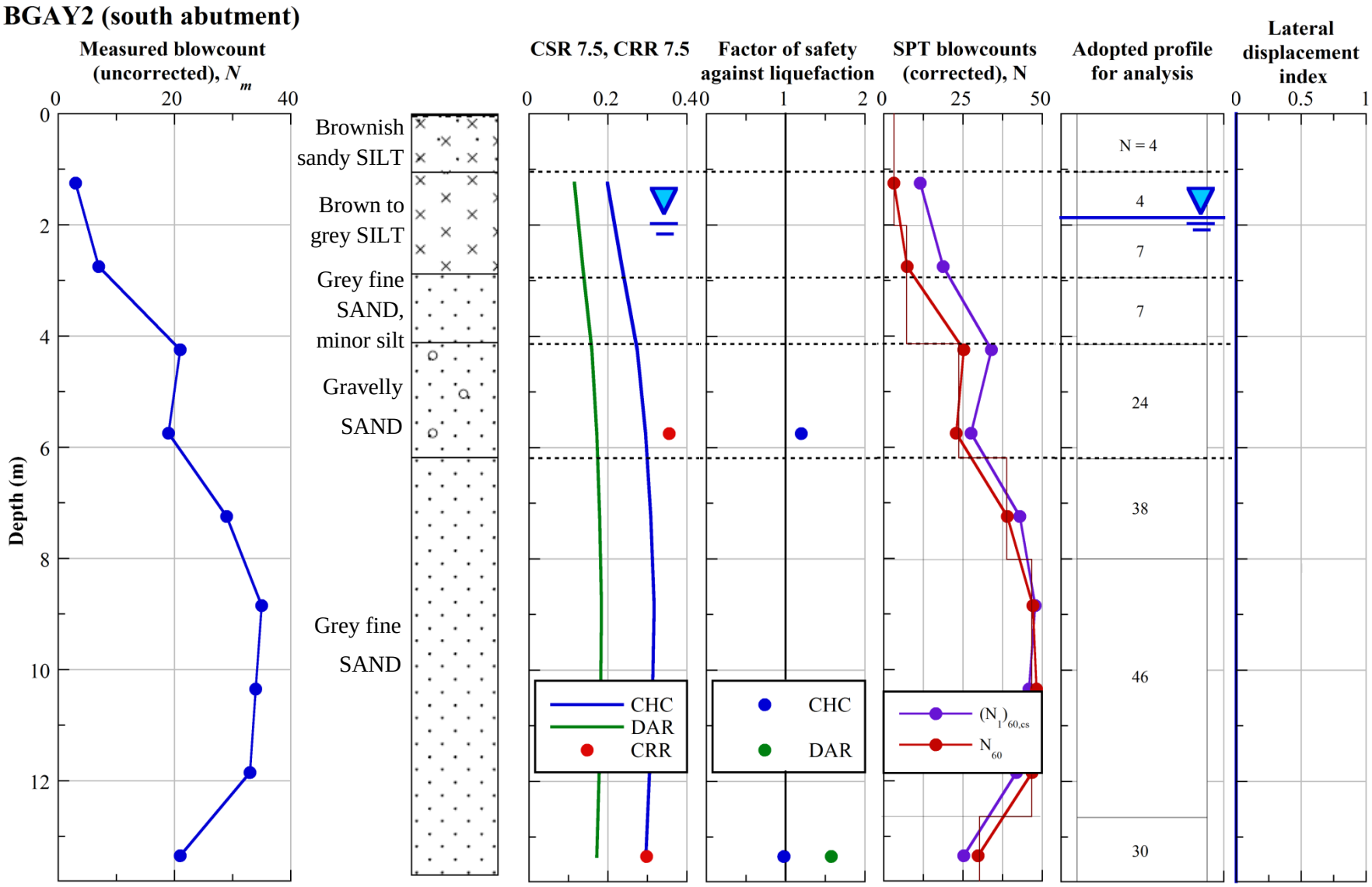

Figure 5-31: Dallington Bridge south abutment SPT data and liquefaction analysis results

5.5.3 Earthquake observations

Subsequent to the Darfield earthquake significant liquefaction occurred on the northern inner bank of the river. As a result, ground settlement and lateral spreading occurred around the entire Dallington Loop. Some small cracking in the northern abutment wall and northern pier were visible following this event. No land or bridge damage was apparent on the southern bank.

The Christchurch earthquake caused additional and substantial land damage to the north of the bridge; the cumulative effects of both events led to more than half a metre of ground settlement in the vicinity. Free-field lateral spreading displacements in the order of 0.7-0.9 m were measured on either side of the north abutment of the bridge, while the measured lateral displacement at the bridge deck was constrained to 0.2-0.35 m. The bridge had evidently restrained free-field displacements and this was especially evident where the wingwalls had independently displaced an additional 0.4-0.7 m towards the river. No land or bridge damage was apparent on the southern bank.

Although Dallington Bridge is an integral structure, some back-rotation of the northern abutment wall was measured. This ranged from 0.8° to 2.2° across the width of the wall. Extensive cracking occurred along the northern abutment wall and reinforcing connecting the wingwalls to the abutment was completely exposed. Pile investigations carried out on the northern abutment indicated that severe flexural cracking had occurred in the river-facing sides of some piles immediately beneath the abutment-pile interface, to the point where transverse reinforcing was exposed and confinement lost.

For more information relating to observed damages to Dallington Bridge and its surrounds refer to the detailed observations in Section 3.7.7.2.

5.5.4 Pseudo-static analysis

Two separate series of PSAs were carried out on Dallington Bridge; the first to simulate the post-liquefaction lateral spreading phase, and the second to simulate the cyclic loading phase which occurs during earthquake shaking. The single pile set of analyses is confined to the north abutment piles only, due to negligible displacements, damages or liquefaction effects being observed on the southern abutment. Within each set of analyses the single pile models were first constructed followed by a model of the whole structure. The models are based on a representative tributary bridge width of 1.8 metres (centre-to-centre pier pile spacing, smaller than abutment-pile spacing), and all beam element and soil-spring properties have been scaled to this accordingly. First the lateral spreading phase of loading is presented and single pile model results are shown followed by the whole bridge model. Secondly, the cyclic loading phase in the longitudinal direction is considered represented firstly by the

single pile model followed by the global bridge model. All analyses are based on measurements made following the 22nd February 2011 earthquake.

5.5.4.1 Beam elements

The global bridge model comprises 3 beam elements which represent the abutment piles, pier piles and abutment walls/pier walls/bridge deck respectively. The abutment walls, pier walls and bridge deck are assumed to remain in the elastic range[3] and thus have linear moment-curvature relationships with a flexural stiffness (EI) found by multiplying Young's modulus (E) of concrete by the sections' second moment of area (I). The reinforced concrete piles have tri-linear moment-curvature relationships with the three points defined by: concrete cracking (M_c), reinforcing yielding (M_y) and concrete crushing (M_u).

Knowing each pile's cross-section, material properties and other characteristics (i.e. axial load, position of reinforcement, spacing of transverse reinforcement) the moment-curvature relationships for each pile were calculated using *CUMBIA* (Montejo and Kowalsky 2007) and are shown in Figure 5-32. Note that these have been scaled to be representative of a 1.8 m tributary bridge width (i.e. scaled to the width of the bridge supported by one pier pile).

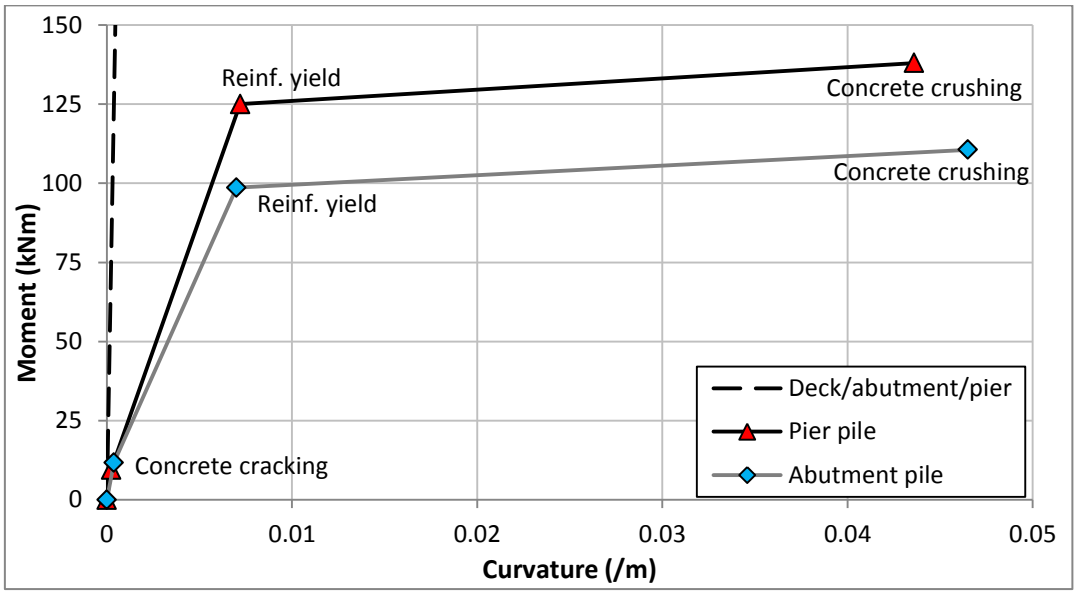

Figure 5-32: Moment-curvature relationships for beam elements, Dallington Bridge

[3] Although, as one parametric study, the stiffness of the abutment will be reduced in order to see what effect cracking might have had.

5.5.4.2 Soil springs

Each soil spring is assigned a bi-linear load-deflection (*p*-*δ* or *p*-*y*) relationship in order to account for soil yielding once it reaches its ultimate pressure. Reduced stiffness due to liquefaction or other nonlinearity can be accounted for by applying a degradation factor β to the initial spring stiffness.

The soil springs were divided into layers at each abutment based on the analysis results from the CPT and SPTs as discussed previously. The RM for the north abutment was based on the CPT test rather than the SPT. For the purposes of the global bridge model it was necessary to interpolate between these in order to create assumed profiles for the central pier piles. This interpolation is shown in Figure 5-33, where the layers deemed to have liquefied are shaded blue. The exact formulation of each soil spring is treated separately for each of three distinct zones within a soil column; the crust layer, liquefied layers, and deeper non-liquefied layers. On the south abutment (deemed not to liquefy) the soil springs are all assigned *p*-*y* relationships with a stiffness based on the subgrade reaction coefficient and an ultimate pressure equivalent to the Rankine passive pressure. Otherwise, the calculations performed to establish the soil spring relationships are exactly the same as demonstrated in Appendix C, which shows an example spreadsheet from ANZAC Bridge.

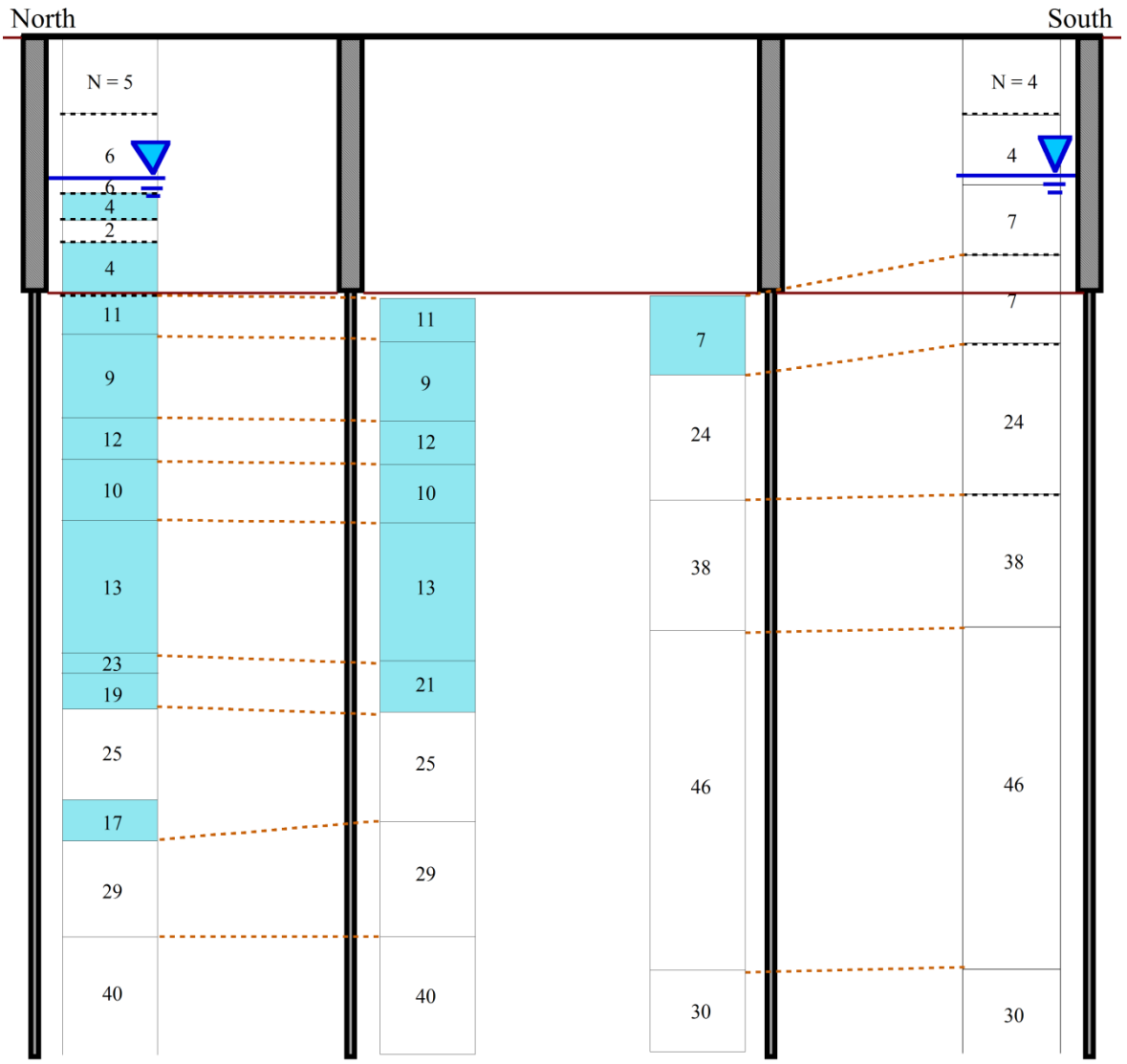

Figure 5-33: Dallington whole-bridge model assumed soil-spring columns

5.5.4.3 Lateral spreading phase

The permanent lateral spreading displacements to apply to the north abutment/pile system were deemed to range between 0.2 and 0.7 metres, and a best estimate of 0.35 m was chosen. These values were then multiplied throughout depth based on the computed lateral displacement index from CPT-DAL-07. Since Dallington Bridge is an integral structure the top of the abutment is considered to be restrained both laterally and rotationally in the single pile model. The results of the parametric study are presented below, and the effects of changing variables in each layer are

examined separately. Horizontal pile displacements and bending moments throughout depth are shown to represent the response of the system.

Single pile model

The results of the parametric studies on the north abutment/pile system are shown below. The top of the abutment is considered to be constrained both laterally and rotationally.

Effect of crust layer

Figure 5-34 displays the results of the abutment-pile system's response to variations in the crust parameters. The pile response shows negligible sensitivity to these parameters, both in terms of computed displacements and bending moments. Computed bending moments indicate that cracking moments are exceeded near the pile/abutment interface, at the liquefied/non-liquefied base layer interface and also throughout the middle of the pile. The computed displacement at the base of the abutment corresponds to an abutment back-rotation of approximately 0.3°, much smaller than that measured (0.8-2.2°). Variations in crust thickness (H_c) of plus or minus one metre did little to affect pile response also, indicating that while the thickness of the crust remains less than the height of the abutment then system response is insensitive to changes in crust parameters. The constrained rotation at the top of the abutment also means that yielding in the deck/abutment connection is not considered and, if yielding in this connection were initiated, then the result would be increased abutment rotation and subsequently altered pile response.

Effect of liquefied layers

Figure 5-36 illustrates the effect that changes in liquefied layer properties have on pile response. While displacement response remains relatively unaffected (governed, as mentioned previously, by constrained abutment rotation), there is some noticeable effect on bending moment response. Yielding is still not computed to be initiated anywhere in the pile, however, and the general response varies only a few percent from the RM over depth.

Effect of deeper non-liquefied layers

Figure 5-35 shows that reducing spring stiffness in deeper non-liquefied layers slightly reduced pile bending moments between the depths of 7 and 13 metres. It is likely that this response is more representative of soil behaviour post-liquefaction, where some degree of stiffness reduction is likely to have occurred to the effects of pore pressure dissipation.

Effect of ground displacement

Figure 5-37 presents the results of system response based on different magnitudes of applied ground displacements. An additional displacement profile was also applied which corresponded to the LDI

computed from the SPT performed on the northern abutment (BH-GAY-01) multiplied by the best estimate surface ground displacement. The effect of this different displacement profile was to reduce computed bending moments throughout depth when compared with the CPT model with the same $U_{G\text{-}max}$.

It is evident that the magnitude of ground displacement has a significant effect on the computed bending moment response, yet still a minimal effect on displacement response. The upper bound applied displacement of 0.7 m was substantial enough to cause the computed bending moments at the pile top to approach ultimate, and to induce yielding at depths of around 9 and 12 metres. Since some pile hinging was observed in the tops of the northern abutment piles it is likely that the ground displacements causing this lie somewhere between the best estimate and upper bound displacements chosen for this PSA. It may be argued that the large degree of restraint provided by the 3.4 m tall abutment wall caused an increased volume of soil to be forced to flow directly under the abutment as a compensatory measure, thus lateral spreading displacements at this depth may have tended towards those more likely encountered in the free field.

Effect of stiffness degradation in abutment

Cubrinovski and Ishihara (2004) showed that reducing the initial flexural stiffness, EI, of a beam (pile) element to a fraction of its original value, was equivalent to modelling an equivalent nonlinear stiffness in that element. It is appreciated that the northern abutment of Dallington Bridge did sustain cracking damages, and so a set of parametric studies was run which investigated the effects of member stiffness degradation in the abutment wall. For the reference models, the wall was modelled to remain in the elastic range, and as such this governed the behaviour of the wall and pile response. Stiffness degradation is not considered in the RM and sensitivity analysis of other variables due to the fact that the construction design drawing layouts of reinforcing in the abutments were very poor, and as such accurate tri-linear moment-curvature relationships were not able to be calculated. For the purposes of this investigation, the initial abutment stiffness was degraded to 50%, 25% and 10% of its reference value. The results are presented in Figure 5-38.

As expected, the reduction in abutment wall stiffness corresponds to an increase in rotation of the abutment wall. With a stiffness of 10% of the initial elastic one, an abutment wall rotation of 0.8 degrees is computed – the lower bound of what was observed in the field. This indicates that the substantial cracking which occurred throughout the abutment wall may have greatly contributed to the observed response. The bending moment response for the 10% stiffness shows that substantial cracking, and nearly yielding, are approached near the head of the pile in the opposite direction. This, again, is more consistent with what was observed in the field (tension cracking on river-faces of piles).

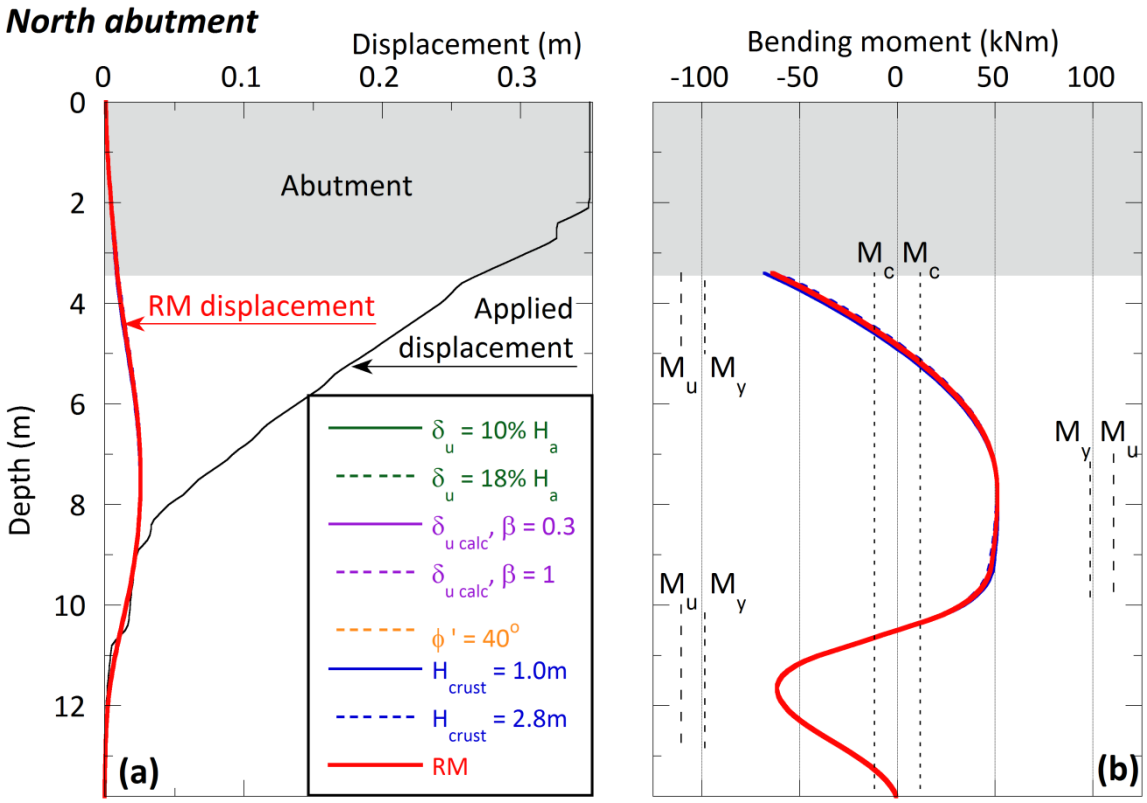

Figure 5-34: Single pile lateral spreading analyses, Dallington Bridge, effect of crust layer, (a) displacements, (b) bending moments

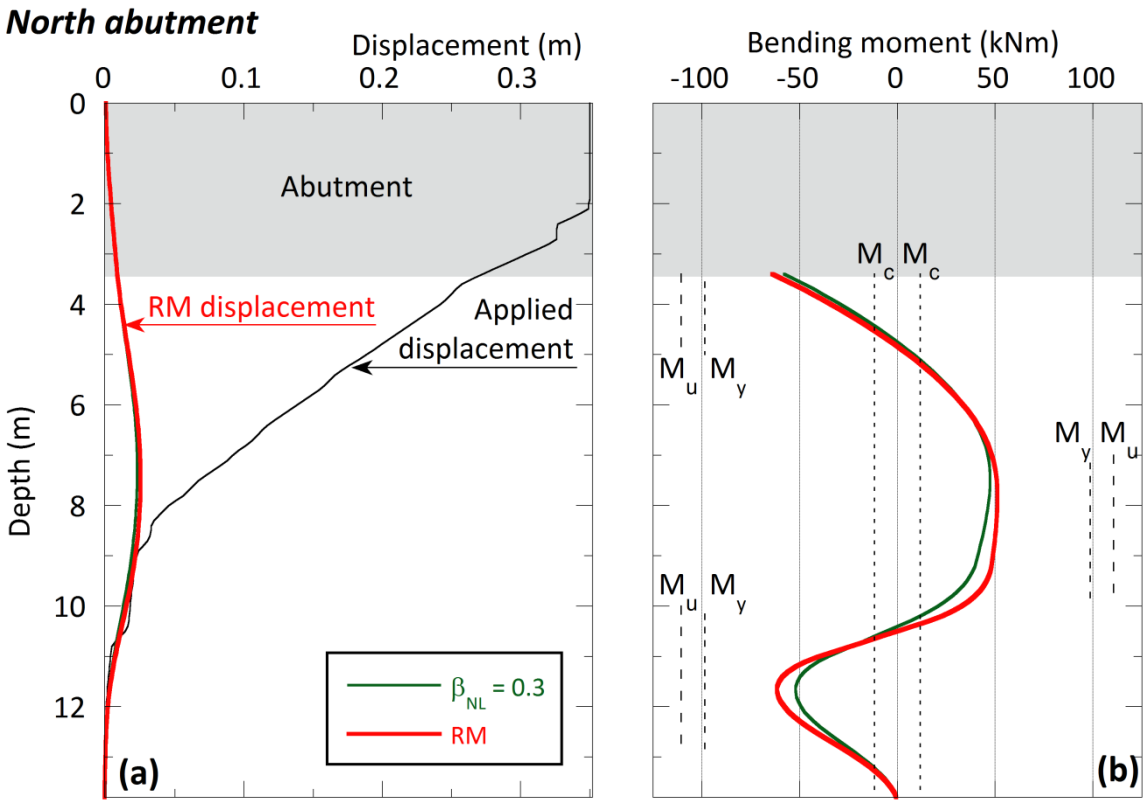

Figure 5-35: Single pile lateral spreading analyses, Dallington Bridge, effect of non-liquefied layers, (a) displacements, (b) bending moments

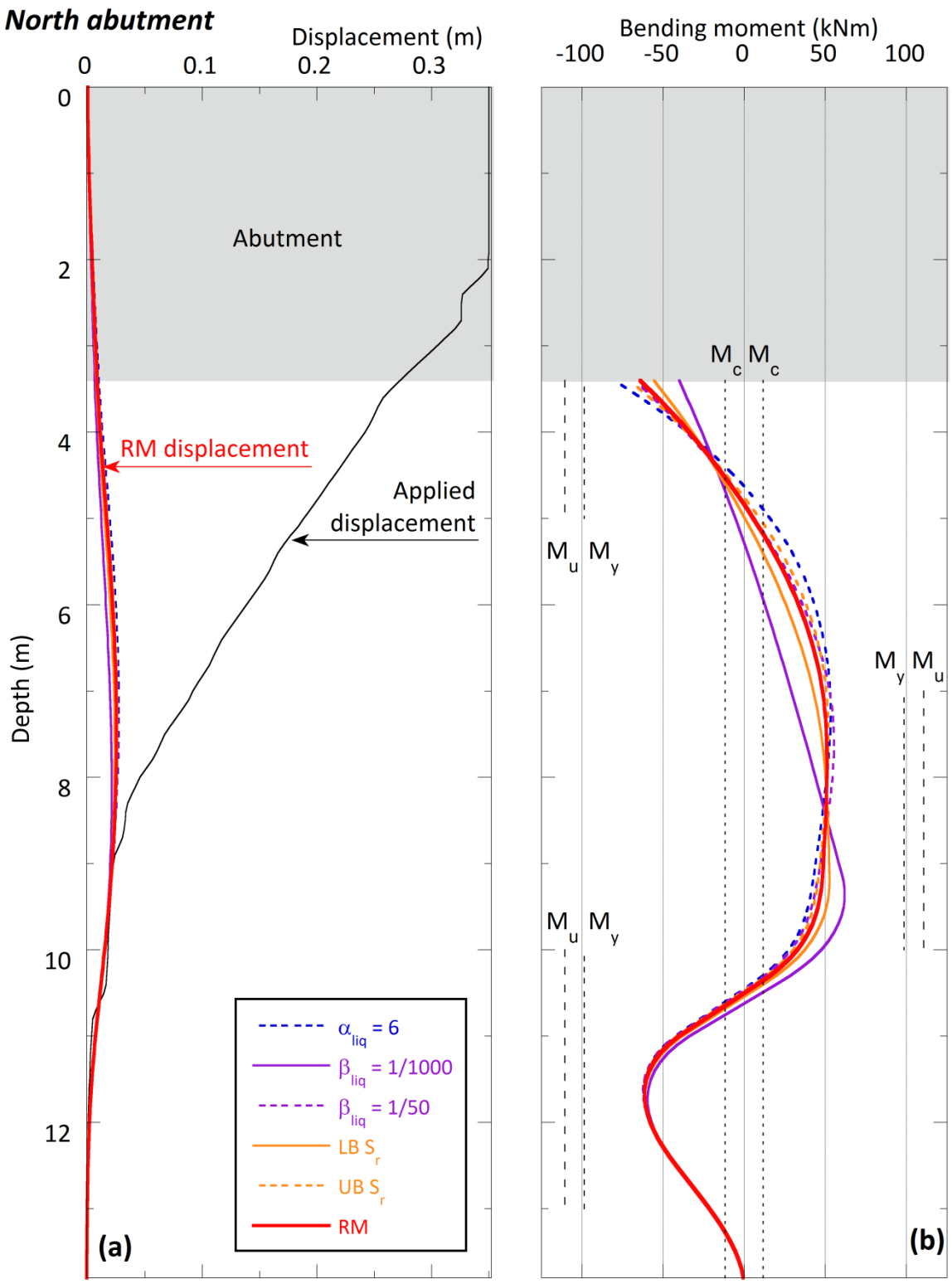

Figure 5-36: Single pile lateral spreading analyses, Dallington Bridge, effect of liquefied layers, (a) displacements, (b) bending moments

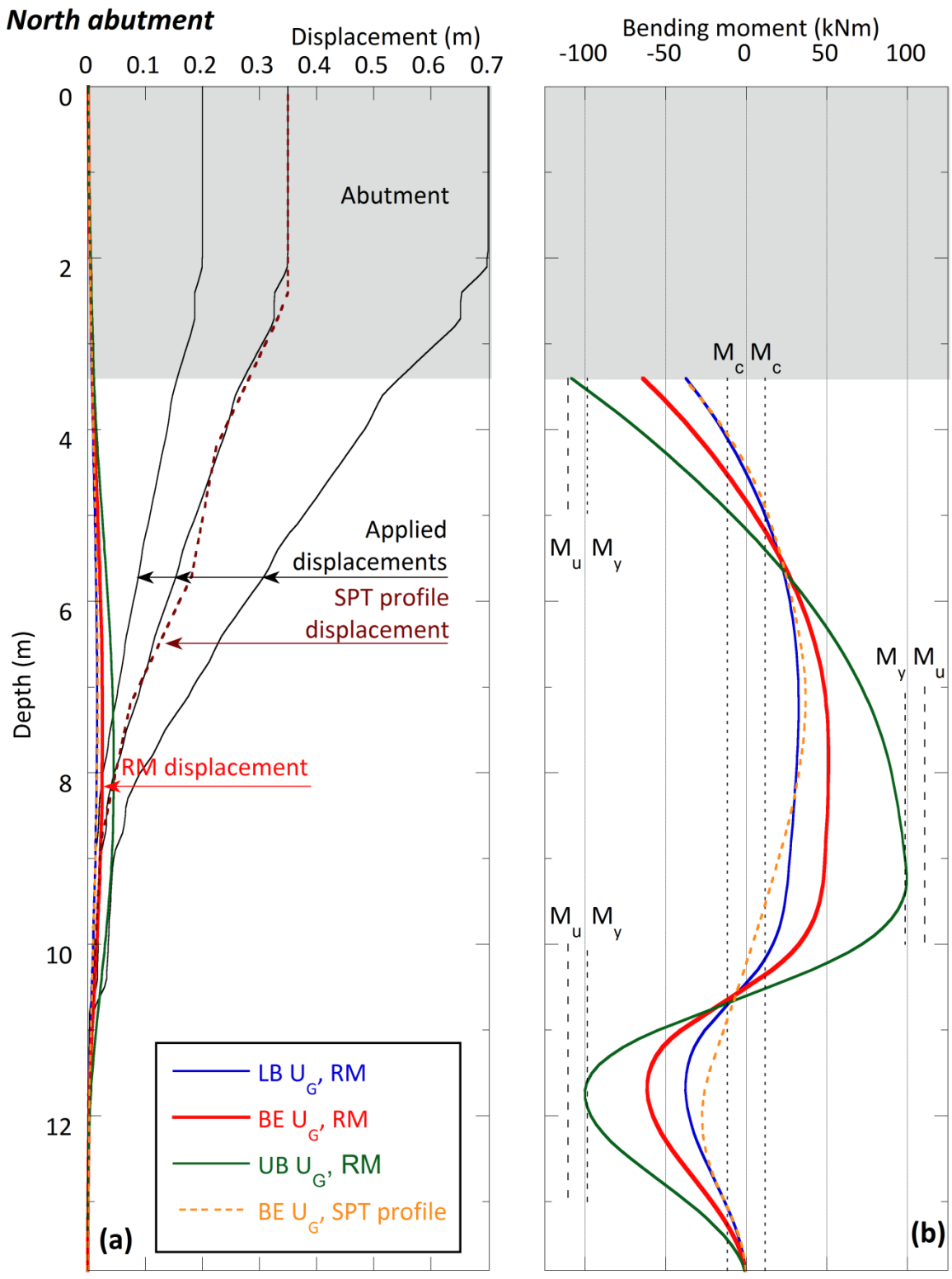

Figure 5-37: Single pile lateral spreading analyses, Dallington Bridge, effect of ground displacements, (a) displacements, (b) bending moments

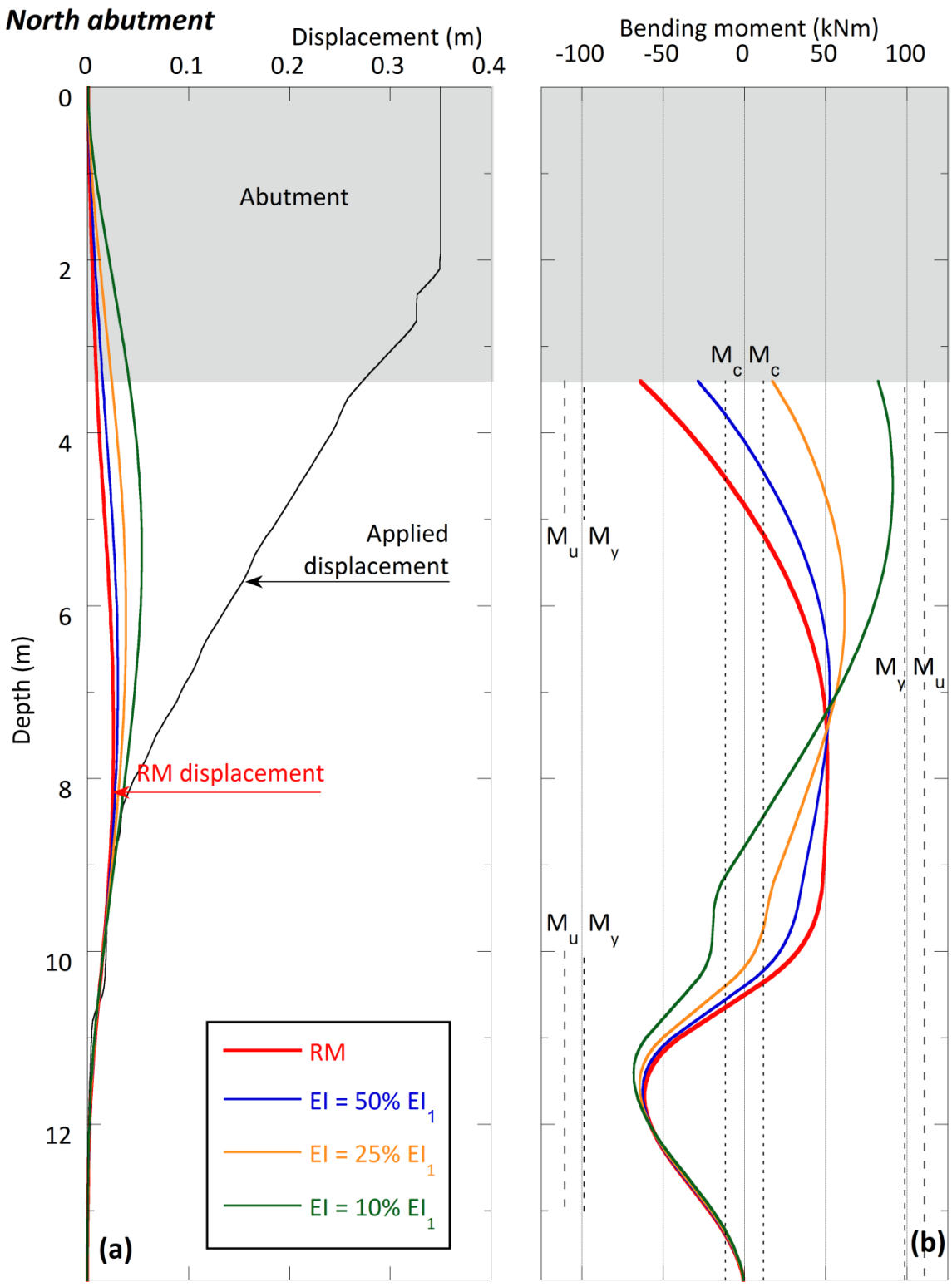

Figure 5-38: Single pile lateral spreading analyses, Dallington Bridge, effects of reduction in abutment wall stiffness, (a) displacements, (b) bending moments

Whole bridge model

In the whole bridge model each abutment/deck and pier/deck connection is considered to be constrained rotationally to reflect the integral nature of the bridge. This allows full moment transfer through the joints.

Figure 5-39 shows a schematic view of the global bridge model subjected to lateral spreading loads, resulting bridge deformed shape and computed bending moments in the abutment piles and pier piles. The first analysis run was that where the only applied displacements were the spreading displacements at the north abutment ("A" analysis in Figure 5-39). The response of the north abutment pile was fully consistent with that found from the single pile analysis.

Next, lateral spreading displacements were applied to the central piles in addition to that at the north abutment ("A + P" analysis). The displacements applied to the northern pier piles were distributed throughout depth based on the methodology of Zhang *et al.* (2004) and the displacement at the ground surface was taken to be 50% of the lateral displacement applied at the same elevation of the north abutment. A nominal spreading displacement of 50 mm was applied to the southern pier piles to reflect the fact that a relatively weak layer (N = 7) is assumed to exist at the ground surface and is likely to have liquefied in the Christchurch earthquake.

An additional analysis was carried out where the residual strength of the liquefied soils in the pier pile soil columns was calculated using the normalised relationship proposed by Olson and Stark.

Effect of applied displacement

As can be seen in Figure 5-39, the inclusion of lateral displacements on the pier piles ("A + P") had negligible effect on all components except the northern pier piles. Yield moments were not approached in any components, but cracking moments were exceeded in many places as can be seen in the plot.

Effect of liquefied layers

The shear-strength normalisation of liquefied layers in the central pier pile soil columns served only to affect the north pier pile response such that it tended back towards that of the "A" analysis. This is because the normalised shear strengths were significantly smaller than the non-normalised ones.

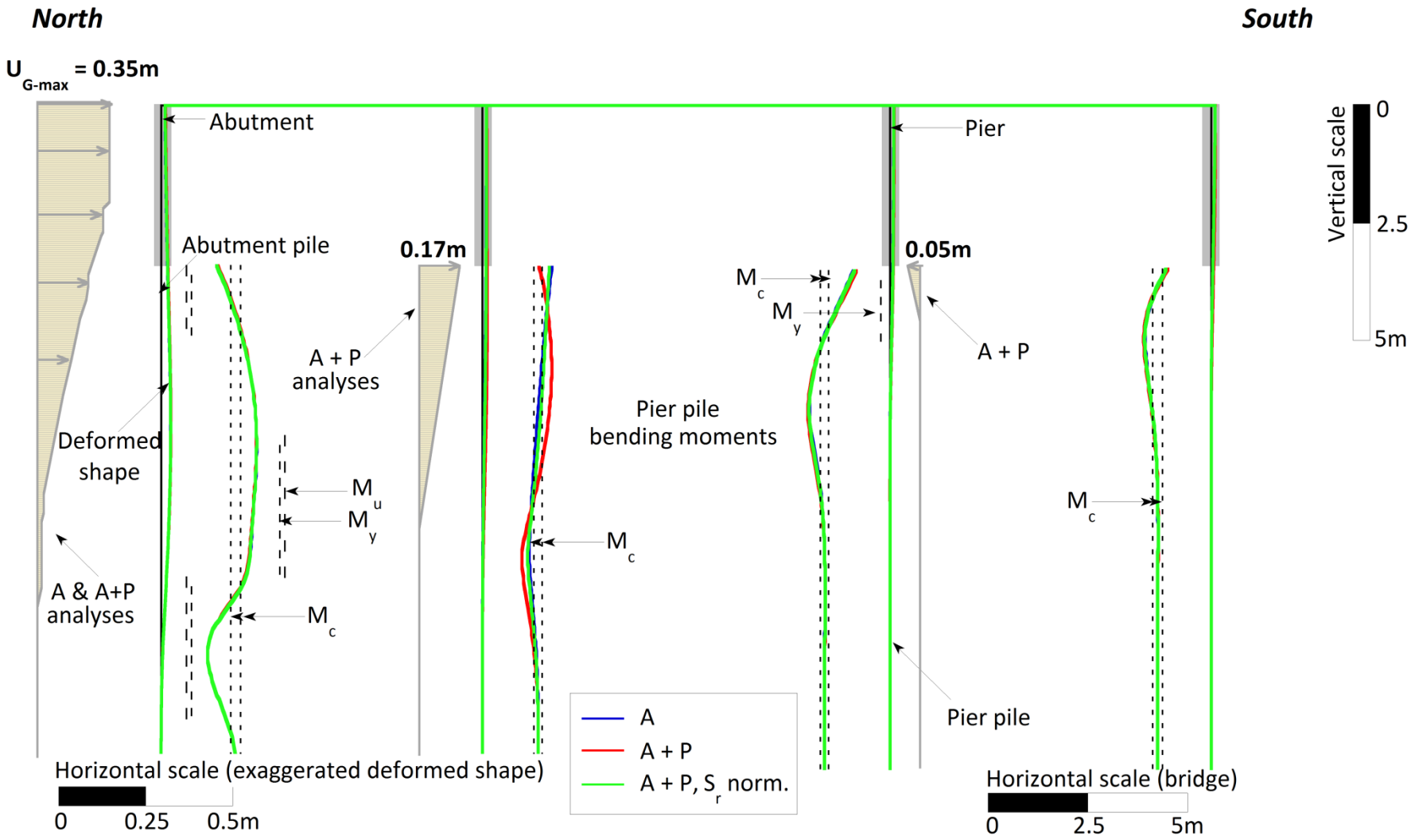

Figure 5-39: Whole bridge lateral spreading analysis, Dallington Bridge, applied ground displacements, deformed shape and bending moments in all piles shown

5.5.4.4 Cyclic loading phase

Cyclic ground displacements throughout depth were established using the method of Tokimatsu and Asaka (1998), and inertial loads on each component were calculated by multiplying the superstructure weight by the PGA and correcting for tributary area. The single pile model considers the effects of cyclic ground displacements only, while the global bridge model considers the effects of ground displacements and inertial loads. The computed cyclic ground displacements at the top of each soil column are 0.14, 0.11 and 0.01 m for the north abutment, north pier and south pier respectively. Cyclic loadings in the longitudinal direction only are considered.

Single pile model

Effect of liquefied layers

Figure 5-40 shows the applied cyclic ground displacements in the downslope direction (towards the river) at the north abutment. Changes in liquefied layer properties have some effect on both displacement and bending moment response, most notably arising from changes in the strength parameter α_{Liq}. It is predicted that the cracking moment is exceeded at the pile top, as well as many other places throughout depth.

Effect of displacement in the opposite direction

Figure 5-41 demonstrates the effect of applying cyclic ground displacements to the abutment piles in the direction away from the river. These are only applied to the piles and not the abutment due to the riverbed being approximately level with the tops of the piles. The plot shows applied displacements both equal to, and half of that applied in the downslope direction. In reality, at Dallington Bridge there is no natural “downslope” feature due to the abutment wall effectively acting as a retaining wall, such that it meets the riverbed at an approximate right angle. The response of the model to these applied displacements predicts bending moments greater than the cracking moment extensively throughout depth.

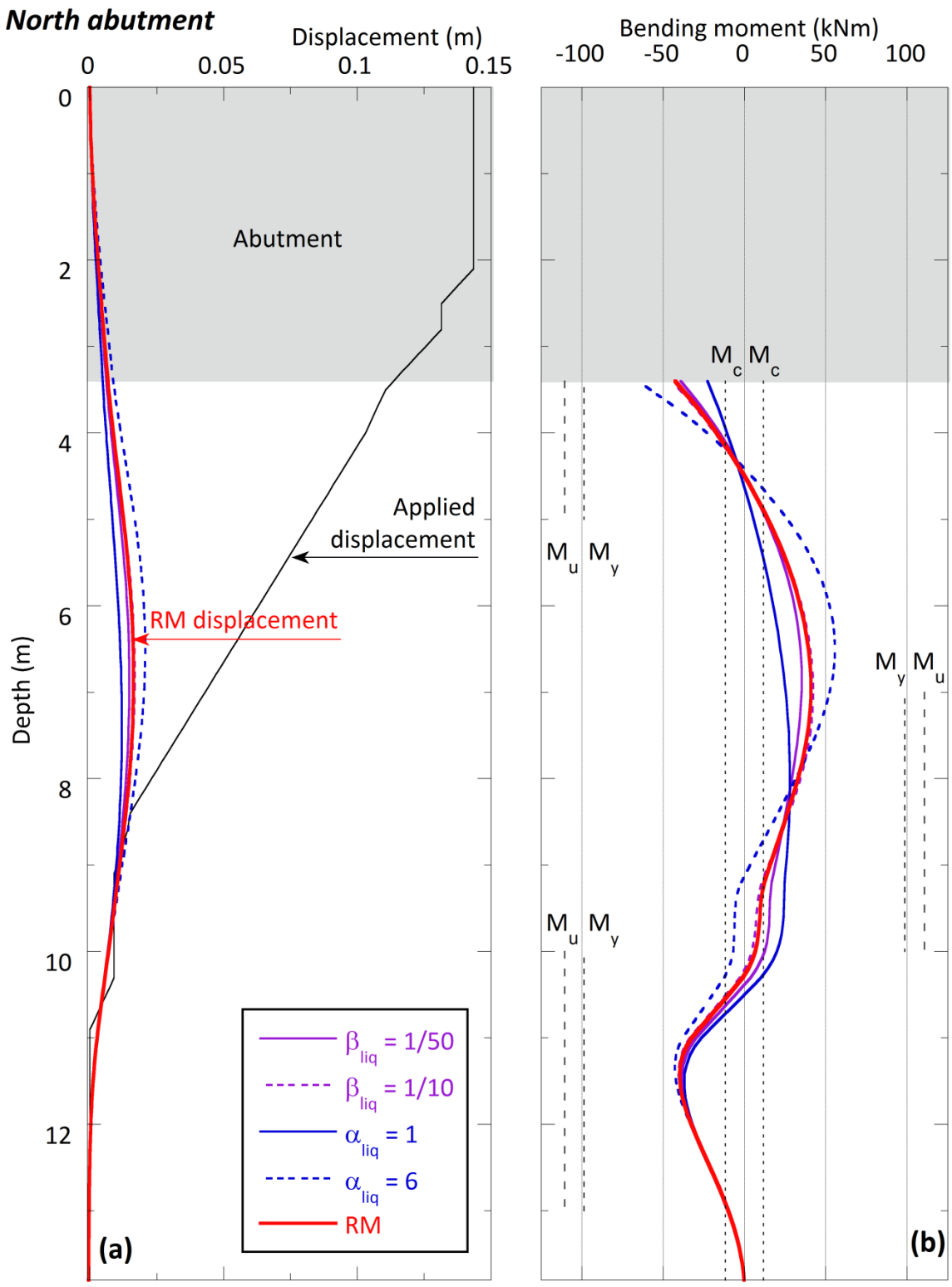

Figure 5-40: Single pile cyclic analyses, Dallington Bridge, effect of liquefied layers, (a) displacement, (b) bending moments

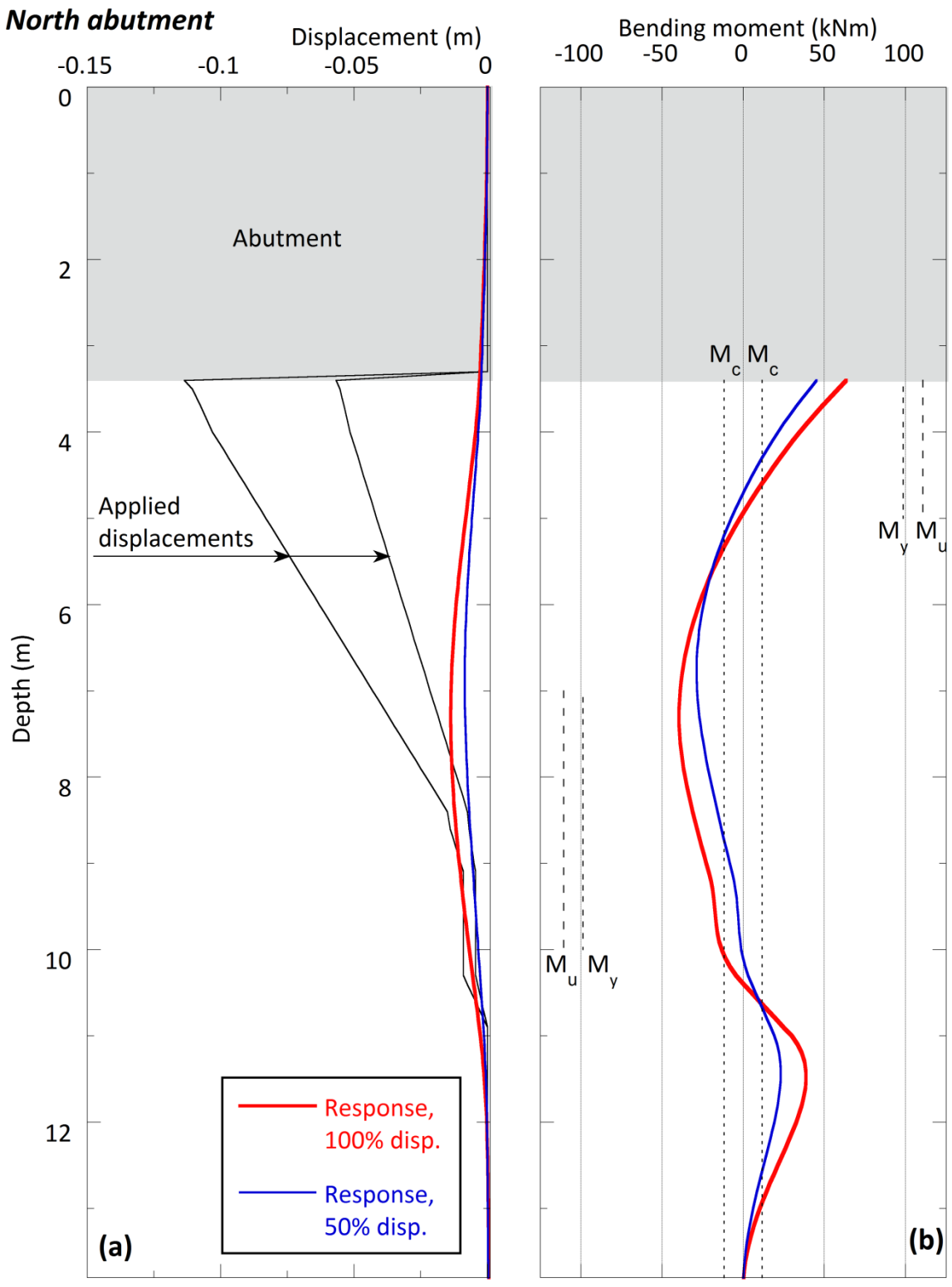

Figure 5-41: Single pile cyclic analyses, Dallington Bridge, effect of displacement in opposite direction, (a) displacement, (b) bending moments

Whole bridge model

Cyclic analyses were carried out on the whole bridge model in both the north to south (Figure 5-42) and south to north (Figure 5-43) directions. The loading scenarios involved the application of inertial loads only ("I" analyses), followed by the application of cyclic displacements alone ("D" analyses) and then the combination of these ("I + D").

Effect of inertial loads

In both directions of loading the inertial loads alone induced bending moments in all of the pile tops greater than the cracking moment. This rapidly reduced to almost zero within the top 2 metres of each pile.

Effect of ground displacements and combined effects

The effects of applied cyclic ground displacements can be seen in Figures 5-42 and 5-43 where, again, it is computed that pile yielding does not occur anywhere, but substantial cracking does occur. The same effect can be seen for the analyses which combine the applied cyclic displacements with the inertial loads.

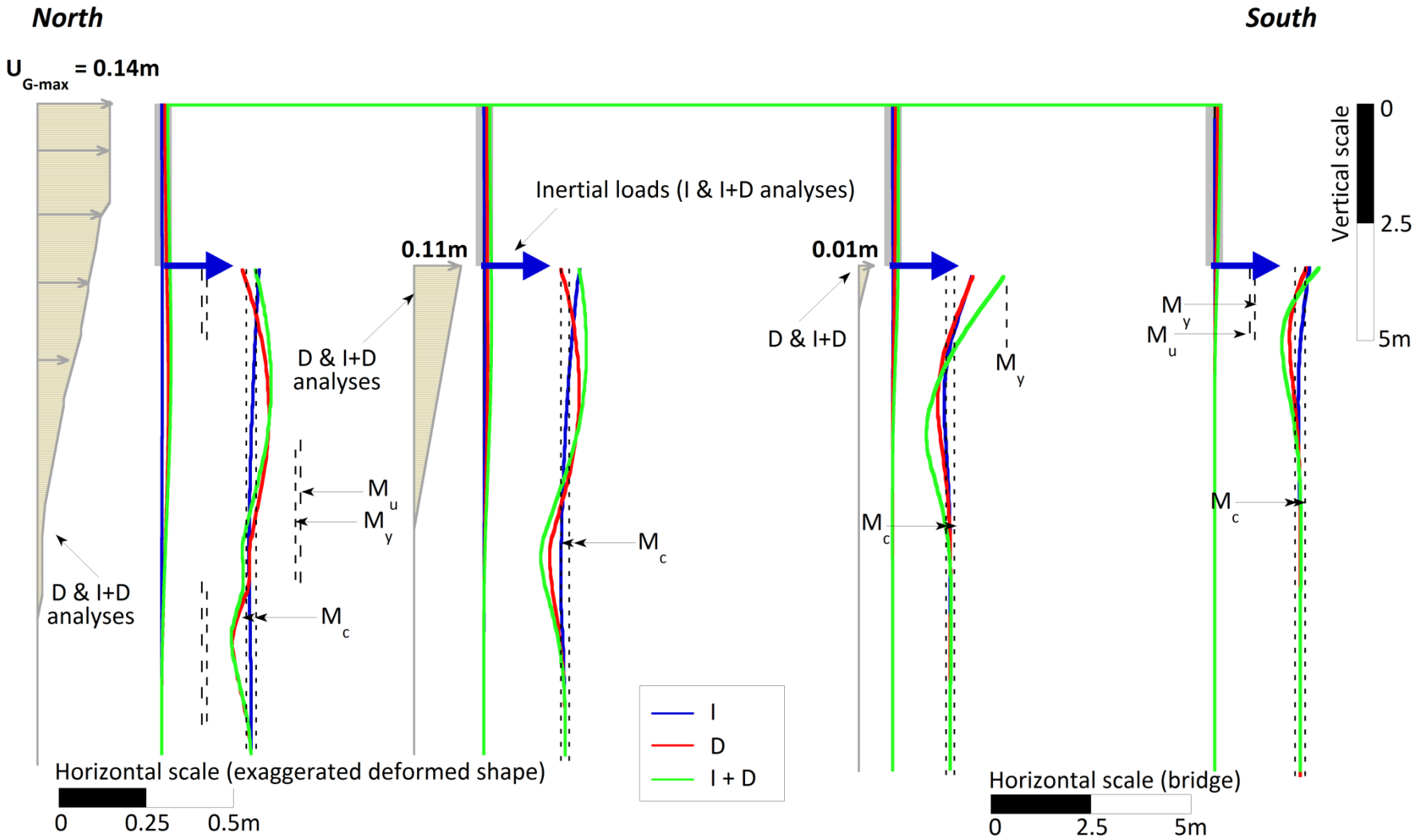

Figure 5-42: Whole bridge cyclic analyses (North to South direction), Dallington Bridge, applied ground displacements, deformed shape and bending moments in abutment piles and pier piles shown

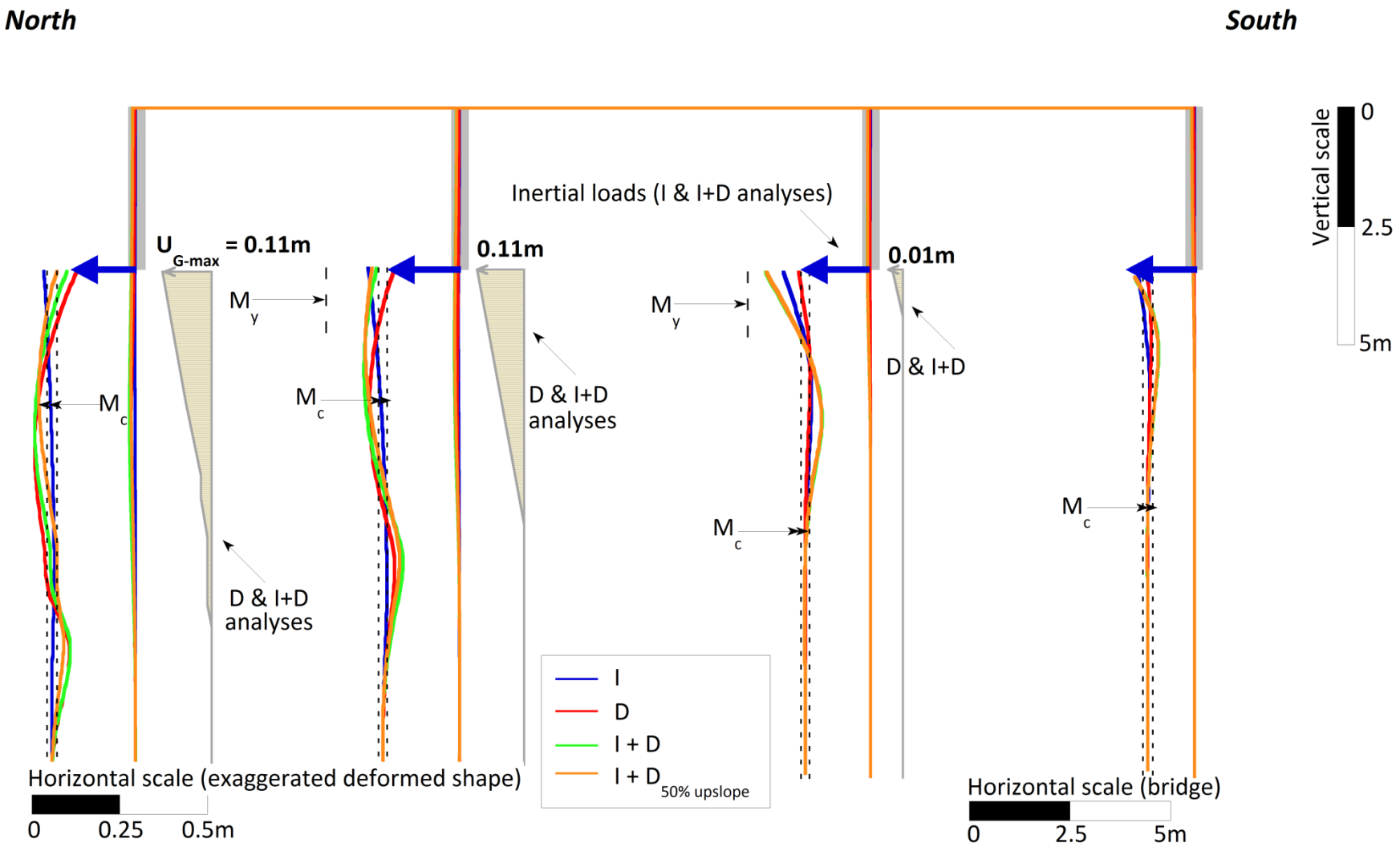

Figure 5-43: Whole bridge cyclic analyses (South to North direction), Dallington Bridge, applied ground displacements, deformed shape and bending moments in abutment piles and pier piles shown

5.5.4.5 Comparison between PSA model results and observed damages

The single pile and global bridge PSAs produced results consistent with one another in the abutments and abutment piles in both loading phases. It was apparent, however, that the system response was greatly affected by an assumed stiffness degradation in the abutment wall following cracking, and as such, it is difficult to draw firm comparisons between parametric variations and observations made in the field.

The cyclic loading phase was shown to have a much smaller effect on pile response than the lateral spreading phase in both directions of longitudinal analysis. Inertial loads were also shown to be insignificant in comparison with applied cyclic ground displacements.

The observed rotations of the abutment wall were small and there could be errors in the observation measurements due to construction tolerances on the existing abutment wall angle.

5.6 Summary

The PSA of piles and bridges in liquefying and laterally spreading soils is burdened with many uncertainties. This chapter presented two case studies of bridges subjected to cyclic and lateral spreading loads in the February 22nd 2011 Christchurch earthquake.

Key points of discussion concerning the PSAs are:

- That PSA has the ability to capture the characteristic spreading-induced deck-pinning, abutment back-rotation mechanism of bridges subjected to lateral spreading, both in single pile and global bridge analyses.
- The effects of uncertainties in key parameters can be accounted for and their effect on system response quantified.
- It was shown that where the piles extended into the crust layer, the ultimate lateral crust pressure (p_u) was a key factor controlling pile response, and as such the parameters controlling strength in the nonliquefied crust layers should be treated with due acknowledgement paid to their uncertainties.
- It was shown that, in this instance, the stiffness and strength of the liquefied layers had negligible effect on pile response, and this is due the governing loads being primarily in the crust layer.
- The magnitude of applied ground displacement was also critical in controlling pile response.

- The choice of boundary condition (fixity) at the top of a local system (e.g. abutment/pile top at point of rotation) enables the use of single pile PSA to be an effective means of isolating local system response in the case of liquefaction and lateral spreading.
- In general, the inertial loads from the superstructure were shown to be relatively small in comparison to the kinematic loads from the soil in the cyclic loading phase.
- It is noted that only the longitudinal directions of loading were considered in the cyclic analyses, and that transverse analyses could also be carried out to fully analyse the behaviour of the structure.
- The cyclic loading scenarios that were presented represent the worst possible case cyclic loading scenarios in the longitudinal direction, given that they combine the maximum inertial forces (from PGAs) with the maximum predicted cyclic ground displacements.
- Pile group effects were not considered, and this is due to the fact that pile spacings in all models considered were either equal to or greater than *4D*.
- It is important to conduct global bridge analyses as well as isolated system analyses so that more representative distributions of bending moment and displacement demands can be evaluated, especially for the central piers and pier piles.
- The type of bridge construction (i.e. segmental vs. integral) does not limit the use of PSA, rather the choice of appropriate beam element properties and fixity conditions is more important with regards to structural components.
- The restraint provided by the bridge superstructure (in this case, short stiff deck components) meant that the use of free-field lateral spreading displacements presents an upper bound solution and for these cases the model results were overly conservative.
- The results presented herein were computed based on the ground accelerations and movements of the February 22nd 2011 earthquake only, and as such it is expected that they represent the cumulative effects of both the Darfield and Christchurch events.
- Following on from the above considerations, the first case study, ANZAC Bridge, generally showed good agreement with observations made in the field, and the effects of variations in certain key parameters on system response were investigated.
- The second case study, Dallington Bridge, showed that the stiffness reduction factor for the abutment governed the behaviour for this case.
- It is recommended that further investigations be carried out on Dallington Bridge in order to investigate the effects of applying stiffness reductions to the abutment wall and pier wall components which account for cracking, where section properties are not fully known.

Surveys of existing wall properties (i.e. as-built reinforcing spacings, full extent of cracking, actual material properties) would greatly affect and enhance the use of PSA in this instance.

- Following on from this, parametric studies on the effects of crust properties, liquefied layer properties and applied ground displacements could be reassessed based on the variations in abutment stiffness.

6 Concluding remarks

6.1 Canterbury earthquakes and liquefaction-induced lateral spreading damage to bridges

The 2010-2011 Canterbury earthquake sequence, in particular the February 22nd 2011 event, caused widespread liquefaction throughout Christchurch's eastern suburbs and parts of its CBD. Along the Avon River, liquefaction was commonly accompanied by lateral spreading of the river banks in the order of several centimetres to more than two metres. This spreading was particularly damaging to bridges, infrastructure, houses and other buildings close to river banks.

Following the Christchurch earthquake, detailed bridge reconnaissance works were carried out by a University of Canterbury team on road bridges across the Avon River. Nine bridges were investigated in detail; three in the CBD on shallow foundations, and six east of the CBD on pile foundations. All those investigated were short-mid length reinforced concrete structures with high stiffness in the longitudinal direction.

The most commonly observed spreading-induced damage mechanism was that of deck-pinning and abutment back-rotation, whereby the stiff bridge decks provided restraint against lateral ground movements, and as a result, back-rotation of abutments occurred due to the abutment piles not being able to resist the large lateral forces arising from spreading ground movements. Associated damages included substantial approach settlements and pile damages immediately beneath the abutment-pile interfaces.

It was found that both segmental and integral bridges exhibited the same deformation mechanism, with abutment rotations being higher in segmental bridges than in integral. The case studies also suggested that the lateral movements of the foundation soils were larger than the displacements of the abutments pile tops but smaller than the free field lateral spreading displacements. This suggests that the use of free field lateral spreading displacements in bridge performance analysis may be over-conservative.

6.2 Case histories and experimental studies of bridge and pile damage in liquefying and laterally spreading soils

Investigations into the behaviour of pile foundations and/or bridges in liquefying and laterally spreading soils come from case histories as well as experimental studies. In general, the loads on such piles can be divided into two separate phases; the cyclic phase which occurs during earthquake shaking, and the lateral spreading phase which occurs post-liquefaction. Different combinations of kinematic and inertial loads act on the structure during each of these phases. In both cases, pile response depends on pile stiffness, liquefied soil stiffness, fixity conditions at the head and tip of the pile, and the lateral loads exerted on the pile by a nonliquefied crust layer. It was shown that pile damages are most pronounced at the interface between the liquefied layer and non-liquefied base layer, as well as at the pile head when fixity is significant.

The occurrence of liquefaction results in a significant decrease in soil stiffness and strength, and where lateral spreading occurs, large unilateral ground displacements can be applied to pile systems. Many studies have shown that passive failure modes due to lateral spreading of the non-liquefied crust layer govern the pile response.

6.3 Pseudo-static analysis

PSA is one of many computational methods available for assessing the response of soil-pile systems in liquefying and laterally spreading ground. While it is a simplified analysis method, it is shown that it is able to capture the basic mechanisms of pile behaviour without excessive computational effort and as such is attractive to designing engineers. Many design guidelines worldwide adopt pseudo-static approaches for the design of piles in liquefying and laterally spreading soils.

The application of PSA to piles in liquefying soils still retains significant uncertainties associated with capturing dynamic spatial and temporal changes in a static analysis, and it can be said that the most important consideration in a PSA is not the modelling itself, but rather the way in which key uncertainties are handled.

The case studies carried out in this research project showed that reasonable approximations of pile behaviour can be computed by PSA, especially when particular attention is paid to the key parameters affecting pile and system response. It was shown that PSA has the ability to capture the characteristic deformation of bridges and piles in laterally spreading soils, involving deck-pinning and abutment back-rotation. The choices of certain boundary (fixity) conditions at abutment/pile tops

enable the use of PSA for local-system evaluations also. It was also found through parametric analysis that the use of free-field lateral spreading displacements as inputs presented an upper bound solution and was overly conservative; and this is a direct result of the pinning forces provided by the stiff bridge superstructure.

6.4 Recommendations for further research

In order to further assess and develop the use of PSA as a seismic modelling tool, it is recommended that the following be taken into consideration:

- Transverse analyses should be carried out on the case study bridges in order to assess the effects that they would have in comparison with those from longitudinal loading cases (in particular with regard to the cyclic phase).
- More consideration could be paid to the combined effects of kinematic and inertial forces in the cyclic loading phase, and the approximation of cyclic loading displacements could be varied to analyse these effects in more depth.
- It would be most valuable to know the actual soil conditions at central bridge piers/pier piles such that more rigorous global bridge analyses could be carried out, and further site investigations at the abutments would be extremely valuable also.
- It would be interesting to calculate the pinning forces provided by the bridge superstructures in order to assess the restraining forces at the embankments against lateral soil movements.
- It is recommended that further investigations be carried out on Dallington Bridge in order to investigate the effects of applying stiffness reductions to the abutment wall and pier wall components which account for cracking, where section properties are not fully known. Surveys of existing wall properties (i.e. as-built reinforcing spacings, full extent of cracking, actual material properties) would greatly affect and enhance the use of PSA in this instance.

7 References

Abdoun, T., Dobry, R., O'Rourke, T. D., Goh, S. H. (2003). "Pile response to lateral spreads: Centrifuge modelling." *Journal of Geotechnical and Geoenvironmental Engineering,* **129**(10), 869-878.

Abdoun, T., Dobry, R., Zimmie, T. F. and Zeghal, M. (2005). "Centrifuge research of countermeasures to protect pile foundations against liquefaction-induced lateral spreading." *Journal of Earthquake Engineering,* **9**(S1), 105-125.

Architectural Institute of Japan (AIJ) (2001). "Recommendations for the design of building foundations." *In Japanese.*

Ashford, S. A., Boulanger, R. W. and Brandenberg, S. J. (2011). "Recommended Design Practice for Pile Foundations in Laterally Spreading Ground." *Pacific Earthquake Engineering Research Center,* PEER Report 2011/04.

ASTM International (2007). "Standard test method for determining particle size distribution of alumina or quartz by laser light scattering." *Designation: C 1070-01.*

Berrill, J. B., Christensen, S. A., Keenan, R. P., Okada, W. and Pettinga, J. R. (2001). "Case study of lateral spreading forces on a piled foundation." *Géotechnique* **51**(6), 501-517.

Berrill, J. & Yasuda, S. (2002). "Liquefaction and piled foundations: Some issues." *Journal of Earthquake Engineering*, **6**(Spec. Issue 1), 1-41.

Bhattacharya, S. & Madabhushi, S. G. P. (2008). "A critical review of methods for pile design in seismically liquefiable soils." *Bulletin of Earthquake Engineering,* **6***,* 407-446.

Boulanger, R. W., Kutter, B. L., Brandenberg, S. J., Singh, P. and Chang, P. (2003). "Pile Foundations in Liquefied and Laterally Spreading Ground during Earthquakes: Centrifuge Experiments and Analyses." *Report No. UCD/CGM-03/01*, Department of Civil and Environmental Engineering, University of California.

Boulanger, R. W., Chang, D., Brandenberg, S. J., Armstrong, R. J. & Kutter, B. L. (2007). "Seismic design of pile foundations for liquefaction effects." In K. D. Pitilakis (ed.), *Earthquake Geotechnical Engineering*, London & New York: Springer (Chapter 12 in book).

Bowen, H. (2007). "Behaviour of Piles in Liquefiable Deposits during Strong Earthquakes." *Thesis submitted in partial fulfilment of the requirements for the Degree of Master of Engineering in the University of Canterbury,* Department of Civil Engineering, University of Canterbury, Christchurch, New Zealand.

Bowen, H., Cubrinovski, M. and Jacka, M. (2007). "Pseudo-static analysis of piles in liquefied soils: a case study of a bridge foundation." *10th Australia New Zealand Conference on Geomechanics, 2007, Common Ground,* 130-135.

Bowen, H. J. and Cubrinovksi, M. (2008). "Pseudo-static analysis of piles in liquefiable soils: Parametric evaluation of liquefied layer properties." *Bulletin of the New Zealand Society for Earthquake Engineering,* **41**(4), 234-246.

Bradley, B. A. (2010). "NZ-specific pseudo-spectral acceleration ground motion prediction equations based on foreign models." *Research Report 2010-03.* Department of Civil Engineering, University of Canterbury, Christchurch, New Zealand, 22 September 2010. 324 pp.

Bradley, B. A. and Cubrinovski, M. (2011). "Near-source Strong Ground Motions Observed in the 22 February 2011 Christchurch Earthquake." *Seismological Research Letters,* **82**(6), 853-865.

Brandenberg, S. J. (2005). "Behavior of pile foundations in liquefied and laterally spreading ground." *PhD dissertation,* Department of Civil and Environmental Engineering, University of California, Davis, California.

Brandenberg, S. J., Boulanger, R. W., Kutter, B. L. & Chang, D. (2005). "Behavior of pile foundations in laterally spreading ground during centrifuge tests." *Journal of Geotechnical and Geoenvironmental Engineering,* **131**(11), 1378-1391.

Brandenberg, S. J., Boulanger, R. W., Kutter, B. L. & Chang, D. (2007): *Liquefaction-induced softening of load transfer between pile groups and laterally spreading crusts. Journal of Geotechnical and Geoenvironmental Engineering,* **133**(9), 1055-1066.

Brown, L. J. & Weeber, J. H. (1992). "Geology of the Christchurch Urban Area". *Institute of Geological and Nuclear Sciences, Lower Hutt, New Zealand.*

Brown, L. J., Beetham, R. D., Paterson, B. R. and Weeber, J. H. (1995). "Geology of Christchurch, New Zealand." *Environmental and Engineering Geoscience,* **1**(4), 427-488.

BS-Pile, In-house developed computer programme, University of Canterbury, New Zealand.

Christchurch City Council. (2011a). "R104 Avondale Road – Bridge Status Summary Report." *Report to CCC by Michael Cowan, Principal Civil Structures Engineer, Opus,* http://resources.ccc.govt.nz/files/R104AvondaleRoadBridge.pdf

Christchurch City Council. (2011b). "R102 Pages Road – Bridge Status Summary Report." *Report to CCC by Michael Cowan, Principal Civil Structures Engineer, Opus,* http://resources.ccc.govt.nz/files/R102PagesRoadBridge.pdf

Christchurch City Council. (2011c). "R101 South Brighton – Bridge Status Summary Report." *Report to CCC by Michael Cowan, Principal Civil Structures Engineer, Opus,* http://resources.ccc.govt.nz/files/R101SouthBrightonBridge.pdf

Christchurch City Council. (2013). "Repairs Underway on Historic Monuments." *Christchurch City Council Media Release, 22 March 2013, CCC Communications,* http://ccc.govt.nz/thecouncil/newsmedia/mediareleases/2013/201303221.aspx

Christchurch City Libraries. http://christchurchcitylibraries.com/Heritage/Maps/433589.asp

Conte, J. P. and Zhang, Y. (2007). "Performance based earthquake engineering: Application to an actual Bridge-Foundation-Ground system." *Keynote paper*, 12th Italian National Conference on Earthquake Engineering, Pisa, Italy, June 10-14, 2007.

Cubrinovski, M., Ishihara, K. and Tanizawa, F. (1996). "Numerical simulation of the Kobe Port Island liquefaction." *Eleventh World Conference on Earthquake Engineering*, Acapulco, Mexico, June 1996.

Cubrinovski, M., Ishihara, K. and Furukawazono, K. (1999). "Analysis of full-scale tests on piles in deposits subjected to liquefaction." *Second International Conference on Earthquake Geotechnical Engineering*, Lisbon, Portugal, June 1999.

Cubrinovski, M., Ishihara, K. and Kijima, T. (2001). "Effects of liquefaction on seismic response of a storage tank of pile foundations." *Fourth International Conference on Recent Advances in Geotechnical Earthquake Engineering & Soil Dynamics*, San Diego, California, March 2001.

Cubrinovski, M. and Ishihara, K. (2003). "Liquefaction-induced ground deformation and damage to piles in the 1995 Kobe earthquake." *International Conference, Skopje Earthquake. 40 Years of European Earthquake Engineering,* August 2003.

Cubrinovski, M. and Ishihara, K. (2004). "Simplified method for analysis of piles undergoing lateral spreading in liquefied soils." *Soils and Foundations,* **44**(5), 119-133.

Cubrinovski, M., Kokusho, T. and Ishihara, K. (2006a). "Interpretations from large-scale shake table tests on piles undergoing lateral spreading in liquefied soils." *Soil Dynamics and Earthquake Engineering,* **26**, 275-286.

Cubrinovski, M. and Ishihara, K. (2006b). "Assessment of pile group response to lateral spreading by single pile analysis." *ACSE Geotechnical Special Publication 145*, 242-254.

Cubrinovksi, M. (2007). "Key parameters in pseudo-static analysis of piles in liquefying sand." *10th Australian New Zealand Conference on Geomechanics,* Brisbane, pp 218-223.

Cubrinovski, M., Uzuoka, R., Sugita, H., Tokimatsu, K., Sato, M., Ishihara, K., Tsukamoto, Y. and Kamata, T. (2008). "Prediction of pile response to lateral spreading by 3-D soil-water coupled dynamic analysis: Shaking in the direction of ground flow." *Soil Dynamics and Earthquake Engineering,* **28,** 421-435.

Cubrinovksi, M. and Bradley, B.A. (2009). "Evaluation of seismic performance of geotechnical structures." In Kokusho, Tsukamoto and Yoshimine (eds.), *Performance-Based Design in Earthquake Geotechnical Engineering*, Taylor & Francis Group, London.

Cubrinovski, M., Ishihara, K. and Poulos, H. (2009a). "Pseudo-static analysis of piles subjected to lateral spreading." *Bulletin of the NZ Society for Earthquake Engineering*, **42**(1), 28-38.

Cubrinovski, M., Haskell, J. J. M. and Bradley, B. (2009b). "The effect of shear strength normalisation on the response of piles in laterally spreading soils." *Earthquake Geotechnical Engineering Satellite Conference. XVIIth International Conference on Soil Mechanics & Geotechnical Engineering 2-3.* 10. 2009, Alexandria, Egypt.

Cubrinovski, M., Haskell, J. M. M. and Bradley, B. A. (2010a). "Soil-pile interaction in liquefying soils: modelling issues." *International Workshop on Soil-Foundation-Structure-Interaction*, Auckland, Nov 2009, pp 93-100.

Cubrinovski, M., Green, R. (eds.), Allen, J., Ashford, S., Bowman, E., Bradley, B., Cox, B., Hutchinson, T., Kavazanjian, E., Orense, R., Pender, M., Quigley, M. and Wotherspoon, L. (2010b): "Geotechnical Reconnaissance of the 2010 Darfield (Canterbury) Earthquake." *Bulletin of the New Zealand Society for Earthquake Engineering,* **43**(4), 243-320.

Cubrinovski, M. (2011). "Seismic effective stress analysis: Modelling and application." *5ICEGE,* Santiago, Chile, January 2011.

Cubrinovski, M., Bradley, B., Wotherspoon, L., Green, R., Bray, J., Wood, C., Pender, M., Allen, J., Bradshaw, A., Rix, G., Taylor, M., Robinson, K., Henderson, D., Giorgini, S., Ma, K., Winkley, A. and Zupan, J. (2011). "Geotechnical Aspects of the 22 February 2011 Christchurch Earthquake." *Bulletin of the New Zealand Society for Earthquake Engineering,* **44**(4), 205-226.

Cubrinovski, M., Haskell, J. J. M. and Bradley B. A. (2012). "Analysis of Piles in Liquefying Soils by the Pseudo-Static Approach." In M.A. Sakr and A. Ansal (eds.), *Advances in Earthquake Geotechnical Engineering.* London & New York: Springer (Chapter 6 in Book).

Cubrinovski, M., Haskell, J., Winkley, A., Robinson, K. and Wotherspoon, L. (2013). "Performance of bridges in liquefied deposits during the 2010-2011 Christchurch (New Zealand) earthquakes." *ASCE Journal of Performance of Constructed Facilities, Special Issue,* in press.

Cubrinovski, M., Winkley, A., Haskell, J., Palermo, A., Wotherspoon, L., Robinson, K., Bradley, B., Brabhaharan, P. and Hughes, M. (2014). "Spreading-induced damage to short-span bridges in Christchurch (New Zealand)." *EERI Christchurch Special Issue*, accepted for print.

Di Stefano, C., Ferro, V. and Mirabile, S. (2010). "Comparison between grain-size analyses using laser diffraction and sedimentation methods." *Biosystems Engineering,* **106,** 205-215.

Elgamal, A., Yan, L., Yang, Z. and Conte, J. P. (2008). "Three-dimensional seismic response of Humboldt Bay Bridge-Foundation-Ground system." *Journal of Structural Engineering*, **134**(7), 1165-1176.

Finn, W. D. L., Byrne, P. M., Evans, S. and Law, T. (1996). "Some geotechnical aspects of the Hyogo-ken Nambu (Kobe) earthquake of January 17, 1995." *Canadian Journal of Civil Engineering,* **23**(3), 778-796.

GEER Association: Cubrinovski, M., Green, R., Wotherspoon, L. (eds), Allen, J., Bradley, B., Bradshaw, A., Bray, J., DePascale, G., Orense, R., O'Rourke, T., Pender, M., Rix, G., Wells, D., Wood, C., Cox, B., Henderson, D., Hogan, L., Kailey, P., Lasley, S., Robinson, K., Taylor, M., Winkley, A. and Zupan, J. (2011). "2011 Christchurch, New Zealand Earthquake. Version 1: November 8, 2011." *Report for Web Dissemination.* GEER Association Report No. GEER-027.

GNS Science. http://geonet.org.nz

Gregg Drilling (2010). "Guide to Cone Penetration Testing." http://www.greggdrilling.com/PDF_files/Guides/GuidetoConePenetrationTesting.pdf

Hamada, M. and O'Rourke, T. D. (eds.) (1992). "Case studies of liquefaction and lifeline performance during past earthquakes." *National Centre for Engineering Research,* State University of New York at Buffalo, Buffalo, NY, Feb 1992, Technical Report NCEER-92-0001.

Haskell, J. J. M., Cubrinovski, M. and Bradley, B. A. (2012). "Sensitivity analysis and its role in pseudo-static design of pile foundations." *Soil Dynamics and Earthquake Engineering,* **42,** 80-94.

Horikoshi, K., Tateishi, A. & Ohtsu, H. (2000). "Detailed investigation of piles damaged by Hyogoken Nambu earthquake." *12WCEE,* Paper 2477.

Ince, J. A. (1998). "A City of Bridges: A History of Bridges over the Avon and Heathcote Rivers in Christchurch." *Christchurch City Council, Christchurch, New Zealand,* 188 pp.

Ishihara, K. and Cubrinovski, M. (1998). "Performance of large-diameter piles subjected to lateral spreading of liquefied deposits." *Thirteenth Southeast Asian Geotechnical Conference*, Taipei, Taiwan, 16-20 November 1998.

Ishihara, K. and Cubrinovski, M. (2004). "Performance of piles as evaluated by three-layer model." *Geo-trans*, 2004, Los Angeles, pp 167-191.

Jefferies, M. G. and Davies, M. P. (1993). "Use of CPTu to estimate equivalent SPT N_{60}." *Geotechnical Testing Journal,* **16**, Dec, 458.

Liao, S. S. C. and Whitman, R. V. (1986). "Catalogue of liquefaction and non-liquefaction occurrences during earthquakes." *Research Report,* Department of Civil Engineering, Massachusetts Institute of Technology, Cambridge, Massachusetts.

Liyanapathirana, D. S. and Poulos, H. G. (2005). "Pseudostatic Approach for Seismic Analysis of Piles in Liquefying Soil." *Journal of Geotechnical and Geoenvironmental Engineering,* **131**(12), 1480-1487.

Le Heux, M., Palermo, A., Mackenzie, J. R. and Cubrinovski, M. (2011). "Darfield Earthquake 2010: Lateral spreading actions on the Dallington pedestrian bridge." *Proceedings of the Ninth Pacific Conference on Earthquake Engineering, 14-16 April 2011, Auckland, New Zealand,* Paper 176.

Loizeau, J. –L., Arbouille, S., Santiago, S. and Vernet, J. –P. (1994). "Evaluation of a wide range laser diffraction grain size analyser for use with sediments." *Sedimentology*, **41**(2), 353-361.

Madabhushi, G., Knappett, J. and Haigh, S. (2010). "Design of Pile Foundations in Liquefiable Soils." Imperial College Press © 2010.

Martin, G. R., Marsh, M. L., Anderson, D. G., Mayes, R. L. and Power, M. S. (2002). "Recommended Design Approach for Liquefaction Induced Lateral Spreads." *Proceedings of the third National Seismic Conference and Workshop on Bridges and Highways,* Portland, Oregon, May.

Matlock, H. (1970). "Correlations of design of laterally loaded piles in soft clay." *Proceedings, Offshore Technical Conference,* Houston, Texas, 1(1204): 577-594.

McKerchar, A. (2001). "Avon and Heathcote flow analysis." *NIWA Client Report CHC 01/42*, prepared for Environment Canterbury, May 2001.

MCEER/ATC 49-1 (2003). "Liquefaction Study Report; Recommended LRFD guidelines for the seismic design of highway bridges." *Prepared under NCHRP Project 12-49,* MCEER/ATC 49-1.

Montejo, L. A. and Kowalsky, M. J. (2007). "CUMBIA". *Set of Codes for the Analysis of Reinforced Concrete Members* (Computer Programme). Department of Civil, Construction and Environmental Engineering, North Carolina State University, Raleigh, NC.

New Zealand Transport Agency (NZTA) (2011). "Tables of state highways in each category." http://www.nzta.govt.nz/planning/process/doc/criteria-and-thresholds.pdf

Norris, R. J. and Cooper, A. F. (2001). "Late Quaternary slip rates and slip partitioning on the Alpine Fault, New Zealand." *Journal of Structural Geology,* **23**, 507-520.

Olson, S. M. and Stark, T. D. (2002). "Liquefied strength ratio from liquefaction flow failure case histories." *Canadian Geotechnical Journal*, **39**(3), 629-647.

Olson, S. M. and Stark, T. D. (2003). "Use of laboratory data to confirm yield and liquefied strength ratio concepts." *Canadian Geotechnical Journal,* **40**: 1164-1184.

Palermo, A., Le Heux, M., Bruneau, M., Anagnostopoulou, M., Wotherspoon, L. and Hogan, L. (2010). "Preliminary Findings on Performance of Bridges in the 2010 Darfield Earthquake." *Bulletin of the New Zealand Society for Earthquake Engineering,* **43**(4), 412-420.

Palermo, A., Wotherspoon, L., Wood, J., Chapman, H., Scott, A., Hogan, L., Kivell, A., Camnasio, E., Yashinsky, M., Bruneau, M. and Chouw, N. (2011). "Lessons Learnt from 2011 Christchurch Earthquakes: Analysis and Assessment of Bridges." *Bulletin of the New Zealand Society for Earthquake Engineering,* **44**(4), 319-333.

Powrie, W. (2004). "Soil mechanics: Concepts and applications." 2nd ed, Spon Press.

Project Orbit, Canterbury Geotechnical Database managed by Tonkin and Taylor, https://canterburygeotechnicaldatabase.projectorbit.com/

Reese, L. C. and Van Impe, W. F. (2001). "Single piles and pile groups under lateral loading." *Taylor and Francis Group, London, UK.*

Reese, L. C., Cox, W. R. and Koop, F. D. (1974). "Analysis of laterally loaded piles in sand." *Proceedings, Offshore Technology Conference,* Houston, TX, Paper OTC 2080, 473-483.

Robertson, P. K., Campanella, R. G. and Wightman, A. (1983). "SPT-CPT Correlations." *Journal of Geotechnical Engineering*, **109**(11), 1449-1460.

Robertson, P. K. and Wride, C. E. (1998). "Evaluating cyclic liquefaction potential using the cone penetration test." *Canadian Geotechnical Journal,* **35,** 442-459.

Robinson, K., Cubrinovski, M., Kailey, P. and Orense, R. (2011). "Field Measurements of Lateral Spreading following the 2010 Darfield Earthquake." *Proceedings of the Ninth Pacific Conference on Earthquake Engineering, 14-16 April 2011, Auckland, New Zealand,* Paper 52.

Seed, R. B. and Harder, L. F. (1990). "SPT-based analysis of cyclic pore pressure generation and undrained residual strength." *H. Bolton Seed Memorial Symposium Proceedings*, Vancouver, Canade, 2: 351-376.

Soils & Foundations (1994). "Avon Bridge – Burwood Expressway Site Investigation Report." *Report prepared for Christchurch City Council*, Soils & Foundations, Geotechnical Consulting Engineers.

Standards New Zealand (2004). "Structural Design Actions, Part 5: Earthquake Actions - New Zealand (NZS 1170.5:2004)". *Wellington, New Zealand: Standards New Zealand*, 80 pp.

Takata, T., Tada, Y., Toshida, I. and Kuribayashi, E. (1965). "Damage to bridges in the Niigata earthquake." *Report no. 125-5*, Public Works Research Institute (in Japanese).

Tamura, K. (2013). "Design Requirements of Highway Bridges for Soil Liquefaction." *Proceedings of the International Symposium for Bridge Earthquake Engineering in Honour of Prof. Kazuhiko Kawashima,* Tokyo, Japan, March 15, 2013.

Tatsuoka, F., Zhou, S., Sato, T. and Shibuya, S. (1990). "Method of evaluating liquefaction potential and its application." *Report on Seismic hazards in soil deposits in urban areas,* Ministry of Education of Japan, 75-109, In Japanese.

Tokimatsu, K. and Asaka, Y. (1998). "Effects of liquefaction-induced ground displacements on pile performance in the 1995 Hyogoken-Nambu earthquake." *Special Issue of Soils and Foundations*, JGS, 163-177.

Tokimatsu, K., Suzuki, H. and Sato, M. (2005). "Effects of inertial and kinematic interaction on seismic behaviour of pile with embedded foundation." *Soil Dynamics and Earthquake Engineering,* **25**, 753-762.

Uchida, A. and Tokimatsu, K. (2005). "Comparison of current Japanese design specifications for pile foundations in liquefiable and laterally spreading ground." In R. W. Boulanger and K. Tokimatsu (eds.), *Seismic Performance and Simulation of Pile Foundations in Liquefied and Laterally Spreading Ground (Geotechnical Special Publication No. 145).* Proceedings of a workshop, March 16-18, University of California, Davis, California, pp 61-70.

University of Canterbury Department of Geology. http://www.geol.canterbury.ac.nz/earthquake/

Villemure, M., Wilson, T. M., Bristow, D., Gallagher, M., Giovinazzi, S. and Brown, C. (2012). "Liquefaction ejecta clean-up in Christchurch during the 2010-2011 earthquake sequence." *New Zealand Society for Earthquake Engineering: 2012 Annual Technical Conference (NZSEE), 13-15 April 2012,* Paper 131.

Waldin, J., Jennings, J. and Routledge, P. (2012). "Critically damaged bridges and concepts for earthquake recovery." *New Zealand Society for Earthquake Engineering: 2012 Annual Technical Conference (NZSEE), 13-15 April 2012,* Paper 104.

Wang, S. T. and Reese, L. C. (1998). "Design of pile foundations in liquefied soils." *Geotechnical Earthquake Engineering and Soil Dynamics III, GSP No. 75,* P. Dakoulas and M. Yegian (eds), Vol. 2, ASCE, Reston, Va.

Weaver, T. S., Ashford, S. A. and Rollins, K. M. (2005). "Response of liquefied sand to a 0.6-m CISS pile under lateral loading." *Journal of Geotechnical and Geoenvironmental Engineering,* ASCE, **131**(1): 94-102.

Wen, B., Aydin, A. and Duzgoren-Aydin, N. S. (2002). "A comparative study of particle size analyses by sieve-hydrometer and laser diffraction methods." *Geotechnical Testing Journal,* **25**(4), 434-442.

Wilson, D. W., Boulanger, R. W. and Kutter, B. L. (2000). "Observed seismic lateral resistance of liquefying sand." *Journal of Geotechnical and Geoenvironmental Engineering,* ASCE, **126**(10): 898-906.

Wotherspoon, L. and Palermo, A. (2012). "Geotechnical Investigation of Earthquake Damaged Christchurch Bridges." *Report documenting locations and data of geotechnical site investigations,* Universities of Auckland and Canterbury.

Wotherspoon, L., Bradshaw, A., Green, R., Wood, C., Palermo, A., Cubrinovski, M. and Bradley, B. (2011). "Performance of Bridges during the 2012 Darfield and 2011 Christchurch Earthquakes." *Seismological Research Letters,* **82**(6), 950-964.

Youd., T. L. and Idriss, I. M. (2001). "Liquefaction Resistance of Soils: Summary Report from the 1996 NCEER/NSF Workshops of Evaluation of Liquefaction Resistance of Soils." *Journal of Geotechnical and Geoenvironmental Engineering,* **127**(4), 297-313.

Youd, T. L., Rollins, K. M., Salazar, A. F. and Wallace, R. M. (1992). "Bridge damage caused by liquefaction during the 22 April 1991 Costa Rica earthquake." *Earthquake Engineering, Tenth World Conference,* Balkema, Rotterdam.

Zhang, G., Robertson, P. K. and Brachman, R. W. I. (2002). "Estimating liquefaction-induced ground settlements from CPT for level ground." *Canadian Geotechnical Journal,* **39**(5), 1168-1180.

Zhang, G., Robertson, P. K. and Brachman, R. W. I. (2004). "Estimating liquefaction-induced lateral displacements using the standard penetration test or cone penetration test." *Journal of Geotechnical and Geoenvironmental Engineering*, **127**(10), 861-871.

Zhang, Y., Conte, J. P., Yang, Z., Elgamal, A., Bielak, J. and Acero, G. (2008). "Two-dimensional nonlinear earthquake response analysis of a Bridge-Foundation-Ground system." *Earthquake Spectra*, **24**(2), 343-386.

Appendix A – Original site investigation data

ANZAC Bridge

North Abutment

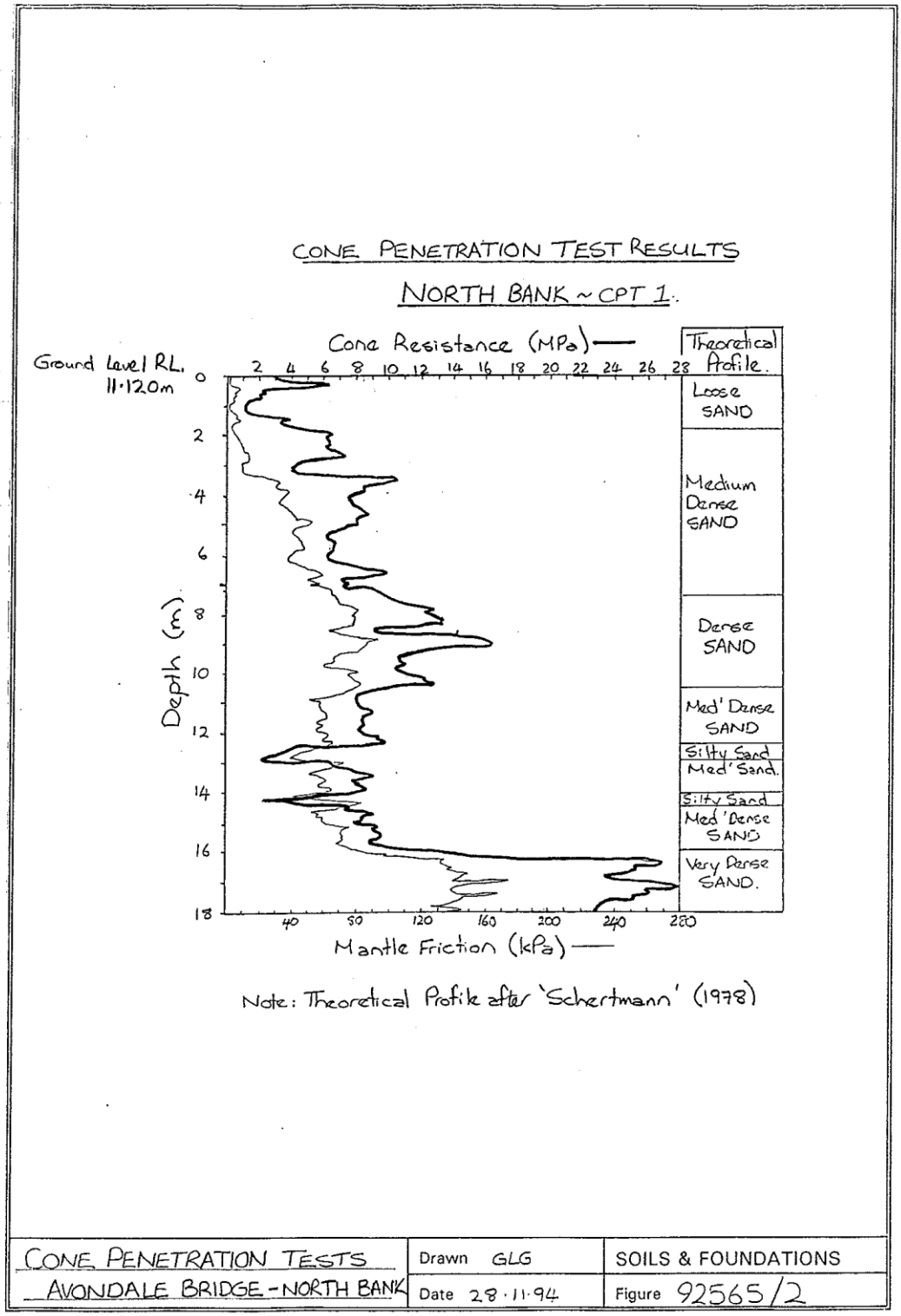

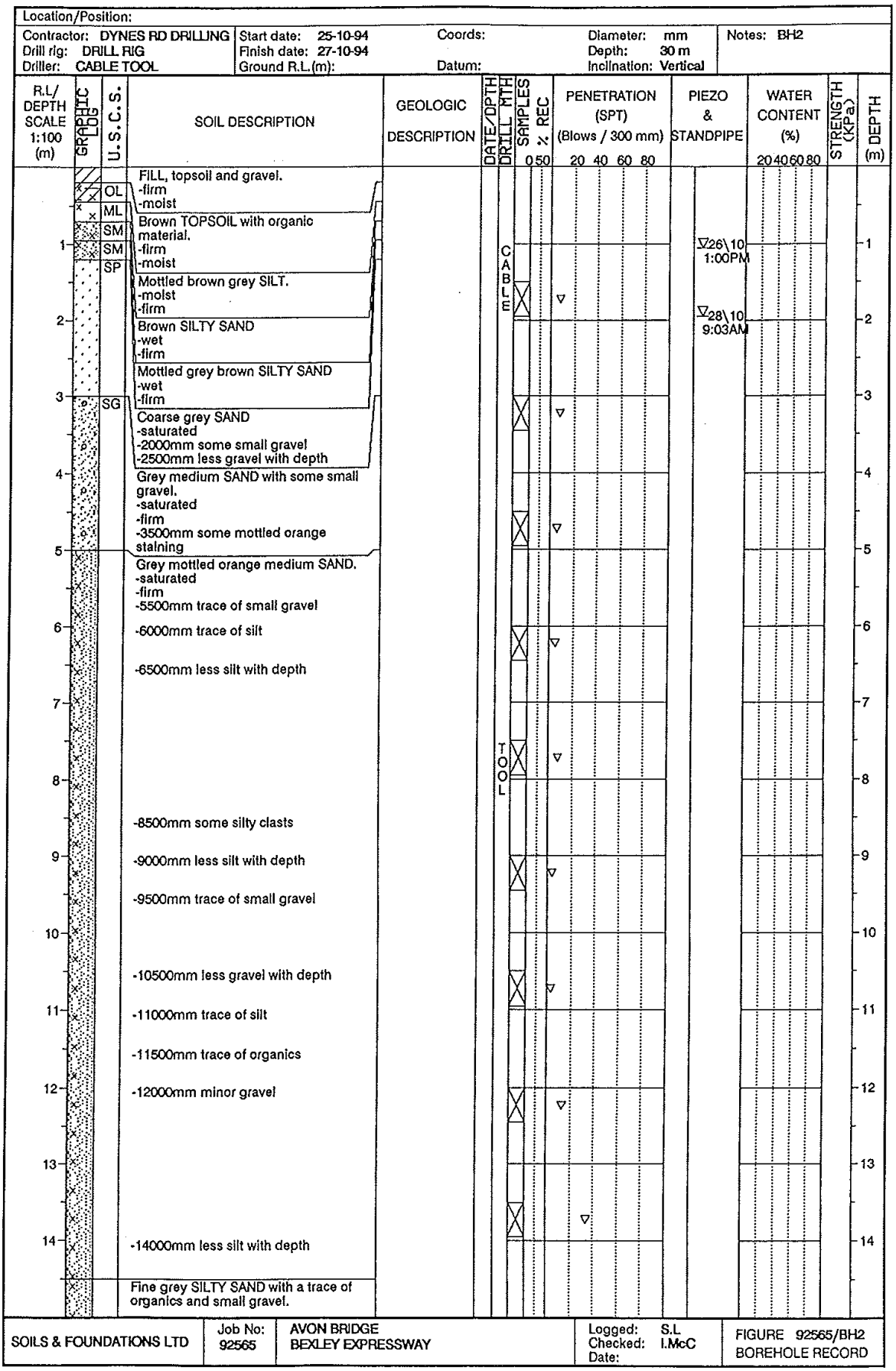
Location/Position:
Contractor: DYNES RD DRILLING
Drill rig: DRILL RIG
Driller: CABLE TOOL
Start date: 25-10-94
Finish date: 27-10-94
Ground R.L.(m):
Coords:
Datum:
Diameter: mm
Depth: 30 m
Inclination: Vertical
Notes: BH2
R.L/ DEPTH SCALE 1:100 (m)
GRAPHIC LOG
U.S.C.S.
SOIL DESCRIPTION
GEOLOGIC DESCRIPTION
DATE/DPTH
DRILL MTH
SAMPLES
% REC
PENETRATION (SPT)
(Blows / 300 mm)
PIEZO & STANDPIPE
WATER CONTENT (%)
STRENGTH (KPa)
DEPTH (m)
FILL, topsoil and gravel.
-firm
-moist
OL
ML
Brown TOPSOIL with organic material.
-firm
-moist
SM
SM
SP
Mottled brown grey SILT.
-moist
-firm
Brown SILTY SAND
-wet
-firm
Mottled grey brown SILTY SAND
-wet
-firm
SG
Coarse grey SAND
-saturated
-2000mm some small gravel
-2500mm less gravel with depth
Grey medium SAND with some small gravel.
-saturated
-firm
-3500mm some mottled orange staining
Grey mottled orange medium SAND.
-saturated
-firm
-5500mm trace of small gravel
-6000mm trace of silt
-6500mm less silt with depth
-8500mm some silty clasts
-9000mm less silt with depth
-9500mm trace of small gravel
-10500mm less gravel with depth
-11000mm trace of silt
-11500mm trace of organics
-12000mm minor gravel
-14000mm less silt with depth
Fine grey SILTY SAND with a trace of organics and small gravel.
CABLE TOOL
26\10 1:00PM
28\10 9:03AM
SOILS & FOUNDATIONS LTD
Job No: 92565
AVON BRIDGE
BEXLEY EXPRESSWAY
Logged: S.L
Checked: I.McC
Date:
FIGURE 92565/BH2
BOREHOLE RECORD

Location/Position:

Contractor: DYNES RD DRILLING | Start date: 25-10-94 | Coords: | Diameter: mm | Notes: BH2
Drill rig: DRILL RIG | Finish date: 27-10-94 | Depth: 30 m
Driller: CABLE TOOL | Ground R.L.(m): | Datum: | Inclination: Vertical

R.L/ DEPTH SCALE 1:100 (m)	GRAPHIC LOG	U.S.C.S.	SOIL DESCRIPTION	GEOLOGIC DESCRIPTION	DATE/DPTH DRILL MTH	SAMPLES	% REC	PENETRATION (SPT) (Blows / 300 mm)	PIEZO & STANDPIPE	WATER CONTENT (%)	STRENGTH (KPa)	DEPTH (m)
16			-saturated -15000mm less organics -15500mm less gravel with depth -16000mm trace of organics		CABLE TOOL		0 50	20 40 60 80		20 40 60 80		16
17			-17000mm less organics with depth									17
18												18
19												19
20			-20000mm trace of small gravel									20
21			-21500mm trace of silt									21
22												22
23			-23000mm trace of silt and gravel and some broken sea shells									23
24		SM	Grey fine SILTY SAND. -saturated -firm -24500mm minor small gravel and trace of silt									24
25			Grey fine SAND. -saturated -firm									25
26			-26000mm some small shell fragments									26
27			-27500mm trace of silt and organics									27
28			-28000mm less silt and organics with depth									28
29												29

SOILS & FOUNDATIONS LTD | Job No: 92565 | AVON BRIDGE BEXLEY EXPRESSWAY | Logged: S.L Checked: I.McC Date: | FIGURE 92565/BH2 BOREHOLE RECORD

South abutment

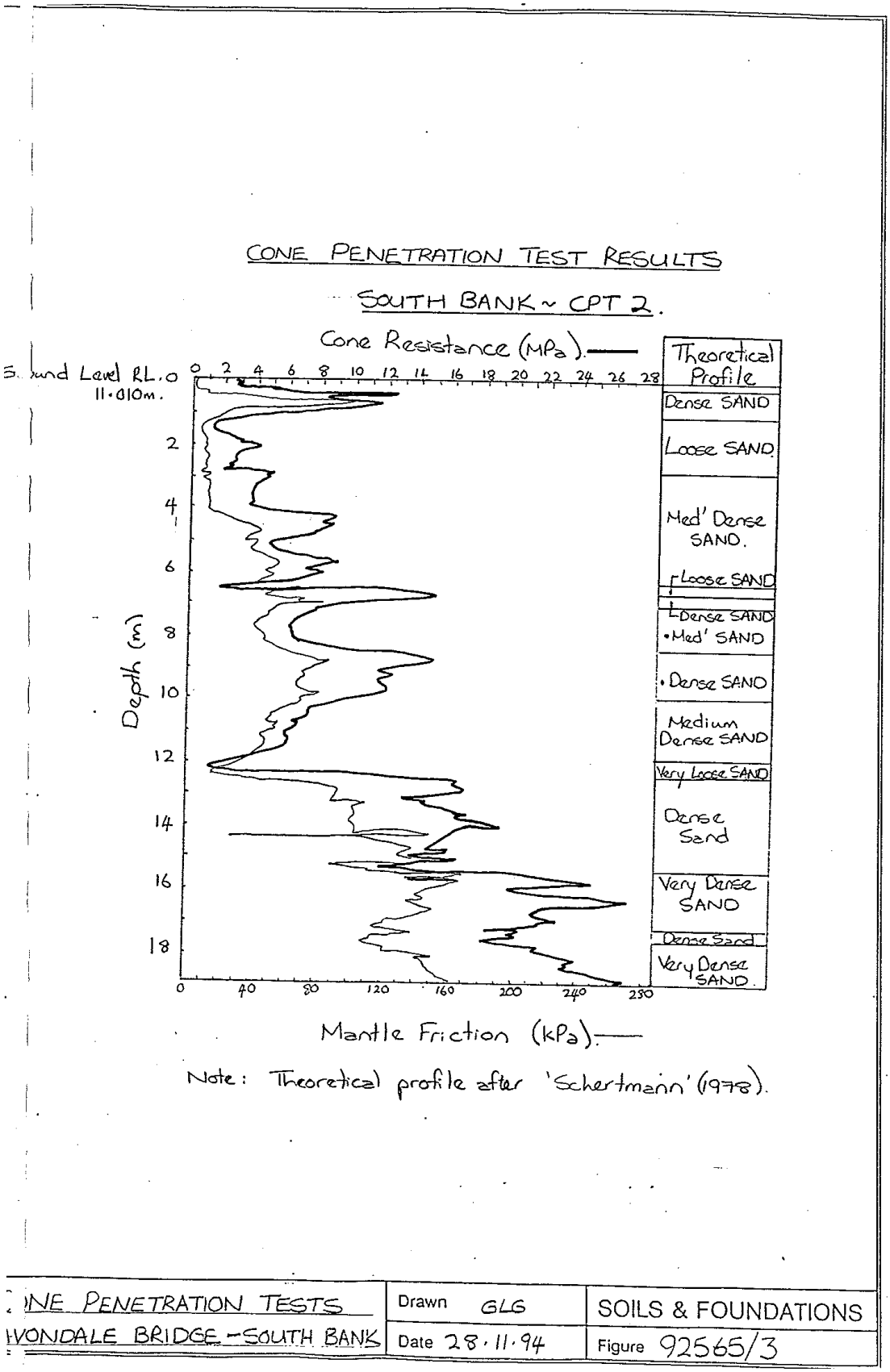

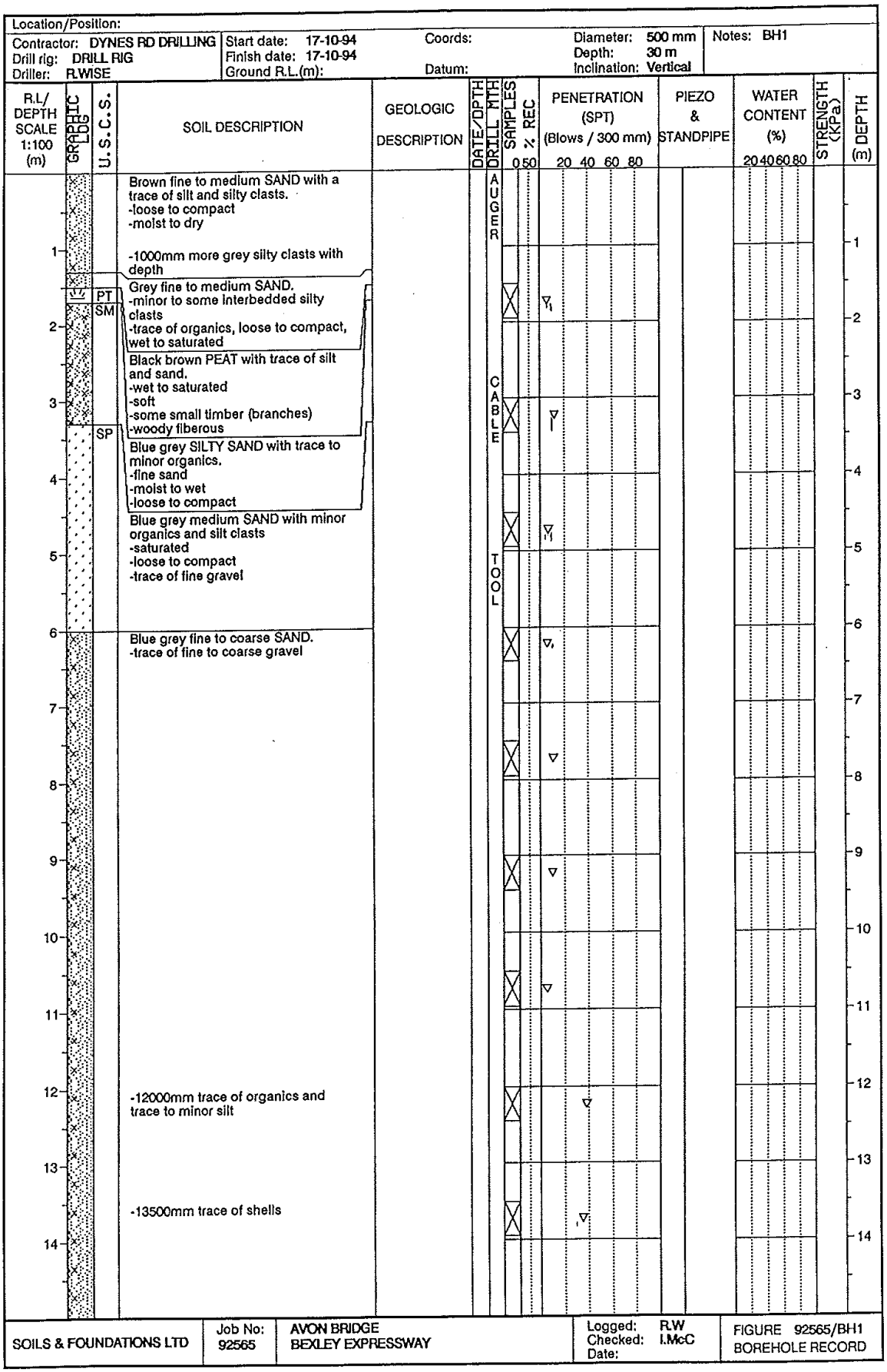
Location/Position:
Contractor: DYNES RD DRILLING
Drill rig: DRILL RIG
Driller: R.WISE
Start date: 17-10-94
Finish date: 17-10-94
Ground R.L.(m):
Coords:
Datum:
Diameter: 500 mm
Depth: 30 m
Inclination: Vertical
Notes: BH1
R.L/ DEPTH SCALE 1:100 (m)
GRAPHIC LOG
U.S.C.S.
SOIL DESCRIPTION
GEOLOGIC DESCRIPTION
DATE/DEPTH
DRILL MTR
SAMPLES
% REC
PENETRATION (SPT) (Blows / 300 mm)
PIEZO & STANDPIPE
WATER CONTENT (%)
STRENGTH (KPa)
DEPTH (m)
AUGER
CABLE
TOOL
Brown fine to medium SAND with a trace of silt and silty clasts.
-loose to compact
-moist to dry
-1000mm more grey silty clasts with depth
PT
SM
Grey fine to medium SAND.
-minor to some interbedded silty clasts
-trace of organics, loose to compact, wet to saturated
Black brown PEAT with trace of silt and sand.
-wet to saturated
-soft
-some small timber (branches)
-woody fiberous
SP
Blue grey SILTY SAND with trace to minor organics.
-fine sand
-moist to wet
-loose to compact
Blue grey medium SAND with minor organics and silt clasts
-saturated
-loose to compact
-trace of fine gravel
Blue grey fine to coarse SAND.
-trace of fine to coarse gravel
-12000mm trace of organics and trace to minor silt
-13500mm trace of shells
SOILS & FOUNDATIONS LTD
Job No: 92565
AVON BRIDGE
BEXLEY EXPRESSWAY
Logged: R.W
Checked: I.McC
Date:
FIGURE 92565/BH1
BOREHOLE RECORD

Location/Position:

Contractor: DYNES RD DRILLING | Start date: 17-10-94 | Coords: | Diameter: 500 mm | Notes: BH1
Drill rig: DRILL RIG | Finish date: 17-10-94 | | Depth: 30 m
Driller: R.WISE | Ground R.L.(m): | Datum: | Inclination: Vertical

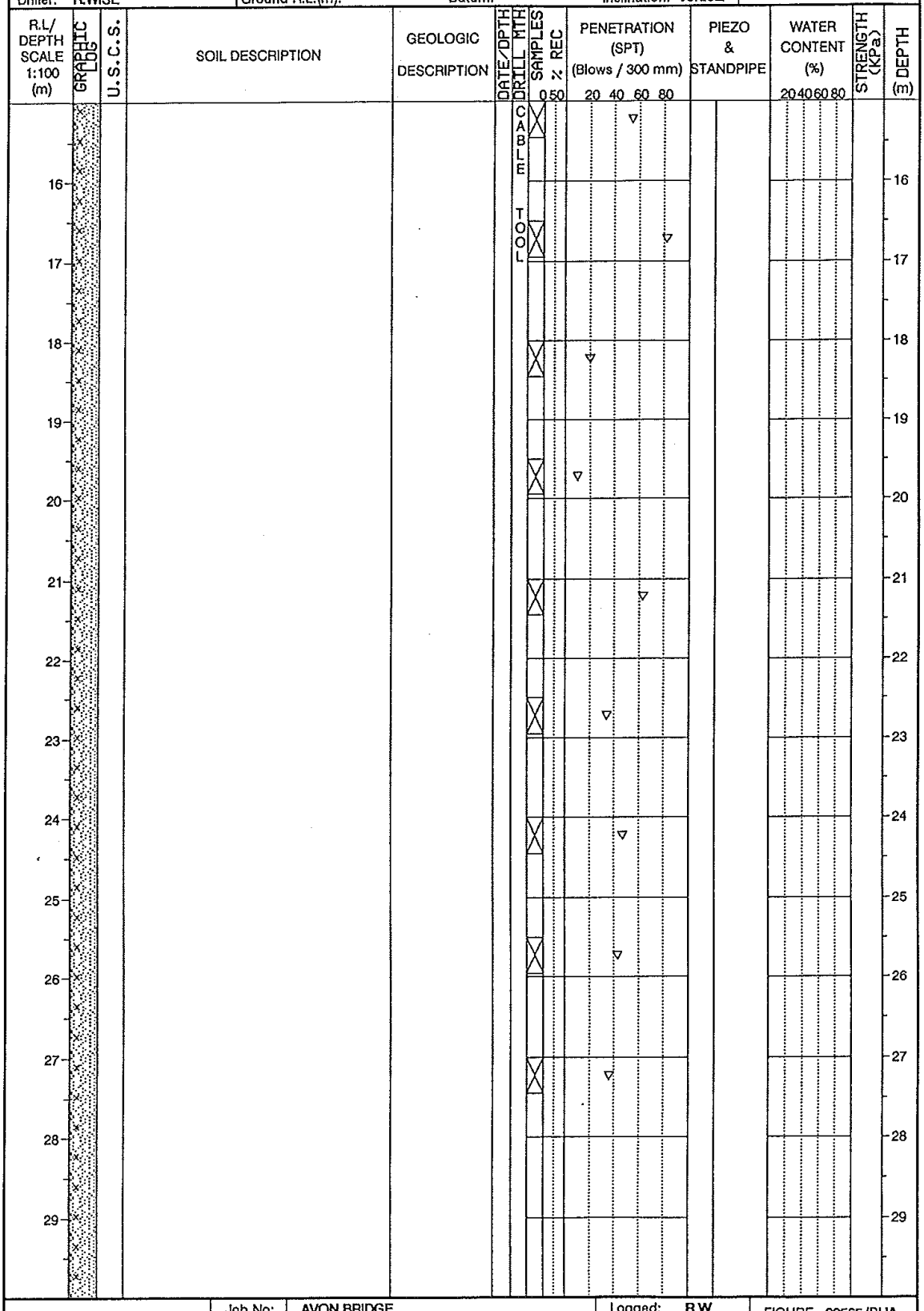

SOILS & FOUNDATIONS LTD | Job No: 92565 | AVON BRIDGE BEXLEY EXPRESSWAY | Logged: R.W Checked: I.McC Date: | FIGURE 92565/BHA BOREHOLE RECORD

Dallington Bridge

North abutment

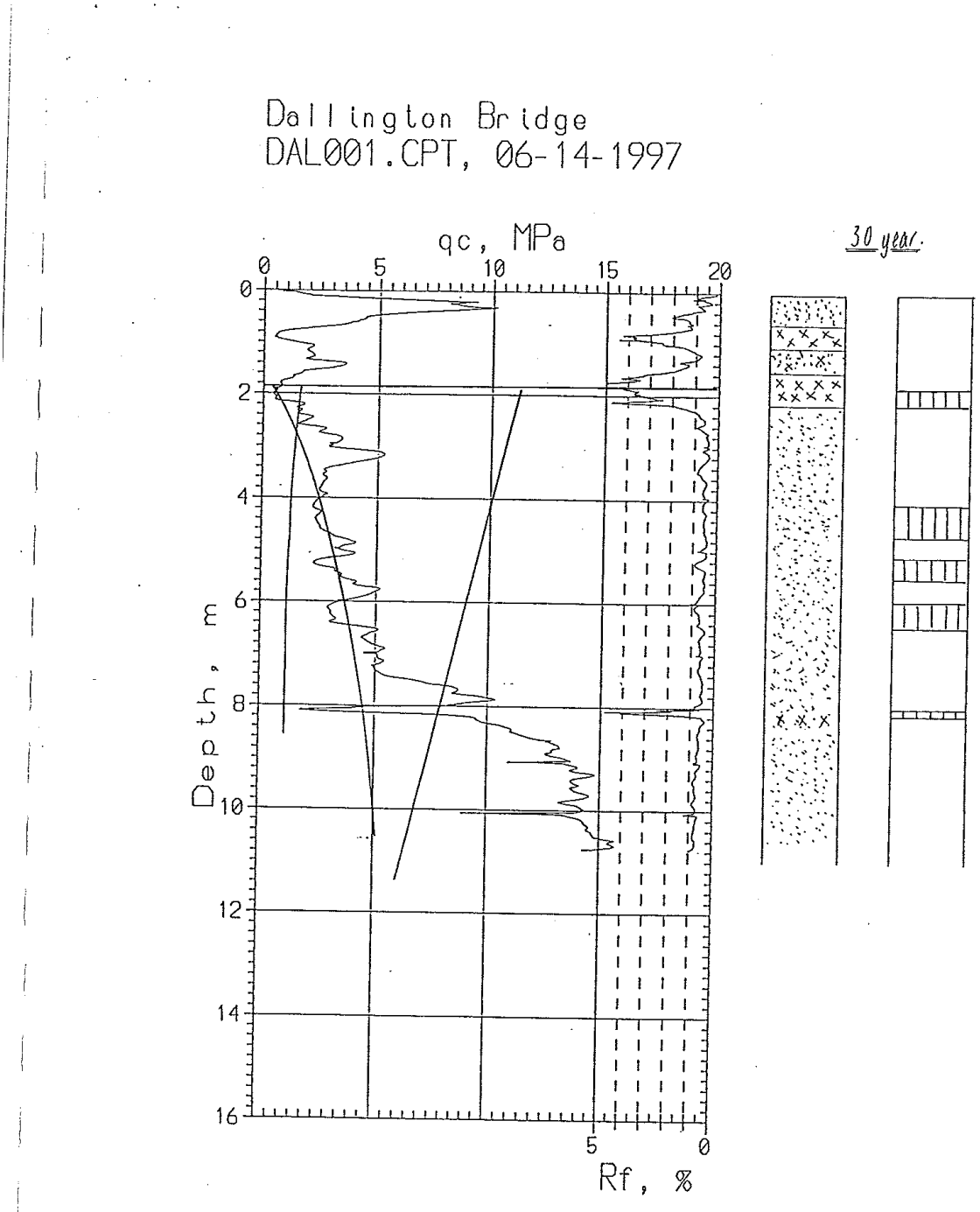

Project:	Darfield 2010 Earthquake - EQC Ground Investigations			Page: 1 of 2	CPT-DAL-07
Test Date:	18-Nov-2010	Location:	Dallington	Operator:	Perry
Pre-Drill:	0.8m	Assumed GWL:	2.7mBGL	Located By:	Survey GPS
Position:	2483566.1mE	5742841.9mN	3.04mRL	Coord. System:	NZMG & MSL
Other Tests:				Comments:	

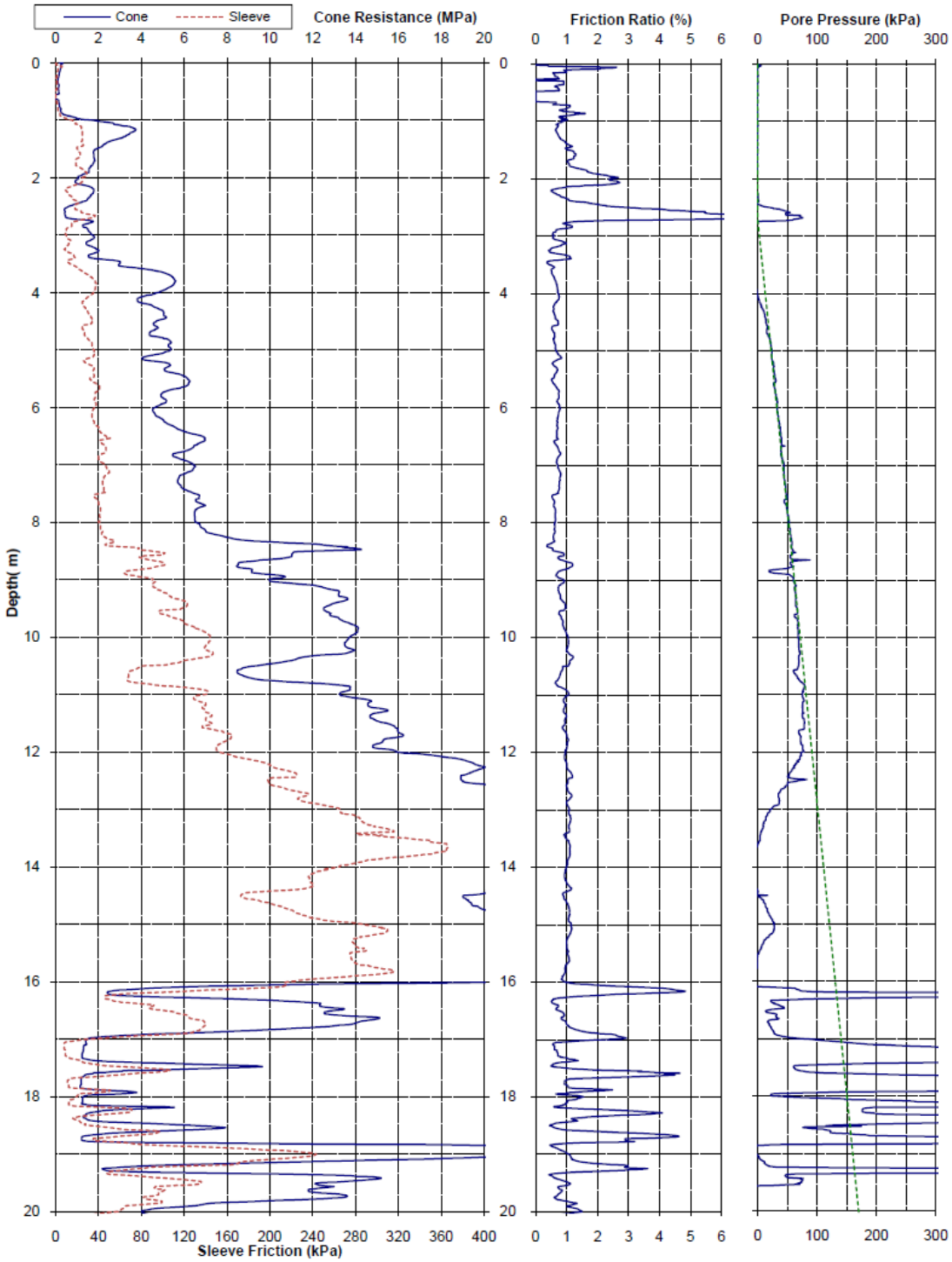

Project:	Darfield 2010 Earthquake - EQC Ground Investigations			Page: 2 of 2	CPT-DAL-07
Test Date:	18-Nov-2010	Location:	Dallington	Operator:	Perry
Pre-Drill:	0.8m	Assumed GWL:	2.7mBGL	Located By:	Survey GPS
Position:	2483566.1mE	5742841.9mN	3.04mRL	Coord. System:	NZMG & MSL
Other Tests:				Comments:	

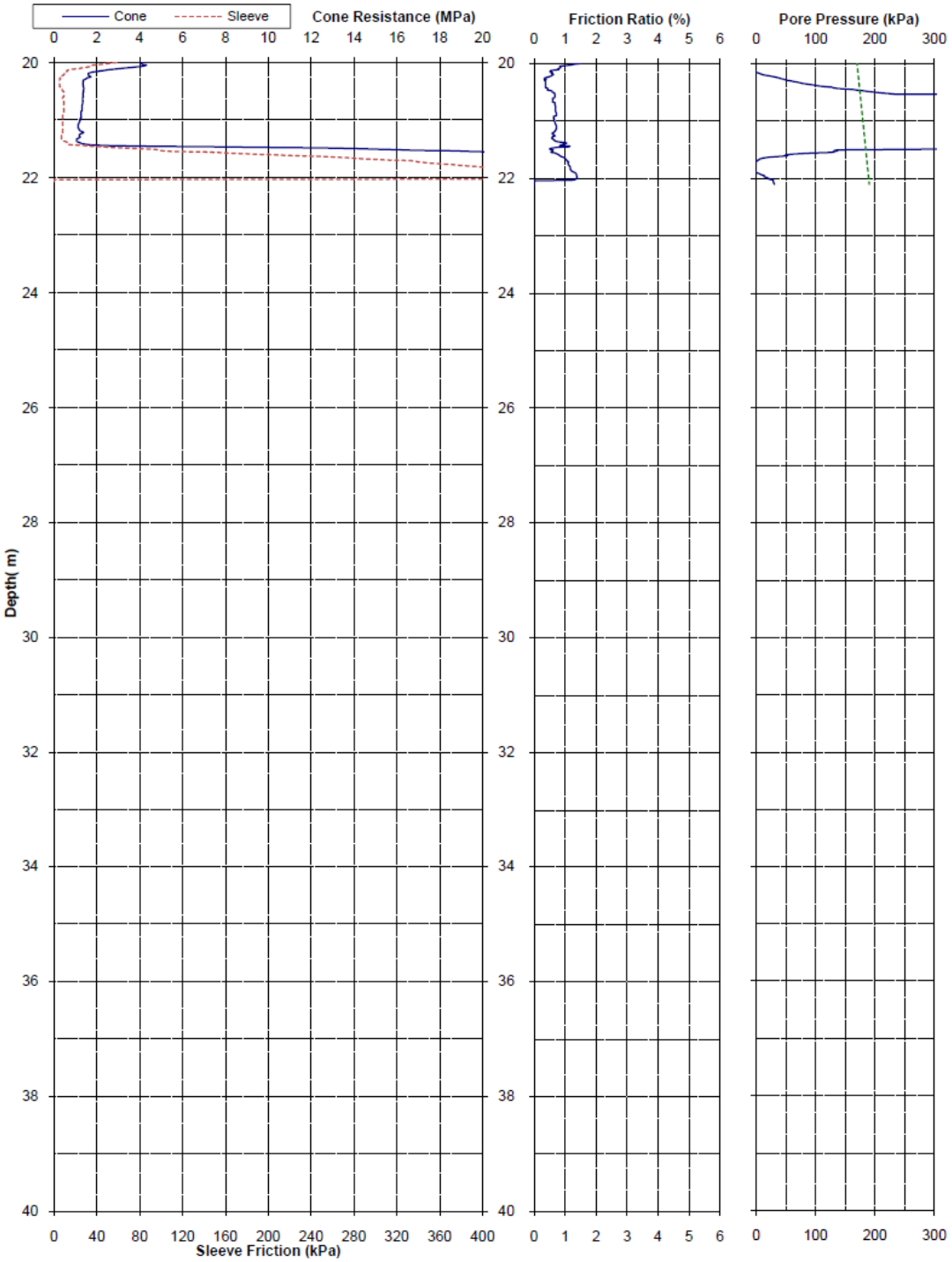

Project:	Darfield 2010 Earthquake - EQC Ground Investigations			Page: 1 of 2	CPT-DAL-49
Test Date:	8-Dec-2010	Location:	Dallington	Operator:	Perry
Pre-Drill:	1.2m	Assumed GWL:	1.2mBGL	Located By:	Survey GPS
Position:	2483520.9mE	5742834.4mN	2.16mRL	Coord. System:	NZMG & MSL
Other Tests:				Comments:	

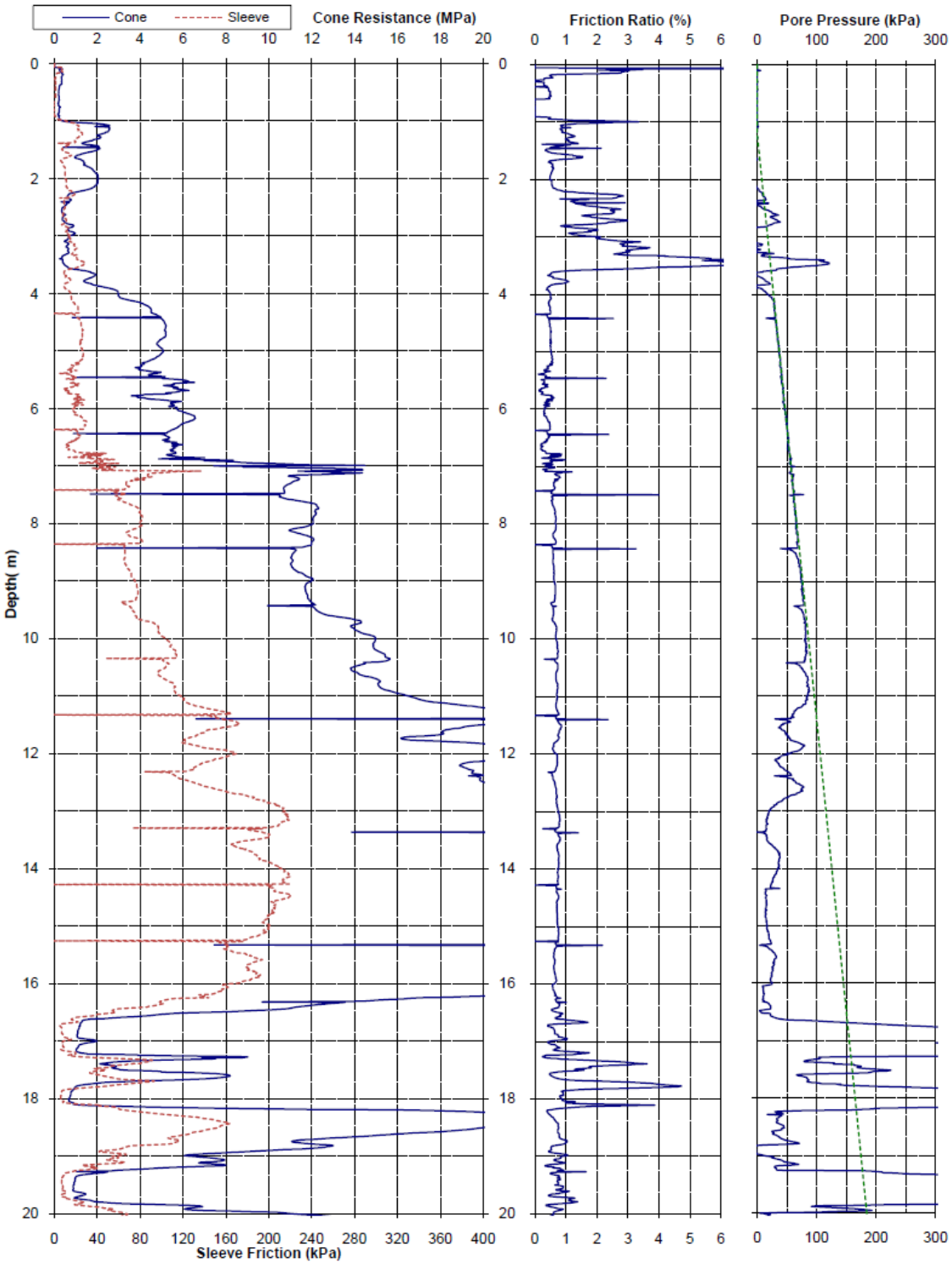

Project:	Darfield 2010 Earthquake - EQC Ground Investigations			Page: 2 of 2	CPT-DAL-49
Test Date:	8-Dec-2010	Location:	Dallington	Operator:	Perry
Pre-Drill:	1.2m	Assumed GWL:	1.2mBGL	Located By:	Survey GPS
Position:	2483520.9mE	5742834.4mN	2.16mRL	Coord. System:	NZMG & MSL
Other Tests:				Comments:	

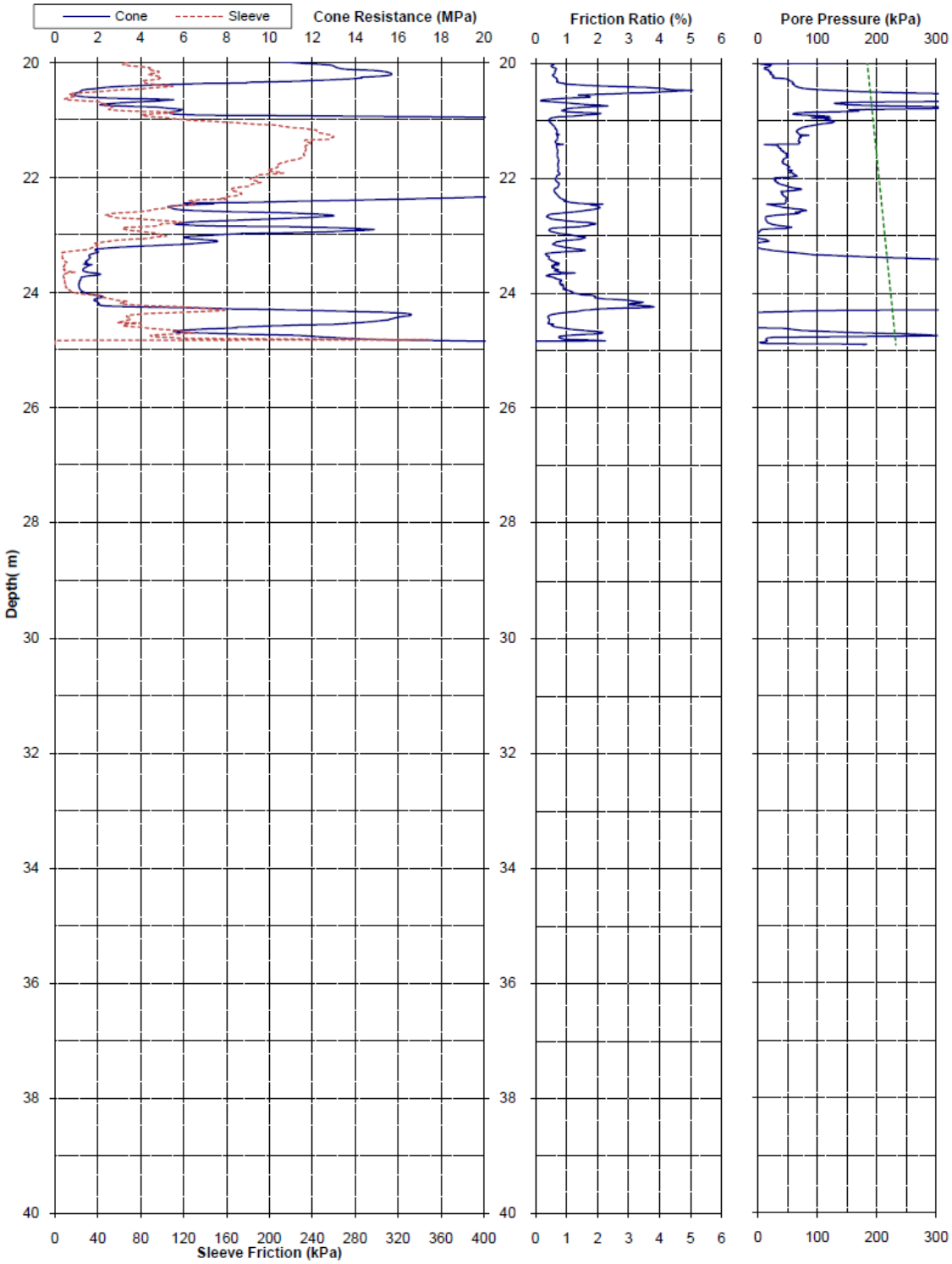

Bore Log

McMILLAN DRILLING SERVICES

Client:	University of Auckland
Project:	Christchurch Bridges
Bore No.:	/BGAY1
Job No.:	9338

Site Location: Gayhurst Road Bridge - Site One
Grid Reference: 2483569 mE, 5742841 mN (NZMG)
Rig Operator: D. Keown
Rig Model and Mounting: Geoprobe 8140LS (DT45)

Date Commenced: 18/11/2011
Date Completed: 19/11/2011
Consent:
Datum: Ground

Description	Depth	Method	Drivability (1 2 3 4)	Recovery (25 50 75)	Graphic Log	SPT N-Value (uncorrected) (10 20 30 40)	SPT Data (uncorrected)
Fine brownish SAND	0			40%			
Grey brownish SILT	1			100%			N = 5 (C) 1.1m 2, 2 / 2, 1, 1, 1 450 mm
PEAT	2			100%			N = 5 (C) 2.6m 1, 1 / 1, 1, 1, 2 450 mm
Grey fine SAND; saturated	3			60%			N = 10 (C) 4.1m 3, 2 / 2, 2, 3, 3 450 mm
	4			90%			N = 7 (C) 5.6m 4, 2 / 1, 1, 2, 3 450 mm
	5			10%			N = 11 (C) 7.1m 2, 2 / 3, 2, 3, 3 450 mm
	6			100%			N = 17 (C) 8.7m 10, 4 / 4, 4, 4, 5 450 mm
	7			100%			N = 18 (C) 10.2m 4, 4 / 4, 4, 5, 5 450 mm
	8			100%			N = 30 (C) 11.7m 7, 5 / 6, 7, 8, 9 450 mm
	9			100%			N = 40 (C) 13.2m 6, 7 / 7, 9, 12, 12 450 mm
	10			100%			N = 37 (C) 14.7m 5, 10 / 7, 10, 9, 11 450 mm
Grey Sandy SILT, trace wood	11			100%			N = 12 (C) 16.3m 0, 0 / 1, 4, 4, 3 450 mm
	12			100%			N = 50 (C) 17.8m 1, 3 / 10, 14, 13, 13 450 mm
	13			100%			N = 0 (C) 19.3m 0, 0 / 0, 0, 0, 0 450 mm Weight of Hammer
	14			100%			N = 22 (C) 20.8m 6, 7 / 5, 5, 6, 6 450 mm
	15			100%			N = 29 (C) 22.3m 2, 7 / 10, 7, 6, 6 450 mm
Grey fine SAND	16			100%			N = 24 (C) 23.9m 2, 2 / 3, 5, 8, 8 450 mm
Sandy SILT	17			100%			N = 39 (C) 25.4m 2, 4 / 5, 8, 13, 13 450 mm
	18			100%			
	19			100%			
Grey fine SAND, minor silt -20.81 - 24.3m; no silt	20			100%			
	21			100%			
	22			100%			
	23			100%			
	24			100%			
Organic SILT	25			100%			
Silty Sandy GRAVEL							
E.O.H 25.8m							

Installation & Resources

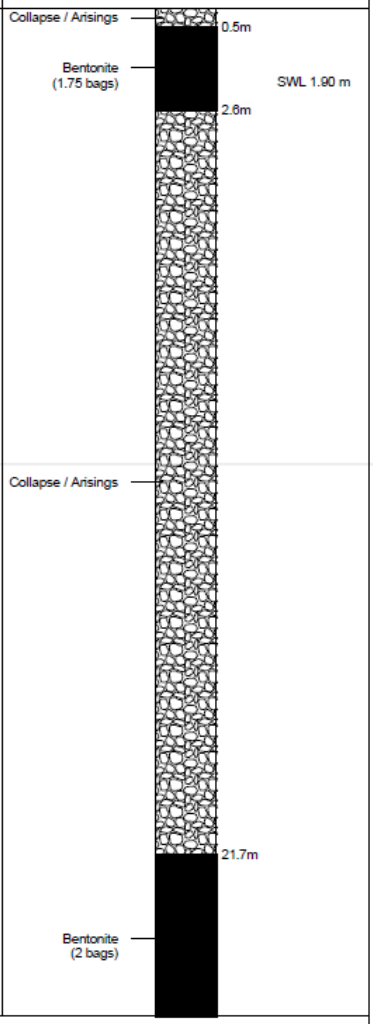

Remarks:
Geotechnical Investigation Borehole BH-GAY-01 with SPT Testing.
3000 litres water added.
SPT: Safety Auto Trip Hammer #368 used (energy ratio 85% - estimated, yet to be PDA tested)

Drivability
1 Easy Push - No Hammer \ Fast Penetration
2 Relatively Easy Push - Light Hammer \ Relatively Fast
3 Medium Push - Consistent Hammer \ Medium
4 Hard Push - Full Hammer \ Somewhat Slow
5 Very Hard Push - Very Slow, Full Hammer \ Very Slow

Additional Resources:

Plastic Liner	m	25.5
Flush Mounted Toby Box		
- Standard	ea	
- Environmental	ea	
Above Ground Protective Surround	ea	
Geotextile Sock	m	
Handclear Location	ea	
Decontaminate Equipment	ea	

120 High Street, Southbridge 7602, Canterbury, New Zealand | ph: (03) 324 2571 fax: +64 3 324 2431 web: www.drilling.co.nz

Report Created: 16/12/2011 10:25:58 a.m.

South abutment

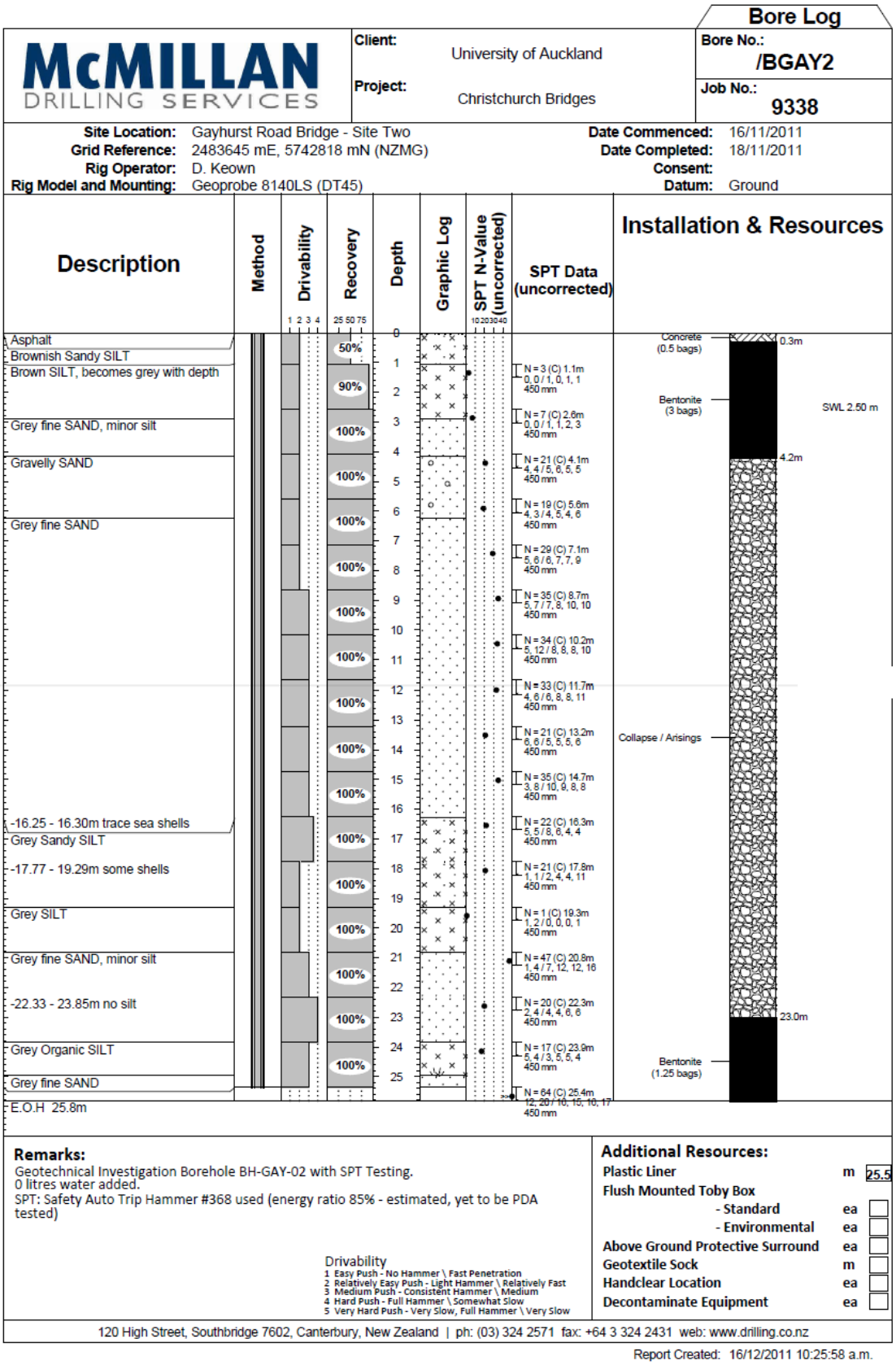

Appendix B – Processing of site investigation data

Test	**ANZ-CPT-2 (South abutment)**		
Time + date	28/11/94		
Latitude	43.50121	S	
Longitude	172.7013	E	
Elevation	11.01		
Performed by			
Predrilled	0	m	
Other comments	Avon Bridge - Burwood Expressway SI Report - Nov 1994		

Unit weight dry soil =	18	kN/m^3
Unit weight sat soil =	19	kN/m^3
Depth to GWT =	1.4	m (before 2 m of FILL overlaid)
Unit weight water =	9.81	kN/m^3

PGA (g)	Feb - D	Sept - D
cond. Σ	0.158	0.149
+ σ	0.3279	0.1834
cond. Med	**0.28**	**0.158**
- σ	0.2391	0.1361

Legend for pages in the *EXCEL* spreadsheet, processing of CPT-2, ANZAC

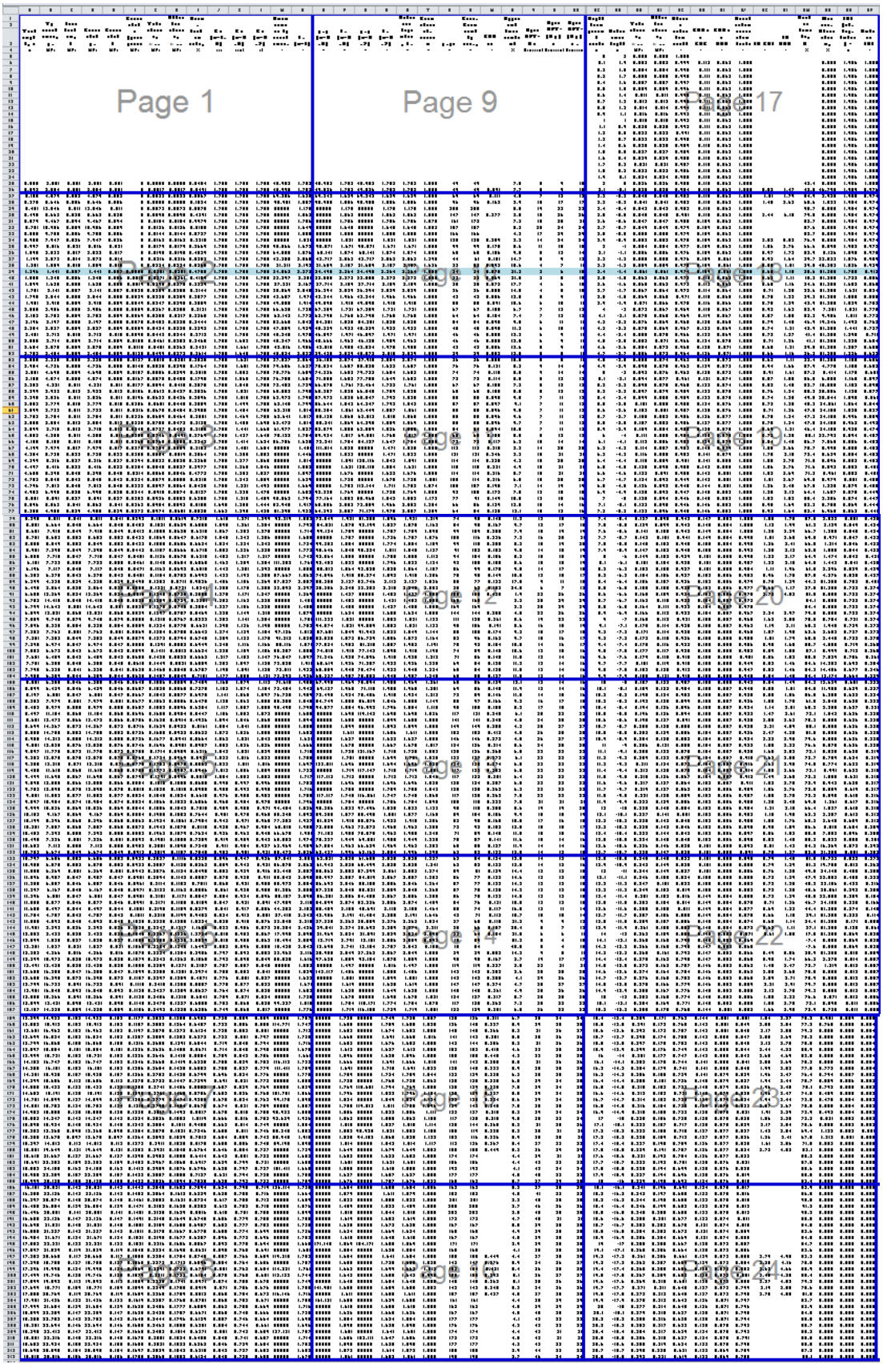

1

	A	B	C	D	E	F	G	H	I	J	K	L	M	N
1														
2														
3	Test length, z	Tip resistance, q_c	Local friction, f_s	Corrected q_c	Corrected f_s	Corrected u (pore pressure)	Total stress, σ_{vo}	Effective stress, σ'_{vo}	Norm. friction ratio, F	C_Q (n=1.0)	C_Q (n=0.5)	C_Q (n=0.7)	Dimensionless tip resistance, Q_1	I_c (n=1)
4	m	MPa	MPa	MPa	MPa	MPa	MPa	MPa	%	clay	sand	silt	-	-
5														
6														
7														
8														
9														
10														
11														
12														
13														
14														
15														
16														
17														
18														
19														
20														
21														
22														
23														
24														
25	0.000	2.881	0.001	2.881	0.001	0	0.0000	0.0000	0.0484	1.700	1.700	1.700	48.982	1.782
26	0.093	2.884	0.001	2.884	0.001	0	0.0017	0.0017	0.0491	1.700	1.700	1.700	48.998	1.782

2

27	0.185	4.079	0.002	4.079	0.002	0	0.0033	0.0033	0.0567	1.700	1.700	1.700	69.286	1.630
28	0.275	5.646	0.006	5.646	0.006	0	0.0050	0.0050	0.1034	1.700	1.700	1.700	95.901	1.507
29	0.401	12.046	0.011	12.046	0.011	0	0.0072	0.0072	0.0875	1.700	1.700	1.700	204.662	1.170
30	0.498	8.663	0.038	8.663	0.038	0	0.0090	0.0090	0.4391	1.700	1.700	1.700	147.123	1.562
31	0.579	9.467	0.094	9.467	0.094	0	0.0104	0.0104	0.9979	1.700	1.700	1.700	160.768	1.756
32	0.701	10.986	0.089	10.986	0.089	0	0.0126	0.0126	0.8150	1.700	1.700	1.700	186.543	1.649
33	0.800	9.755	0.056	9.755	0.056	0	0.0144	0.0144	0.5737	1.700	1.700	1.700	165.587	1.588
34	0.900	7.947	0.026	7.947	0.026	0	0.0162	0.0162	0.3318	1.700	1.700	1.700	134.820	1.531
35	0.997	5.816	0.021	5.816	0.021	0	0.0179	0.0179	0.3669	1.700	1.700	1.700	98.566	1.672
36	1.098	3.832	0.017	3.832	0.017	0	0.0198	0.0198	0.4539	1.700	1.700	1.700	64.805	1.876
37	1.199	2.572	0.014	2.572	0.014	0	0.0216	0.0216	0.5383	1.700	1.700	1.700	43.350	2.065
38	1.301	1.859	0.010	1.859	0.010	0	0.0234	0.0234	0.5368	1.700	1.700	1.700	31.211	2.192
39	1.396	1.441	0.007	1.441	0.007	0.0000	0.0251	0.0251	0.4708	1.700	1.700	1.700	24.062	2.272
40	1.500	1.345	0.006	1.345	0.006	0.0010	0.0271	0.0261	0.4189	1.700	1.700	1.700	22.397	2.281
41	1.599	1.630	0.005	1.630	0.005	0.0019	0.0290	0.0270	0.3339	1.700	1.700	1.700	27.221	2.167
42	1.701	2.141	0.007	2.141	0.007	0.0030	0.0309	0.0280	0.3144	1.700	1.700	1.700	35.869	2.045
43	1.798	2.544	0.008	2.544	0.008	0.0039	0.0328	0.0289	0.3077	1.700	1.700	1.700	42.687	1.971
44	1.901	2.918	0.009	2.918	0.009	0.0049	0.0347	0.0298	0.3059	1.700	1.700	1.700	49.008	1.914
45	2.005	3.956	0.008	3.956	0.008	0.0059	0.0367	0.0308	0.2131	1.700	1.700	1.700	66.635	1.735
46	2.102	3.753	0.009	3.753	0.009	0.0069	0.0385	0.0317	0.2360	1.700	1.700	1.700	63.143	1.772
47	2.196	3.197	0.008	3.197	0.008	0.0078	0.0403	0.0325	0.2444	1.700	1.700	1.700	53.665	1.843
48	2.304	2.837	0.009	2.837	0.009	0.0089	0.0424	0.0335	0.3292	1.700	1.700	1.700	47.509	1.939
49	2.401	2.712	0.010	2.712	0.010	0.0098	0.0442	0.0344	0.3712	1.700	1.700	1.700	45.345	1.978
50	2.500	2.714	0.009	2.714	0.009	0.0108	0.0461	0.0353	0.3465	1.700	1.683	1.700	45.347	1.966
51	2.604	2.578	0.009	2.578	0.009	0.0118	0.0481	0.0363	0.3431	1.700	1.661	1.700	43.016	1.986
52	2.702	2.404	0.009	2.404	0.009	0.0128	0.0499	0.0372	0.3614	1.700	1.640	1.700	40.024	2.023

3

53	2.800	2.230	0.008	2.230	0.008	0.0137	0.0518	0.0381	0.3825	1.700	1.621	1.700	37.037	2.064
54	2.904	4.736	0.008	4.736	0.008	0.0148	0.0538	0.0390	0.1764	1.700	1.601	1.700	79.606	1.637
55	3.001	4.690	0.009	4.690	0.009	0.0157	0.0556	0.0399	0.2018	1.700	1.583	1.700	78.776	1.659
56	3.100	4.574	0.008	4.574	0.008	0.0167	0.0575	0.0408	0.1795	1.700	1.565	1.700	76.780	1.654
57	3.202	4.321	0.011	4.321	0.011	0.0177	0.0594	0.0418	0.2570	1.700	1.548	1.700	72.453	1.729
58	3.299	3.932	0.012	3.932	0.012	0.0186	0.0613	0.0427	0.3036	1.700	1.531	1.700	65.803	1.795
59	3.398	3.826	0.011	3.826	0.011	0.0196	0.0632	0.0436	0.2896	1.700	1.515	1.700	63.973	1.798
60	3.502	3.779	0.010	3.779	0.010	0.0206	0.0651	0.0445	0.2809	1.700	1.499	1.700	63.140	1.799
61	3.599	3.732	0.011	3.732	0.011	0.0216	0.0670	0.0454	0.2985	1.700	1.484	1.700	62.310	1.814
62	3.703	3.754	0.011	3.754	0.011	0.0226	0.0689	0.0464	0.3081	1.700	1.469	1.700	62.641	1.817
63	3.800	3.804	0.012	3.804	0.012	0.0235	0.0708	0.0473	0.3125	1.700	1.455	1.690	63.472	1.814
64	3.899	3.718	0.012	3.718	0.012	0.0245	0.0727	0.0482	0.3180	1.700	1.441	1.668	61.977	1.827
65	4.002	4.200	0.011	4.200	0.011	0.0255	0.0746	0.0491	0.2769	1.700	1.427	1.645	70.123	1.754
66	4.100	5.180	0.011	5.180	0.011	0.0265	0.0765	0.0500	0.2242	1.700	1.414	1.624	86.756	1.635
67	4.199	7.979	0.017	7.979	0.017	0.0275	0.0784	0.0509	0.2153	1.700	1.401	1.604	134.316	1.451
68	4.304	8.735	0.022	8.735	0.022	0.0285	0.0804	0.0519	0.2564	1.700	1.388	1.583	147.127	1.446
69	4.399	8.316	0.027	8.316	0.027	0.0294	0.0822	0.0528	0.3265	1.700	1.377	1.565	139.978	1.514
70	4.497	8.416	0.033	8.416	0.033	0.0304	0.0840	0.0537	0.3977	1.700	1.365	1.546	141.642	1.553
71	4.600	8.398	0.040	8.398	0.040	0.0314	0.0860	0.0546	0.4773	1.700	1.353	1.527	141.307	1.597
72	4.702	8.048	0.042	8.048	0.042	0.0324	0.0879	0.0555	0.5318	1.700	1.342	1.509	135.319	1.639
73	4.796	7.512	0.040	7.512	0.040	0.0333	0.0897	0.0564	0.5430	1.700	1.331	1.493	126.174	1.669
74	4.903	6.995	0.035	6.995	0.035	0.0344	0.0918	0.0574	0.5137	1.700	1.320	1.475	117.356	1.682
75	5.001	5.891	0.037	5.891	0.037	0.0353	0.0936	0.0583	0.6305	1.700	1.310	1.459	98.562	1.794
76	5.096	5.062	0.041	5.062	0.041	0.0363	0.0954	0.0592	0.8188	1.690	1.300	1.444	83.940	1.917
77	5.200	4.985	0.039	4.985	0.039	0.0373	0.0974	0.0601	0.8025	1.663	1.290	1.428	81.295	1.923
78	5.300	5.271	0.038	5.271	0.038	0.0383	0.0993	0.0610	0.7269	1.638	1.280	1.413	84.728	1.883

4

79	5.395	5.811	0.041	5.811	0.041	0.0392	0.1011	0.0619	0.7218	1.615	1.271	1.399	92.219	1.852
80	5.501	6.664	0.045	6.664	0.045	0.0402	0.1031	0.0629	0.6805	1.590	1.261	1.384	104.324	1.793
81	5.601	7.918	0.049	7.918	0.049	0.0412	0.1050	0.0638	0.6215	1.567	1.252	1.370	122.443	1.714
82	5.701	8.683	0.053	8.683	0.053	0.0422	0.1069	0.0647	0.6175	1.545	1.243	1.356	132.494	1.685
83	5.800	8.049	0.053	8.049	0.053	0.0432	0.1088	0.0656	0.6624	1.524	1.234	1.343	120.977	1.734
84	5.901	7.395	0.049	7.395	0.049	0.0442	0.1107	0.0666	0.6715	1.502	1.226	1.330	109.442	1.773
85	6.000	7.710	0.047	7.710	0.047	0.0451	0.1126	0.0675	0.6210	1.482	1.217	1.317	112.599	1.743
86	6.101	7.732	0.050	7.732	0.050	0.0461	0.1145	0.0684	0.6568	1.462	1.209	1.304	111.353	1.761
87	6.196	7.117	0.048	7.117	0.048	0.0471	0.1163	0.0693	0.6815	1.443	1.201	1.293	101.058	1.805
88	6.303	6.278	0.043	6.278	0.043	0.0481	0.1184	0.0703	0.6992	1.423	1.193	1.280	87.667	1.862
89	6.399	4.235	0.039	4.235	0.039	0.0490	0.1202	0.0711	0.9526	1.406	1.186	1.269	57.837	2.087
90	6.498	2.564	0.025	2.564	0.025	0.0500	0.1221	0.0721	1.0241	1.388	1.178	1.258	33.892	2.297
91	6.600	13.269	0.034	13.269	0.034	0.0510	0.1240	0.0730	0.2585	1.370	1.171	1.247	180.103	1.369
92	6.702	14.415	0.048	14.415	0.048	0.0520	0.1259	0.0739	0.3381	1.353	1.163	1.235	193.289	1.401
93	6.799	14.642	0.051	14.642	0.051	0.0530	0.1278	0.0748	0.3504	1.337	1.156	1.225	194.014	1.408
94	6.899	12.531	0.068	12.531	0.068	0.0539	0.1297	0.0757	0.5469	1.320	1.149	1.215	163.743	1.579
95	7.009	9.745	0.079	9.745	0.079	0.0550	0.1318	0.0767	0.8232	1.303	1.141	1.204	125.252	1.781
96	7.096	8.328	0.054	8.328	0.054	0.0559	0.1334	0.0775	0.6631	1.290	1.136	1.195	105.679	1.782
97	7.202	7.762	0.051	7.762	0.051	0.0569	0.1354	0.0785	0.6642	1.274	1.129	1.184	97.136	1.812
98	7.301	7.383	0.049	7.383	0.049	0.0579	0.1373	0.0794	0.6740	1.259	1.122	1.175	91.213	1.838
99	7.395	6.974	0.047	6.974	0.047	0.0588	0.1391	0.0803	0.6949	1.245	1.116	1.166	85.116	1.871
100	7.502	6.672	0.043	6.672	0.043	0.0599	0.1411	0.0813	0.6634	1.230	1.109	1.156	80.357	1.880
101	7.601	6.459	0.042	6.459	0.042	0.0608	0.1430	0.0822	0.6663	1.217	1.103	1.147	76.847	1.897
102	7.701	6.255	0.040	6.255	0.040	0.0618	0.1449	0.0831	0.6589	1.203	1.097	1.138	73.528	1.911
103	7.798	6.238	0.041	6.238	0.041	0.0628	0.1468	0.0840	0.6757	1.190	1.091	1.130	72.511	1.922
104	7.900	6.289	0.044	6.289	0.044	0.0638	0.1487	0.0849	0.7151	1.177	1.085	1.121	72.293	1.936

5

105	8.001	6.300	0.046	6.300	0.046	0.0648	0.1506	0.0859	0.7459	1.165	1.079	1.113	71.618	1.950
106	8.099	6.439	0.046	6.439	0.046	0.0657	0.1525	0.0868	0.7378	1.153	1.074	1.104	72.454	1.943
107	8.197	6.881	0.047	6.881	0.047	0.0667	0.1543	0.0877	0.6970	1.141	1.068	1.097	76.735	1.909
108	8.303	7.979	0.051	7.979	0.051	0.0677	0.1563	0.0886	0.6470	1.128	1.062	1.088	88.255	1.840
109	8.403	8.979	0.055	8.979	0.055	0.0687	0.1583	0.0896	0.6204	1.117	1.057	1.080	98.490	1.790
110	8.497	11.104	0.060	11.104	0.060	0.0696	0.1600	0.0904	0.5447	1.106	1.052	1.073	121.025	1.685
111	8.601	13.473	0.066	13.473	0.066	0.0706	0.1620	0.0914	0.4926	1.094	1.046	1.065	145.669	1.594
112	8.699	14.267	0.073	14.267	0.073	0.0716	0.1639	0.0923	0.5161	1.084	1.041	1.058	152.839	1.588
113	8.800	14.758	0.082	14.758	0.082	0.0726	0.1658	0.0932	0.5623	1.073	1.036	1.050	156.560	1.602
114	8.900	14.212	0.080	14.212	0.080	0.0736	0.1677	0.0941	0.5664	1.062	1.031	1.043	149.208	1.621
115	9.001	13.030	0.076	13.030	0.076	0.0746	0.1696	0.0951	0.5907	1.052	1.026	1.036	135.298	1.666
116	9.097	11.770	0.072	11.770	0.072	0.0755	0.1714	0.0959	0.6216	1.042	1.021	1.029	120.896	1.718
117	9.202	12.075	0.070	12.075	0.070	0.0765	0.1734	0.0969	0.5921	1.032	1.016	1.022	122.828	1.700
118	9.300	12.215	0.071	12.215	0.071	0.0775	0.1753	0.0978	0.5863	1.022	1.011	1.016	123.100	1.697
119	9.400	11.610	0.068	11.610	0.068	0.0785	0.1772	0.0987	0.5946	1.013	1.006	1.009	115.804	1.722
120	9.499	11.690	0.067	11.690	0.067	0.0795	0.1791	0.0996	0.5815	1.004	1.002	1.003	115.532	1.717
121	9.598	12.005	0.066	12.005	0.066	0.0804	0.1810	0.1005	0.5605	0.995	0.997	0.996	117.604	1.702
122	9.703	12.095	0.070	12.095	0.070	0.0815	0.1830	0.1015	0.5900	0.985	0.993	0.990	117.347	1.716
123	9.801	11.852	0.077	11.852	0.077	0.0824	0.1848	0.1024	0.6610	0.976	0.988	0.983	113.927	1.755
124	9.897	10.954	0.074	10.954	0.074	0.0834	0.1866	0.1033	0.6866	0.968	0.984	0.978	104.246	1.796
125	9.999	10.036	0.069	10.036	0.069	0.0844	0.1886	0.1042	0.7015	0.959	0.980	0.971	94.484	1.836
126	10.103	9.167	0.069	9.167	0.069	0.0854	0.1905	0.1052	0.7644	0.951	0.975	0.965	85.348	1.893
127	10.199	8.396	0.065	8.396	0.065	0.0863	0.1924	0.1061	0.7904	0.943	0.971	0.960	77.353	1.937
128	10.301	7.557	0.060	7.557	0.060	0.0873	0.1943	0.1070	0.8110	0.935	0.967	0.954	68.810	1.985
129	10.403	7.392	0.055	7.392	0.055	0.0883	0.1963	0.1079	0.7624	0.926	0.963	0.948	66.670	1.981
130	10.498	7.326	0.051	7.326	0.051	0.0893	0.1981	0.1088	0.7209	0.919	0.959	0.943	65.503	1.974
131	10.603	7.112	0.050	7.112	0.050	0.0903	0.2001	0.1098	0.7240	0.911	0.954	0.937	62.969	1.989
132	10.702	6.674	0.049	6.674	0.049	0.0913	0.2019	0.1107	0.7540	0.903	0.951	0.931	58.473	2.026

6

133	10.797	6.656	0.053	6.656	0.053	0.0922	0.2037	0.1116	0.8230	0.896	0.947	0.926	57.841	2.051
134	10.900	6.570	0.053	6.570	0.053	0.0932	0.2057	0.1125	0.8363	0.889	0.943	0.921	56.570	2.063
135	11.000	6.269	0.051	6.269	0.051	0.0942	0.2076	0.1134	0.8495	0.882	0.939	0.916	53.440	2.087
136	11.096	5.987	0.047	5.987	0.047	0.0951	0.2094	0.1143	0.8057	0.875	0.935	0.911	50.543	2.095
137	11.200	6.087	0.046	6.087	0.046	0.0961	0.2114	0.1153	0.7811	0.868	0.931	0.905	50.972	2.084
138	11.297	6.167	0.048	6.167	0.048	0.0971	0.2132	0.1162	0.8006	0.861	0.928	0.900	51.256	2.088
139	11.396	6.081	0.047	6.081	0.047	0.0981	0.2151	0.1171	0.8047	0.854	0.924	0.896	50.107	2.098
140	11.500	5.877	0.046	5.877	0.046	0.0991	0.2171	0.1180	0.8189	0.847	0.921	0.891	47.959	2.118
141	11.600	5.497	0.044	5.497	0.044	0.1001	0.2190	0.1189	0.8379	0.841	0.917	0.886	44.382	2.152
142	11.704	4.707	0.042	4.707	0.042	0.1011	0.2210	0.1199	0.9452	0.834	0.913	0.881	37.415	2.242
143	11.800	4.092	0.040	4.092	0.040	0.1020	0.2228	0.1208	1.0234	0.828	0.910	0.876	32.040	2.318
144	11.901	3.292	0.036	3.292	0.036	0.1030	0.2247	0.1217	1.1680	0.822	0.906	0.872	25.204	2.436
145	12.003	2.433	0.030	2.433	0.030	0.1040	0.2267	0.1226	1.3734	0.815	0.903	0.867	17.990	2.598
146	12.099	1.525	0.027	1.525	0.027	0.1050	0.2285	0.1235	2.0539	0.810	0.900	0.863	10.494	2.889
147	12.201	1.527	0.021	1.527	0.021	0.1060	0.2304	0.1245	1.6493	0.803	0.896	0.858	10.420	2.842
148	12.303	4.366	0.016	4.366	0.016	0.1070	0.2324	0.1254	0.3956	0.797	0.893	0.853	32.963	2.116
149	12.399	10.972	0.020	10.972	0.020	0.1079	0.2342	0.1263	0.1860	0.792	0.890	0.849	85.030	1.616
150	12.491	13.420	0.028	13.420	0.028	0.1088	0.2359	0.1271	0.2107	0.787	0.887	0.845	103.707	1.553
151	12.600	16.200	0.047	16.200	0.047	0.1099	0.2380	0.1281	0.2974	0.780	0.883	0.841	124.580	1.539
152	12.688	16.290	0.073	16.290	0.073	0.1107	0.2397	0.1289	0.4571	0.776	0.881	0.837	124.479	1.632
153	12.799	16.732	0.091	16.732	0.091	0.1118	0.2418	0.1300	0.5507	0.770	0.877	0.832	126.892	1.671
154	12.901	16.548	0.092	16.548	0.092	0.1128	0.2437	0.1309	0.5637	0.764	0.874	0.828	124.558	1.683
155	13.000	15.366	0.091	15.366	0.091	0.1138	0.2456	0.1318	0.6041	0.759	0.871	0.824	114.720	1.730
156	13.099	13.431	0.090	13.431	0.090	0.1148	0.2475	0.1327	0.6805	0.753	0.868	0.820	99.337	1.810
157	13.187	14.225	0.089	14.225	0.089	0.1156	0.2492	0.1335	0.6386	0.749	0.865	0.817	104.669	1.776
158	13.298	14.481	0.106	14.481	0.106	0.1167	0.2513	0.1345	0.7484	0.743	0.862	0.812	105.766	1.813

7

159	13.399	14.923	0.102	14.923	0.102	0.1177	0.2532	0.1355	0.6982	0.738	0.859	0.809	108.288	1.787
160	13.503	15.913	0.102	15.913	0.102	0.1187	0.2552	0.1364	0.6487	0.733	0.856	0.805	114.771	1.747
161	13.601	16.962	0.102	16.962	0.102	0.1197	0.2570	0.1373	0.6134	0.728	0.853	0.801	121.647	1.713
162	13.699	16.524	0.102	16.524	0.102	0.1207	0.2589	0.1382	0.6272	0.723	0.851	0.797	117.664	1.730
163	13.799	16.868	0.100	16.868	0.100	0.1216	0.2608	0.1391	0.6044	0.719	0.848	0.794	119.352	1.716
164	13.897	18.054	0.101	18.054	0.101	0.1226	0.2626	0.1400	0.5671	0.714	0.845	0.790	127.039	1.678
165	13.999	18.731	0.103	18.731	0.103	0.1236	0.2646	0.1410	0.5554	0.709	0.842	0.786	130.984	1.661
166	14.102	16.747	0.103	16.747	0.103	0.1246	0.2665	0.1419	0.6225	0.705	0.839	0.783	116.112	1.733
167	14.200	16.181	0.103	16.181	0.103	0.1256	0.2684	0.1428	0.6503	0.700	0.837	0.779	111.411	1.759
168	14.301	15.938	0.107	15.938	0.107	0.1266	0.2703	0.1438	0.6799	0.696	0.834	0.776	108.989	1.778
169	14.399	15.656	0.112	15.656	0.112	0.1275	0.2722	0.1447	0.7299	0.691	0.831	0.772	106.344	1.805
170	14.500	15.433	0.123	15.433	0.123	0.1285	0.2741	0.1456	0.8083	0.687	0.829	0.769	104.123	1.839
171	14.603	15.191	0.130	15.191	0.130	0.1295	0.2761	0.1465	0.8706	0.682	0.826	0.765	101.781	1.866
172	14.701	14.899	0.137	14.899	0.137	0.1305	0.2779	0.1474	0.9355	0.678	0.824	0.762	99.170	1.895
173	14.801	15.752	0.134	15.752	0.134	0.1315	0.2798	0.1484	0.8678	0.674	0.821	0.759	104.289	1.857
174	14.902	15.050	0.130	15.050	0.130	0.1325	0.2817	0.1493	0.8817	0.670	0.818	0.755	98.922	1.880
175	15.002	14.347	0.142	14.347	0.142	0.1334	0.2836	0.1502	1.0119	0.666	0.816	0.752	93.629	1.936
176	15.095	15.934	0.148	15.934	0.148	0.1343	0.2854	0.1511	0.9480	0.662	0.814	0.749	103.593	1.884
177	15.203	13.265	0.095	13.265	0.095	0.1354	0.2875	0.1521	0.7346	0.658	0.811	0.746	85.348	1.883
178	15.300	12.670	0.097	12.670	0.097	0.1364	0.2893	0.1529	0.7812	0.654	0.809	0.743	80.948	1.918
179	15.397	14.012	0.112	14.012	0.112	0.1373	0.2911	0.1538	0.8178	0.650	0.806	0.740	89.195	1.895
180	15.501	19.649	0.131	19.649	0.131	0.1383	0.2931	0.1548	0.6764	0.646	0.804	0.737	125.047	1.729
181	15.615	21.667	0.137	21.667	0.137	0.1395	0.2953	0.1558	0.6414	0.642	0.801	0.733	137.136	1.683
182	15.691	23.283	0.159	23.283	0.159	0.1402	0.2967	0.1565	0.6917	0.639	0.799	0.731	146.839	1.680
183	15.803	24.155	0.162	24.155	0.162	0.1413	0.2989	0.1576	0.6796	0.635	0.797	0.727	151.411	1.665
184	15.900	22.259	0.157	22.259	0.157	0.1422	0.3007	0.1585	0.7127	0.631	0.794	0.725	138.578	1.708
185	15.999	20.138	0.150	20.138	0.150	0.1432	0.3026	0.1594	0.7538	0.628	0.792	0.722	124.470	1.759

8

186	16.101	20.521	0.143	20.521	0.143	0.1442	0.3045	0.1603	0.7094	0.624	0.790	0.719	126.114	1.738
187	16.200	23.126	0.142	23.126	0.142	0.1452	0.3064	0.1612	0.6239	0.620	0.788	0.716	141.546	1.664
188	16.297	25.574	0.145	25.574	0.145	0.1461	0.3082	0.1621	0.5724	0.617	0.785	0.713	155.860	1.609
189	16.400	26.554	0.139	26.554	0.139	0.1471	0.3102	0.1630	0.5282	0.613	0.783	0.710	160.956	1.576
190	16.496	25.851	0.141	25.851	0.141	0.1481	0.3120	0.1639	0.5516	0.610	0.781	0.708	155.790	1.599
191	16.600	22.126	0.147	22.126	0.147	0.1491	0.3140	0.1649	0.6745	0.606	0.779	0.705	132.282	1.708
192	16.698	21.521	0.148	21.521	0.148	0.1501	0.3159	0.1658	0.6957	0.603	0.777	0.702	127.906	1.728
193	16.800	21.337	0.142	21.337	0.142	0.1511	0.3178	0.1667	0.6775	0.600	0.774	0.699	126.071	1.726
194	16.904	21.671	0.134	21.671	0.134	0.1521	0.3198	0.1677	0.6287	0.596	0.772	0.696	127.332	1.703
195	17.002	22.221	0.122	22.221	0.122	0.1531	0.3216	0.1686	0.5567	0.593	0.770	0.694	129.906	1.665
196	17.097	21.529	0.119	21.529	0.119	0.1540	0.3234	0.1695	0.5631	0.590	0.768	0.691	125.138	1.681
197	17.202	20.660	0.117	20.660	0.117	0.1550	0.3254	0.1704	0.5748	0.587	0.766	0.689	119.318	1.703
198	17.298	18.705	0.127	18.705	0.127	0.1560	0.3273	0.1713	0.6896	0.584	0.764	0.686	107.285	1.787
199	17.396	19.998	0.134	19.998	0.134	0.1569	0.3291	0.1722	0.6791	0.581	0.762	0.684	114.221	1.761
200	17.499	19.746	0.120	19.746	0.120	0.1579	0.3311	0.1732	0.6184	0.578	0.760	0.681	112.123	1.744
201	17.599	19.092	0.112	19.092	0.112	0.1589	0.3330	0.1741	0.5971	0.574	0.758	0.678	107.771	1.749
202	17.699	18.771	0.109	18.771	0.109	0.1599	0.3349	0.1750	0.5919	0.571	0.756	0.676	105.357	1.755
203	17.800	20.769	0.119	20.769	0.119	0.1609	0.3368	0.1759	0.5813	0.568	0.754	0.673	116.146	1.716
204	17.901	21.426	0.122	21.426	0.122	0.1619	0.3387	0.1768	0.5781	0.565	0.752	0.671	119.243	1.705
205	17.999	21.604	0.129	21.604	0.129	0.1628	0.3406	0.1777	0.6059	0.563	0.750	0.669	119.630	1.716
206	18.099	22.359	0.147	22.359	0.147	0.1638	0.3425	0.1787	0.6671	0.560	0.748	0.666	123.232	1.730
207	18.200	23.702	0.143	23.702	0.143	0.1648	0.3444	0.1796	0.6139	0.557	0.746	0.664	130.059	1.690
208	18.301	23.694	0.146	23.694	0.146	0.1658	0.3463	0.1805	0.6251	0.554	0.744	0.661	129.333	1.696
209	18.398	23.412	0.147	23.412	0.147	0.1668	0.3482	0.1814	0.6371	0.551	0.742	0.659	127.131	1.707
210	18.501	23.316	0.148	23.316	0.148	0.1678	0.3501	0.1824	0.6450	0.548	0.741	0.657	125.939	1.714
211	18.603	23.924	0.150	23.924	0.150	0.1688	0.3521	0.1833	0.6363	0.546	0.739	0.654	128.604	1.703
212	18.698	25.090	0.154	25.090	0.154	0.1697	0.3539	0.1842	0.6218	0.543	0.737	0.652	134.315	1.682
213	18.810	25.816	0.156	25.816	0.156	0.1708	0.3560	0.1852	0.6134	0.540	0.735	0.650	137.477	1.670

9

	O	P	Q	R	S	T	U	V	W	X	Y	Z	AA
1													
2													
3	q_{c1} (n=0.5)	I_c (n=0.5)	q_{c1} (n=0.7)	I_c (n=0.7)	Behaviour type index, I_c actual	Grain charact. corrxn fact., K_c	q_{c1N}	Corr. Clean sand tip res., $(q_{c1N})_{cs}$	$CRR_{7.5}$	Apparent fines content	Equiv SPT-N_{60}	Equiv SPT-$(N_1)_{60}$	Equiv SPT-$(N_1)_{60cs}$
4	-	-	-	-	-	-	-	-	-	%	Blowcount	Blowcount	Blowcount
5													
6													
7													
8													
9													
10													
11													
12													
13													
14													
15													
16													
17													
18													
19													
20													
21													
22													
23													
24													
25	48.982	1.782	48.982	1.782	1.782	1.000	49	49		7.8	5	9	10
26	49.026	1.782	49.026	1.782	1.782	1.000	49	49	0.091	7.7	5	9	10

10

27	69.343	1.629	69.343	1.629	1.629	1.000	69	69	0.111	4.8	7	13	13
28	95.985	1.506	95.985	1.506	1.506	1.000	96	96	0.162	2.9	10	17	17
29	204.784	1.170	204.784	1.170	1.170	1.000	205	205		0.0	19	32	32
30	147.275	1.562	147.275	1.562	1.562	1.000	147	147	0.377	3.8	15	26	26
31	160.945	1.756	160.945	1.756	1.756	1.075	161	173		7.2	18	30	31
32	186.757	1.648	186.757	1.648	1.648	1.002	187	187		5.2	20	34	34
33	165.832	1.588	165.832	1.588	1.588	1.000	166	166		4.2	17	29	29
34	135.096	1.531	135.096	1.531	1.531	1.000	135	135	0.309	3.3	14	24	24
35	98.871	1.671	98.871	1.671	1.671	1.000	99	99	0.170	5.6	11	18	18
36	65.141	1.874	65.141	1.874	1.874	1.000	65	65	0.106	9.8	8	13	14
37	43.717	2.062	43.717	2.062	2.062	1.390	44	61	0.101	14.7	5	9	12
38	31.609	2.187	31.609	2.187	2.187	1.636	32	52	0.093	18.6	4	7	11
39	24.490	2.264	24.490	2.264	2.264	1.000	24	24	0.070	21.2	3	6	10
40	22.858	2.273	22.858	2.273	2.273	1.000	23	23	0.069	21.5	3	5	10
41	27.714	2.159	27.714	2.159	2.159	1.000	28	28	0.073	17.7	4	6	10
42	36.394	2.039	36.394	2.039	2.039	1.000	36	36	0.080	14.0	4	8	10
43	43.244	1.966	43.244	1.966	1.966	1.000	43	43	0.086	12.0	5	9	11
44	49.598	1.910	49.598	1.910	1.910	1.000	50	50	0.091	10.6	6	10	11
45	67.259	1.731	67.259	1.731	1.731	1.000	67	67	0.108	6.7	7	13	13
46	63.798	1.768	63.798	1.768	1.768	1.000	64	64	0.104	7.4	7	12	12
47	54.351	1.838	54.351	1.838	1.838	1.000	54	54	0.095	9.0	6	11	11
48	48.229	1.933	48.229	1.933	1.933	1.000	48	48	0.090	11.2	6	10	11
49	46.097	1.971	46.097	1.971	1.971	1.000	46	46	0.088	12.2	6	9	11
50	45.666	1.963	46.130	1.959	1.963	1.000	46	46	0.088	12.0	6	9	11
51	42.818	1.988	43.834	1.978	1.988	1.000	43	43	0.086	12.6	5	9	11
52	39.438	2.029	40.873	2.015	2.029	1.000	39	39	0.083	13.8	5	8	11

11

53	36.150	2.074	37.918	2.054	2.074	1.000	36	36	0.080	15.0	5	8	11
54	75.824	1.657	80.520	1.632	1.657	1.000	76	76	0.121	5.3	9	14	14
55	74.226	1.683	79.722	1.654	1.683	1.000	74	74	0.118	5.8	9	14	14
56	71.585	1.683	77.758	1.649	1.683	1.000	72	72	0.114	5.8	8	13	13
57	66.875	1.761	73.464	1.723	1.761	1.000	67	67	0.108	7.3	8	13	13
58	60.207	1.830	66.845	1.789	1.830	1.000	60	60	0.100	8.8	8	12	12
59	57.973	1.838	65.047	1.792	1.838	1.000	58	58	0.098	9.0	7	11	12
60	56.644	1.842	64.247	1.792	1.842	1.000	57	57	0.097	9.1	7	11	12
61	55.384	1.861	63.449	1.807	1.861	1.000	55	55	0.096	9.5	7	11	12
62	55.130	1.868	63.813	1.810	1.868	1.000	55	55	0.096	9.6	7	11	12
63	55.341	1.869	64.290	1.809	1.869	1.000	55	55	0.096	9.7	7	11	12
64	53.579	1.885	62.009	1.826	1.885	1.000	54	54	0.094	10.0	7	11	12
65	59.924	1.817	69.081	1.760	1.817	1.000	60	60	0.100	8.5	8	12	12
66	73.241	1.704	84.127	1.647	1.704	1.000	73	73	0.117	6.2	10	14	14
67	111.814	1.525	127.969	1.471	1.525	1.000	112	112	0.210	3.2	14	20	20
68	121.263	1.522	138.266	1.471	1.522	1.000	121	121	0.246	3.2	15	21	21
69	114.495	1.591	130.116	1.542	1.591	1.000	114	114	0.220	4.2	15	20	20
70	114.887	1.631	130.118	1.584	1.631	1.000	115	115	0.221	4.9	15	21	21
71	113.643	1.676	128.257	1.632	1.676	1.000	114	114	0.216	5.7	15	21	21
72	107.986	1.720	121.462	1.678	1.720	1.051	108	114	0.216	6.5	15	20	20
73	100.012	1.753	112.144	1.711	1.753	1.074	100	107	0.195	7.1	14	19	19
74	92.330	1.769	103.173	1.728	1.769	1.085	92	100	0.173	7.5	13	18	18
75	77.164	1.883	85.960	1.843	1.883	1.173	77	91	0.149	10.0	12	15	16
76	65.806	2.003	73.089	1.966	2.003	1.304	66	86	0.139	13.0	10	14	16
77	64.293	2.007	71.179	1.970	2.007	1.309	64	84	0.135	13.1	10	13	16
78	67.467	1.965	74.468	1.930	1.965	1.257	67	85	0.137	12.0	11	14	16

12

79	73.849	1.931	81.280	1.896	1.931	1.219	74	90	0.148	11.2	12	15	17
80	84.031	1.870	92.199	1.837	1.870	1.162	84	98	0.167	9.7	13	17	18
81	99.124	1.789	108.442	1.757	1.789	1.098	99	109	0.200	7.9	15	19	19
82	107.926	1.757	117.735	1.726	1.757	1.076	108	116	0.226	7.2	16	20	21
83	99.352	1.804	108.082	1.774	1.804	1.109	99	110	0.205	8.2	15	19	20
84	90.646	1.840	98.334	1.811	1.840	1.137	91	103	0.182	9.0	14	18	19
85	93.864	1.808	101.547	1.780	1.808	1.113	94	104	0.186	8.3	15	18	19
86	93.483	1.823	100.859	1.796	1.823	1.124	93	105	0.188	8.6	15	18	19
87	85.512	1.864	92.025	1.838	1.864	1.157	86	99	0.170	9.5	14	17	18
88	74.896	1.918	80.374	1.893	1.918	1.206	75	90	0.149	10.8	13	15	17
89	50.208	2.137	53.746	2.113	2.137	1.526	50	77	0.122	17.0	9	11	15
90	30.206	2.340	32.253	2.315	2.340	2.082	30	63	0.103	24.0	6	7	12
91	155.316	1.427	165.413	1.402	1.427	1.000	155	155	0.428	1.9	22	26	26
92	167.658	1.453	178.099	1.431	1.453	1.000	168	168		2.2	25	29	29
93	169.288	1.458	179.403	1.437	1.458	1.000	169	169		2.3	25	29	29
94	143.990	1.624	152.220	1.605	1.624	1.000	144	144	0.358	4.8	23	26	26
95	111.233	1.821	117.279	1.803	1.821	1.122	111	125	0.261	8.6	19	22	22
96	94.574	1.821	99.509	1.803	1.821	1.123	95	106	0.191	8.6	16	18	19
97	87.601	1.849	91.942	1.832	1.849	1.144	88	100	0.174	9.2	15	17	18
98	82.835	1.873	86.739	1.856	1.873	1.164	83	96	0.163	9.7	15	16	17
99	77.824	1.903	81.315	1.887	1.903	1.191	78	93	0.154	10.5	14	16	17
100	74.010	1.910	77.143	1.895	1.910	1.198	74	89	0.145	10.6	13	15	16
101	71.246	1.925	74.096	1.910	1.925	1.213	71	86	0.140	11.0	13	14	16
102	68.619	1.936	71.207	1.922	1.936	1.225	69	84	0.135	11.3	13	14	16
103	68.059	1.945	70.474	1.932	1.945	1.234	68	84	0.135	11.5	13	14	16
104	68.237	1.957	70.503	1.945	1.957	1.248	68	85	0.137	11.8	13	14	16

13

105	67.990	1.969	70.094	1.958	1.969	1.261	68	86	0.139	12.1	13	14	16
106	69.127	1.960	71.118	1.950	1.960	1.251	69	86	0.140	11.9	13	14	16
107	73.495	1.924	75.456	1.915	1.924	1.212	73	89	0.146	11.0	14	15	16
108	84.749	1.855	86.819	1.846	1.855	1.149	85	97	0.166	9.3	16	17	18
109	94.877	1.804	96.993	1.796	1.804	1.110	95	105	0.188	8.2	17	18	19
110	116.767	1.698	119.142	1.690	1.698	1.036	117	121	0.245	6.1	20	22	22
111	140.942	1.605	143.507	1.599	1.605	1.000	141	141	0.340	4.5	24	25	25
112	148.524	1.599	150.931	1.593	1.599	1.000	149	149	0.385	4.3	25	27	27
113	152.867	1.611	155.032	1.606	1.611	1.000	153	153	0.412	4.5	26	28	28
114	146.489	1.627	148.273	1.623	1.627	1.000	146	146	0.372	4.8	26	27	27
115	133.650	1.670	135.013	1.667	1.670	1.017	134	136	0.314	5.6	24	25	25
116	120.166	1.720	121.167	1.718	1.720	1.052	120	126	0.268	6.5	22	22	23
117	122.671	1.701	123.446	1.699	1.701	1.038	123	127	0.272	6.1	22	23	23
118	123.511	1.696	124.062	1.694	1.696	1.035	124	128	0.274	6.0	23	23	23
119	116.846	1.719	117.147	1.718	1.719	1.051	117	123	0.252	6.5	22	22	22
120	117.113	1.713	117.200	1.712	1.713	1.046	117	123	0.251	6.4	22	22	22
121	119.725	1.696	119.597	1.696	1.696	1.035	120	124	0.257	6.0	22	22	22
122	120.045	1.708	119.686	1.709	1.708	1.043	120	125	0.263	6.3	22	22	23
123	117.117	1.745	116.561	1.747	1.745	1.068	117	125	0.262	7.0	22	22	22
124	107.782	1.784	107.087	1.786	1.784	1.095	108	118	0.233	7.8	21	21	21
125	98.306	1.822	97.496	1.825	1.822	1.123	98	110	0.205	8.6	19	19	20
126	89.388	1.877	88.490	1.881	1.877	1.168	89	104	0.186	9.9	18	18	19
127	81.529	1.918	80.576	1.922	1.918	1.206	82	98	0.168	10.8	17	16	18
128	73.055	1.963	72.073	1.968	1.963	1.255	73	92	0.152	12.0	15	15	17
129	71.153	1.958	70.075	1.963	1.958	1.248	71	89	0.145	11.8	15	15	16
130	70.227	1.949	69.051	1.955	1.949	1.238	70	87	0.141	11.6	15	14	16
131	67.884	1.962	66.629	1.969	1.962	1.253	68	85	0.137	11.9	14	14	16
132	63.437	1.996	62.162	2.004	1.996	1.295	63	82	0.132	12.8	14	13	15

14

133	63.021	2.020	61.658	2.028	2.020	1.327	63	84	0.134	13.5	14	13	16
134	61.942	2.030	60.499	2.038	2.030	1.341	62	83	0.133	13.8	14	13	16
135	58.863	2.052	57.399	2.061	2.052	1.374	59	81	0.129	14.4	13	12	15
136	55.997	2.057	54.519	2.067	2.057	1.383	56	77	0.123	14.6	13	12	15
137	56.693	2.046	55.105	2.056	2.046	1.364	57	77	0.123	14.2	13	12	15
138	57.220	2.048	55.531	2.059	2.048	1.368	57	78	0.125	14.3	13	12	15
139	56.201	2.056	54.458	2.067	2.056	1.380	56	78	0.123	14.5	13	12	15
140	54.099	2.074	52.336	2.086	2.074	1.409	54	76	0.121	15.0	12	12	15
141	50.409	2.105	48.691	2.118	2.105	1.464	50	74	0.117	16.0	12	11	14
142	42.986	2.191	41.454	2.205	2.191	1.646	43	71	0.113	18.7	10	10	14
143	37.238	2.263	35.859	2.276	2.263	1.834	37	68	0.110	21.2	9	9	13
144	29.841	2.374	28.692	2.389	2.374	2.211	30	66	0.107	25.4	8	7	12
145	21.969	2.524	21.091	2.539	2.524	2.895	22	64	0.104	31.8	6	6	11
146	13.719	2.791	13.151	2.806	2.889	5.592	10	59		51.3	5	4	10
147	13.690	2.741	13.104	2.757	2.842	5.155	10	54		48.5	5	4	10
148	38.988	2.049	37.263	2.067	2.049	1.000	39	39	0.082	14.3	9	8	11
149	97.635	1.559	93.184	1.578	1.559	1.000	98	98	0.167	3.7	19	17	17
150	119.022	1.497	113.444	1.516	1.497	1.000	119	119	0.237	2.8	23	21	21
151	143.117	1.486	136.196	1.505	1.486	1.000	143	143	0.353	2.6	28	25	25
152	143.457	1.581	136.347	1.599	1.581	1.000	143	143	0.355	4.1	29	26	26
153	146.774	1.619	139.281	1.638	1.619	1.000	147	147	0.374	4.7	30	27	27
154	144.637	1.630	137.055	1.649	1.630	1.000	145	145	0.361	4.9	30	26	26
155	133.844	1.675	126.653	1.695	1.675	1.021	134	137	0.317	5.7	28	25	25
156	116.587	1.754	110.171	1.774	1.754	1.075	117	125	0.263	7.2	25	22	22
157	123.105	1.719	116.188	1.739	1.719	1.051	123	129	0.281	6.5	26	23	23
158	124.847	1.756	117.654	1.776	1.756	1.076	125	134	0.305	7.2	27	24	24

15

159	128.215	1.728	120.661	1.749	1.728	1.057	128	136	0.311	6.7	28	24	24
160	136.241	1.688	128.034	1.709	1.688	1.030	136	140	0.337	5.9	29	25	25
161	144.746	1.652	135.849	1.674	1.652	1.005	145	145	0.366	5.3	31	26	27
162	140.542	1.668	131.730	1.691	1.668	1.016	141	143	0.351	5.5	30	26	26
163	142.998	1.653	133.856	1.676	1.653	1.005	143	144	0.356	5.3	31	26	26
164	152.558	1.613	142.620	1.637	1.613	1.000	153	153	0.410	4.6	32	28	28
165	157.753	1.596	147.280	1.620	1.596	1.000	158	158	0.445	4.3	33	28	28
166	140.568	1.666	131.060	1.691	1.666	1.015	141	143	0.350	5.5	31	26	26
167	135.394	1.691	126.077	1.715	1.691	1.032	135	140	0.333	5.9	30	25	25
168	132.931	1.709	123.624	1.734	1.709	1.044	133	139	0.328	6.3	30	25	25
169	130.170	1.735	120.903	1.760	1.735	1.062	130	138	0.325	6.8	29	24	25
170	127.907	1.769	118.651	1.794	1.769	1.085	128	139	0.328	7.5	29	24	25
171	125.489	1.796	116.256	1.822	1.796	1.104	125	139	0.327	8.0	29	24	25
172	122.704	1.824	113.537	1.849	1.824	1.124	123	138	0.324	8.6	29	24	25
173	129.323	1.785	119.513	1.811	1.785	1.096	129	142	0.345	7.8	30	25	25
174	123.172	1.806	113.686	1.833	1.806	1.111	123	137	0.318	8.2	29	24	24
175	117.062	1.862	107.915	1.888	1.862	1.155	117	135	0.310	9.5	28	23	24
176	129.644	1.810	119.378	1.837	1.810	1.114	130	144	0.360	8.3	31	25	26
177	107.573	1.802	98.925	1.831	1.802	1.108	108	119	0.238	8.2	25	21	21
178	102.449	1.835	94.102	1.865	1.835	1.133	102	116	0.226	8.9	25	20	21
179	112.975	1.814	103.651	1.843	1.814	1.117	113	126	0.267	8.4	27	22	23
180	157.933	1.649	144.718	1.679	1.649	1.003	158	158	0.449	5.2	36	29	29
181	173.561	1.603	158.824	1.633	1.603	1.000	174	174		4.4	39	31	31
182	186.090	1.601	170.137	1.631	1.601	1.000	186	186		4.4	42	33	33
183	192.436	1.585	175.710	1.615	1.585	1.000	192	192		4.1	43	34	34
184	176.830	1.627	161.278	1.657	1.627	1.000	177	177		4.8	40	32	32
185	159.525	1.676	145.329	1.707	1.676	1.022	160	163		5.7	37	29	30

16

186	162.081	1.654	147.483	1.685	1.654	1.006	162	163		5.3	37	30	30
187	182.135	1.579	165.543	1.611	1.579	1.000	182	182		4.0	41	32	32
188	200.861	1.523	182.363	1.555	1.523	1.000	201	201		3.2	45	35	35
189	207.954	1.489	188.584	1.522	1.489	1.000	208	208		2.7	46	36	36
190	201.905	1.510	182.900	1.544	1.510	1.000	202	202		3.0	45	35	35
191	172.307	1.619	155.907	1.653	1.619	1.000	172	172		4.7	40	31	31
192	167.143	1.638	151.070	1.672	1.638	1.000	167	167		5.0	39	30	30
193	165.246	1.634	149.187	1.669	1.634	1.000	165	165		4.9	39	30	30
194	167.356	1.610	150.918	1.645	1.610	1.000	167	167		4.5	39	30	30
195	171.145	1.569	154.171	1.605	1.569	1.000	171	171		3.9	39	30	30
196	165.382	1.584	148.826	1.620	1.584	1.000	165	165		4.1	38	30	30
197	158.257	1.604	142.252	1.641	1.604	1.000	158	158	0.449	4.4	37	28	28
198	142.917	1.688	128.331	1.725	1.688	1.030	143	147	0.376	5.9	34	26	27
199	152.395	1.662	136.699	1.699	1.662	1.012	152	154	0.421	5.4	36	28	28
200	150.057	1.642	134.453	1.680	1.642	0.998	150	150	0.392	5.1	36	27	27
201	144.710	1.645	129.526	1.684	1.645	1.000	145	145	0.362	5.1	35	26	26
202	141.901	1.650	126.877	1.689	1.650	1.003	142	142	0.348	5.2	34	26	26
203	156.588	1.611	139.861	1.650	1.611	1.000	157	157	0.437	4.5	37	28	28
204	161.121	1.600	143.758	1.639	1.600	1.000	161	161		4.4	38	29	29
205	162.046	1.610	144.437	1.650	1.610	1.000	162	162		4.5	39	29	29
206	167.280	1.626	148.949	1.665	1.626	1.000	167	167		4.8	40	30	30
207	176.863	1.584	157.319	1.624	1.584	1.000	177	177		4.1	42	32	32
208	176.347	1.590	156.698	1.630	1.590	1.000	176	176		4.2	42	32	32
209	173.819	1.601	154.299	1.641	1.601	1.000	174	174		4.4	42	31	31
210	172.660	1.606	153.111	1.647	1.606	1.000	173	173		4.5	42	31	31
211	176.713	1.595	156.544	1.635	1.595	1.000	177	177		4.3	43	32	32
212	184.884	1.573	163.628	1.614	1.573	1.000	185	185		3.9	44	33	33
213	189.705	1.561	167.707	1.602	1.561	1.000	190	190		3.7	46	34	34

17

	AC	AD	AE	AF	AG	AH	AI	AJ	AK	AL	AM	AN	AO	AP
1														
2	Depth from ground surface	Reference depth	Total stress, σ_{vo}	Effective stress, σ'_{vo}	Stress reduction coeff., r_d	$CSR_{7.5}$ CHC	$CSR_{7.5}$ DAR	Overburden correction factor, K_σ	FS CHC	FS DAR	Relative density, D_r	Max cyc. Shear strain, γ_{max}	LDI (lat. disp. Index) - CHC	Unitless LDI
3														
4	m	m	MPa	MPa	-	-	-	-	-	-	%	%	m	-
5	0	2	0.000	0.000	1.000									
6	0.1	1.9	0.002	0.002	0.999	0.112	0.063	1.000				0.000	1.956	1.000
7	0.2	1.8	0.004	0.004	0.998	0.111	0.063	1.000				0.000	1.956	1.000
8	0.3	1.7	0.005	0.005	0.998	0.111	0.063	1.000				0.000	1.956	1.000
9	0.4	1.6	0.007	0.007	0.997	0.111	0.063	1.000				0.000	1.956	1.000
10	0.5	1.5	0.009	0.009	0.996	0.111	0.063	1.000				0.000	1.956	1.000
11	0.6	1.4	0.011	0.011	0.995	0.111	0.063	1.000				0.000	1.956	1.000
12	0.7	1.3	0.013	0.013	0.995	0.111	0.063	1.000				0.000	1.956	1.000
13	0.8	1.2	0.014	0.014	0.994	0.111	0.063	1.000				0.000	1.956	1.000
14	0.9	1.1	0.016	0.016	0.993	0.111	0.063	1.000				0.000	1.956	1.000
15	1	1	0.018	0.018	0.992	0.111	0.063	1.000				0.000	1.956	1.000
16	1.1	0.9	0.020	0.020	0.992	0.111	0.062	1.000				0.000	1.956	1.000
17	1.2	0.8	0.022	0.022	0.991	0.111	0.062	1.000				0.000	1.956	1.000
18	1.3	0.7	0.023	0.023	0.990	0.111	0.062	1.000				0.000	1.956	1.000
19	1.4	0.6	0.025	0.025	0.989	0.110	0.062	1.000				0.000	1.956	1.000
20	1.5	0.5	0.027	0.027	0.989	0.110	0.062	1.000				0.000	1.956	1.000
21	1.6	0.4	0.029	0.029	0.988	0.110	0.062	1.000				0.000	1.956	1.000
22	1.7	0.3	0.031	0.031	0.987	0.110	0.062	1.000				0.000	1.956	1.000
23	1.8	0.2	0.032	0.032	0.986	0.110	0.062	1.000				0.000	1.956	1.000
24	1.9	0.1	0.034	0.034	0.985	0.110	0.062	1.000				0.000	1.956	1.000
25	2	0	0.036	0.036	0.985	0.110	0.062	1.000			43.4	0.000	1.956	1.000
26	2.1	-0.1	0.038	0.038	0.984	0.110	0.062	1.000	0.83	1.47	43.5	46.790	1.909	0.976

18

27	2.2	-0.2	0.040	0.040	0.983	0.110	0.062	1.000	1.01	1.79	54.9	3.930	1.905	0.974
28	2.3	-0.3	0.041	0.041	0.982	0.110	0.062	1.000	1.48	2.62	65.6	1.032	1.904	0.974
29	2.4	-0.4	0.043	0.043	0.982	0.110	0.062	1.000			90.7	0.000	1.904	0.974
30	2.5	-0.5	0.045	0.045	0.981	0.110	0.062	1.000	3.44	6.10	79.8	0.000	1.904	0.974
31	2.6	-0.6	0.047	0.047	0.980	0.109	0.062	1.000			82.7	0.000	1.904	0.974
32	2.7	-0.7	0.049	0.049	0.979	0.109	0.062	1.000			87.6	0.000	1.904	0.974
33	2.8	-0.8	0.050	0.050	0.979	0.109	0.062	1.000			83.7	0.000	1.904	0.974
34	2.9	-0.9	0.052	0.052	0.978	0.109	0.062	1.000	2.83	5.02	76.9	0.000	1.904	0.974
35	3	-1	0.054	0.054	0.977	0.109	0.062	1.000	1.56	2.76	66.6	0.890	1.903	0.973
36	3.1	-1.1	0.056	0.056	0.976	0.109	0.062	1.000	0.97	1.72	52.9	5.136	1.898	0.970
37	3.2	-1.2	0.058	0.058	0.976	0.109	0.061	1.000	0.93	1.64	39.7	22.033	1.876	0.959
38	3.3	-1.3	0.059	0.059	0.975	0.109	0.061	1.000	0.85	1.51	29.0	40.202	1.836	0.939
39	3.4	-1.4	0.061	0.061	0.974	0.109	0.061	1.000	0.65	1.15	20.6	51.200	1.785	0.912
40	3.5	-1.5	0.063	0.062	0.973	0.110	0.062	1.000	0.63	1.11	18.3	51.200	1.733	0.886
41	3.6	-1.6	0.065	0.063	0.972	0.112	0.063	1.000	0.65	1.16	24.6	51.200	1.682	0.860
42	3.7	-1.7	0.067	0.064	0.972	0.114	0.064	1.000	0.71	1.25	33.6	51.200	1.631	0.834
43	3.8	-1.8	0.069	0.065	0.971	0.115	0.065	1.000	0.75	1.33	39.3	51.200	1.580	0.808
44	3.9	-1.9	0.071	0.066	0.970	0.116	0.066	1.000	0.78	1.39	43.9	51.200	1.529	0.782
45	4	-2	0.073	0.067	0.969	0.118	0.067	1.000	0.92	1.63	53.9	7.251	1.521	0.778
46	4.1	-2.1	0.075	0.068	0.969	0.119	0.067	1.000	0.87	1.55	52.2	9.986	1.511	0.773
47	4.2	-2.2	0.076	0.069	0.968	0.120	0.068	1.000	0.79	1.40	46.9	19.246	1.492	0.763
48	4.3	-2.3	0.078	0.069	0.967	0.122	0.069	1.000	0.74	1.31	42.9	51.200	1.441	0.737
49	4.4	-2.4	0.080	0.070	0.966	0.123	0.069	1.000	0.72	1.27	41.4	51.200	1.390	0.711
50	4.5	-2.5	0.082	0.071	0.966	0.124	0.070	1.000	0.71	1.26	41.1	51.200	1.338	0.684
51	4.6	-2.6	0.084	0.072	0.965	0.125	0.071	1.000	0.68	1.21	39.0	51.200	1.287	0.658
52	4.7	-2.7	0.086	0.073	0.964	0.126	0.071	1.000	0.66	1.16	36.3	51.200	1.236	0.632

19

53	4.8	-2.8	0.088	0.074	0.963	0.128	0.072	1.000	0.63	1.11	33.4	51.200	1.185	0.606
54	4.9	-2.9	0.090	0.075	0.963	0.129	0.073	1.000	0.94	1.66	57.9	4.770	1.180	0.603
55	5	-3	0.092	0.076	0.962	0.130	0.073	1.000	0.91	1.61	57.2	5.414	1.175	0.601
56	5.1	-3.1	0.094	0.077	0.961	0.131	0.074	1.000	0.87	1.55	56.0	6.500	1.168	0.597
57	5.2	-3.2	0.095	0.078	0.960	0.132	0.074	1.000	0.82	1.45	53.7	15.080	1.153	0.590
58	5.3	-3.3	0.097	0.079	0.959	0.132	0.075	1.000	0.76	1.34	50.3	25.006	1.128	0.577
59	5.4	-3.4	0.099	0.080	0.959	0.133	0.075	1.000	0.74	1.30	49.0	30.044	1.098	0.561
60	5.5	-3.5	0.101	0.080	0.958	0.134	0.076	1.000	0.72	1.28	48.2	34.061	1.064	0.544
61	5.6	-3.6	0.103	0.081	0.957	0.135	0.076	1.000	0.71	1.26	47.5	34.100	1.030	0.527
62	5.7	-3.7	0.105	0.082	0.956	0.136	0.077	1.000	0.70	1.24	47.3	34.100	0.996	0.509
63	5.8	-3.8	0.107	0.083	0.956	0.137	0.077	1.000	0.70	1.24	47.5	34.100	0.962	0.492
64	5.9	-3.9	0.109	0.084	0.955	0.138	0.078	1.000	0.69	1.21	46.4	34.100	0.928	0.474
65	6	-4	0.111	0.085	0.954	0.138	0.078	1.000	0.72	1.28	50.1	33.793	0.894	0.457
66	6.1	-4.1	0.113	0.086	0.953	0.139	0.079	1.000	0.84	1.48	56.7	7.860	0.886	0.453
67	6.2	-4.2	0.114	0.087	0.953	0.140	0.079	1.000	1.50	2.66	70.7	0.990	0.885	0.452
68	6.3	-4.3	0.116	0.088	0.952	0.141	0.079	1.000	1.75	3.10	73.4	0.639	0.884	0.452
69	6.4	-4.4	0.118	0.089	0.951	0.141	0.080	1.000	1.55	2.75	71.5	0.896	0.883	0.452
70	6.5	-4.5	0.120	0.090	0.950	0.142	0.080	1.000	1.56	2.76	71.6	0.892	0.882	0.451
71	6.6	-4.6	0.122	0.091	0.950	0.143	0.081	1.000	1.52	2.69	71.2	0.961	0.882	0.451
72	6.7	-4.7	0.124	0.092	0.949	0.143	0.081	1.000	1.51	2.67	69.5	0.979	0.881	0.450
73	6.8	-4.8	0.126	0.092	0.948	0.144	0.081	1.000	1.36	2.40	67.0	1.330	0.879	0.450
74	6.9	-4.9	0.128	0.093	0.947	0.145	0.082	1.000	1.20	2.12	64.4	1.607	0.878	0.449
75	7	-5	0.130	0.094	0.946	0.145	0.082	1.000	1.03	1.82	58.4	3.206	0.874	0.447
76	7.1	-5.1	0.132	0.095	0.946	0.146	0.082	1.000	0.95	1.69	53.2	5.785	0.869	0.444
77	7.2	-5.2	0.133	0.096	0.945	0.146	0.083	1.000	0.92	1.64	52.4	6.965	0.862	0.441
78	7.3	-5.3	0.135	0.097	0.944	0.147	0.083	1.000	0.93	1.65	54.0	6.694	0.855	0.437

20

79	7.4	-5.4	0.137	0.098	0.943	0.147	0.083	1.000	1.00	1.78	57.0	3.532	0.851	0.435
80	7.5	-5.5	0.139	0.099	0.943	0.148	0.084	1.000	1.12	1.99	61.3	2.129	0.849	0.434
81	7.6	-5.6	0.141	0.100	0.942	0.149	0.084	1.000	1.35	2.39	66.7	1.355	0.848	0.434
82	7.7	-5.7	0.143	0.101	0.941	0.149	0.084	0.998	1.51	2.68	69.5	0.971	0.847	0.433
83	7.8	-5.8	0.145	0.102	0.940	0.150	0.084	0.995	1.36	2.41	66.8	1.314	0.846	0.432
84	7.9	-5.9	0.147	0.103	0.940	0.150	0.085	0.992	1.20	2.13	63.8	1.588	0.844	0.432
85	8	-6	0.149	0.103	0.939	0.151	0.085	0.990	1.22	2.17	64.9	1.474	0.843	0.431
86	8.1	-6.1	0.151	0.104	0.938	0.151	0.085	0.987	1.23	2.18	64.8	1.443	0.841	0.430
87	8.2	-6.2	0.152	0.105	0.937	0.151	0.085	0.984	1.11	1.96	61.8	2.296	0.839	0.429
88	8.3	-6.3	0.154	0.106	0.937	0.152	0.086	0.982	0.96	1.70	57.5	4.276	0.835	0.427
89	8.4	-6.4	0.156	0.107	0.936	0.152	0.086	0.979	0.78	1.39	44.3	51.200	0.783	0.401
90	8.5	-6.5	0.158	0.108	0.935	0.153	0.086	0.977	0.66	1.17	27.5	51.200	0.732	0.374
91	8.6	-6.6	0.160	0.109	0.934	0.153	0.086	0.975	2.73	4.83	81.5	0.000	0.732	0.374
92	8.7	-6.7	0.162	0.110	0.933	0.154	0.087	0.972			84.1	0.000	0.732	0.374
93	8.8	-6.8	0.164	0.111	0.933	0.154	0.087	0.970			84.4	0.000	0.732	0.374
94	8.9	-6.9	0.166	0.112	0.932	0.154	0.087	0.967	2.24	3.97	79.0	0.000	0.732	0.374
95	9	-7	0.168	0.113	0.931	0.155	0.087	0.965	1.63	2.88	70.5	0.784	0.731	0.374
96	9.1	-7.1	0.170	0.114	0.930	0.155	0.087	0.962	1.19	2.11	65.2	1.945	0.729	0.373
97	9.2	-7.2	0.171	0.114	0.928	0.155	0.088	0.960	1.07	1.90	62.6	2.602	0.727	0.372
98	9.3	-7.3	0.173	0.115	0.926	0.155	0.088	0.958	1.01	1.79	60.8	3.445	0.723	0.370
99	9.4	-7.4	0.175	0.116	0.923	0.155	0.088	0.956	0.95	1.68	58.7	4.505	0.719	0.368
100	9.5	-7.5	0.177	0.117	0.920	0.155	0.088	0.953	0.89	1.58	57.1	5.999	0.713	0.365
101	9.6	-7.6	0.179	0.118	0.918	0.155	0.088	0.951	0.86	1.52	55.8	7.039	0.706	0.361
102	9.7	-7.7	0.181	0.119	0.915	0.155	0.088	0.949	0.83	1.46	54.6	14.252	0.692	0.354
103	9.8	-7.8	0.183	0.120	0.912	0.155	0.088	0.947	0.82	1.46	54.3	14.486	0.677	0.346
104	9.9	-7.9	0.185	0.121	0.910	0.155	0.088	0.945	0.84	1.48	54.4	13.174	0.664	0.339

21

105	10	-8	0.187	0.122	0.907	0.155	0.088	0.942	0.84	1.49	54.3	12.629	0.651	0.333
106	10.1	-8.1	0.189	0.123	0.904	0.155	0.087	0.940	0.85	1.51	54.8	11.908	0.639	0.327
107	10.2	-8.2	0.190	0.124	0.902	0.155	0.087	0.938	0.88	1.56	56.8	6.208	0.633	0.324
108	10.3	-8.3	0.192	0.125	0.899	0.155	0.087	0.936	1.00	1.78	61.5	3.545	0.630	0.322
109	10.4	-8.4	0.194	0.126	0.896	0.155	0.087	0.934	1.14	2.01	65.3	2.208	0.627	0.321
110	10.5	-8.5	0.196	0.126	0.894	0.155	0.087	0.932	1.47	2.61	72.1	1.042	0.626	0.320
111	10.6	-8.6	0.198	0.127	0.891	0.155	0.087	0.930	2.05	3.63	78.3	0.000	0.626	0.320
112	10.7	-8.7	0.200	0.128	0.888	0.155	0.087	0.928	2.31	4.09	80.1	0.000	0.626	0.320
113	10.8	-8.8	0.202	0.129	0.886	0.154	0.087	0.926	2.47	4.38	81.0	0.000	0.626	0.320
114	10.9	-8.9	0.204	0.130	0.883	0.154	0.087	0.924	2.23	3.95	79.6	0.000	0.626	0.320
115	11	-9	0.206	0.131	0.880	0.154	0.087	0.922	1.88	3.33	76.6	0.870	0.626	0.320
116	11.1	-9.1	0.208	0.132	0.878	0.154	0.087	0.920	1.60	2.83	73.1	0.825	0.625	0.319
117	11.2	-9.2	0.209	0.133	0.875	0.154	0.087	0.918	1.62	2.88	73.7	0.789	0.624	0.319
118	11.3	-9.3	0.211	0.134	0.872	0.154	0.087	0.916	1.63	2.90	74.0	0.774	0.623	0.319
119	11.4	-9.4	0.213	0.135	0.870	0.154	0.087	0.914	1.50	2.66	72.1	0.991	0.622	0.318
120	11.5	-9.5	0.215	0.136	0.867	0.154	0.087	0.913	1.49	2.65	72.2	1.005	0.621	0.318
121	11.6	-9.6	0.217	0.137	0.864	0.153	0.087	0.911	1.53	2.70	72.9	0.943	0.620	0.317
122	11.7	-9.7	0.219	0.137	0.862	0.153	0.086	0.909	1.56	2.76	73.0	0.889	0.619	0.317
123	11.8	-9.8	0.221	0.138	0.859	0.153	0.086	0.907	1.55	2.75	72.2	0.895	0.618	0.316
124	11.9	-9.9	0.223	0.139	0.856	0.153	0.086	0.905	1.38	2.45	69.5	1.261	0.617	0.316
125	12	-10	0.225	0.140	0.854	0.153	0.086	0.904	1.21	2.15	66.4	1.827	0.615	0.315
126	12.1	-10.1	0.227	0.141	0.851	0.152	0.086	0.902	1.10	1.95	63.3	2.357	0.613	0.313
127	12.2	-10.2	0.228	0.142	0.848	0.152	0.086	0.900	1.00	1.76	60.3	3.645	0.609	0.312
128	12.3	-10.3	0.230	0.143	0.846	0.152	0.086	0.898	0.90	1.59	56.6	5.818	0.604	0.309
129	12.4	-10.4	0.232	0.144	0.843	0.152	0.086	0.897	0.86	1.52	55.8	7.082	0.596	0.305
130	12.5	-10.5	0.234	0.145	0.840	0.152	0.086	0.895	0.83	1.48	55.3	8.022	0.588	0.301
131	12.6	-10.6	0.236	0.146	0.838	0.151	0.085	0.893	0.81	1.43	54.2	16.269	0.572	0.293
132	12.7	-10.7	0.238	0.147	0.835	0.151	0.085	0.891	0.78	1.37	52.0	21.388	0.551	0.282

22

133	12.8	-10.8	0.240	0.148	0.832	0.151	0.085	0.890	0.79	1.40	51.8	18.732	0.532	0.272
134	12.9	-10.9	0.242	0.149	0.830	0.151	0.085	0.888	0.79	1.39	51.2	19.758	0.512	0.262
135	13	-11	0.244	0.149	0.827	0.151	0.085	0.886	0.76	1.35	49.5	24.140	0.488	0.250
136	13.1	-11.1	0.246	0.150	0.824	0.150	0.085	0.885	0.73	1.29	47.9	32.853	0.455	0.233
137	13.2	-11.2	0.247	0.151	0.822	0.150	0.085	0.883	0.72	1.28	48.3	33.156	0.422	0.216
138	13.3	-11.3	0.249	0.152	0.819	0.150	0.085	0.882	0.73	1.30	48.6	30.561	0.392	0.200
139	13.4	-11.4	0.251	0.153	0.816	0.149	0.084	0.880	0.73	1.29	48.0	32.550	0.359	0.184
140	13.5	-11.5	0.253	0.154	0.814	0.149	0.084	0.878	0.71	1.26	46.7	34.100	0.325	0.166
141	13.6	-11.6	0.255	0.155	0.811	0.149	0.084	0.877	0.69	1.22	44.4	51.200	0.274	0.140
142	13.7	-11.7	0.257	0.156	0.808	0.149	0.084	0.875	0.66	1.18	39.1	51.200	0.223	0.114
143	13.8	-11.8	0.259	0.157	0.806	0.148	0.084	0.874	0.65	1.14	34.4	51.200	0.171	0.088
144	13.9	-11.9	0.261	0.158	0.803	0.148	0.084	0.872	0.63	1.11	27.1	51.200	0.120	0.061
145	14	-12	0.263	0.159	0.800	0.148	0.083	0.871	0.61	1.08	17.0	51.200	0.069	0.035
146	14.1	-12.1	0.265	0.160	0.798	0.148	0.083	0.869			-7.4	0.000	0.069	0.035
147	14.2	-12.2	0.266	0.160	0.795	0.147	0.083	0.868			-7.6	0.000	0.069	0.035
148	14.3	-12.3	0.268	0.161	0.792	0.147	0.083	0.866	0.49	0.86	35.9	51.200	0.018	0.009
149	14.4	-12.4	0.270	0.162	0.790	0.147	0.083	0.865	0.98	1.74	66.2	3.378	0.014	0.007
150	14.5	-12.5	0.272	0.163	0.787	0.146	0.083	0.863	1.40	2.47	72.7	1.219	0.013	0.007
151	14.6	-12.6	0.274	0.164	0.784	0.146	0.082	0.862	2.08	3.68	78.8	0.000	0.013	0.007
152	14.7	-12.7	0.276	0.165	0.782	0.146	0.082	0.860	2.09	3.71	78.9	0.000	0.013	0.007
153	14.8	-12.8	0.278	0.166	0.779	0.146	0.082	0.859	2.21	3.91	79.7	0.000	0.013	0.007
154	14.9	-12.9	0.280	0.167	0.776	0.145	0.082	0.858	2.13	3.78	79.2	0.000	0.013	0.007
155	15	-13	0.282	0.168	0.774	0.145	0.082	0.856	1.88	3.32	76.6	0.871	0.012	0.006
156	15.1	-13.1	0.284	0.169	0.771	0.145	0.082	0.855	1.55	2.75	72.1	0.895	0.011	0.006
157	15.2	-13.2	0.285	0.170	0.768	0.144	0.081	0.853	1.66	2.95	73.9	0.735	0.011	0.005
158	15.3	-13.3	0.287	0.171	0.765	0.144	0.081	0.852	1.81	3.20	74.3	0.579	0.010	0.005

23

159	15.4	-13.4	0.289	0.171	0.763	0.144	0.081	0.851	1.84	3.27	75.2	0.901	0.009	0.005
160	15.5	-13.5	0.291	0.172	0.760	0.143	0.081	0.849	2.00	3.54	77.2	0.765	0.008	0.004
161	15.6	-13.6	0.293	0.173	0.757	0.143	0.081	0.848	2.17	3.85	79.2	0.000	0.008	0.004
162	15.7	-13.7	0.295	0.174	0.755	0.143	0.080	0.847	2.08	3.69	78.2	0.000	0.008	0.004
163	15.8	-13.8	0.297	0.175	0.752	0.142	0.080	0.845	2.12	3.75	78.8	0.000	0.008	0.004
164	15.9	-13.9	0.299	0.176	0.749	0.142	0.080	0.844	2.44	4.32	80.9	0.000	0.008	0.004
165	16	-14	0.301	0.177	0.747	0.142	0.080	0.843	2.65	4.69	82.0	0.000	0.008	0.004
166	16.1	-14.1	0.303	0.178	0.744	0.141	0.080	0.841	2.08	3.69	78.2	0.000	0.008	0.004
167	16.2	-14.2	0.304	0.179	0.741	0.141	0.080	0.840	1.99	3.52	77.0	0.772	0.008	0.004
168	16.3	-14.3	0.306	0.180	0.739	0.141	0.079	0.839	1.96	3.47	76.4	0.794	0.007	0.003
169	16.4	-14.4	0.308	0.181	0.736	0.140	0.079	0.837	1.94	3.44	75.7	0.809	0.006	0.003
170	16.5	-14.5	0.310	0.182	0.733	0.140	0.079	0.836	1.96	3.48	75.1	0.792	0.005	0.003
171	16.6	-14.6	0.312	0.182	0.731	0.140	0.079	0.835	1.96	3.47	74.5	0.459	0.005	0.002
172	16.7	-14.7	0.314	0.183	0.728	0.139	0.079	0.834	1.94	3.44	73.8	0.470	0.004	0.002
173	16.8	-14.8	0.316	0.184	0.725	0.139	0.078	0.832	2.07	3.67	75.5	0.000	0.004	0.002
174	16.9	-14.9	0.318	0.185	0.723	0.138	0.078	0.831	1.91	3.39	73.9	0.492	0.004	0.002
175	17	-15	0.320	0.186	0.720	0.138	0.078	0.830	1.86	3.30	72.2	0.531	0.003	0.002
176	17.1	-15.1	0.322	0.187	0.717	0.138	0.078	0.829	2.17	3.84	75.6	0.000	0.003	0.002
177	17.2	-15.2	0.323	0.188	0.715	0.137	0.077	0.827	1.43	2.54	69.4	1.133	0.002	0.001
178	17.3	-15.3	0.325	0.189	0.712	0.137	0.077	0.826	1.36	2.41	67.8	1.312	0.001	0.000
179	17.4	-15.4	0.327	0.190	0.709	0.136	0.077	0.825	1.61	2.86	71.0	0.803	0.000	0.000
180	17.5	-15.5	0.329	0.191	0.707	0.136	0.077	0.824	2.72	4.82	82.1	0.000	0.000	0.000
181	17.6	-15.6	0.331	0.192	0.704	0.136	0.077	0.823			85.2	0.000	0.000	0.000
182	17.7	-15.7	0.333	0.193	0.701	0.135	0.076	0.821			87.5	0.000	0.000	0.000
183	17.8	-15.8	0.335	0.194	0.699	0.135	0.076	0.820			88.6	0.000	0.000	0.000
184	17.9	-15.9	0.337	0.194	0.696	0.135	0.076	0.819			85.8	0.000	0.000	0.000
185	18	-16	0.339	0.195	0.693	0.134	0.076	0.818			82.4	0.000	0.000	0.000

24

186	18.1	-16.1	0.341	0.196	0.691	0.134	0.075	0.817			82.9	0.000	0.000	0.000
187	18.2	-16.2	0.342	0.197	0.688	0.133	0.075	0.816			86.8	0.000	0.000	0.000
188	18.3	-16.3	0.344	0.198	0.685	0.133	0.075	0.815			90.0	0.000	0.000	0.000
189	18.4	-16.4	0.346	0.199	0.683	0.133	0.075	0.813			91.2	0.000	0.000	0.000
190	18.5	-16.5	0.348	0.200	0.680	0.132	0.075	0.812			90.2	0.000	0.000	0.000
191	18.6	-16.6	0.350	0.201	0.677	0.132	0.074	0.811			85.0	0.000	0.000	0.000
192	18.7	-16.7	0.352	0.202	0.675	0.131	0.074	0.810			84.0	0.000	0.000	0.000
193	18.8	-16.8	0.354	0.203	0.672	0.131	0.074	0.809			83.6	0.000	0.000	0.000
194	18.9	-16.9	0.356	0.204	0.669	0.131	0.074	0.808			84.0	0.000	0.000	0.000
195	19	-17	0.358	0.205	0.667	0.130	0.073	0.807			84.7	0.000	0.000	0.000
196	19.1	-17.1	0.360	0.206	0.664	0.130	0.073	0.806			83.6	0.000	0.000	0.000
197	19.2	-17.2	0.361	0.206	0.661	0.129	0.073	0.805	2.79	4.95	82.2	0.000	0.000	0.000
198	19.3	-17.3	0.363	0.207	0.659	0.129	0.073	0.804	2.35	4.16	78.8	0.000	0.000	0.000
199	19.4	-17.4	0.365	0.208	0.656	0.128	0.072	0.802	2.63	4.66	80.9	0.000	0.000	0.000
200	19.5	-17.5	0.367	0.209	0.653	0.128	0.072	0.801	2.45	4.35	80.4	0.000	0.000	0.000
201	19.6	-17.6	0.369	0.210	0.651	0.128	0.072	0.800	2.27	4.02	79.2	0.000	0.000	0.000
202	19.7	-17.7	0.371	0.211	0.648	0.127	0.072	0.799	2.19	3.88	78.6	0.000	0.000	0.000
203	19.8	-17.8	0.373	0.212	0.645	0.127	0.072	0.798	2.75	4.88	81.8	0.000	0.000	0.000
204	19.9	-17.9	0.375	0.213	0.643	0.126	0.071	0.797			82.7	0.000	0.000	0.000
205	20	-18	0.377	0.214	0.640	0.126	0.071	0.796			82.9	0.000	0.000	0.000
206	20.1	-18.1	0.379	0.215	0.637	0.125	0.071	0.795			84.0	0.000	0.000	0.000
207	20.2	-18.2	0.380	0.216	0.635	0.125	0.071	0.794			85.8	0.000	0.000	0.000
208	20.3	-18.3	0.382	0.217	0.632	0.125	0.070	0.793			85.7	0.000	0.000	0.000
209	20.4	-18.4	0.384	0.217	0.629	0.124	0.070	0.792			85.2	0.000	0.000	0.000
210	20.5	-18.5	0.386	0.218	0.627	0.124	0.070	0.791			85.0	0.000	0.000	0.000
211	20.6	-18.6	0.388	0.219	0.624	0.123	0.070	0.790			85.8	0.000	0.000	0.000
212	20.7	-18.7	0.390	0.220	0.621	0.123	0.069	0.789			87.3	0.000	0.000	0.000
213	20.8	-18.8	0.392	0.221	0.619	0.122	0.069	0.788			88.1	0.000	0.000	0.000

Graphical representation of parameters calculated in previous spreadsheet

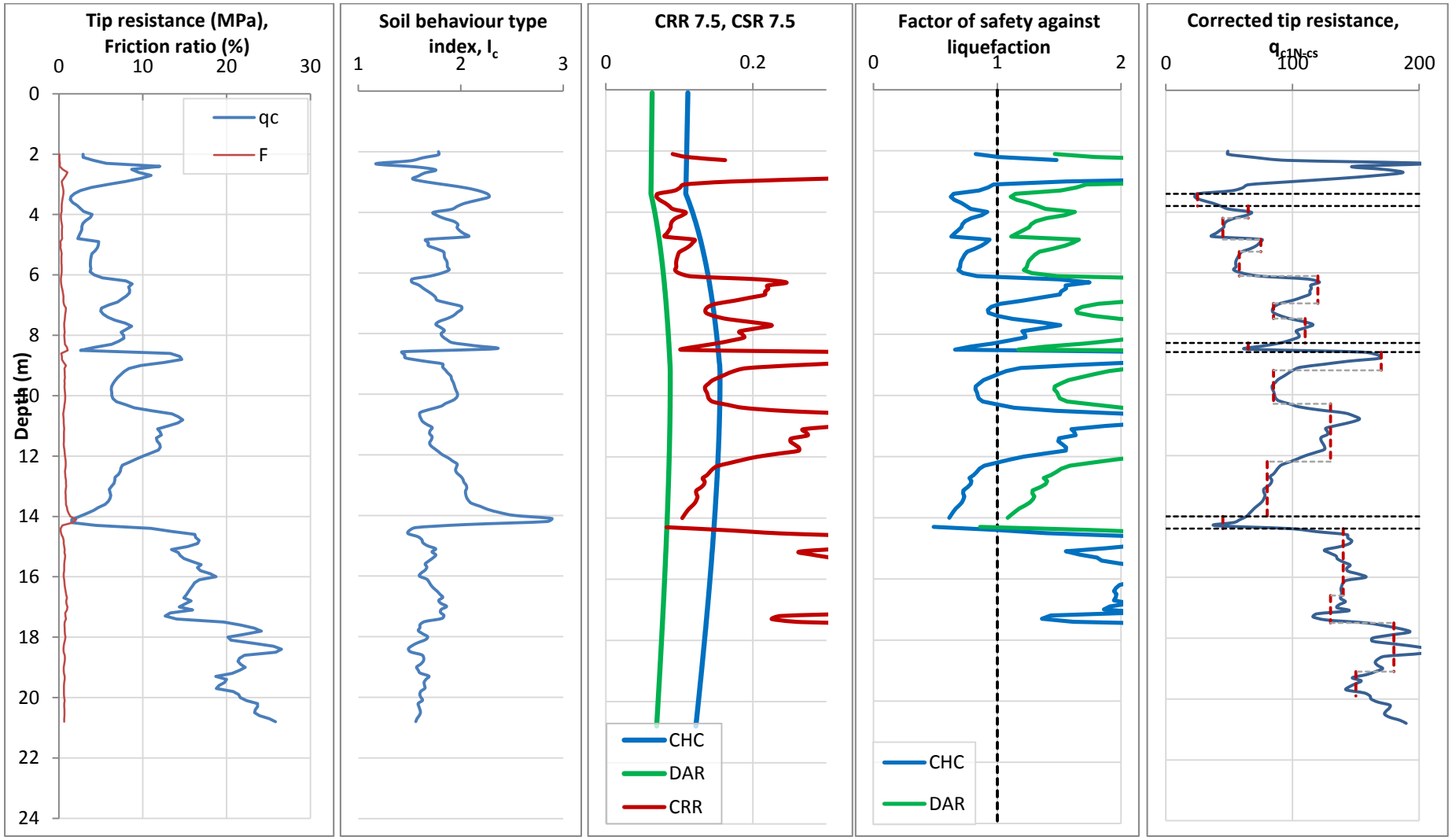

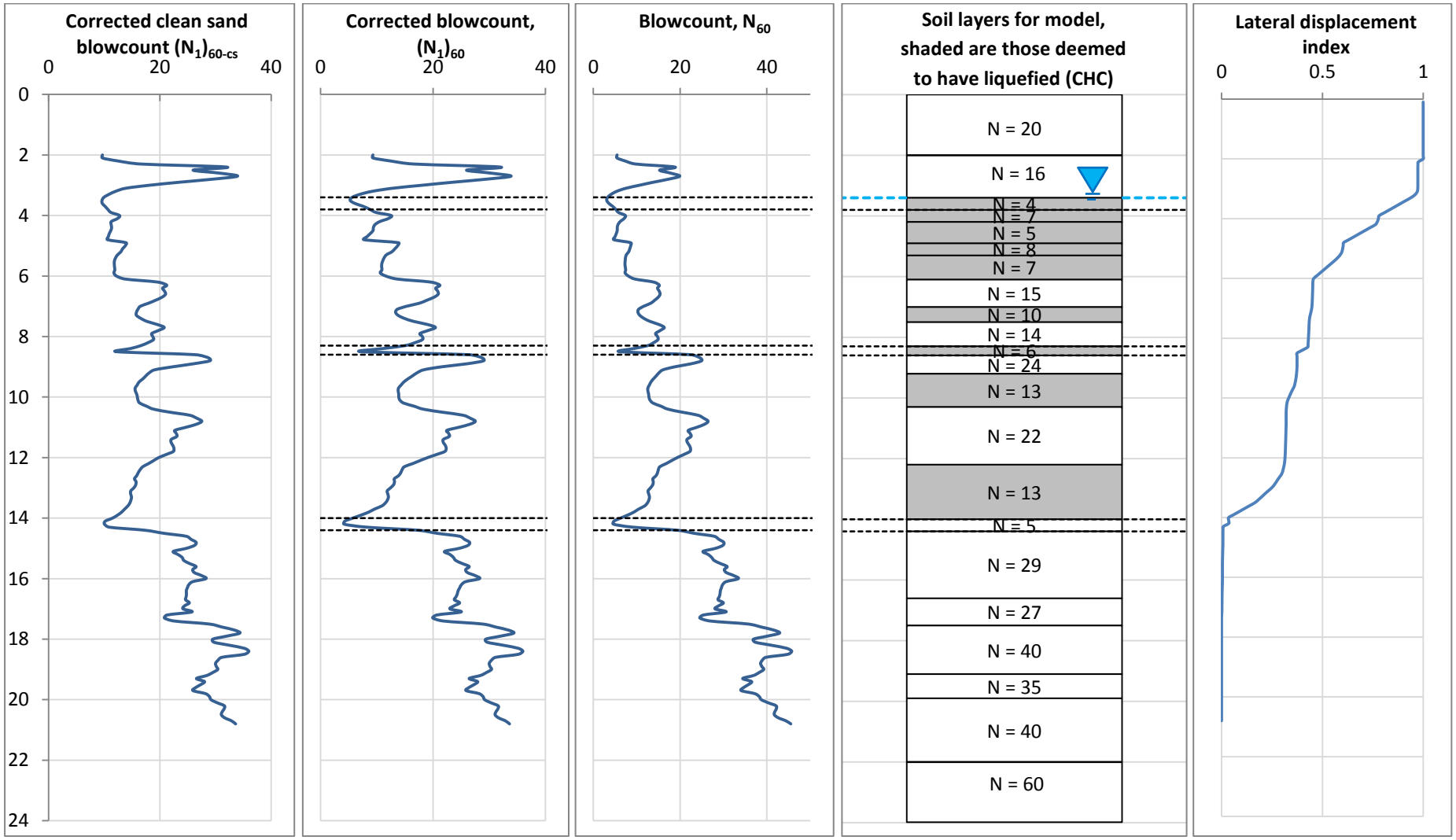
Corrected clean sand blowcount $(N_1)_{60\text{-}cs}$
0
20
40
0
2
4
6
8
10
12
14
16
18
20
22
24
Corrected blowcount, $(N_1)_{60}$
0
20
40
Blowcount, N_{60}
0
20
40
Soil layers for model, shaded are those deemed to have liquefied (CHC)
N = 20
N = 16
N = 4
N = 7
N = 5
N = 8
N = 7
N = 15
N = 10
N = 14
N = 6
N = 24
N = 13
N = 22
N = 13
N = 5
N = 29
N = 27
N = 40
N = 35
N = 40
N = 60
Lateral displacement index
0
0.5
1

Tabulated equivalent SPT blowcount values for each discretised layer

Representative equivalent blowcounts				
Depth below surface – layer top (m)	$(N_1)_{60cs}$	$(N_1)_{60}$	N_{60} (=N for model)	Liq (Y/N)
0	30	30	20	N
2	25	25	16	N
3.4	10	6	4	Y
3.8	12	12	7	Y
4.2	11	8	5	Y
4.9	14	14	8	Y
5.3	13	12	7	Y
6.1	21	21	15	N
7	16	14	10	Y
7.5	18	18	14	N
8.3	12	8	6	Y
8.6	28	28	24	N
9.2	16	14	13	Y
10.3	23	23	22	N
12.2	15	13	13	Y
14	10	5	5	N
14.4	25	25	29	N
16.6	22	22	27	N
17.5	32	32	40	N
19.1	27	27	35	N
19.9	32	32	40	N
22	50	50	60	N

Appendix C – Soil spring calculations

Legend for pages in the *EXCEL* spreadsheet, soil-spring formulations and parametric variations based on CPT-2 (ANZAC) – South abutment, single pile model

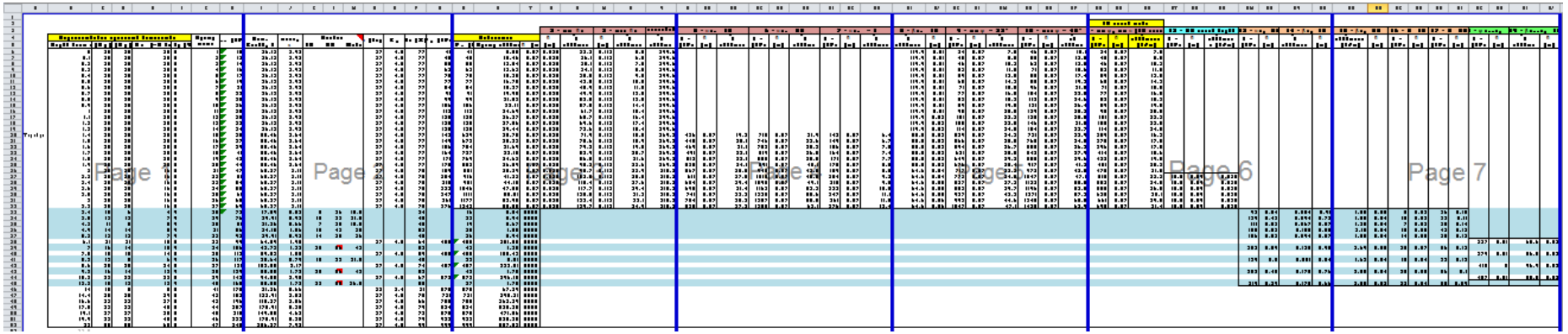

Parametric Study (Lateral Spreading)			
	Reference	LB	UB
α_{Crust}	4.5	3	5
α_{Liq}	1	1	6
$\alpha_{Non\text{-}Liq}$	1	1	3
β_{Crust}	1	0.3	1
β_{Liq}	0.01	0.001	0.02
$\beta_{Non\text{-}Liq}$	1	0.3	1

	A	B	C	D	E	F	G	H
1								
2								
3								
4		Representative equivalent blowcounts					Spring name	σ'_{vo} (kPa)
5		Depth below surface	$(N_1)_{60cs}$	$(N_1)_{60}$	N_{60} (=N for model)	Liq (Y/N)		
6		0	30	30	20	N	1	10
7		0.1	30	30	20	N	2	12
8		0.2	30	30	20	N	3	14
9		0.3	30	30	20	N	4	16
10		0.4	30	30	20	N	5	17
11		0.5	30	30	20	N	6	19
12		0.6	30	30	20	N	7	21
13		0.7	30	30	20	N	8	23
14		0.8	30	30	20	N	9	25
15		0.9	30	30	20	N	10	26
16		1	30	30	20	N	11	28
17		1.1	30	30	20	N	12	30
18		1.2	30	30	20	N	13	32
19		1.3	30	30	20	N	14	34
20	Top of pile	1.4	30	30	20	N	15	35
21		1.5	30	30	20	N	16	37
22		1.6	30	30	20	N	17	39
23		1.7	30	30	20	N	18	41
24		1.8	30	30	20	N	19	43
25		1.9	30	30	20	N	20	44
26		2	25	25	16	N	21	47
27		2.2	25	25	16	N	22	51
28		2.4	25	25	16	N	23	54
29		2.6	25	25	16	N	24	58
30		2.8	25	25	16	N	25	61
31		3	25	25	16	N	26	65
32		3.2	25	25	16	N	27	69
33		3.4	10	6	4	Y	28	72
34		3.8	12	12	7	Y	29	76
35		4.2	11	8	5	Y	30	81
36		4.9	14	14	8	Y	31	86
37		5.3	13	12	7	Y	32	92
38		6.1	21	21	15	N	33	99
39		7	16	14	10	Y	34	106
40		7.5	18	18	14	N	35	112
41		8.3	12	8	6	Y	36	117
42		8.6	28	28	24	N	37	121
43		9.2	16	14	13	Y	38	129
44		10.3	23	23	22	N	39	143
45		12.2	15	13	13	Y	40	160
46		14	10	5	5	N	41	170
47		14.4	25	25	29	N	42	182
48		16.6	22	22	27	N	43	196
49		17.5	32	32	40	N	44	207
50		19.1	27	27	35	N	45	218
51		19.9	32	32	40	N	46	232
52		22	50	50	60	N	47	248
53		23.5						

1

I	J	K	L	M	N	O	P	Q
Sub. Rxn. Coeff, k (MN/m^3)	Stiffness, κ (MN/m)	Residual Strength, S_r (kPa)			ϕ (deg)	K_p	Dr (%)	P_p (kPa)
		LB	UB	Median				
26.13	3.92				37	4.0	77	41
26.13	3.92				37	4.0	77	48
26.13	3.92				37	4.0	77	55
26.13	3.92				37	4.0	77	62
26.13	3.92				37	4.0	77	70
26.13	3.92				37	4.0	77	77
26.13	3.92				37	4.0	77	84
26.13	3.92				37	4.0	77	91
26.13	3.92				37	4.0	77	99
26.13	3.92				37	4.0	77	106
26.13	3.92				37	4.0	77	113
26.13	3.92				37	4.0	77	120
26.13	3.92				37	4.0	77	128
26.13	3.92				37	4.0	77	135
85.46	2.64				37	4.0	77	142
85.46	2.64				37	4.0	77	149
85.46	2.64				37	4.0	77	156
85.46	2.64				37	4.0	77	164
85.46	2.64				37	4.0	77	171
85.46	2.64				37	4.0	77	178
68.37	2.11				37	4.0	70	189
68.37	2.11				37	4.0	70	204
68.37	2.11				37	4.0	70	218
68.37	2.11				37	4.0	70	233
68.37	2.11				37	4.0	70	247
68.37	2.11				37	4.0	70	261
68.37	2.11				37	4.0	70	276
17.09	0.53	5	26	15.5			34	
29.91	0.92	10	33	21.5			48	
21.36	0.66	7	30	18.5			40	
34.18	1.06	18	42	30			52	
29.91	0.92	14	38	26			48	
64.09	1.98				37	4.0	64	400
42.73	1.32	28	56	42			52	
59.82	1.85				37	4.0	59	450
25.64	0.79	10	33	21.5			40	
102.55	3.17				37	4.0	74	487
55.55	1.72	28	56	42			52	
94.00	2.90				37	4.0	67	573
55.55	1.72	23	50	36.5			50	
21.36	0.66				33	3.4	31	575
123.91	3.83				37	4.0	70	731
115.37	3.56				37	4.0	66	788
170.91	5.28				37	4.0	79	834
149.55	4.62				37	4.0	73	878
170.91	5.28				37	4.0	79	932
256.37	7.92				37	4.0	99	999

2

	R	S	T	U	V	W	X	Y
1								
2								
3				2 - min δy		3 - max δy		4 - calculated δy
4	Reference			δ_y (m)	Degraded stiffness (t/m)	δ_y (m)	Degraded stiffness (t/m)	Degraded stiffness (t/m)
5	P_u (kPa)	Spring stiffness (t'/m)	δ_y (m)					
6	41	8.88	0.07	0.028	22.2	0.112	5.5	399.6
7	48	10.46	0.07	0.028	26.1	0.112	6.5	399.6
8	55	12.04	0.07	0.028	30.1	0.112	7.5	399.6
9	62	13.62	0.07	0.028	34.1	0.112	8.5	399.6
10	70	15.20	0.07	0.028	38.0	0.112	9.5	399.6
11	77	16.78	0.07	0.028	42.0	0.112	10.5	399.6
12	84	18.37	0.07	0.028	45.9	0.112	11.5	399.6
13	91	19.95	0.07	0.028	49.9	0.112	12.5	399.6
14	99	21.53	0.07	0.028	53.8	0.112	13.5	399.6
15	106	23.11	0.07	0.028	57.8	0.112	14.4	399.6
16	113	24.69	0.07	0.028	61.7	0.112	15.4	399.6
17	120	26.27	0.07	0.028	65.7	0.112	16.4	399.6
18	128	27.86	0.07	0.028	69.6	0.112	17.4	399.6
19	135	29.44	0.07	0.028	73.6	0.112	18.4	399.6
20	639	28.75	0.07	0.028	71.9	0.112	18.0	269.2
21	672	30.22	0.07	0.028	75.6	0.112	18.9	269.2
22	704	31.69	0.07	0.028	79.2	0.112	19.8	269.2
23	737	33.15	0.07	0.028	82.9	0.112	20.7	269.2
24	769	34.62	0.07	0.028	86.5	0.112	21.6	269.2
25	802	36.09	0.07	0.028	90.2	0.112	22.6	269.2
26	851	38.29	0.07	0.028	95.7	0.112	23.9	215.3
27	916	41.22	0.07	0.028	103.0	0.112	25.8	215.3
28	981	44.15	0.07	0.028	110.4	0.112	27.6	215.3
29	1046	47.08	0.07	0.028	117.7	0.112	29.4	215.3
30	1111	50.01	0.07	0.028	125.0	0.112	31.3	215.3
31	1177	52.95	0.07	0.028	132.4	0.112	33.1	215.3
32	1242	55.88	0.07	0.028	139.7	0.112	34.9	215.3
33	16	0.54	0.09069					
34	22	0.94	0.07188					
35	19	0.67	0.08659					
36	30	1.08	0.08776					
37	26	0.94	0.08693					
38	400	201.88	0.00624					
39	42	1.35	0.09829					
40	450	188.42	0.00752					
41	22	0.81	0.08386					
42	487	323.01	0.00474					
43	42	1.75	0.07561					
44	573	296.10	0.00610					
45	37	1.75	0.06571					
46	575	67.29	0.02694					
47	731	390.31	0.00590					
48	788	363.39	0.00683					
49	834	538.35	0.00488					
50	878	471.06	0.00587					
51	932	538.35	0.00545					
52	999	807.53	0.00389					
53								

3

Z	AA	AB	AC	AD	AE	AF	AG	AH
5 - α_{Crust} LB			6 - α_{Crust} UB			7 - α_{Crust} = 1		
p_{max} (kPa)	δ_y (m)	Degraded stiffness (t/m)	p_{max} (kPa)	δ_y (m)	Degraded stiffness (t/m)	p_{max} (kPa)	δ_y (m)	Degraded stiffness (t/m)
426	0.07	19.2	710	0.07	31.9	142	0.07	6.4
448	0.07	20.1	746	0.07	33.6	149	0.07	6.7
469	0.07	21.1	782	0.07	35.2	156	0.07	7.0
491	0.07	22.1	819	0.07	36.8	164	0.07	7.4
513	0.07	23.1	855	0.07	38.5	171	0.07	7.7
535	0.07	24.1	891	0.07	40.1	178	0.07	8.0
567	0.07	25.5	945	0.07	42.5	189	0.07	8.5
611	0.07	27.5	1018	0.07	45.8	204	0.07	9.2
654	0.07	29.4	1090	0.07	49.1	218	0.07	9.8
698	0.07	31.4	1163	0.07	52.3	233	0.07	10.5
741	0.07	33.3	1235	0.07	55.6	247	0.07	11.1
784	0.07	35.3	1307	0.07	58.8	261	0.07	11.8
828	0.07	37.3	1380	0.07	62.1	276	0.07	12.4

4

5

	AI	AJ	AK	AL	AM	AN	AO	AP
1								
2								
3	8 - β_{Crust} LB		9 - min ϕ = 33°			10 - max ϕ = 40°		
4	Degraded stiffness (t/m)	δ_y (m)	p_{max} (kPa)	δ_y (m)	Degraded stiffness (t/m)	p_{max} (kPa)	δ_y (m)	Degraded stiffness (t/m)
5								
6	119.9	0.00518	34	0.07	7.5	46	0.07	10.1
7	119.9	0.00611	40	0.07	8.8	55	0.07	12.0
8	119.9	0.00703	46	0.07	10.2	63	0.07	13.8
9	119.9	0.00795	53	0.07	11.5	71	0.07	15.6
10	119.9	0.00888	59	0.07	12.8	80	0.07	17.4
11	119.9	0.0098	65	0.07	14.2	88	0.07	19.2
12	119.9	0.01073	71	0.07	15.5	96	0.07	21.0
13	119.9	0.01165	77	0.07	16.8	104	0.07	22.8
14	119.9	0.01257	83	0.07	18.2	113	0.07	24.6
15	119.9	0.0135	89	0.07	19.5	121	0.07	26.4
16	119.9	0.01442	95	0.07	20.8	129	0.07	28.2
17	119.9	0.01534	101	0.07	22.2	138	0.07	30.0
18	119.9	0.01627	108	0.07	23.5	146	0.07	31.8
19	119.9	0.01719	114	0.07	24.8	154	0.07	33.7
20	80.8	0.02493	539	0.07	24.2	731	0.07	32.9
21	80.8	0.0262	566	0.07	25.5	768	0.07	34.5
22	80.8	0.02747	594	0.07	26.7	805	0.07	36.2
23	80.8	0.02874	621	0.07	28.0	842	0.07	37.9
24	80.8	0.03001	649	0.07	29.2	880	0.07	39.6
25	80.8	0.03128	676	0.07	30.4	917	0.07	41.3
26	64.6	0.04148	717	0.07	32.3	973	0.07	43.8
27	64.6	0.04466	772	0.07	34.8	1047	0.07	47.1
28	64.6	0.04784	827	0.07	37.2	1122	0.07	50.5
29	64.6	0.05102	882	0.07	39.7	1196	0.07	53.8
30	64.6	0.05419	937	0.07	42.2	1271	0.07	57.2
31	64.6	0.05737	992	0.07	44.6	1345	0.07	60.5
32	64.6	0.06055	1047	0.07	47.1	1420	0.07	63.9
33								
34								
35								
36								
37								
38								
39								
40								
41								
42								
43								
44								
45								
46								
47								
48								
49								
50								
51								
52								

AQ	AR	AS	AT	AU	AV	AW	AX	AY	AZ
LB crust model									
11 - min ϕ, min α (LB crust)			12 - NA crust depth			13 - α_{Liq} UB		14 - β_{Liq} LB	
p_{max} (kPa)	δ_y (m)	Degraded stiffness (t/m)	p_{max} (kPa)	δ_y (m)	Degraded stiffness (t/m)	p_{max} (kPa)	δ_y (m)	Degraded stiffness (t/m)	δ_y (m)
34	0.07	7.5							
40	0.07	8.8							
46	0.07	10.2							
53	0.07	11.5							
59	0.07	12.8							
65	0.07	14.2							
71	0.07	15.5							
77	0.07	16.8							
83	0.07	18.2							
89	0.07	19.5							
95	0.07	20.8							
101	0.07	22.2							
108	0.07	23.5							
114	0.07	24.8							
359	0.07	16.2							
378	0.07	17.0							
396	0.07	17.8							
414	0.07	18.6							
432	0.07	19.5							
451	0.07	20.3							
478	0.07	21.5							
515	0.07	23.2	15.5	0.09069	0.538				
552	0.07	24.8	15.5	0.09069	0.538				
588	0.07	26.5	15.5	0.09069	0.538				
625	0.07	28.1	15.5	0.09069	0.538				
661	0.07	29.8	15.5	0.09069	0.538				
698	0.07	31.4	15.5	0.09069	0.538				
						93	0.54413	0.054	0.90689
						129	0.43129	0.094	0.71882
						111	0.51956	0.067	0.86593
						180	0.52658	0.108	0.87763
						156	0.52156	0.094	0.86927
						252	0.58977	0.135	0.98295
						129	0.50318	0.081	0.83863
						252	0.45367	0.175	0.75611
						219	0.39426	0.175	0.6571

BA	BB	BC	BD	BE	BF	BG	BH	BI	BJ
15 - β_{Liq} UB		16 - S_r LB		17 - S_r UB		18 - $\phi_{Non\text{-}Liq}$ LB		19 - $\beta_{Non\text{-}Liq}$ LB	
Degraded stiffness (t/m)	δ_y (m)	p_{max} (kPa)	δ_y (m)	p_{max} (kPa)	δ_y (m)	p_{max} (kPa)	δ_y (m)	Degraded stiffness (t/m)	δ_y (m)
1.08	0.04534	5	0.02925	26	0.15212				
1.88	0.03594	10	0.03343	33	0.11033				
1.35	0.0433	7	0.03276	30	0.14042				
2.15	0.04388	18	0.05266	42	0.12287				
1.88	0.04346	14	0.04681	38	0.12705				
						337.002	0.00526	60.6	0.02079
2.69	0.04915	28	0.06553	56	0.13106				
						379	0.00634	56.5	0.02505
1.62	0.04193	10	0.03901	33	0.12872				
						410	0.004	96.9	0.01581
3.50	0.03781	28	0.05041	56	0.10082				
						487	0.00518	88.8	0.02046
3.50	0.03285	23	0.04141	50	0.09001				

Appendix D

Particle size distributions – BH-GAY-01 (to establish fines content)

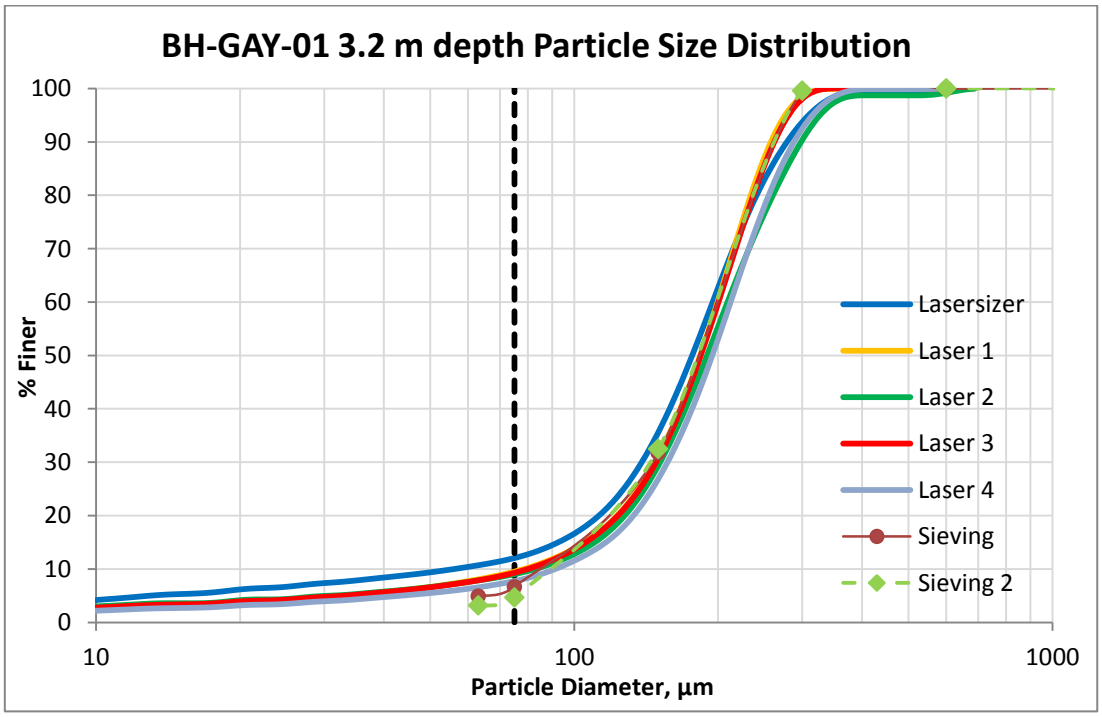

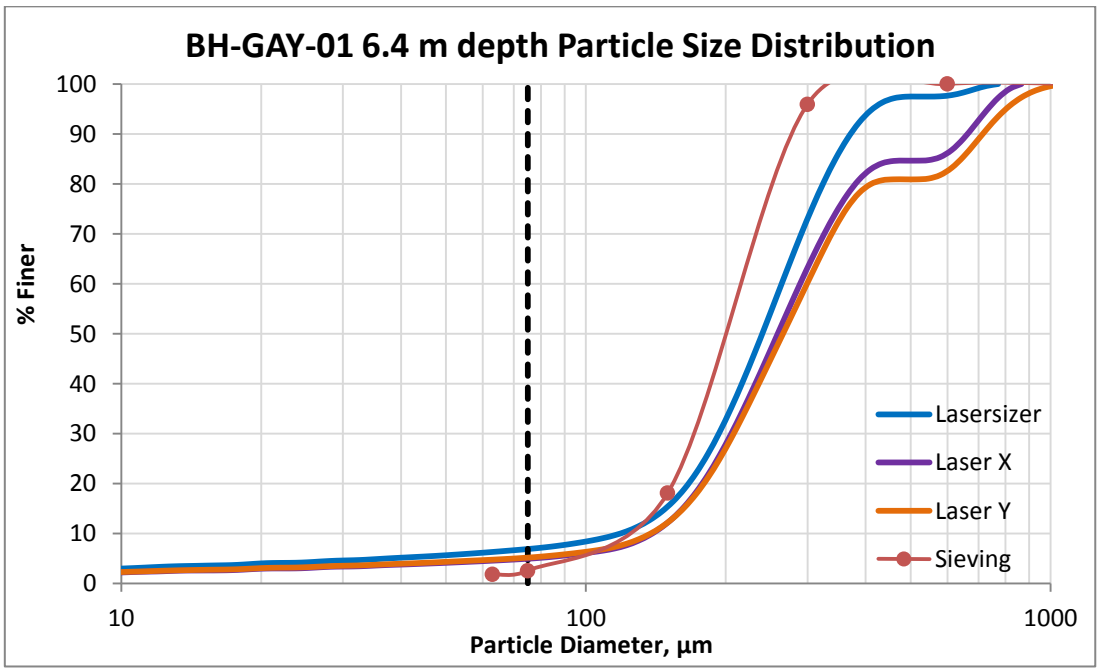

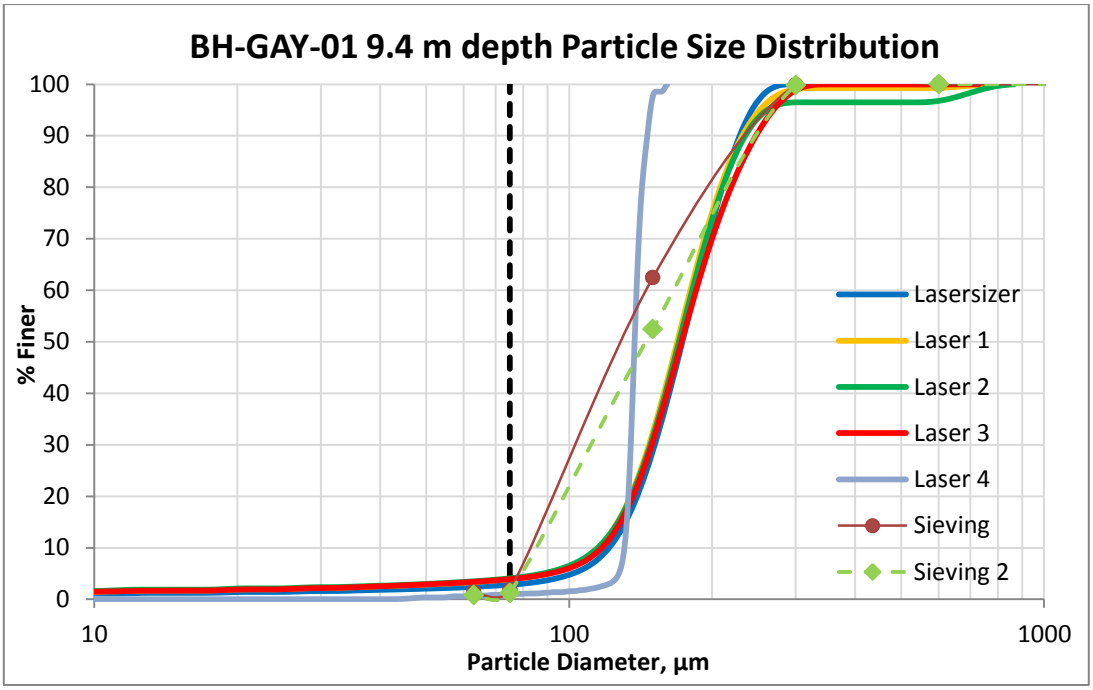
BH-GAY-01 9.4 m depth Particle Size Distribution
% Finer
100
90
80
70
60
50
40
30
20
10
0
10
100
1000
Particle Diameter, µm
Lasersizer
Laser 1
Laser 2
Laser 3
Laser 4
Sieving
Sieving 2

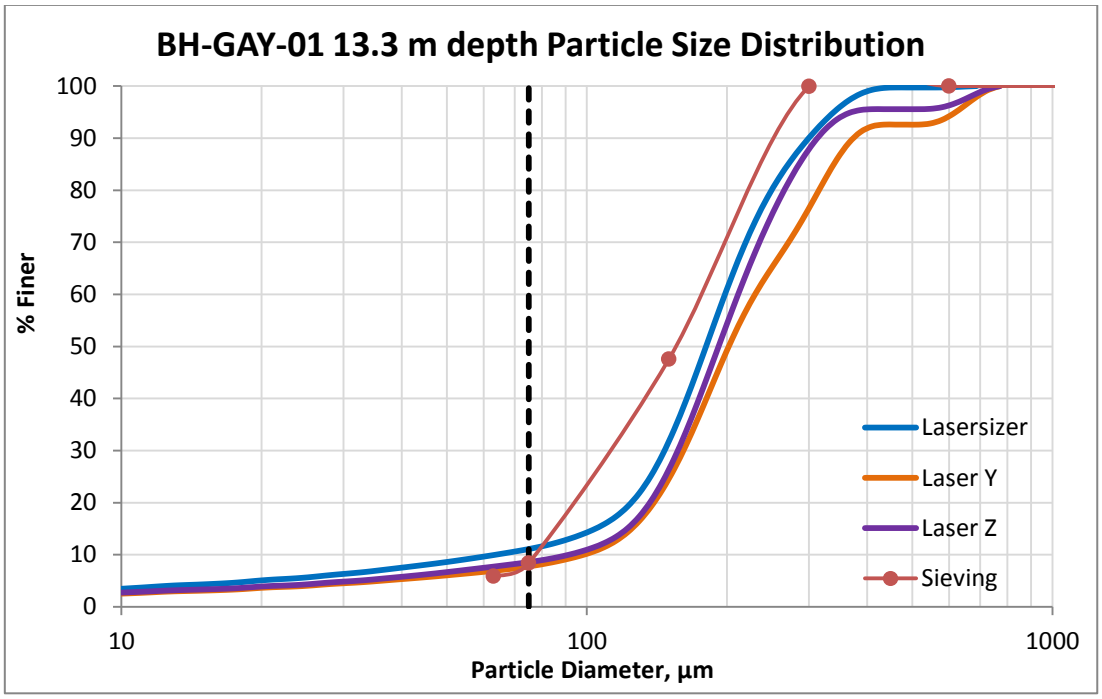
BH-GAY-01 13.3 m depth Particle Size Distribution
% Finer
100
90
80
70
60
50
40
30
20
10
0
10
100
1000
Particle Diameter, µm
Lasersizer
Laser Y
Laser Z
Sieving

Particle size distributions – BH-GAY-02 (to establish fines content)

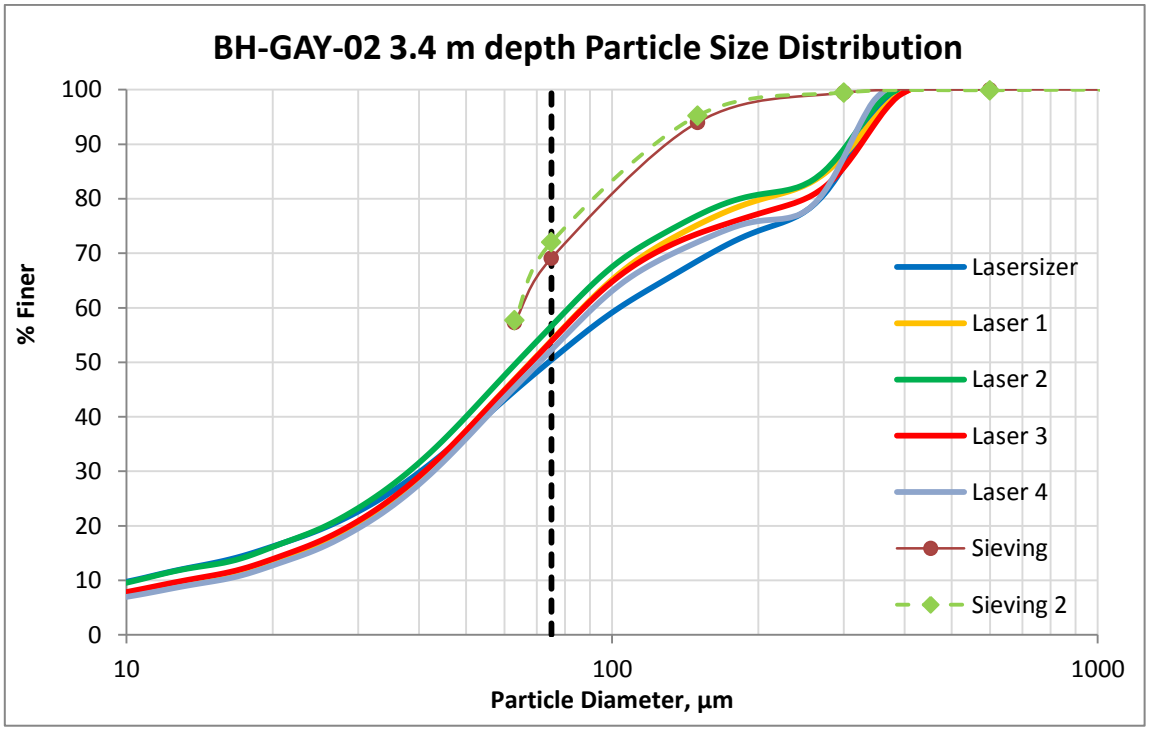

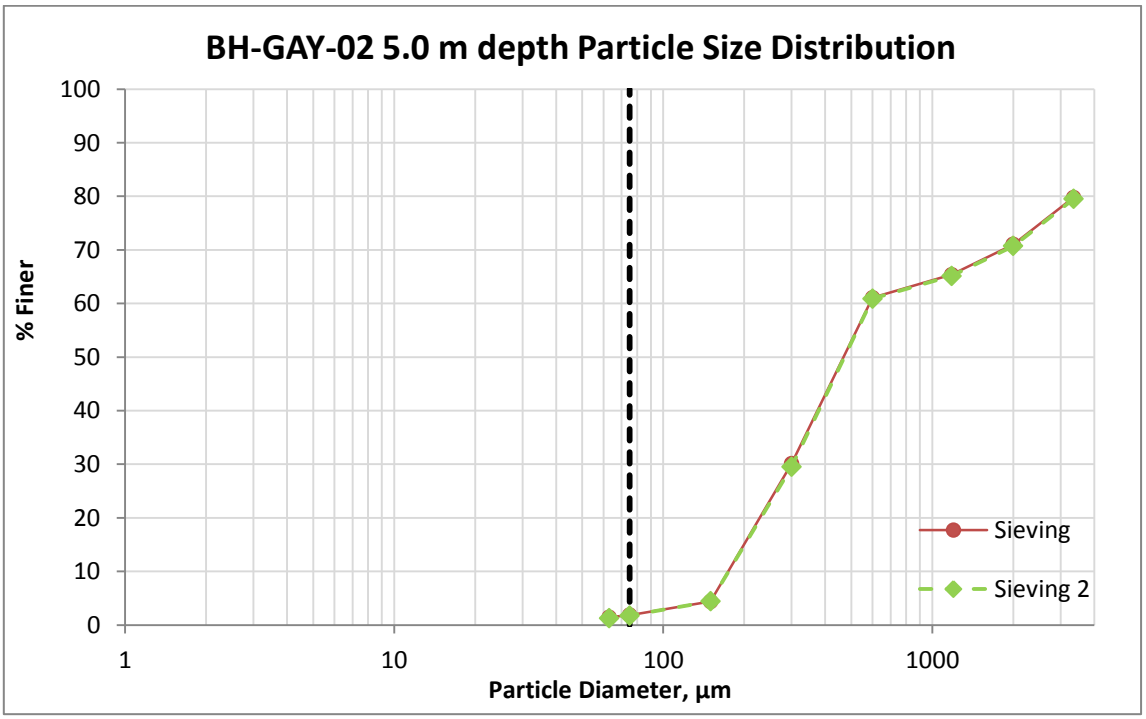

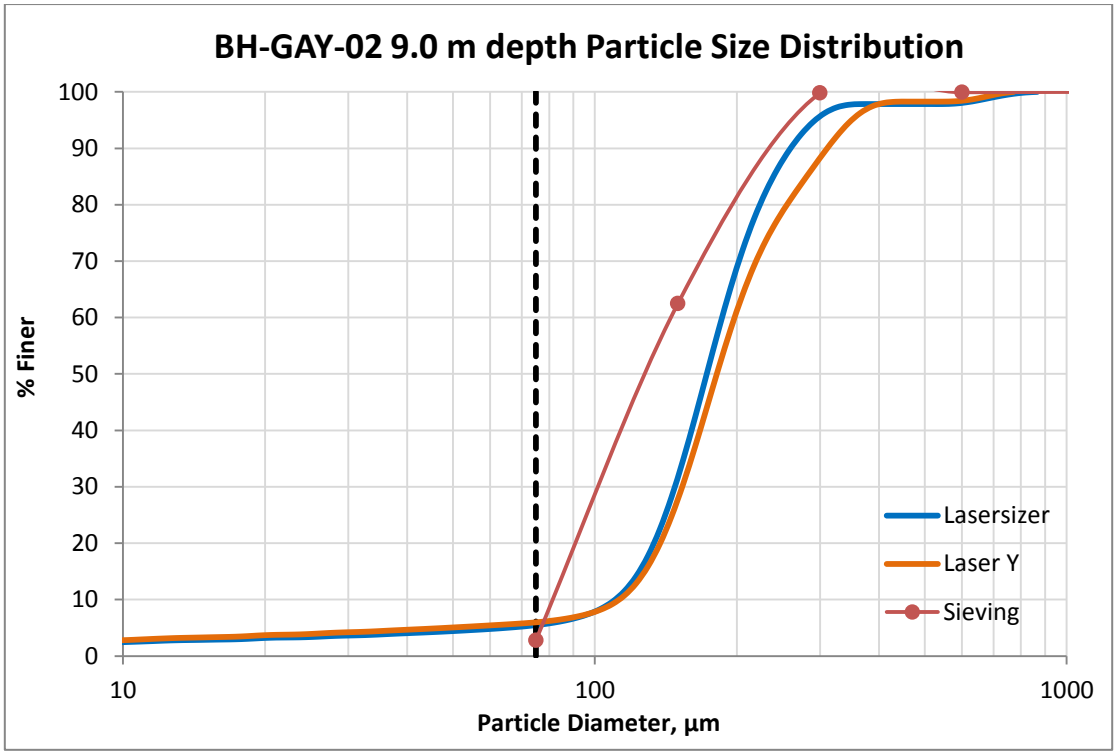
BH-GAY-02 9.0 m depth Particle Size Distribution
% Finer
100
90
80
70
60
50
40
30
20
10
0
10
100
1000
Particle Diameter, µm
Lasersizer
Laser Y
Sieving